Masters of the tips:

End Binding proteins orchestrate microtubule plus- and minus-end dynamics

Chao YANG

Masters of the tips:
End Binding proteins orchestrate microtubule plus- and minus-end dynamics

Chao YANG

ISBN: 978-94-6375-797-3

The research described in this thesis was performed in the division of Cell Biology, Neurobiology and Biophysics in the Department of Biology, Faculty of Science, Utrecht University, the Netherlands.

The printing of this thesis was financially supported by Alzheimer Nederland.

Cover: Fireworks of dynamic cells
Layout by: Chao YANG

Print: Ridderprint

Masters of the tips:
End Binding proteins orchestrate microtubule plus- and minus-end dynamics

Maestro's van de uiteinden:
Eind Bindende eiwitten dirigeren de dynamiek van microtubuli plus- en min-uiteinden
(met een samenvatting in het Nederlands)

Proefschrift
ter verkrijging van de graad van doctor aan de Universiteit Utrecht
op gezag van de rector magnificus, prof.dr. H.R.B.M. Kummeling,
ingevolge het besluit van het college voor promoties in het openbaar te
verdedigen op woensdag 23 maart 2020 des middags te 2.30 uur

door

Chao YANG

geboren op 26 augustus 1988 te Chengdu, China

Promotor: Prof. dr. A.S. Akhmanova

A journey of a thousand miles begins with a single step.

千里之行，始于足下

Lao Tzu

Table of contents

1

Introduction

End Binding proteins at dynamic microtubule ends: Mechanisms, regulation andfunction

Chao YANG

1.1 Microtubules and their dynamics

Microtubules (MTs) are components of the cytoskeleton, which are important for cell morphology, migration, intracellular trafficking and cell division (Howard and Hyman, 2003; Akhmanova and Steinmetz, 2008). MTs are hollow tubes with an outer diameter of 25 nm diameter and inner diameter of 12 nm. They are composed of rows of tubulin dimers, termed protofilaments, and most mammalian MTs have 13 protofilaments (Desai and Mitchison, 1997). MTs deviating from this protofilament number, ranging from 4 to 40 protofilaments, can be found in plants, animals, and protists (Chaaban and Brouhard, 2017). To perform different functions, MTs can form different stable or dynamic structures. An example of a structure composed of stable MTs is the centriole, which contains nine stable, symmetrically organized MT triplets. Centrioles form the core of centrosomes, the major animal MT organizing centers (MTOCs). Centrioles can also be converted into the basal bodies of cilia or flagella, cell protrusions supported by another stable MT structure, the axoneme with nine MT doublets (Kobayashi and Dynlacht, 2011). In addition to these stable structures, MTs form highly dynamic cytoplasmic networks of various geometry, such as mitotic and meiotic spindles, MT asters, as well as parallel and antiparallel linear arrays found in different cell types (Lüders and Stearns, 2007; Akhmanova and Hoogenraad, 2015).

MTs are polymers of α- and β-tubulin heterodimers, which attach to each other by noncovalent bonds in a head-to-tail fashion. As a result, MTs have two distinct ends, the end where β-tubulin protrudes, the plus end, and the end where α-tubulin is exposed, the minus end. MTs are dynamic: both MT ends can grow and shrink, but the addition and removal of tubulin dimers occurs faster at the plus end, and therefore MT mass is generated by MT plus end polymerization. In contrast, MT minus ends display relatively slow dynamics and their organization controls the geometry of MT networks (Martin and Akhmanova, 2018; Lüders and Stearns, 2007).

Both α- and β-tubulin bind to GTP. During polymerization, the GTP bound to β-tubulin (at the E-site) is hydrolyzed, while the GTP bound to α-tubulin is non-exchangeable (Desai and Mitchison, 1997). During MT polymerization, tubulin dimers with GTP-bound β-tubulin are incorporated into MTs. Because of the delay between incorporation and GTP hydrolysis by β-tubulin, an extended region enriched in GTP-tubulin subunits, termed the GTP cap (Figure 1A), forms at MT ends. The GTP cap protects MTs from depolymerization (Brouhard and Rice, 2018; Desai and Mitchison, 1997). Below the cap, tubulin dimers are in the GDP state (Hyman et al., 1995), which has a destabilizing effect on the MT lattice, and if the cap is lost, MT undergoes a catastrophe and starts shrinking (Mitchison and Kirschner, 1984). Reformation of the GTP cap on a depolymerizing MT promotes switching back to growth, known as rescue (Seetapun et al., 2012; Vemu et al., 2018; Aumeier et al., 2016; Dimitrov et al., 2008).

Many MT-associated proteins (MAPs) interact with MT ends directly or indirectly. MAPs can promote MT growth (MT polymerases), MT disassembly (MT depolymerases), or regulate transitions between growth and shortening; they can cooperate and compete with each other and collectively control MT dynamics (Brouhard and Rice, 2018; Akhmanova and Steinmetz, 2008). An important group of MAPs are MT plus end tracking proteins (+TIPs). +TIPs are structurally and functionally diverse proteins, which specifically accumulate at growing MT ends and fulfil various functions related to different aspects of cell activity (Jiang and Akhmanova, 2011; Akhmanova and Steinmetz, 2008). End binding proteins (EBs) are at the core of +TIP network, because they can autonomously recognize growing MT ends and recruit to them numerous additional proteins with various functions (Jiang et al., 2012; Honnappa et al., 2009).

1.2 MT minus ends

MT organization strongly depends on the arrangement of MT minus ends. Compared to the growing complexity of the protein machinery regulating MT plus ends, the work on minus end regulators has been for a long time dominated by one major player: γ-tubulin ring complex (γ-TuRC). In animal cells, γ-TuRC is often concentrated at centrosomes, which represent major MT organizing centers (MTOCs). However, it is becoming increasingly clear that even in dividing mammalian cells, various non-centrosomal MTOCs, which depend on specific MT minus-end binding proteins, play very important roles in MT organization. For example, in mitotic cells, MTs can be nucleated from spindle MTs (Petry et al., 2013) and kinetochores (Maiato et al., 2004), whereas in interphase, the Golgi apparatus (Chabin-brion et al., 2001; Efimov et al., 2007; Miller et al., 2009; Rivero et al., 2009) and the nuclear envelope (Tassin et al., 1985; Sun et al., 2019) can strongly participate in MT minus-end organization.

The Golgi apparatus has recently emerged as a major MTOC for non-centrosomal MTs in animal cells (Sanders and Kaverina, 2015; Petry and Vale, 2015; Martin and Akhmanova, 2018). Unlike centrosomal MTs, Golgi MTs are organized asymmetrically, and can thus enable polarized trafficking, Golgi reorientation, cell polarity and cell migration, and are particularly important for cell movement in 3D matrix (Efimov et al., 2007; Wu et al., 2016; Martin et al., 2018; Miller et al., 2009; Yang et al., 2017). In addition to γ-TuRC, recent work has shown that Calmodulin-regulated spectrin-associated proteins (CAMSAPs) in mammals and their homologs Patronins in invertebrates, are the key players to regulate non-centrosomal MTs in interphase cells, including the Golgi-derived ones (Jiang et al., 2014; Tanaka et al., 2012; Meng et al., 2008; Wu et al., 2016; Martin et al., 2018). A highly conserved domain of CAMSAPs, CKK, specifically recognizes MT minus ends by binding to the site between two tubulin dimers at the interprotofilament interface on the outer MT surface (Atherton et al., 2017).

MTOC activity can be separated into two distinct steps: nucleation and anchoring. Centrosomes and Golgi membranes can nucleate and anchor MT (Petry and Vale, 2015; Martin and Akhmanova, 2018). At the centrosome, γ-TuRC is recruited by pericentriolar material (PCM) components, such as Pericentrin (Zimmerman et al., 2004), AKAP450 (also known as CGNAP or AKAP9)(Takahashi et al., 2002) and CDK5RAP2 (Fong et al., 2008). Other PCM proteins, like NEDD1(Haren et al., 2006) and Ninein (Delgehyr et al., 2005), are required for stabilizing and anchoring MTs. Centrosomes and Golgi share some common factors involved in the MT nucleation pathways. On the Golgi membranes, two homologous proteins, myomegalin (MMG) and CDK5RAP2, cooperate with AKAP450 to recruit γ-TuRC and nucleate MT. In addition to MT nucleation, Golgi membranes can also anchor CAMSAP2-decorated MTs though the interaction with AKAP450 and MMG (Wu et al., 2016). Other MT-binding proteins, such as CLASP1/2 (Efimov et al., 2007; Miller et al., 2009) and MTCL, which interacts with AKAP450 and CLASPs (Sato et al., 2014), contribute to MT nucleation and/or anchoring at the Golgi.

1.3 +TIPs: EBs and their structure

Whereas the diversity of mechanisms underlying the regulation of MT minus ends started to emerge only recently (Martin and Akhmanova, 2018; Strothman et al., 2019), the factors controlling MT plus ends have received a lot of attention in the past 20 years. End binding proteins (EBs) are the key regulators of MT plus-end interactome, which consists of numerous structurally and functionally diverse proteins that accumulate at MT plus ends and regulate various aspects of cell activity (Akhmanova and Steinmetz, 2015; Van De Willige et al., 2016). EBs are encoded by evolutionarily conserved genes designed MT-associated protein RP/EB family members (MAPREs) (Su and Qi, 2001). They were initially discovered through the interaction with the tumor suppressor protein Adenomatous Polyposis Coli (APC)(Su et al.,

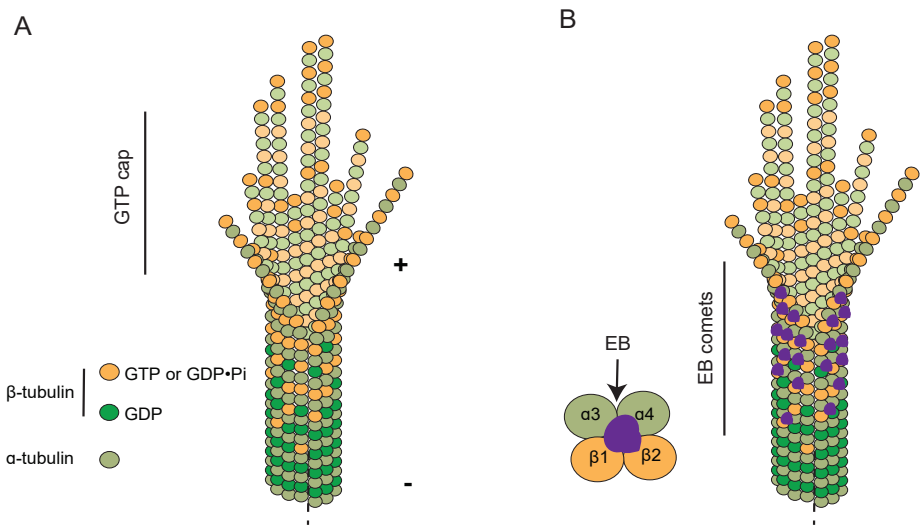

Figure 1. GTP cap and EB comets at growing MT plus ends.

A. MTs are polymers of α- and β-tubulin dimers organized in a head-to-tail fashion. β-tubulin can hydrolyze GTP and can exist in three different nucleotide states, GTP, GDP·Pi and GDP. GTP and/or GDP-Pi bound β-tubulin subunits form a stabilizing GTP cap at growing MT ends.

B. EBs form comet-like accumulations at growing MT plus ends. The CH domain of EB binds at the vertex of four tubulin dimers between the protofilaments, except the seam.

1995), but the subsequent work showed that they accumulate at MT plus ends independently of APC (Morrison et al., 1998; Mimori-Kiyosue et al., 2000). EBs are highly conserved from yeast to human; their homologs in the worm Caenorhabditis elegans are named ebp-1, ebp-2 and ebp-3, and yeast counterparts are named Bim1 in Saccharomyces cerevisiae, and Mal3 in Schizosaccharomyces pombe (Tirnauer and Bierer, 2000).

EBs are composed of a highly conserved N-terminal Calponin Homology (CH) domain, which is related to the CH domains that are found in actin-binding proteins (Gimona et al., 2002). In the EBs, the CH domain is followed by a flexible and unstructured linker region and a C-terminal coiled-coil domain, which overlaps with the end-binding homology (EBH) domain, and terminates with a flexible tail, that contains the EEY/F sequence motif. Similar C-terminal acidic-aromatic motifs are also found in α-tubulin and CLIP170 (Slep and Vale, 2007; Akhmanova and Steinmetz, 2008).

The CH domain is necessary and sufficient for MT binding (Komarova et al., 2009). Structural analysis showed that the CH domain of the EBs binds at the vertex of four tubulin dimers between the protofilaments, except the seam (Figure 1B) (Maurer et al., 2012). This binding site is the same as the site recognized by the MT-binding protein Doublecortin (DCX), although some important mechanistic details are different, because the EBs but not DCX bind to MTs in nucleotide-specific manner (Fourniol et al., 2010; Bechstedt et al., 2014; Maurer et al., 2012). The binding of CH domain to an extended conformation of MT lattice promotes its compaction and twist, and leads to seam closure and GTP hydrolysis (Zhang et al., 2015, 2018). However, these effects vary dependent on the origin of EBs and tubulin (e.g. human versus yeast) (Howes et al., 2017; Von Loeffelholz et al., 2017; Maurer et al., 2012), the presence of different nucleotides or GTP analogs (GDP, GMPCPP or GTPγS) (Zhang et al., 2015, 2018), as well as the presence of EBs during MT polymerization (Zhang et al., 2018). Importantly, the currently available data were all collected with monomeric CH domains. However the EBs are

constitutive dimers in vitro and in vivo (Komarova et al., 2009; De Groot et al., 2010), and it is currently unclear whether and how the dimerization would affect the EB specificity and the structure of MT lattice (Honnappa et al., 2005; Von Loeffelholz et al., 2017; Roth et al., 2018).
The linker region of EBs contributes to the MT plus-end specific accumulation (Des Georges et al., 2008; Komarova et al., 2009; Buey et al., 2011), and this property is controlled by phosphorylation. Multiple sites in the linker regions of EBs can be phosphorylated, because they are enriched in serines, threonines and tyrosines. For example, yeast EB1, Bim1, is regulated by the Aurora B/lpl1p kinase, which phosphorylates a cluster of six serine residues and affects Bim1 dimerization and its tip-tracking activity (Zimniak et al., 2009). Phosphorylation of EBs is extensively regulated during the cell cycle. For example, the phosphorylation of Ser-176 by Aurora A and Aurora B can stabilize EB3 during mitosis by blocking EB3 ubiquitylation by the ubiquitin protein isopeptide ligase SIAH-1 (Ban et al., 2009).
The negatively charged C terminal coil-coil domain is responsible for EB dimerization (Honnappa et al., 2005; De Groot et al., 2010), and it also affects specific accumulation of the EBs at MT plus ends (Buey et al., 2011). Another major function of this domain is the recruitment of protein partners to MT tips (Honnappa et al., 2009; Jiang et al., 2012). EB partners can be divided into two groups. One group is represented by numerous structurally and functionally diverse proteins containing an SxIP motif (Honnappa et al., 2009; Jiang et al., 2012). Structural analysis showed that a hydrophobic cavity of the highly conserved EBH domain is responsible for the interaction (Honnappa et al., 2009, 2005). Another group of EB partners comprises proteins with a CAP-Gly domain, including CLIP170 (a plus end recruitment factor for cytoplasmic dynein), CLIP115 and p150Glued (the large subunit of the dynein-associated complex dynactin), which all interact with C-terminal EEY tail of EBs (Komarova et al., 2005; Dixit et al., 2009). The two groups of partners can both cooperate and compete with each other for the limited space at growing MT plus ends (Duellberg et al., 2014; Honnappa et al., 2009; van der Vaart et al., 2011). In vitro work has shown that the two groups of partners can display a hierarchy: CLIP170 could displace SxIP ligands, which showed lower affinity, and this resulted in the accumulation of dynein and dynactin at MT plus ends (Duellberg et al., 2014). These in vitro observations reflect the in vivo situation where CLIP170 promotes efficient accumulation of dynein and dynactin at MT plus ends (Lansbergen et al., 2004).
In addition, it has been suggested that EBs can be autoinhibited, through the direct binding of their C-terminus to the N-terminus (Kanaba et al., 2013), and this auto-inhibition could be released by GTP or partner binding (Hayashi et al., 2005; Gireesh et al., 2018). The importance of this mechanism requires further investigation.

1.4 MT dynamics and EBs

MTs grow and shrink by adding or removing tubulin subunits from their ends, and the description of this process is usually focused on the fast growing plus ends rather than the slow growing minus ends (Akhmanova and Steinmetz, 2015; Martin and Akhmanova, 2018). MTs display dynamic instability – spontaneous switching between phases of growth and shortening. It is thought that dynamic instability is driven by GTP hydrolysis on tubulin: the chemical state of the tubulin-bound nucleotide (GTP or GDP) determines the rate of tubulin addition and removal (Bergen and Borisy, 1980; Margolis and Wilson, 1978; Wegner, 1976; Surrey et al., 2006). At growing MT ends, due to the GTPase activity of tubulin, GTP is converted to GDP-Pi, and then Pi is released leaving behind GDP-bound tubulin (Mitchison and Kirschner, 1984; Roostalu and Surrey, 2017). The presence of GTP-tubulin promotes formation of lateral interactions between tubulin dimers (Jánosi et al., 1998; VanBuren et al., 2002; Nawrotek et al., 2011). Because of the delay between tubulin incorporation and GTP hydrolysis, a cap of GTP-bound

tubulin subunits forms at the plus end, stabilizing the growing MT (Desai and Mitchison, 1997; Maurer et al., 2012). Formation of the GTP cap is central for explaining MT dynamics (Caplow and Shanks, 1996; Desai and Mitchison, 1997; Seetapun et al., 2012). However, the exact properties of the GTP cap are unknown because the GTP in the growing MT end region cannot be directly visualized (Brouhard and Rice, 2018; Seetapun et al., 2012). Furthermore, although it is generally thought that nucleotide exchange takes place on free tubulin, recently it was proposed that the exchange of GDP to GTP at the MT ends can contribute to the formation of GTP cap and catastrophe suppression (Piedra et al., 2016).

EBs track growing MT ends and form 0.5-2 μm long comet-like structures at such ends (Komarova et al., 2009; Bieling et al., 2007). Within these comets, EBs exchange rapidly with the cytosolic pool, and dissociate when a MT switches to depolymerization (Dragestein et al., 2008; Mimori-Kiyosue et al., 2000). Detailed imaging demonstrated that the comet region does not extend all the way to the very end of a growing MT, in contrast to the localization of another MT tip-tracking protein, XMAP215/chTOG. Instead, an EB comet is positioned several tens of nanometers behind the accumulation of XMAP215, which labels the outermost MT ends (Maurer et al., 2014). Cryo-electron tomography imaging showed that EBs interact with the outer surface of the curved and straight tubulin sheets as well as closed regions of the MT lattice (Guesdon et al., 2016). Detailed structural analysis revealed that the CH domain of EB binds to the vertex of four tubulin dimers (Maurer et al., 2012). By binding close to the exchangeable GTP-binding site on β-tubulin, the CH domain is ideally positioned to sense the nucleotide state of tubulin (Maurer et al., 2012; Zhang et al., 2015; Von Loeffelholz et al., 2017). To analyze nucleotide preference of EBs, GMPCPP, GTPγS and GDP-BeF3-bound MTs were used to represent the GTP and GDP-Pi state of tubulin, respectively (Maurer et al., 2011;Zanic et al., 2009). It was found that EBs bind to MTs in the presence of GTPγS or GDP-BeF3-, which are reminiscent of the GDP-Pi nucleotide state and promote the transition from GDP-Pi to GDP state (Zhang et al., 2015, 2018). However, it is still unclear how exactly the structures of MTs bound to GMPCPP and GTPγS relate to GTP and GDP-bound MT lattices, and how the tubulin dimers with different nucleotide states are distributed within the GTP cap.

Multiple structural states at MT ends have been observed, including partially curved sheet-like structures (Vitre et al., 2008; Guesdon et al., 2016) and fully curved separated protofilaments (McIntosh et al., 2018). To investigate how EB comets relate to MT stability with a high spatial and temporal solution, the microfluidics-assisted Total Internal Reflection Fluorescence (TIRF) microscopy assay was deployed. This assay showed that the stabilizing caps are formed by the extended EB-binding regions of EB comets, and a short region at the end of the cap can trigger MT depolymerization if the density of EB-binding sites in this region is low. The cap size can vary at a particular growth speed, and fluctuations in MT growth speed correlate with the fluctuations in the EB comets size. At higher EB concentrations, EB comets become shorter and catastrophe frequency is increased, which suggests EB binding promotes GTP hydrolysis (Duellberg et al., 2016; Rickman et al., 2017).

Another emerging concept that helps to explain MT dynamic instability is MT plasticity, which regards MT lattice as a continuous stiff material under tension (VanBuren et al., 2002; Kueh and Mitchison, 2009; Schaedel et al., 2015; Cross, 2019). At the heart of the MT plasticity view is the tubulin conformational cycle: curved, straight expanded and compacted (and/or twisted) (Manka and Moores, 2018; Brouhard and Rice, 2018). At growing MT ends, soluble curved GTP-tubulin is first incorporated into the straight tubulin lattice and then compacted (McIntosh et al., 2018). GTP-tubulin is thought to be more flexible than GDP-tubulin. Tubulin gains flexibility upon GTP binding, but the binding itself does not force GTP-tubulin to adopt the straight MT-like conformation (Igaev and Grubmüller, 2018). A loop movement in GTP-bound tubulin favors

its recruitment to the ends of growing MT, promotes its curved-to-straight transition, which occurs as MT specific contacts between tubulin dimers are established (Nawrotek et al., 2011), and this conformation transition affects MT dynamics (Geyer et al., 2015).

EBs bind tightly to both straight and curved regions of growing MT tips, and more weakly to the straight GDP-MT lattice. As already mentioned above, at growing MT tips, their binding leads to the loss of their own high-affinity binding sites (Maurer et al., 2014; Duellberg et al., 2016). Structural analysis showed that EBs facilitate the transition of longitudinally expanded tubulin to a compacted conformation, and from 14-protofilament MTs to 13-protofilament ones, as well as tubulin sheet closure into a tube (Vitre et al., 2008; Zhang et al., 2015, 2018).

To visualize the mechanical force acting during MT polymerization, optical tweezers or beads were applied in reconstitution experiments. It was shown that applying tension to a growing MT via a bead promotes rapid MT growth (Akiyoshi et al., 2010), while a shrinking MT can push a bead (Driver et al., 2017). Such mechanical forces generated during MT depolymerization play key roles when MTs segregate chromosome during cell division.

The concept of MT plasticity can help to explain MT catastrophes and rescues. In this view, the compacted GDP-tubulin in the MT lattice tends to adopt an outwardly curved conformation when MTs depolymerize, causing mechanical stress to accumulate in the MT lattice, because protofilaments are trapped in the straight configuration by interactions with their neighbors (Geyer et al., 2015; Driver et al., 2017; Memet et al., 2018; VanBuren et al., 2002). Defects accumulate between protofilaments at the ends or within a MT, allowing protofilaments to peel apart and curl outward, releasing the stored energy of GTP hydrolysis (Hemmat et al., 2018; Kueh and Mitchison, 2009; Driver et al., 2017).

An interesting example of MT lattice plasticity is provided by MT bending assays. MTs bent by hydrodynamic flow display increasing softening after each bending cycle, and the MT stiffness can be restored by incorporating new tubulin dimers into the MT lattice (Schaedel et al., 2015). The newly incorporated tubulin dimers can accumulate at the mechanical defect sites and form areas enriched in GTP-bound tubulin. Such “GTP-islands” are important for MT self-repair in cells and in vitro (Aumeier et al., 2016). Interestingly, EBs are recruited to GTP-islands and might participate in repairing MT defects (Aumeier et al., 2016; Vemu et al., 2018). Cells can protect their MT from bending-induced lattice damage by acetylation, which makes MTs more resistant to bending-induced breakage (Xu et al., 2018; Portran et al., 2017). In addition, motor proteins such as kinesins may also play a role in modulating MT lattices. It was shown that the binding of kinesin-1 can change the conformation of GDP MTs to a conformation resembling that of GTP MTs, and this change promotes further kinesin-1 binding (Shima et al., 2018). Kinesin binding may also affect EB binding as there are overlaps between the binding sites (Zhang et al., 2015, 2018).

As mentioned above, structural conformational transitions in tubulin are often accompanied by biochemical transitions, and vice versa. Therefore, the combined mechanochemical view is believed to better and more accurately describe the structural complexity associated with MT dynamic instability (Manka and Moores, 2018; Peet et al., 2018; Brouhard and Rice, 2018). At MT plus ends, a mixture GTP and GDP-bound tubulin is present. For example, a GTP-bound tubulin subunit, which favors expanded conformation, can be compacted by its neighboring GDP-bound tubulin in the MT lattice. This mismatch would result in the stress for the neighboring GDP-bound tubulin, forcing it to expand. The compacted or expanded conformation could be propagated to more distant subunits in the MT lattice. Such long-range mechanical coupling mechanism would make the conformation of an individual tubulin dimer to be determined not only by its nucleotide state but also by long-range interactions with other subunits in the lattice. And such conformational coupling effects could enforce or modulate

each other, resulting in a highly cooperative structure capable of abrupt transitions. This view can explain how EBs promote GTP hydrolysis by tubulin at MT plus ends: Even if EBs bind to a post-GTPase tubulin state, through long-range coupling mechanism, the effects of their binding could be transferred to the outermost tips where they would facilitate GTP hydrolysis (Maurer et al., 2014; Brouhard and Rice, 2018). A long-range coupling mechanism can also be applied to explain how EBs synergize with ch-TOG/XMAP215 to accelerate MT growth (Zanic et al., 2013; Brouhard and Rice, 2018).

1.5 The function of EB family proteins

EBs are highly conserved proteins in animals, plants and fungi (Slep et al., 2005; Skube et al., 2010). In mammalian cells, the EB family includes three members: EB1, EB2 (RP1) and EB3 (Figure 2) (Komarova et al., 2009; Skube et al., 2010; Roth et al., 2018). In HeLa cells, EB1 is the most abundant family member, followed by EB3 and EB2 (Liu et al., 2019; Itzhak et al., 2016). EB1, EB2 and EB3 can compete for the binding sites at the MT plus ends. Results in cells showed that after the depletion of EB1 or EB1 and EB3 together, EB2 can replace EB1 at the very end of the MT, followed by EB3 (Komarova et al., 2009; Yang et al., 2017; Roth et al., 2018). In vitro experiments showed that EB1 and EB3 distribute in a similar region relative to MT tip, but EB2 locates further behind the MT tip (Roth et al., 2018). EBs constitutively dimerize through a thermodynamically stable coiled-coil domain in the C-terminal part of the protein (Honnappa et al., 2005; Slep et al., 2005; Slep and Vale, 2007; Buey et al., 2011). However, EB1 and EB3 are kinetically unstable and efficiently form heterodimers, while EB2 preferentially forms a homodimer (Komarova et al., 2009; De Groot et al., 2010).

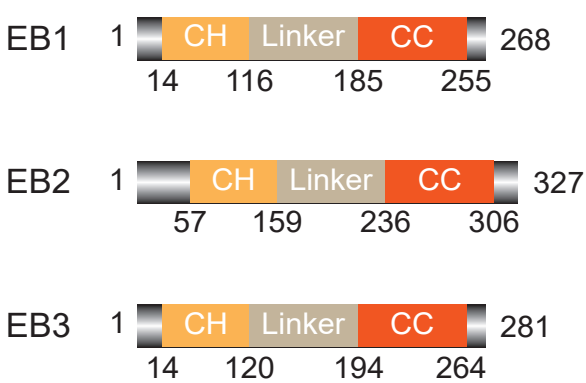

Figure 2. Scheme of mammalian EB family members. The schemes show human EB1, EB2 and EB3, with the amino acid positions of the domain boundaries indicated.

Sequence alignment showed that EB2 N-terminus differs from EB1 and EB3 including the presence of a 42 amino acid extension and several substitutions in the CH domain. These differences have a great impact on EB2 activity. EB1 and EB3 promote persistent MT growth by suppress catastrophe, whereas EB2 lacks this activity. This difference is not due to the N-terminal 42 amino acid-long extension, but rather to the substitutions in the N-terminal part of the CH domain. Chimeric constructs showed that fusing the EB2-specific extension to EB3 does not prevent EB3 from suppressing catastrophes, while swapping 29 amino acids of EB2 to EB3 in the N-terminal part of the CH domain inhibits the ability of EB3 to suppress catastrophes (Komarova et al., 2009).

Structural analysis revealed that the CH domains of EB1 and EB3 are very similar to each other,

with few substitutions that do not affect MT binding. Therefore, EB1 and EB3 are generally considered equivalent in their ability to track MT tips and regulate MT dynamics. However, the modeled EB2 CH domain structure is different from their EB1 and EB3 counterparts, with most divergent residues found around the conserved sequence segment 16-SRHD-19, which is critical for MT binding (Komarova et al., 2009). Several reports also suggested that the C-terminal part of EB2, particularly the EBH domain, also strongly deviates from its EB1 and EB3 counterparts. EB1 and EB3 are generally thought to have similar binding affinities to partners, including the CAP-Gly partner CLIP170 and the SxIP partner CLASP, whereas EB2 has a low affinity for these proteins (Schrøder et al., 2011; Yang et al., 2017; Komarova et al., 2005; Leterrier et al., 2011; Arens et al., 2013).

EBs are also differentially regulated to exert diverse functions, particularly in differentiated cell types, including neurons and muscle cells. EB3 is specifically upregulated during neuronal development and myogenic differentiation (Straube and Merdes, 2007; Jaworski et al., 2009). Though EB1 and EB3 are quite similar with respect to interactions with their partners, small differences within the partner binding sites can make them favor some specific flanking sequences of SxIP motif of the partners (Lesniewska et al., 2014; Jiang et al., 2012). Viruses can manipulate EBs to infect cells (Naghavi and Walsh, 2017; Jovasevic et al., 2015), and they can make full use of these small differences. Human cytomegalovirus (HCMV) specifically recruits EB3, but not EB1 or EB2, to its assembly compartment to promote formation of Golgi-derived MTs (Procter et al., 2018). SxIP-containing aptamers specifically binding EB3 due to variations in their SxIP flanking amino acid sequence can be applied to control viral infection, showing that targeting EB3 might have therapeutic potential (Procter et al., 2018).

EB1 has also been implicated in disease. Many cancers, including breast (Xin et al., 2010; Luo et al., 2014) and colon cancer (Islam et al., 2018; Sugihara et al., 2012) as well as hepatocellular carcinoma (Orimo et al., 2008) and glioblastoma (Rovini et al., 2013; Berges et al., 2016) overexpress EB1 instead of EB3, though it is currently unclear what role EB1 plays in these cancers. Importantly, MT targeting agents (MTAs) are widely used for cancer treatment. The effects of MT targeting agents on MTs can be modulated by EBs, which sensitize MTs to the action of MTAs (Mohan et al., 2013). EBs are also required for tumor invasion and metastasis. Knockout cells lacking EB1, EB2 and EB3 showed migration defects in both 2D and 3D matrices (this this thesis, Yang et al., 2017). Furthermore, an optogenetic assay clearly showed that EBs can regulate subcellular MT dynamics and affect cancer cell migration (Van Haren et al., 2018). Mechanistic studies revealed that EB1 recruits +TIPs to coordinate protrusion dynamics (Gierke and Wittmann, 2012), and further work showed that the EB-dependent +TIPs, SLAIN2 and CLASP1, are essential for mesenchymal cell morphogenesis and migration in soft 3D matrices, because they can suppress catastrophe and support persistent MT growth (Bouchet et al., 2016b). EBs and their partners thus represent potentially promising targets for inhibiting metastasis.

1.6 EBs and +TIP network

EBs orchestrate other MT plus end tracking proteins (+TIP) to modulate MT dynamics. Numerous structurally and functionally diverse proteins can accumulate at MT plus ends by directly or indirectly interacting with EBs. The ones that directly interact with EBs can be classified into two main groups: the CAP-Gly proteins, which contain globular CAP-Gly domains and include CLIP170 and CLIP115, and the SxIP proteins, such as CLASPs and SLAIN2, which contain linear SxIP motifs embedded in unstructured polypeptide regions (Honnappa et al., 2009). chTOG/XMAP215 represent MT regulators that interact with EBs indirectly (Figure 3).

The CAP-Gly group is featured by containing cytoskeleton-associated protein Gly-rich (CAP-

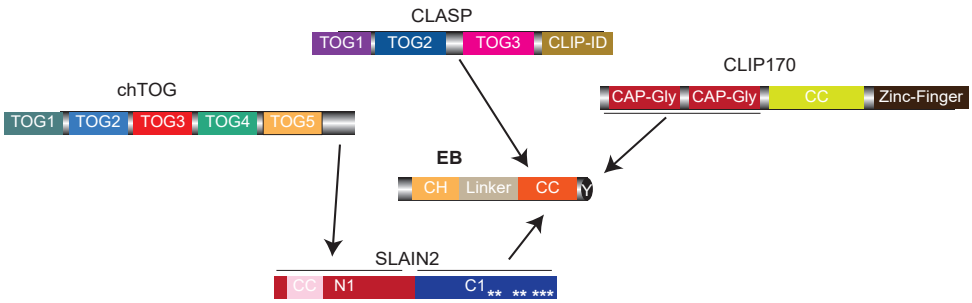

Figure 3. A scheme of the domain organization of EB, SLAIN2, chTOG, CLASP and CLIP170 and their interactions.

Gly) domains. It contains two cytoplasmic linker proteins (CLIPs), CLIP170 and CLIP115, and the structurally related large subunit of dynactin complex, p150Glued (reviewed in Akhmanova and Steinmetz, 2008). CLIP170 contains two tandemly arranged CAP-Gly domains, which interact with the C-terminal EEY/F sequence motifs, found in EBs and α-tubulin as well as its own C terminus. The C-terminal part of CLIP170 is the cargo-binding domain, which comprises two zinc knuckle domains and terminates with EEY motif that can mediate CLIP170 autoinhibition by interacting with the N-terminal CAP-Gly domains in the same molecule (Lansbergen et al., 2004; Weisbrich et al., 2007).

CLIP170 was originally described as the linker between MTs and endocytic vesicles, although this function was not confirmed in subsequent studies; it plays a role in trafficking and cell migration (Pierre et al., 1992; Zaoui et al., 2019). Because the CAP-Gly domains can interact with the C-terminal tails of EBs and α-tubulin, CLIP170 can bind to MTs and is enriched at growing MT plus ends (Bieling et al., 2008; Diamantopoulos et al., 1999; Komarova et al., 2005). When bound to MTs, CLIP-170 can recruit other factors, including the dynein-dynactin complex, which drives MT minus end-directed cargo transport (Lansbergen et al., 2004).

CLASPs were identified as CLIP-associated proteins that track growing MT plus ends by binding to the coiled coil region of CLIPs (Akhmanova et al., 2001) or targeting EBs though the SxIP motif (Mimori-Kiyosue et al., 2005). CLASPs are highly conserved from lower eukaryotes to plants and humans (Young and Bisgrove, 2011; Al-Bassam and Chang, 2011), and they are among the most abundant SxIP containing EB partners. CLASPs are important regulators of MT dynamics. In vitro experiments showed that they can suppress MT catastrophes and induce rescues without significantly affecting the rate of MT growth and shrinkage, and these effects on MT dynamics are enhanced when EBs are present (Aher et al., 2018; Lawrence et al., 2018; Lawrence and Zanic, 2019). In cells, CLASPs promote MT rescue, particularly at the cell periphery, where they participate in the formation of the cortical MT stabilizing complexes (CMSCs). These multiprotein assemblies is linked to focal adhesions (FA) by the CMSC component KANK1, which interacts with the integrin-binding protein Talin (Lansbergen et al., 2006; Kumar et al., 2009; van der Vaart et al., 2013; Bouchet et al., 2016a). In addition, CLASPs also play essential roles in regulating spindle MT dynamics, particularly in the formation and stabilization of kinetochore MTs (Maiato et al., 2005; Bratman and Chang, 2007).

Human CLASPs contain three tumor overexpressed gene-like (TOG) domains, and between the second and third TOG domains there are two SxIP motifs, which interact with EBs. CLASPs are autoinhibited, and TOG1 domain can release the autoinhibition by interacting with the CLASP C-terminus. TOG2 is necessary and sufficient for catastrophe suppression. When targeted to MT plus ends, TOG2 is sufficient to stabilize incomplete or damaged MT tips, thereby enabling their restoration to promote processive MT growth. TOG3 mildly promotes rescues but does

not inhibit catastrophes (Aher et al., 2018). The C-terminal domain of CLASPs (termed CLIP-ID for CLIP-interacting domain) can interact with CLIP-170 and SLAIN2 (Akhmanova et al., 2001; Liu et al., 2017). In vitro experiments showed that the autoinhibitory activity of CLIP-ID on TOG2 and TOG3 can be relieved by TOG1 or other partners, such as CLIPs (Aher et al., 2018).
Though we have a clear idea of how single CLASP domains determine its activities, we lack the structural understanding of CLASP effects on the conformational transitions in MT lattices. TOG domains are known for their ability to bind to free tubulin (Leano et al., 2013), and it has been proposed that CLASPs act like MT polymerases, such as chTOG, by promoting the recruitment of tubulin dimers (Al-Bassam et al., 2010; Yu et al., 2016). However, it appears that TOG domains of CLASPs cannot bind to free tubulin (Aher et al., 2018). X-ray crystallography showed that the second and the third TOG domain of human CLASP have distinct curvatures at the tubulin-binding interface, and they can bind to taxol-stabilized MTs, but cannot interact with unpolymerized tubulin dimers. It was implied that there is a conformational change either in TOG2 or tubulin dimers upon their binding (Leano et al., 2013), but this idea has not been proven. Since CLASPs do not accelerate MT polymerization but instead stabilize incomplete MT tip structures, it is possible that their TOG domains interact with specific tubulin arrangements at MT tips (Aher et al., 2018; Maki et al., 2015).
SLAIN2 is a protein that can interact with CLASPs, CLIP170 as well as EBs. The SLAIN family has two members: SLAIN1 and SLAIN2, and they are highly conserved in vertebrates. SLAIN proteins are named after an amino acid stretch in the C terminus of SLAIN1 that reads “SLAIN”, although SLAIN2 does not share these amino acids (Hirst et al., 2006). They have a coiled-coil domain at the N terminus, which is responsible for dimerization, followed by an intrinsically disordered region (IDR), which is enriched in serines, prolines and basic residues. SLAINs terminate with a tyrosine, which is critical for CLIP170 interaction, similar to the C-terminal aromatic residues found in EBs, α-tubulin and CLIP170 (van der Vaart et al., 2011).
It was demonstrated that the N-terminal half of SLAIN2 can interact with chTOG, and the C-terminal half can interact with CLASPs and EBs. The C-terminal part of SLAIN2 contains four SxIP and three SxIP-like motifs, which were reported to participate in the interaction with EBs. SLAIN2 contributes to the accumulation of both chTOG and EBs at MT tips: it was proposed to link chTOG and EBs to promote persistent MT growth (van der Vaart et al., 2011). Similar to the adaptor function of SLAIN2, Sentin is an EB1 dependent +TIP in Drosophila, which promotes the accumulation of Msps, the orthologue of chTOG, at MT tips (Li et al., 2012b).
SLAIN2 is an important regulator of MT dynamics. It was shown that SLAIN2 suppresses catastrophes and promotes persistent MT growth, and SLAIN2 depletion leads to shorter EB comets and affects the radial MT organization (van der Vaart et al., 2011). It was suggested that SLAIN2 depletion may affect MT nucleation, as there are less EB comets, representing growing MT ends, in SLAIN2 depleted cells (van der Vaart et al., 2011). Though SLAIN2 depletion does not significantly affect 2D cell migration on hard substrates, it is important for cell movement in soft 3D matrices and tumor invasion in a mouse model (Bouchet et al., 2016b). In addition, SLAIN2 was also suggested to be important for neuronal development (van der Vaart et al., 2012).
chTOG (colonic and hepatic tumor-overexpressed gene), which is also known as cytoskeleton associated protein 5 (CKAP5), is a protein that can target both growing and shortening MT plus ends independently of EBs. Though chTOG cannot directly interact with EBs, the two proteins can be linked by SLAIN2 (van der Vaart et al., 2011). chTOG is the human homologue of XMAP215, a MT-associated protein (MAP) with a molecular weight of 215 kD that was found and characterized in Xenopus egg extracts (Charrasse et al., 1995, 1998). chTOG belongs to the protein family, which is highly conserved in animals, plants and fungi (Gard et al., 2004; Young

and Bisgrove, 2011). Members of this family accumulate at MT tips and act as MT polymerases (Brouhard et al., 2008). They contain several tumor-overexpressed gene (TOG) domains, which bind to tubulin or MTs (Al-Bassam et al., 2007; Widlund et al., 2011). The C terminal domain (CTD) of chTOG/XMAP215 has a low affinity for MTs, and it was predicted that it contains an additional TOG domain (Hood et al., 2013). It was shown that CTD of chTOG/XMAP215 is important for partner interactions, including SLAIN2 (van der Vaart et al., 2011), γ-TuRC (Thawani et al., 2018) and TACC3 (Hood et al., 2013). However, the molecular details of these interactions are still unclear.

chTOG is expressed at low levels in all cells, but is highly expressed in neurons and tumor cells (Charrasse et al., 1995; van der Vaart et al., 2012). Based on the number of TOG domains, XMAP215 homologs can be divided into 3 groups, and among them the human chTOG, Xenopus laevis XMAP215 and Drosophila melanogaster Msps belong to the higher eukaryotic group, which has five TOG domains (Al-Bassam et al., 2007). It is generally accepted that the arrangement of this pentameric TOG domain array is critical for the protein functions, including the association with free tubulin, tracking MT plus ends and polymerization. The structure of each TOG domain has a subtle specificity, by either binding to free or lattice incorporated tubulin dimers. Among the five TOG domains, TOG1 and TOG2 are critical for binding free tubulin (Slep and Vale, 2007; Widlund et al., 2011), and TOG3 is similar to TOG1 and TOG2, because it shares the same tubulin-binding mode (Howard et al., 2015). TOG4 has a unique architecture, similar to CLASP2 TOG3 (Byrnes and Slep, 2017), which is predicted to have a distinct engagement with tubulin (Fox et al., 2014), and TOG5 is critical for MT lattice binding (Byrnes and Slep, 2017). It is thought that the XMAP215/chTOG is positioned at MT plus end, where TOG1 and TOG2 domains recruit free αβ-tubulin dimers, and TOG3 and TOG4 might stabilize the newly formed protofilament tips, and TOG5 interacts with MT lattice. The CTD binds to partners (Zanic et al., 2013; Maurer et al., 2014; Akhmanova and Steinmetz, 2015; Thawani et al., 2018; Byrnes and Slep, 2017), resulting in specific localization, including the accumulation at growing MT plus ends by the interaction with the EB binding proteins SLAIN2/Sentin (Li et al., 2012b; van der Vaart et al., 2011), or centrosomal localization through interactions with γ-TuRC (Thawani et al., 2018) and TACC3 (Gergely et al., 2000, 2003; Hood et al., 2013).

It is still unclear how chTOG uses its specific TOG array to recognize both growing and shortening MT tips, and how exactly MT plus end tracking of this protein relates to its function as a MT polymerase. The polymerase activity depends on the N-terminal four to five TOG domains (Widlund et al., 2011; Thawani et al., 2018), and it was shown that TOG1, 2 and 5 are sufficient to fully rescue interphase MT polymerization rates in cells (Byrnes and Slep, 2017). Although chTOG cannot directly interact with EBs, the two proteins can synergistically increase MT polymerization rate to a physiological value (Zanic et al., 2013). chTOG also participates in MT nucleation (Roostalu and Surrey, 2017). This activity depends on the presence of other factors; for example, similar to CDK5RAP2 (Fong et al., 2008; Wang et al., 2010), chTOG can interact and cooperate with γ-TURC (Thawani et al., 2018).

When chTOG and its orthologs are depleted, cells display perturbed proliferation with reduced MT growth rate and shorter average MT length (van der Vaart et al., 2011). In mitotic and meiotic cells, chTOG depletion leads to downscaling of the spindle and centrosomal aster size (Cassimeris and Morabito, 2004);(Cullen and Ohkura, 2001). In addition, chTOG also plays a role in the regulation of MT assembly during neuronal development (van der Vaart et al., 2012).

1.7 Phase separation

Phase transition is a process whereby a substance switches from one physical state to another, for example from a liquid to solid state. Liquid-liquid phase separation (LLPS) occurs when a homogenous solution of molecules (such as biological polymers) separates into two liquid phases, a dense phase that has a high concentration of these molecules and a light phase that has a low concentration of these molecules (Kurimoto and Niiyama, 2016; Kulkarni and Rao, 2013). Liquid droplets or condensates formed by such phase separation can form distinct compartments, which subsequently can acquire different physical properties, e.g. become liquid, gel or a solid crystal. LLPS occurs widely in cells, leading, for example, to formation of classical membraneless organelles (Zeng et al., 2016; Brangwynne et al., 2009; Banani et al., 2016), signaling complexes (Su et al., 2016; Huang et al., 2019; Case et al., 2019) and cytoskeletal structures (Li et al., 2012a; Woodruff et al., 2017; Hernández-Vega et al., 2017).

The driving forces for the protein phase separation in vitro and in cells can be different, including temperature, salt concentration, pH, concentrations of binding partners, and the volume excluded by other macromolecules (Holehouse and Pappu, 2018; Alberti et al., 2019). It is believed that multivalent interactions provide an critical driving force for protein phase transitions (Li et al., 2012a; Holehouse and Pappu, 2018). There are many ways to form multivalent interactions, as shown for many high-resolution structures, where the molecular basis for multi-point interaction was investigated in detail. It is frequently found that many proteins undergoing phase separation contain IDRs, which can promote multivalent interactions. A specific subset of IDRs are low-complexity domains (LCDs), because they have a biased amino acid composition and/or are repetitive in sequence. It is believed that the IDR length, phosphorylation, the repeat number, patterning, etc, are factors that can affect protein phase separation (Holehouse and Pappu, 2018; Boeynaems et al., 2018), but the exact mechanism underlying IDR-mediated LLPS is still unclear.

Based on the physicochemical properties of participating molecules, a variety of possible functions associated with LLPS can be defined, including confinement of biochemical reactions ("filter and sequester"), signal amplification and force generation. LLPS can locally concentrate molecules in condensates to promote certain chemical reactions, signaling processes and nucleation of cytoskeletal structures, including actin filaments and MTs (Boeynaems et al., 2018; Alberti et al., 2019). For example, multivalent interactions with T cell receptors drive clustering of the downstream signaling proteins by phase separation at the membrane, and these protein clusters can efficiently promote actin polymerization (Su et al., 2016). Similarly, phase separation of centrosomal components can concentrate tubulin and promote MT polymerization. Centrosomes can be regarded as autocatalytic droplets of pericentriolar material organized by centrioles (Zwicker et al., 2014). An in vitro study showed that crowding agents drive the worm centrosomal scaffold protein SPD-5 to form condensates, which recruit tubulins and MT-binding proteins, TPXL-1 (TPX2 homolog) and ZYG-9 (XMAP215 homolog), and these molecules together can concentrate tubulin and promote MT nucleation and tubulin polymerization (Woodruff et al., 2017). Cytoplasm contains many neutral and relatively hydrophilic macromolecules that can act as crowding agents and effectively affect local protein concentration via the excluded volume effect (Breydo et al., 2014). However, quantitative characterization of such effects is still lacking, and it is unclear how protein phase separation participates in the nucleation of cytoskeletal filaments and their regulation in cells.

Protein phase separation is also implicated in many pathological conditions, including neurodegenerative disorders and cancers (Shin and Brangwynne, 2017; Boeynaems et al., 2018). For example, neurodegenerative diseases are closely associated with abnormalities in RNA-binding proteins, like the heterogeneous nuclear ribonucleoproteins (hnRNPs): hnRNPA1

and hnRNPA2B1, TDP-43 (Mann et al., 2019) and fused in sarcoma (FUS)(Burke et al., 2015), which contain distinctive IDRs. Disease mutations in IDRs can promote their phase separation and dramatically reduce their dynamics in cells (Kim et al., 2013; Patel et al., 2015; Molliex et al., 2015). In addition, phase separation is also been implicated in cancer (Kwon et al., 2013). The relationship between the propensity of certain proteins for phase separation and formation of pathological protein aggregates is subject of intense investigation.

Scope of the thesis

In Chapter 2, we used CRISPR/Cas9 technology to generate combined EB1, EB2 and EB3 mutant cell lines. Surprisingly, we found that the loss of all three EBs strongly affected MT minus-end organization and Golgi morphology, but had only a relatively mild effect on cell division and MT dynamics. In EB1 and EB3 mutated cell lines, CAMSAP2-positive MT minus ends were dispersed, and the Golgi apparatus compacted. Further study showed that the interaction of EB1/EB3 with myomegalin can tether CAMSAP2-decorated MT minus ends to the Golgi apparatus and counteract compacting of Golgi stacks. In addition, we found that the disruption of EB1 and EB3 also affected cell migration, intracellular trafficking and the distribution of focal adhesions.

In Chapter 3, we further investigated how EBs and their partners affect the properties of growing MT plus ends. To achieve this, we generated cells lines that completely lacked EB1, EB2 and EB3. We used these cells to compare EB comet length in vivo and in vitro and found that they depended on the EB protein used. We also applied MT severing and inducible protein heterodimerization assays to explore how EBs and their partners affect MT tip behavior.

In Chapter 4, we probed the possibility that SLAIN2, one of the EB-binding +TIPs, undergoes phase separation at MT ends. We found SLAIN2 can form droplets both in cells and in vitro. In cells, EBs and chTOG were recruited to the SLAIN2 droplets, whereas CLASPs and CLIP170 were not. In vitro, SLAIN2 and chTOG, but not EB3, could efficiently form droplets in the presence of crowding reagents. We further found that the presence of crowding reagents promotes spontaneous MT nucleation, but were unable to find conclusive evidence supporting formation of SLAIN2 condensates at MT tips.

In Chapter 5, we artificially targeted specific MT-binding domains to MT plus ends by fusing them to EBs and showed that they can exert very distinct effects on MT growth in vitro. The fusions of EB to SLAIN2 or the MT binding C-terminal peptide of spectraplakin had little effect on MT dynamics, whereas the EB fusions of the TOG domains of CLASP2 promoted persistent MT growth or rescue. All EB fusions of the TOG domain of chTOG induced catastrophes, whereas the EB fusions of the GAR domain of spectraplakin and the CAP-Gly domain of CLIP170 promoted rescues, and the EB fusion of the MT binding domain of MAP7 reduced MT depolymerization rate. We also tested the impact of these fusion proteins on MT dynamics in EB1, EB2 and EB3 triple knockout cells, but found that their effects could not be easily matched to those observed in vitro.

In Chapter 6, we discuss our findings and put them into perspective of the current scientific literature.

References

Aher, A., M. Kok, A. Sharma, A. Rai, N. Olieric, R. Rodriguez-Garcia, E.A. Katrukha, T. Weinert, V. Olieric, L.C. Kapitein, M.O. Steinmetz, M. Dogterom, and A. Akhmanova. 2018. CLASP Suppresses Microtubule Catastrophes through a Single TOG Domain. Dev. Cell. 46:40-58.e8. doi:10.1016/j.devcel.2018.05.032.

Akhmanova, A., and C.C. Hoogenraad. 2015. Microtubule minus-end-targeting proteins. Curr. Biol. 25:R162–R171. doi:10.1016/j.cub.2014.12.027.

Akhmanova, A., C.C. Hoogenraad, K. Drabek, T. Stepanova, B. Dortland, T. Verkerk, W. Vermeulen, B.M. Burgering, C.I. De Zeeuw, F. Grosveld, and N. Galjart. 2001. CLASPs are CLIP-115 and -170 associating proteins involved in the regional regulation of microtubule dynamics in motile fibroblasts. Cell. 104:923–935. doi:10.1016/S0092-8674(01)00288-4.

Akhmanova, A., and M.O. Steinmetz. 2008. Tracking the ends: a dynamic protein network controls the fate of microtubule tips. Nat. Rev. Mol. Cell Biol. 9:309–322. doi:10.1038/nrm2369.

Akhmanova, A., and M.O. Steinmetz. 2015. Control of microtubule organization and dynamics: two ends in the limelight. Nat. Rev. Mol. Cell Biol. 16:711–26. doi:10.1038/nrm4084.

Akiyoshi, B., K.K. Sarangapani, A.F. Powers, C.R. Nelson, S.L. Reichow, H. Arellano-Santoyo, T. Gonen, J.A. Ranish, C.L. Asbury, and S. Biggins. 2010. Tension directly stabilizes reconstituted kinetochore-microtubule attachments. Nature. 468:576–579. doi:10.1038/nature09594.

Al-Bassam, J., and F. Chang. 2011. Regulation of microtubule dynamics by TOG-domain proteins XMAP215/Dis1 and CLASP. Trends Cell Biol. 21:604–614. doi:10.1016/j.tcb.2011.06.007.

Al-Bassam, J., H. Kim, G. Brouhard, A. van Oijen, S.C. Harrison, and F. Chang. 2010. CLASP promotes microtubule rescue by recruiting tubulin dimers to the microtubule. Dev. Cell. 19:245–258. doi:10.1016/j.devcel.2010.07.016.

Al-Bassam, J., N.A. Larsen, A.A. Hyman, and S.C. Harrison. 2007. Crystal Structure of a TOG Domain: Conserved Features of XMAP215/Dis1-Family TOG Domains and Implications for Tubulin Binding. Structure. 15:355–362. doi:10.1016/j.str.2007.01.012.

Alberti, S., A. Gladfelter, and T. Mittag. 2019. Considerations and Challenges in Studying Liquid-Liquid Phase Separation and Biomolecular Condensates. Cell. 176:419–434. doi:10.1016/j.cell.2018.12.035.

Arens, J., T.T. Duong, and L. Dehmelt. 2013. A morphometric screen identifies specific roles for microtubule-regulating genes in neuronal development of P19 stem cells. PLoS One. 8. doi:10.1371/journal.pone.0079796.

Atherton, J., K. Jiang, M.M. Stangier, Y. Luo, S. Hua, K. Houben, J.J.E. Van Hooff, A.P. Joseph, G. Scarabelli, B.J. Grant, A.J. Roberts, M. Topf, M.O. Steinmetz, M. Baldus, C.A. Moores, and A. Akhmanova. 2017. A structural model for microtubule minus-end recognition and protection by CAMSAP proteins. Nat. Struct. Mol. Biol. 24:931–943. doi:10.1038/nsmb.3483.

Aumeier, C., L. Schaedel, J. Gaillard, K. John, L. Blanchoin, and M. Théry. 2016. Self-repair promotes microtubule rescue. Nat. Cell Biol. 18:1054–1064. doi:10.1038/ncb3406.

Ban, R., H. Matsuzaki, T. Akashi, G. Sakashita, H. Taniguchi, S.Y. Park, H. Tanaka, K. Furukawa, and T. Urano. 2009. Mitotic regulation of the stability of microtubule plus-end tracking protein EB3 by ubiquitin ligase SIAH-1 and aurora mitotic kinases. J. Biol. Chem. 284:28367–28381. doi:10.1074/jbc.M109.000273.

Banani, S.F., A.M. Rice, W.B. Peeples, Y. Lin, S. Jain, R. Parker, and M.K. Rosen. 2016. Compositional Control of Phase-Separated Cellular Bodies. Cell. 166:651–663. doi:10.1016/j.cell.2016.06.010.

Bechstedt, S., K. Lu, and G.J. Brouhard. 2014. Doublecortin recognizes the longitudinal curvature of the microtubule end and lattice. Curr. Biol. 24:2366–2375. doi:10.1016/j.cub.2014.08.039.

Bergen, L.G., and G.G. Borisy. 1980. Head-to-tail polymerization of microtubules in vitro. Electron microscope analysis of seeded assembly. J. Cell Biol. 84:141–150. doi:10.1083/jcb.84.1.141.

Berges, R., A. Tchoghandjian, S. Honore, M.-A. Esteve, D. Figarella-Branger, F. Bachmann, H.A. Lane, and D. Braguer. 2016. The Novel Tubulin-Binding Checkpoint Activator BAL101553 Inhibits EB1-Dependent Migration and Invasion and Promotes Differentiation of Glioblastoma Stem-like Cells. Mol. Cancer Ther. 15:2740–2749. doi:10.1158/1535-7163.mct-16-0252.

Bieling, P., S. Kandels-Lewis, I.A. Telley, J. Van Dijk, C. Janke, and T. Surrey. 2008. CLIP-170 tracks growing microtubule ends by dynamically recognizing composite EB1/tubulinbinding sites. J. Cell Biol. 183:1223–1233. doi:10.1083/jcb.200809190.

Bieling, P., L. Laan, H. Schek, E.L. Munteanu, L. Sandblad, M. Dogterom, D. Brunner, and T. Surrey. 2007. Reconstitution of a microtubule plus-end tracking system in vitro. Nature. 450:1100–1105. doi:10.1038/nature06386.

Boeynaems, S., S. Alberti, N.L. Fawzi, T. Mittag, M. Polymenidou, F. Rousseau, J. Schymkowitz, J. Shorter, B. Wolozin, L. Van Den Bosch, P. Tompa, and M. Fuxreiter. 2018. Protein Phase Separation: A New Phase in Cell Biology. Trends Cell Biol. 28:420–435. doi:10.1016/j.tcb.2018.02.004.

Bouchet, B.P., R.E. Gough, Y.C. Ammon, D. van de Willige, H. Post, G. Jacquemet, A.F. Maarten Altelaar, A.J.R.

Heck, B.T. Goult, and A. Akhmanova. 2016a. Talin-KANK1 interaction controls the recruitment of cortical microtubule stabilizing complexes to focal adhesions. Elife. 5. doi:10.7554/eLife.18124.

Bouchet, B.P., I. Noordstra, M. van Amersfoort, E.A. Katrukha, Y.C. Ammon, N.D. ter Hoeve, L. Hodgson, M. Dogterom, P.W.B. Derksen, and A. Akhmanova. 2016b. Mesenchymal Cell Invasion Requires Cooperative Regulation of Persistent Microtubule Growth by SLAIN2 and CLASP1. Dev. Cell. 39:708–723. doi:10.1016/j.devcel.2016.11.009.

Brangwynne, C.P., C.R. Eckmann, D.S. Courson, A. Rybarska, C. Hoege, J. Gharakhani, F. Jülicher, and A.A. Hyman. 2009. Germline P granules are liquid droplets that localize by controlled dissolution/condensation. Science (80-.). 324:1729–1732. doi:10.1126/science.1172046.

Bratman, S. V., and F. Chang. 2007. Stabilization of Overlapping Microtubules by Fission Yeast CLASP. Dev. Cell. 13:812–827. doi:10.1016/j.devcel.2007.10.015.

Breydo, L., K.D. Reddy, A. Piai, I.C. Felli, R. Pierattelli, and V.N. Uversky. 2014. The crowd you ' re in with : Effects of different types of crowding agents on protein aggregation. BBA - Proteins Proteomics. 1844:346–357. doi:10.1016/j.bbapap.2013.11.004.

Brouhard, G.J., and L.M. Rice. 2018. Microtubule dynamics: An interplay of biochemistry and mechanics. Nat. Rev. Mol. Cell Biol. 19:451–463. doi:10.1038/s41580-018-0009-y.

Brouhard, G.J., J.H. Stear, T.L. Noetzel, J. Al-Bassam, K. Kinoshita, S.C. Harrison, J. Howard, and A.A. Hyman. 2008. XMAP215 Is a Processive Microtubule Polymerase. Cell. 132:79–88. doi:10.1016/j.cell.2007.11.043.

Buey, R.M., R. Mohan, K. Leslie, T. Walzthoeni, J.H. Missimer, A. Menzel, S. Bjelic, K. Bargsten, I. Grigoriev, I. Smal, E. Meijering, R. Aebersold, A. Akhmanova, and M.O. Steinmetz. 2011. Insights into EB1 structure and the role of its C-terminal domain for discriminating microtubule tips from the lattice. Mol. Biol. Cell. 22:2912–2923. doi:10.1091/mbc.e11-01-0017.

Burke, K.A., A.M. Janke, C.L. Rhine, and N.L. Fawzi. 2015. Residue-by-Residue View of In Vitro FUS Granules that Bind the C-Terminal Domain of RNA Polymerase II. Mol. Cell. 60:231–241. doi:10.1016/j.molcel.2015.09.006.

Byrnes, A.E., and K.C. Slep. 2017. TOG-tubulin binding specificity promotes microtubule dynamics and mitotic spindle formation. J. Cell Biol. 216:1641–1657. doi:10.1083/jcb.201610090.

Caplow, M., and J. Shanks. 1996. Evidence that a single monolayer tubulin-GTP cap is both necessary and sufficient to stabilize microtubules. Mol. Biol. Cell. 7:663–675. doi:10.1091/mbc.7.4.663.

Case, L.B., X. Zhang, J.A. Ditlev, and M.K. Rosen. 2019. Stoichiometry controls activity of phase-separated clusters of actin signaling proteins. Science (80-.). 363:1093–1097. doi:10.1126/science.aau6313.

Cassimeris, L., and J. Morabito. 2004. TOGp, the Human Homolog of XMAP215/Dis1, Is Required for Centrosome Integrity, Spindle Pole Organization, and Bipolar Spindle Assembly. Mol. Biol. Cell. 15:1580–1590. doi:10.1091/mbc.e03-07-0544.

Chaaban, S., and G.J. Brouhard. 2017. A microtubule bestiary: structural diversity in tubulin polymers. Mol. Biol. Cell. 28:2924–2931. doi:10.1091/mbc.e16-05-0271.

Chabin-brion, K., F. Perez, A. Drechou, and C. Pou. 2001. The Golgi Complex Is a Microtubule-organizing Organelle. Mol. Biol. Cell. 12:2047–2060.

Charrasse, S., M. Mazel, S. Taviaux, P. Berta, T. Chow, and C. Larroque. 1995. Characterization of the cDNA and Pattern of Expression of a New Gene Over-Expressed in Human Hepatomas and Colonic Tumors. Eur. J. Biochem. 234:406–413. doi:10.1111/j.1432-1033.1995.406_b.x.

Charrasse, S., M. Schroeder, C. Gauthier-Rouviere, F. Ango, L. Cassimeris, D.L. Gard, and C. Larroque. 1998. The TOGp protein is a new human microtubule-associated protein homologous to the Xenopus XMAP215. J. Cell Sci. 111 (Pt 1:1371–83.

Cross, R.A. 2019. Microtubule lattice plasticity. Curr. Opin. Cell Biol. 56:88–93. doi:10.1016/j.ceb.2018.10.004.

Cullen, C.F., and H. Ohkura. 2001. Msps protein is localized to acentrosomal poles to ensure bipolarity of Drosophila meiotic spindles. Nat. Cell Biol. 3:637–642. doi:10.1038/35083025.

Delgehyr, N., J. Sillibourne, and M. Bornens. 2005. Microtubule nucleation and anchoring at the centrosome are independent processes linked by ninein function. J. Cell Sci. 118:1565–1575. doi:10.1242/jcs.02302.

Desai, A., and T.J. Mitchison. 1997. Microtubule Polymerization Dynamics. Annu. Rev. Cell Dev. Biol. 13:83–117. doi:10.1146/annurev.cellbio.13.1.83.

Diamantopoulos, G.S., F. Perez, H. V. Goodson, G. Batelier, R. Melki, T.E. Kreis, and J.E. Rickard. 1999. Dynamic localization of CLIP-170 to microtubule plus ends is coupled to microtubule assembly. J. Cell Biol. 144:99–112. doi:10.1083/jcb.144.1.99.

Dimitrov, A., S. Moutel, I. Cantaloube, and F. Perez. 2008. Detection of GTP-Tubulin conformation in vivo reveals a role for GTP remnants - Supp data. Science (80-.). 4:1353–1357. doi:10.1126/science.

Dixit, R., B. Barnett, J.E. Lazarus, M. Tokito, Y.E. Goldman, and E.L.F. Holzbaur. 2009. Microtubule plus-end tracking by CLIP-170 requires EB1. Proc. Natl. Acad. Sci. 106:492–497. doi:10.1073/pnas.0807614106.

Dragestein, K.A., W.A. Van Cappellen, J. Van Haren, G.D. Tsibidis, A. Akhmanova, T.A. Knoch, F. Grosveld, and N.

Galjart. 2008. Dynamic behavior of GFP-CLIP-170 reveals fast protein turnover on microtubule plus ends. J. Cell Biol. 180:729–737. doi:10.1083/jcb.200707203.

Driver, J.W., E.A. Geyer, M.E. Bailey, L.M. Rice, and C.L. Asbury. 2017. Direct measurement of conformational strain energy in protofilaments curling outward from disassembling microtubule tips. Elife. 6:1–18. doi:10.7554/elife.28433.

Duellberg, C., N.I. Cade, D. Holmes, and T. Surrey. 2016. The size of the EB cap determines instantaneous microtubule stability. Elife. 5:1–23. doi:10.7554/eLife.13470.

Duellberg, C., M. Trokter, R. Jha, I. Sen, M.O. Steinmetz, and T. Surrey. 2014. Reconstitution of a hierarchical +TIP interaction network controlling microtubule end tracking of dynein. Nat. Cell Biol. 16:804–811. doi:10.1038/ncb2999.

Efimov, A., A. Kharitonov, N. Efimova, J. Loncarek, P.M. Miller, N. Andreyeva, P. Gleeson, N. Galjart, A.R.R. Maia, I.X. McLeod, J.R. Yates, H. Maiato, A. Khodjakov, A. Akhmanova, and I. Kaverina. 2007. Asymmetric CLASP-Dependent Nucleation of Noncentrosomal Microtubules at the trans-Golgi Network. Dev. Cell. 12:917–930. doi:10.1016/j.devcel.2007.04.002.

Fong, K., Y. Choi, J.B. Rattner, and R.Z. Qi. 2008. CDK5RAP2 Is a Pericentriolar Protein That Functions in Centrosomal Attachment of the γ-Tubulin Ring Complex. Mol. Biol. Cell. 19:115–125. doi:10.1091/mbc.E07.

Fourniol, F.J., C. V. Sindelar, B. Amigues, D.K. Clare, G. Thomas, M. Perderiset, F. Francis, A. Houdusse, and C.A. Moores. 2010. Template-free 13-protofilament microtubule-MAP assembly visualized at 8 Å resolution. J. Cell Biol. 191:463–470. doi:10.1083/jcb.201007081.

Fox, J.C., A.E. Howard, J.D. Currie, S.L. Rogers, and K.C. Slep. 2014. The XMAP215 family drives microtubule polymerization using a structurally diverse TOG array. Mol. Biol. Cell. 25:2375–2392. doi:10.1091/mbc.e13-08-0501.

Gard, D.L., B.E. Becker, and S. Josh Romney. 2004. MAPping the eukaryotic tree of life: Structure, function, and evolution of the MAP215/Dis1 family of microtubule-associated proteins. Int. Rev. Cytol. 239:179–272. doi:10.1016/S0074-7696(04)39004-2.

Des Georges, A., M. Katsuki, D.R. Drummond, M. Osei, R.A. Cross, and L.A. Amos. 2008. Mal3, the Schizosaccharomyces pombe homolog of EB1, changes the microtubule lattice. Nat. Struct. Mol. Biol. 15:1102–1108. doi:10.1038/nsmb.1482.

Gergely, F., V.M. Draviam, and J.W. Raff. 2003. The ch-TOG/XMAP215 protein is essential for spindle pole organization in human somatic cells. Genes Dev. 17:336–341. doi:10.1101/gad.245603.

Gergely, F., C. Karlsson, I. Still, J. Cowell, J. Kilmartin, and J.W. Raff. 2000. The TACC domain identifies a family of centrosomal proteins that can interact with microtubules. Proc. Natl. Acad. Sci. U. S. A. 97:14352–14357. doi:10.1073/pnas.97.26.14352.

Geyer, E.A., A. Burns, B.A. Lalonde, X. Ye, F.A. Piedra, T.C. Huffaker, and L.M. Rice. 2015. A mutation uncouples the tubulin conformational and GTPase cycles, revealing allosteric control of microtubule dynamics. Elife. 4:1–20. doi:10.7554/eLife.10113.

Gierke, S., and T. Wittmann. 2012. EB1-recruited microtubule +TIP complexes coordinate protrusion dynamics during 3D epithelial remodeling. Curr. Biol. 22:753–762. doi:10.1016/j.cub.2012.02.069.

Gimona, M., K. Djinovic-Carugo, W.J. Kranewitter, and S.J. Winder. 2002. Functional plasticity of CH domains. FEBS Lett. 513:98–106. doi:10.1016/S0014-5793(01)03240-9.

Gireesh, K.K., A. Shine, R.B. Lakshmi, V. Vijayan, and T.K. Manna. 2018. GTP-binding facilitates EB1 recruitment onto microtubules by relieving its auto-inhibition. Sci. Rep. 8:1–13. doi:10.1038/s41598-018-28056-y.

De Groot, C.O., I. Jelesarov, F.F. Damberger, S. Bjelić, M.A. Schärer, N.S. Bhavesh, I. Grigoriev, R.M. Buey, K. Wüthrich, G. Capitani, A. Akhmanova, and M.O. Steinmetz. 2010. Molecular insights into mammalian end-binding protein heterodimerization. J. Biol. Chem. 285:5802–5814. doi:10.1074/jbc.M109.068130.

Guesdon, A., F. Bazile, R.M. Buey, R. Mohan, S. Monier, R.R. García, M. Angevin, C. Heichette, R. Wieneke, R. Tampé, L. Duchesne, A. Akhmanova, M.O. Steinmetz, and D. Chrétien. 2016. EB1 interacts with outwardly curved and straight regions of the microtubule lattice. Nat. Cell Biol. 18:1102–1108. doi:10.1038/ncb3412.

Van Haren, J., R.A. Charafeddine, A. Ettinger, H. Wang, K.M. Hahn, and T. Wittmann. 2018. Local control of intracellular microtubule dynamics by EB1 photodissociation. Nat. Cell Biol. 20:252–261. doi:10.1038/s41556-017-0028-5.

Haren, L., M. Remy, I. Bazin, I. Callebaut, M. Wright, and A. Merdes. 2006. NEDD1-dependent recruitment of the γ-tubulin ring complex to the centrosome is necessary for centriole duplication and spindle assembly. J. Cell Biol. 172:505–515. doi:10.1083/jcb.200510028.

Hayashi, I., A. Wilde, T.K. Mal, and M. Ikura. 2005. Structural basis for the activation of microtubule assembly by the EB1 and p150Glued complex. Mol. Cell. 19:449–460. doi:10.1016/j.molcel.2005.06.034.

Hemmat, M., B.T. Castle, and D.J. Odde. 2018. Microtubule dynamics: moving toward a multi-scale approach. Curr. Opin. Cell Biol. 50:8–13. doi:10.1016/j.ceb.2017.12.013.

Hernández-Vega, A., M. Braun, L. Scharrel, M. Jahnel, S. Wegmann, B.T. Hyman, S. Alberti, S. Diez, and A.A. Hyman. 2017. Local Nucleation of Microtubule Bundles through Tubulin Concentration into a Condensed Tau Phase. Cell Rep. 20:2304–2312. doi:10.1016/j.celrep.2017.08.042.

Hirst, C.E., E.S. Ng, L. Azzola, A.K. Voss, T. Thomas, E.G. Stanley, and A.G. Elefanty. 2006. Transcriptional profiling of mouse and human ES cells identifies SLAIN1, a novel stem cell gene. Dev. Biol. 293:90–103. doi:10.1016/j.ydbio.2006.01.023.

Holehouse, A.S., and R. V. Pappu. 2018. Functional Implications of Intracellular Phase Transitions. Biochemistry. 57:2415–2423. doi:10.1021/acs.biochem.7b01136.

Honnappa, S., S.M. Gouveia, A. Weisbrich, F.F. Damberger, N.S. Bhavesh, H. Jawhari, I. Grigoriev, F.J.A.A. van Rijssel, R.M. Buey, A. Lawera, I. Jelesarov, F.K. Winkler, K. Wüthrich, A. Akhmanova, M.O. Steinmetz, K. W??thrich, A. Akhmanova, M.O. Steinmetz, K. Wüthrich, A. Akhmanova, and M.O. Steinmetz. 2009. An EB1-Binding Motif Acts as a Microtubule Tip Localization Signal. Cell. 138:366–376. doi:10.1016/j.cell.2009.04.065.

Honnappa, S., C.M. John, D. Kostrewa, F.K. Winkler, and M.O. Steinmetz. 2005. Structural insights into the EB1-APC interaction. EMBO J. 24:261–9. doi:10.1038/sj.emboj.7600529.

Hood, F.E., S.J. Williams, S.G. Burgess, M.W. Richards, D. Roth, A. Straube, M. Pfuhl, R. Bayliss, and S.J. Royle. 2013. Coordination of adjacent domains mediates TACC3-ch-TOG-clathrin assembly and mitotic spindle binding. J. Cell Biol. 202:463–478. doi:10.1083/jcb.201211127.

Howard, A.E., J.C. Fox, and K.C. Slep. 2015. Drosophila melanogaster mini spindles TOG3 utilizes unique structural elements to promote domain stability and maintain a TOG1- and TOG2-like tubulin-binding surface. J. Biol. Chem. 290:10149–10162. doi:10.1074/jbc.M114.633826.

Howard, J., and A.A. Hyman. 2003. Dynamics and mechanics of the microtubule plus end. Nature. 422:753–758. doi:10.1038/nature01600.

Howes, S.C., B. LaFrance, R. Zhang, E. Kellogg, E. Greyer, S. Westermann, L. Rice, and E. Nogales. 2017. Structural differences between yeast and mammalian microtubules revealed by cryo-EM. J. Cell Biol. 216:1–28. doi:10.1083/jcb.201612195.

Huang, W.Y.C., S. Alvarez, Y. Kondo, Y.K. Lee, J.K. Chung, H. Yue, M. Lam, K.H. Biswas, J. Kuriyan, and J.T. Groves. 2019. A molecular assembly phase transition and kinetic proofreading modulate Ras activation by SOS. Science (80-.). 363:1098–1103.

Hyman, A.A., D. Chretien, I. Arnal, and Richard H. Wade. 1995. Structural Changes Accompanying GTP Hydrolysis in Microtubules : J. Cell Biol. 128:117–125.

Igaev, M., and H. Grubmüller. 2018. Microtubule assembly governed by tubulin allosteric gain in flexibility and lattice induced fit. Elife. 7:1–21. doi:10.7554/eLife.34353.

Islam, F., S. Chaousis, R. Wahab, V. Gopalan, and A.K.Y. Lam. 2018. Protein interactions of FAM134B with EB1 and APC/beta-catenin in vitro in colon carcinoma. Mol. Carcinog. 57:1480–1491. doi:10.1002/mc.22871.

Itzhak, D.N., S. Tyanova, J. Cox, and G.H. Borner. 2016. Global, quantitative and dynamic mapping of protein subcellular localization. Elife. 5:1–36. doi:10.7554/elife.16950.

Jánosi, I.M., D. Chrétien, and H. Flyvbjerg. 1998. Modeling elastic properties of microtubule tips and walls. Eur. Biophys. J. 27:501–513. doi:10.1007/s002490050160.

Jaworski, J., L.C. Kapitein, S.M. Gouveia, B.R. Dortland, P.S. Wulf, I. Grigoriev, P. Camera, S.A. Spangler, P. Di Stefano, J. Demmers, H. Krugers, P. Defilippi, A. Akhmanova, and C.C. Hoogenraad. 2009. Dynamic Microtubules Regulate Dendritic Spine Morphology and Synaptic Plasticity. Neuron. 61:85–100. doi:10.1016/j.neuron.2008.11.013.

Jiang, K., and A. Akhmanova. 2011. Microtubule tip-interacting proteins: A view from both ends. Curr. Opin. Cell Biol. 23:94–101. doi:10.1016/j.ceb.2010.08.008.

Jiang, K., S. Hua, R. Mohan, I. Grigoriev, K.W. Yau, Q. Liu, E.A. Katrukha, A.F.M. Altelaar, A.J.R. Heck, C.C. Hoogenraad, and A. Akhmanova. 2014. Microtubule minus-end stabilization by polymerization-driven CAMSAP deposition. Dev. Cell. 28:295–309. doi:10.1016/j.devcel.2014.01.001.

Jiang, K., G. Toedt, S. Montenegro Gouveia, N.E. Davey, S. Hua, B. Van Der Vaart, I. Grigoriev, J. Larsen, L.B. Pedersen, K. Bezstarosti, M. Lince-Faria, J. Demmers, M.O. Steinmetz, T.J. Gibson, and A. Akhmanova. 2012. A proteome-wide screen for mammalian SxIP motif-containing microtubule plus-end tracking proteins. Curr. Biol. 22:1800–1807. doi:10.1016/j.cub.2012.07.047.

Jovasevic, V., M.H. Naghavi, and D. Walsh. 2015. Microtubule plus end-associated CLIP-170 initiates HSV-1 retrograde transport in primary human cells. J. Cell Biol. 211:323–337. doi:10.1083/jcb.201505123.

Kanaba, T., R. Maesaki, T. Mori, Y. Ito, T. Hakoshima, and M. Mishima. 2013. Microtubule-binding sites of the CH domain of EB1 and its autoinhibition revealed by NMR. Biochim. Biophys. Acta - Proteins Proteomics. 1834:499–507. doi:10.1016/j.bbapap.2012.10.013.

Kim, H.J., N.C. Kim, Y.D. Wang, E.A. Scarborough, J. Moore, Z. Diaz, K.S. MacLea, B. Freibaum, S. Li, A. Molliex, A.P. Kanagaraj, R. Carter, K.B. Boylan, A.M. Wojtas, R. Rademakers, J.L. Pinkus, S.A. Greenberg, J.Q. Trojanowski, B.J. Traynor, B.N. Smith, S. Topp, A.S. Gkazi, J. Miller, C.E. Shaw, M. Kottlors, J. Kirschner, A. Pestronk, Y.R.

Li, A.F. Ford, A.D. Gitler, M. Benatar, O.D. King, V.E. Kimonis, E.D. Ross, C.C. Weihl, J. Shorter, and J.P. Taylor. 2013. Mutations in prion-like domains in hnRNPA2B1 and hnRNPA1 cause multisystem proteinopathy and ALS. Nature. 495:467–473. doi:10.1038/nature11922.

Kobayashi, T., and B.D. Dynlacht. 2011. Regulating the transition from centriole to basal body. J. Cell Biol. 193:435–444. doi:10.1083/jcb.201101005.

Komarova, Y., C.O. De Groot, I. Grigoriev, S.M. Gouveia, E.L. Munteanu, J.M. Schober, S. Honnappa, R.M. Buey, C.C. Hoogenraad, M. Dogterom, G.G. Borisy, M.O. Steinmetz, and A. Akhmanova. 2009. Mammalian end binding proteins control persistent microtubule growth. J. Cell Biol. 184:691–706. doi:10.1083/jcb.200807179.

Komarova, Y., G. Lansbergen, N. Galjart, F. Grosveld, G.G. Borisy, and A. Akhmanova. 2005. EB1 and EB3 control CLIP dissociation from the ends of growing microtubules. Mol. Biol. Cell. 16:5334–5345. doi:10.1091/mbc.E05.

Kueh, H.Y., and T.J. Mitchison. 2009. Structural plasticity in actin and tubulin polymer dynamics. Science (80-.). 325:960–964. doi:10.1126/science.1168823.

Kulkarni, A.A., and P.S. Rao. 2013. Synthesis of polymeric nanomaterials for biomedical applications. Woodhead Publishing. 27–63 pp.

Kumar, P., K.S. Lyle, S. Gierke, A. Matov, G. Danuser, and T. Wittmann. 2009. GSK3β phosphorylation modulates CLASP–microtubule association and lamella microtubule attachment. J. Cell Biol. 184:895–908. doi:10.1083/jcb.200901042.

Kurimoto, R., and E. Niiyama. 2016. Fibrous Materials. William Andrew Publishing. 267–278 pp.

Kwon, I., M. Kato, S. Xiang, L. Wu, P. Theodoropoulos, H. Mirzaei, T. Han, S. Xie, J.L. Corden, and S.L. McKnight. 2013. Phosphorylation-regulated binding of RNA polymerase II to fibrous polymers of low-complexity domains. Cell. 155:1049. doi:10.1016/j.cell.2013.10.033.

Lansbergen, G., I. Grigoriev, Y. Mimori-Kiyosue, T. Ohtsuka, S. Higa, I. Kitajima, J. Demmers, N. Galjart, A.B. Houtsmuller, F. Grosveld, and A. Akhmanova. 2006. CLASPs Attach Microtubule Plus Ends to the Cell Cortex through a Complex with LL5β. Dev. Cell. 11:21–32. doi:10.1016/j.devcel.2006.05.012.

Lansbergen, G., Y. Komarova, M. Modesti, C. Wyman, C.C. Hoogenraad, H. V. Goodson, R.P. Lemaitre, D.N. Drechsel, E. Van Munster, T.W.J. Gadella, F. Grosveld, N. Galjart, G.G. Borisy, and A. Akhmanova. 2004. Conformational changes in CLIP-170 regulate its binding to microtubules and dynactin localization. J. Cell Biol. 166:1003–1014. doi:10.1083/jcb.200402082.

Lawrence, E.J., G. Arpag, S.R. Norris, and M. Zanic. 2018. Human CLASP2 specifically regulates microtubule catastrophe and rescue. Mol. Biol. Cell. 29:1168–1177. doi:10.1091/mbc.E18-01-0016.

Lawrence, E.J., and M. Zanic. 2019. Rescuing microtubules from the brink of catastrophe: CLASPs lead the way. Curr. Opin. Cell Biol. 56:94–101. doi:10.1016/j.ceb.2018.10.011.

Leano, J.B., S.L. Rogers, and K.C. Slep. 2013. A cryptic TOG domain with a distinct architecture underlies CLASP-dependent bipolar spindle formation. Structure. 21:939–950. doi:10.1016/j.str.2013.04.018.

Lesniewska, K., E. Warbrick, and H. Ohkura. 2014. Peptide aptamers define distinct EB1- and EB3-binding motifs and interfere with microtubule dynamics. Mol. Biol. Cell. 25:1025–1036. doi:10.1091/mbc.e13-08-0504.

Leterrier, C., H. Vacher, M.-P. Fache, S.A. d'Ortoli, F. Castets, A. Autillo-Touati, and B. Dargent. 2011. End-binding proteins EB3 and EB1 link microtubules to ankyrin G in the axon initial segment. Proc. Natl. Acad. Sci. 108:8826–8831. doi:10.1073/pnas.1018671108.

Li, P., S. Banjade, H.C. Cheng, S. Kim, B. Chen, L. Guo, M. Llaguno, J. V. Hollingsworth, D.S. King, S.F. Banani, P.S. Russo, Q.X. Jiang, B.T. Nixon, and M.K. Rosen. 2012a. Phase transitions in the assembly of multivalent signalling proteins. Nature. 483:336–340. doi:10.1038/nature10879.

Li, W., T. Moriwaki, T. Tani, T. Watanabe, K. Kaibuchi, and G. Goshima. 2012b. Reconstitution of dynamic microtubules with drosophila XMAP215, EB1, and sentin. J. Cell Biol. 199:849–862. doi:10.1083/jcb.201206101.

Liu, Q., S. Remmelzwaal, A.J.R. Heck, A. Akhmanova, and F. Liu. 2017. Facilitating identification of minimal protein binding domains by cross-linking mass spectrometry. Sci. Rep. 7:1–11. doi:10.1038/s41598-017-13663-y.

Liu, Y., Y. Mi, T. Mueller, S. Kreibich, E.G. Williams, A. Van Drogen, C. Borel, M. Frank, P.L. Germain, I. Bludau, M. Mehnert, M. Seifert, M. Emmenlauer, I. Sorg, F. Bezrukov, F.S. Bena, H. Zhou, C. Dehio, G. Testa, J. Saez-Rodriguez, S.E. Antonarakis, W.D. Hardt, and R. Aebersold. 2019. Multi-omic measurements of heterogeneity in HeLa cells across laboratories. Nat. Biotechnol. 37:314–322. doi:10.1038/s41587-019-0037-y.

Von Loeffelholz, O., N.A. Venables, D.R. Drummond, M. Katsuki, R. Cross, and C.A. Moores. 2017. Nucleotide- and Mal3-dependent changes in fission yeast microtubules suggest a structural plasticity view of dynamics. Nat. Commun. 8:1–13. doi:10.1038/s41467-017-02241-5.

Lüders, J., and T. Stearns. 2007. Microtubule-organizing centres: a re-evaluation. Nat. Rev. Mol. Cell Biol. 8:161–167.

Luo, Y., D. Li, J. Ran, B. Yan, J. Chen, X. Dong, Z. Liu, R. Liu, J. Zhou, and M. Liu. 2014. End-binding protein 1 stimulates paclitaxel sensitivity in breast cancer by promoting its actions toward microtubule assembly and

stability. Protein Cell. 5:469–479. doi:10.1007/s13238-014-0053-0.
Maiato, H., A. Khodjakov, and C.L. Rieder. 2005. Drosophila CLASP is required for the incorporation of microtubule subunits into fluxing kinetochore fibres. Nat. Cell Biol. 7:42–47. doi:10.1038/ncb1207.
Maiato, H., C.L. Rieder, and A. Khodjakov. 2004. Kinetochore-driven formation of kinetochore fibers contributes to spindle assembly during animal mitosis. J. Cell Biol. 167:831–840. doi:10.1083/jcb.200407090.
Maki, T., A.D. Grimaldi, S. Fuchigami, I. Kaverina, and I. Hayashi. 2015. CLASP2 has two distinct TOG domains that contribute differently to microtubule dynamics. J. Mol. Biol. 427:2379–2395. doi:10.1016/j.jmb.2015.05.012.
Manka, S.W., and C.A. Moores. 2018. Microtubule structure by cryo-EM: snapshots of dynamic instability. Essays Biochem. 62:737–751. doi:10.1042/ebc20180031.
Mann, J.R., A.M. Gleixner, J.C. Mauna, E. Gomes, M.R. DeChellis-Marks, P.G. Needham, K.E. Copley, B. Hurtle, B. Portz, N.J. Pyles, L. Guo, C.B. Calder, Z.P. Wills, U.B. Pandey, J.K. Kofler, J.L. Brodsky, A. Thathiah, J. Shorter, and C.J. Donnelly. 2019. RNA Binding Antagonizes Neurotoxic Phase Transitions of TDP-43. Neuron. 102:321-338. e8. doi:10.1016/j.neuron.2019.01.048.
Margolis, R.L., and L. Wilson. 1978. Opposite end assembly and disassembly of microtubules at steady state in vitro. Cell. 13:1–8. doi:10.1016/0092-8674(78)90132-0.
Martin, M., and A. Akhmanova. 2018. Coming into Focus: Mechanisms of Microtubule Minus-End Organization. Trends Cell Biol. 28:574–588. doi:10.1016/j.tcb.2018.02.011.
Martin, M., A. Veloso, J. Wu, E.A. Katrukha, and A. Akhmanova. 2018. Control of endothelial cell polarity and sprouting angiogenesis by non-centrosomal microtubules. Elife. 7:1–37. doi:10.7554/elife.33864.
Maurer, S.P., P. Bieling, J. Cope, A. Hoenger, and T. Surrey. 2011. GTP S microtubules mimic the growing microtubule end structure recognized by end-binding proteins (EBs). Proc. Natl. Acad. Sci. 108:3988–3993. doi:10.1073/pnas.1014758108.
Maurer, S.P., N.I. Cade, G. Bohner, N. Gustafsson, E. Boutant, and T. Surrey. 2014. EB1 accelerates two conformational transitions important for microtubule maturation and dynamics. Curr. Biol. 24:372–384. doi:10.1016/j.cub.2013.12.042.
Maurer, S.P., F.J. Fourniol, G. Bohner, C.A. Moores, and T. Surrey. 2012. EBs recognize a nucleotide-dependent structural cap at growing microtubule ends. Cell. 149:371–382. doi:10.1016/j.cell.2012.02.049.
McIntosh, J.R., E. O'Toole, G. Morgan, J. Austin, E. Ulyanov, F. Ataullakhanov, and N. Gudimchuk. 2018. Microtubules grow by the addition of bent guanosine triphosphate tubulin to the tips of curved protofilaments. J. Cell Biol. 217:2691–2708. doi:10.1083/jcb.201802138.
Memet, E., F. Hilitski, M.A. Morris, W.J. Schwenger, Z. Dogic, and L. Mahadevan. 2018. Microtubules soften due to cross-sectional flattening. Elife. 7:1–22. doi:10.7554/eLife.34695.
Meng, W., Y. Mushika, T. Ichii, and M. Takeichi. 2008. Anchorage of Microtubule Minus Ends to Adherens Junctions Regulates Epithelial Cell-Cell Contacts. Cell. 135:948–959. doi:10.1016/j.cell.2008.09.040.
Miller, P.M., A.W. Folkmann, A.R.R. Maia, N. Efimova, A. Efimov, and I. Kaverina. 2009. Golgi-derived CLASP-dependent microtubules control Golgi organization and polarized trafficking in motile cells. Nat. Cell Biol. 11:1069–80. doi:10.1038/ncb1920.
Mimori-Kiyosue, Y., I. Grigoriev, G. Lansbergen, H. Sasaki, C. Matsui, F. Severin, N. Galjart, F. Grosveld, I. Vorobjev, S. Tsukita, and A. Akhmanova. 2005. CLASP1 and CLASP2 bind to EB1 and regulate microtubule plus-end dynamics at the cell cortex. J. Cell Biol. 168:141–153. doi:10.1083/jcb.200405094.
Mimori-Kiyosue, Y., N. Shiina, and S. Tsukita. 2000. The dynamic behavior of the APC-binding protein EB1 on the distal ends of microtubules. Curr. Biol. 10:865–868. doi:10.1016/S0960-9822(00)00600-X.
Mitchison, T.J., and M. Kirschner. 1984. Dynamic instability of microtubule growth. Nature. 312:237–242. doi:10.1038/309126a0.
Mohan, R., E. a Katrukha, H. Doodhi, I. Smal, E. Meijering, L.C. Kapitein, M.O. Steinmetz, and A. Akhmanova. 2013. End-binding proteins sensitize microtubules to the action of microtubule-targeting agents. Proc. Natl. Acad. Sci. U. S. A. 110:8900–5. doi:10.1073/pnas.1300395110.
Molliex, A., J. Temirov, J. Lee, M. Coughlin, A.P. Kanagaraj, H.J. Kim, T. Mittag, and J.P. Taylor. 2015. Phase Separation by Low Complexity Domains Promotes Stress Granule Assembly and Drives Pathological Fibrillization. Cell. 163:123–133. doi:10.1016/j.cell.2015.09.015.
Morrison, E.E., B.N. Wardleworth, J.M. Askham, A.F. Markham, and D.M. Meredith. 1998. EB1, a protein which interacts with the APC tumour suppressor, is associated with the microtubule cytoskeleton throughout the cell cycle. Oncogene. 17:3471–3477. doi:10.1038/sj.onc.1202247.
Naghavi, M.H., and D. Walsh. 2017. Microtubule Regulation and Function during Virus Infection. J. Virol. 91:1–16. doi:10.1128/jvi.00538-17.
Nawrotek, A., M. Knossow, and B. Gigant. 2011. The determinants that Govern microtubule assembly from the atomic structure of GTP-tubulin. J. Mol. Biol. 412:35–42. doi:10.1016/j.jmb.2011.07.029.
Orimo, T., H. Ojima, N. Hiraoka, S. Saito, T. Kosuge, T. Kakisaka, H. Yokoo, K. Nakanishi, T. Kamiyama, S. Todo, S.

Hirohashi, and T. Kondo. 2008. Proteomic profiling reveals the prognostic value of adenomatous polyposis coli-end-binding protein 1 in hepatocellular carcinoma. Hepatology. 48:1851–1863. doi:10.1002/hep.22552.

Patel, A., H.O. Lee, L. Jawerth, S. Maharana, M. Jahnel, M.Y. Hein, S. Stoynov, J. Mahamid, S. Saha, T.M. Franzmann, A. Pozniakovski, I. Poser, N. Maghelli, L.A. Royer, M. Weigert, E.W. Myers, S. Grill, D. Drechsel, A.A. Hyman, and S. Alberti. 2015. A Liquid-to-Solid Phase Transition of the ALS Protein FUS Accelerated by Disease Mutation. Cell. 162:1066–1077. doi:10.1016/j.cell.2015.07.047.

Peet, D.R., N.J. Burroughs, and R.A. Cross. 2018. Kinesin expands and stabilises the GDP-microtubule lattice. Nat. Nanotechnol. 13:386–391. doi:10.1038/s41565-018-0084-4.Kinesin.

Petry, S., A.C. Groen, K. Ishihara, T.J. Mitchison, and R.D. Vale. 2013. Branching microtubule nucleation in xenopus egg extracts mediated by augmin and TPX2. Cell. 152:768–777. doi:10.1016/j.cell.2012.12.044.

Petry, S., and R.D. Vale. 2015. Microtubule nucleation at the centrosome and beyond. Nat. Cell Biol. 17:1089–1093. doi:10.1038/ncb3220.

Piedra, F.-A., T. Kim, E.S. Garza, E.A. Geyer, A. Burns, X. Ye, and L.M. Rice. 2016. GDP-to-GTP exchange on the microtubule end can contribute to the frequency of catastrophe. Mol. Biol. Cell. 27:3515–3525. doi:10.1091/mbc.e16-03-0199.

Pierre, P., J. Scheel, J.E. Rickard, and T.E. Kreis. 1992. CLIP-170 links endocytic vesicles to microtubules. Cell. 70:887–900. doi:10.1016/0092-8674(92)90240-D.

Portran, D., L. Schaedel, Z. Xu, M. Théry, and M. V. Nachury. 2017. Tubulin acetylation protects long-lived microtubules against mechanical ageing. Nat. Cell Biol. 19:391–398. doi:10.1038/ncb3481.

Procter, D.J., A. Banerjee, M. Nukui, K. Kruse, V. Gaponenko, E.A. Murphy, Y. Komarova, and D. Walsh. 2018. The HCMV Assembly Compartment Is a Dynamic Golgi-Derived MTOC that Controls Nuclear Rotation and Virus Spread. Dev. Cell. 45:83-100.e7. doi:10.1016/j.devcel.2018.03.010.

Rickman, J., C. Duellberg, N.I. Cade, L.D. Griffin, and T. Surrey. 2017. Steady-state EB cap size fluctuations are determined by stochastic microtubule growth and maturation. Proc. Natl. Acad. Sci. 114:3427–3432. doi:10.1073/pnas.1620274114.

Rivero, S., J. Cardenas, M. Bornens, and R.M. Rios. 2009. Microtubule nucleation at the cis-side of the Golgi apparatus requires AKAP450 and GM130. EMBO J. 28:1016–1028. doi:10.1038/emboj.2009.47.

Roostalu, J., and T. Surrey. 2017. Microtubule nucleation : beyond the template. Nat. Rev. Mol. Cell Biol. 18:702–710. doi:10.1038/nrm.2017.75.

Roth, D., B.P. Fitton, N.P. Chmel, N. Wasiluk, and A. Straube. 2018. Spatial positioning of EB family proteins at microtubule tips involves distinct nucleotide-dependent binding properties. J. Cell Sci. 132:jcs219550. doi:10.1242/jcs.219550.

Rovini, A., G. Gauthier, R. Bergès, A. Kruczynski, D. Braguer, and S. Honoré. 2013. Anti-Migratory Effect of Vinflunine in Endothelial and Glioblastoma Cells Is Associated with Changes in EB1 C-Terminal Detyrosinated/Tyrosinated Status. PLoS One. 8:1–12. doi:10.1371/journal.pone.0065694.

Sanders, A.A.W.M., and I. Kaverina. 2015. Nucleation and dynamics of Golgi-derived microtubules. Front. Neurosci. 9:1–7. doi:10.3389/fnins.2015.00431.

Sato, Y., K. Hayashi, Y. Amano, M. Takahashi, S. Yonemura, I. Hayashi, H. Hirose, S. Ohno, and A. Suzuki. 2014. MTCL1 crosslinks and stabilizes non-centrosomal microtubules on the Golgi membrane. supp. 5:5266. doi:10.1017/CBO9781107415324.004.

Schaedel, L., K. John, J. Gaillard, M. V. Nachury, L. Blanchoin, and M. Thery. 2015. Microtubules self-repair in response to mechanical stress. Nat. Mater. 14:1156–1163. doi:10.1038/nmat4396.

Schrøder, J.M., J. Larsen, Y. Komarova, A. Akhmanova, R.I. Thorsteinsson, I. Grigoriev, R. Manguso, S.T. Christensen, S.F. Pedersen, S. Geimer, and L.B. Pedersen. 2011. EB1 and EB3 promote cilia biogenesis by several centrosome-related mechanisms. J. Cell Sci. 124:2539–2551. doi:10.1242/jcs.085852.

Seetapun, D., B.T. Castle, A.J. McIntyre, P.T. Tran, and D.J. Odde. 2012. Estimating the microtubule GTP cap size in vivo. Curr. Biol. 22:1681–1687. doi:10.1016/j.cub.2012.06.068.

Shima, T., M. Morikawa, J. Kaneshiro, T. Kambara, S. Kamimura, T. Yagi, H. Iwamoto, S. Uemura, H. Shigematsu, M. Shirouzu, T. Ichimura, T.M. Watanabe, R. Nitta, Y. Okada, and N. Hirokawa. 2018. Kinesin-binding–triggered conformation switching of microtubules contributes to polarized transport. J. Cell Biol. 217:4164–4183. doi:10.1083/jcb.201711178.

Shin, Y., and C.P. Brangwynne. 2017. Liquid phase condensation in cell physiology and disease. Science (80-.). 357. doi:10.1126/science.aaf4382.

Skube, S.B., J.M. Chaverri, and H. V. Goodson. 2010. Effect of GFP tags on the localization of EB1 and EB1 fragments in vivo. Cytoskeleton. 67:1–12. doi:10.1002/cm.20409.

Slep, K.C., S.L. Rogers, S.L. Elliott, H. Ohkura, P.A. Kolodziej, and R.D. Vale. 2005. Structural determinants for EB1-mediated recruitment of APC and spectraplakins to the microtubule plus end. J. Cell Biol. 168:587–598. doi:10.1083/jcb.200410114.

Slep, K.C., and R.D. Vale. 2007. Structural Basis of Microtubule Plus End Tracking by XMAP215, CLIP-170, and EB1. Mol. Cell. 27:976–991. doi:10.1016/j.molcel.2007.07.023.

Straube, A., and A. Merdes. 2007. EB3 Regulates Microtubule Dynamics at the Cell Cortex and Is Required for Myoblast Elongation and Fusion. Curr. Biol. 17:1318–1325. doi:10.1016/j.cub.2007.06.058.

Strothman, C., V. Farmer, G. Arpağ, N. Rodgers, M. Podolski, S. Norris, R. Ohi, and M. Zanic. 2019. Microtubule minus-end stability is dictated by the tubulin off-rate. J. Cell Biol. 218:2841–2853. doi:10.1083/jcb.201905019.

Su, L., M. Burrell, D.E. Hill, J. Gyuris, R. Brent, R. Wiltshire, J. Trent, B. Vogelstein, and K.W. Kinzler. 1995. APC Binds to the Novel Protein EB1. Cancer Res. 2972–2977.

Su, L.K., and Y. Qi. 2001. Characterization of human MAPRE genes and their proteins. Genomics. 71:142–9. doi:10.1006/geno.2000.6428.

Su, X., J. Ditlev, E. Hui, S. Banjade, J. Okrut, J. Taunton, M. Rosen, and R. Vale. 2016. Phase separation of signaling molecules promotes T cell receptor signal transduction. Science (80-.). 352:595–599. doi:10.1158/2326-6074.cricimteatiaacr15-a087.

Sugihara, Y., H. Taniguchi, R. Kushima, H. Tsuda, D. Kubota, H. Ichikawa, K. Sakamoto, Y. Nakamura, T. Tomonaga, S. Fujita, and T. Kondo. 2012. Proteomic-based identification of the APC-binding protein EB1 as a candidate of novel tissue biomarker and therapeutic target for colorectal cancer. J. Proteomics. 75:5342–5355. doi:10.1016/j.jprot.2012.06.013.

Sun, T., Y. Song, J. Dai, D. Mao, M. Ma, J. Ni, and X. Liang. 2019. Spectraplakin Shot Maintains Perinuclear Microtubule Organization in Drosophila Article Spectraplakin Shot Maintains Perinuclear Microtubule Organization in Drosophila Polyploid Cells. Dev. Cell. 49:1–17. doi:10.1016/j.devcel.2019.03.027.

Surrey, T., E. Karsenti, and F.J. Nedelec. 2006. Modelling microtubule patterns. Nat. Cell Biol. 8:1204–1211. doi:10.1038/ncb1498.

Takahashi, M., A. Yamagiwa, T. Nishimura, H. Mukai, and Y. Ono. 2002. Centrosomal Proteins CG-NAP and Kendrin Provide Microtubule Nucleation Sites by Anchoring γ -Tubulin Ring Complex. Mol. Biol. Cell. 13:3235–3245. doi:10.1091/mbc.E02.

Tanaka, N., W. Meng, S. Nagae, and M. Takeichi. 2012. Nezha/CAMSAP3 and CAMSAP2 cooperate in epithelial-specific organization of noncentrosomal microtubules. Proc. Natl. Acad. Sci. U. S. A. 109:20029–34. doi:10.1073/pnas.1218017109.

Tassin, A., B. Maro, and M. Bornens. 1985. Fate of Microtubule-organizing Centers during Myogenesis in Vitro. J. Cell Biol. 100:35–46.

Thawani, A., R.S. Kadzik, and S. Petry. 2018. XMAP215 is a microtubule nucleation factor that functions synergistically with the γ-tubulin ring complex. Nat. Cell Biol. 20:575–585. doi:10.1038/s41556-018-0091-6.

Tirnauer, J.S., and B.E. Bierer. 2000. EB1 proteins regulate microtubule dynamics, cell polarity, and chromosome stability. J. Cell Biol. 149:761–766. doi:10.1083/jcb.149.4.761.

van der Vaart, B., M.A.M. Franker, M. Kuijpers, S. Hua, B.P. Bouchet, K. Jiang, I. Grigoriev, C.C. Hoogenraad, and A. Akhmanova. 2012. Microtubule plus-end tracking proteins SLAIN1/2 and ch-TOG promote axonal development. J. Neurosci. 32:14722–14728. doi:10.1523/JNEUROSCI.1240-12.2012.

van der Vaart, B., C. Manatschal, I. Grigoriev, V. Olieric, S.M. Gouveia, S. Bjelić, J. Demmers, I. Vorobjev, C.C. Hoogenraad, M.O. Steinmetz, and A. Akhmanova. 2011. SLAIN2 links microtubule plus end-tracking proteins and controls microtubule growth in interphase. J. Cell Biol. 193:1083–1099. doi:10.1083/jcb.201012179.

van der Vaart, B., W.E. van Riel, H. Doodhi, J.T. Kevenaar, E.A. Katrukha, L. Gumy, B.P. Bouchet, I. Grigoriev, S.A. Spangler, K. Lou Yu, P.S. Wulf, J. Wu, G. Lansbergen, E.Y. van Battum, R.J. Pasterkamp, Y. Mimori-Kiyosue, J. Demmers, N. Olieric, I. V. Maly, C.C. Hoogenraad, and A. Akhmanova. 2013. CFEOM1-associated kinesin KIF21A is a cortical microtubule growth inhibitor. Dev. Cell. 27:145–160. doi:10.1016/j.devcel.2013.09.010.

VanBuren, V., D.J. Odde, and L. Cassimeris. 2002. Estimates of lateral and longitudinal bond energies within the microtubule lattice. Proc. Natl. Acad. Sci. 99:6035–6040. doi:10.1073/pnas.092504999.

Vemu, A., E. Szczesna, E.A. Zehr, J.O. Spector, N. Grigorieff, A.M. Deaconescu, and A. Roll-Mecak. 2018. Severing enzymes amplify microtubule arrays through lattice GTP-tubulin incorporation. Science (80-.). 361:eaau1504. doi:10.1126/science.aau1504.

Vitre, B., F.M. Coquelle, C. Heichette, C. Garnier, D. Chrétien, and I. Arnal. 2008. EB1 regulates microtubule dynamics and tubulin sheet closure in vitro. Nat. Cell Biol. 10:415–421. doi:10.1038/ncb1703.

Wang, Z., T. Wu, L. Shi, L. Zhang, W. Zheng, J.Y. Qu, R. Niu, and R.Z. Qi. 2010. Conserved motif of CDK5RAP2 mediates its localization to centrosomes and the Golgi complex. J. Biol. Chem. 285:22658–22665. doi:10.1074/jbc.M110.105965.

Wegner, A. 1976. Head to Tail Poloymerization of Actin. J. Mol. Biol. 108:139–150. doi:10.1016/S0022-2836(76)80100-3.

Weisbrich, A., S. Honnappa, R. Jaussi, O. Okhrimenko, D. Frey, I. Jelesarov, A. Akhmanova, and M.O. Steinmetz. 2007. Structure-function relationship of CAP-Gly domains. Nat Struct Mol Biol. 14:959–967. doi:10.1038/

nsmb1291.
Widlund, P.O., J.H. Stear, A. Pozniakovsky, M. Zanic, S. Reber, G.J. Brouhard, A.A. Hyman, and J. Howard. 2011. XMAP215 polymerase activity is built by combining multiple tubulin-binding TOG domains and a basic lattice-binding region. Proc. Natl. Acad. Sci. U. S. A. 108:2741–2746. doi:10.1073/pnas.1016498108.
Van De Willige, D., C.C. Hoogenraad, and A. Akhmanova. 2016. Microtubule plus-end tracking proteins in neuronal development. Cell. Mol. Life Sci. 73:2053–2077. doi:10.1007/s00018-016-2168-3.
Woodruff, J.B., B. Ferreira Gomes, P.O. Widlund, J. Mahamid, A. Honigmann, and A.A. Hyman. 2017. The Centrosome Is a Selective Condensate that Nucleates Microtubules by Concentrating Tubulin. Cell. 169:1066-1077.e10. doi:10.1016/j.cell.2017.05.028.
Wu, J., C. de Heus, Q. Liu, B.P. Bouchet, I. Noordstra, K. Jiang, S. Hua, M. Martin, C. Yang, I. Grigoriev, E.A. Katrukha, A.F.M. Altelaar, C.C. Hoogenraad, R.Z. Qi, J. Klumperman, and A. Akhmanova. 2016. Molecular Pathway of Microtubule Organization at the Golgi Apparatus. Dev. Cell. 1–17. doi:10.1016/j.devcel.2016.08.009.
Xin, D., L. Fangfang, S. Lei, L. Min, L. Dengwen, S. Dan, Z. Zhengmao, D. Jintang, F. Li, and Z. Jun. 2010. oncogenic function of microtubule end-binding protein 1 in breast cancer. J. Pathol. 220:361–396. doi:10.1002/path.2662.
Xu, Z., L. Schaedel, M.P. Marinkovich, J. Gaillard, and M. V. Nachury. 2018. Microtubules acquire resistance from mechanical breakage through intralumenal acetylation. Science (80-.). 356:328–332. doi:10.1126/science.aai8764.
Yang, C., J. Wu, C. de Heus, I. Grigoriev, N. Liv, Y. Yao, I. Smal, E. Meijering, J. Klumperman, R.Z. Qi, and A. Akhmanova. 2017. EB1 and EB3 regulate microtubule minus end organization and Golgi morphology. J. Cell Biol. 216:3179–3198. doi:https://doi.org/10.1083/jcb.201701024.
Young, R.E., and S.R. Bisgrove. 2011. Microtubule Plus End-Tracking Proteins and Their Activities in Plants. In The Plant Cytoskeleton. B. Liu, editor. Springer New York, New York, NY. 95–117.
Yu, N., L. Signorile, S. Basu, S. Ottema, J.H.G. Lebbink, K. Leslie, I. Smal, D. Dekkers, J. Demmers, and N. Galjart. 2016. Isolation of Functional Tubulin Dimers and of Tubulin-Associated Proteins from Mammalian Cells. Curr. Biol. 26:1728–1736. doi:10.1016/j.cub.2016.04.069.
Zanic, M., J.H. Stear, A.A. Hyman, and J. Howard. 2009. EB1 recognizes the nucleotide state of tubulin in the microtubule lattice. PLoS One. 4:1–5. doi:10.1371/journal.pone.0007585.
Zanic, M., P.O. Widlund, A. a Hyman, and J. Howard. 2013. Synergy between XMAP215 and EB1 increases microtubule growth rates to physiological levels. Nat. Cell Biol. 15:1–8. doi:10.1038/ncb2744.
Zaoui, K., S. Duhamel, C.A. Parachoniak, and M. Park. 2019. CLIP-170 spatially modulates receptor tyrosine kinase recycling to coordinate cell migration. Traffic. 20:187–201. doi:10.1111/tra.12629.
Zeng, M., Y. Shang, Y. Araki, T. Guo, R.L. Huganir, and M. Zhang. 2016. Phase Transition in Postsynaptic Densities Underlies Formation of Synaptic Complexes and Synaptic Plasticity. Cell. 166:1163-1175.e12. doi:10.1016/j.cell.2016.07.008.
Zhang, R., G.M. Alushin, A. Brown, and E. Nogales. 2015. Mechanistic origin of microtubule dynamic instability and its modulation by EB proteins. Cell. 162:849–859. doi:10.1016/j.cell.2015.07.012.
Zhang, R., B. LaFrance, and E. Nogales. 2018. Separating the effects of nucleotide and EB binding on microtubule structure. Proc. Natl. Acad. Sci. 115:E6191–E6200. doi:10.1073/pnas.1802637115.
Zimmerman, W.C., J. Sillibourne, J. Rosa, and S.J. Doxsey. 2004. Mitosis-specific Anchoring of γ Tubulin Complexes by Pericentrin Controls Spindle Organization and Mitotic Entry. Mol. Biol. Cell. 15:3642–3657. doi:10.1091/mbc.E03.
Zimniak, T., K. Stengl, K. Mechtler, and S. Westermann. 2009. Phosphoregulation of the budding yeast EB1 homologue Bim1p by Aurora/Ipl1p. J. Cell Biol. 186:379–391. doi:10.1083/jcb.200901036.
Zwicker, D., M. Decker, S. Jaensch, A.A. Hyman, and F. Jülicher. 2014. Centrosomes are autocatalytic droplets of pericentriolar material organized by centrioles. Proc. Natl. Acad. Sci. U. S. A. 111:E2636-2645. doi:10.1073/pnas.1404855111. Figure 3. A scheme of the domain organization of EB, SLAIN2, chTOG, CLASP and CLIP170 and their interactions.

2

EB1 and EB3 regulate microtubule minus end organization and Golgi morphology

Chao Yang [1*], Jingchao Wu [1*], Cecilia de Heus [3], Ilya Grigoriev [1], Nalan Liv[3], Yao Yao [4], Ihor Smal [4], Erik Meijering[4], Judith Klumperman[3], Robert Z. Qi [2] and Anna Akhmanova [1#]

J Cell Biol (2017) 216 (10): 3179-3198.

[1] Cell Biology, Department of Biology, Faculty of Science, Utrecht University, Padualaan 8, 3584 CH Utrecht, the Netherlands

[2] Division of Life Science, The Hong Kong University of Science and Technology, Clear Water Bay, Kowloon, Hong Kong, China

[3] Department of Cell Biology, Center for Molecular Medicine, University Medical Center Utrecht, Heidelberglaan 100, 3584CX, Utrecht, the Netherlands.

[4] Departments of Medical Informatics and Radiology, Biomedical Imaging Group Rotterdam, Erasmus University Medical Center, 2040, 3000 CA, Rotterdam, the Netherlands.

* These authors contributed equally to this paper

Corresponding author: a.akhmanova@uu.nl

EB1 and EB3 regulate microtubule minus end organization and Golgi morphology

Chao Yang,[1]* Jingchao Wu,[1]* Cecilia de Heus,[2] Ilya Grigoriev,[1] Nalan Liv,[2] Yao Yao,[4,5] Ihor Smal,[4,5] Erik Meijering,[4,5] Judith Klumperman,[2] Robert Z. Qi,[3] and Anna Akhmanova[1]

[1]Cell Biology, Department of Biology, Faculty of Science, Utrecht University, Utrecht, Netherlands
[2]Department of Cell Biology, Center for Molecular Medicine, University Medical Center Utrecht, Utrecht, Netherlands
[3]Division of Life Science, The Hong Kong University of Science and Technology, Kowloon, Hong Kong, China
[4]Department of Medical Informatics and [5]Department of Radiology, Biomedical Imaging Group Rotterdam, Erasmus University Medical Center, Rotterdam, Netherlands

End-binding proteins (EBs) are the core components of microtubule plus end tracking protein complexes, but it is currently unknown whether they are essential for mammalian microtubule organization. Here, by using CRISPR/Cas9-mediated knockout technology, we generated stable cell lines lacking EB2 and EB3 and the C-terminal partner-binding half of EB1. These cell lines show only mild defects in cell division and microtubule polymerization. However, the length of CAMSAP2-decorated stretches at noncentrosomal microtubule minus ends in these cells is reduced, microtubules are detached from Golgi membranes, and the Golgi complex is more compact. Coorganization of microtubules and Golgi membranes depends on the EB1/EB3–myomegalin complex, which acts as membrane–microtubule tether and counteracts tight clustering of individual Golgi stacks. Disruption of EB1 and EB3 also perturbs cell migration, polarity, and the distribution of focal adhesions. EB1 and EB3 thus affect multiple interphase processes and have a major impact on microtubule minus end organization.

Introduction

Microtubules (MTs) are dynamic polymers essential for cell division, organization of intracellular compartments, and cell polarity. Many MT-associated processes critically depend on the proteins that bind to the two MT ends, the plus and minus ends, which have different growth rates and cellular functions (Howard and Hyman, 2003; Akhmanova and Steinmetz, 2015). MT plus ends polymerize rapidly in vitro; in cells, they are the sites where MT elongation takes place. MT minus ends grow slowly in vitro and in cells are often anchored to MT organizing centers (MTOCs). Until recently, it was believed that in cells, MT minus ends do not grow. However, studies of calmodulin-regulated spectrin-associated (CAMSAP)/Patronin proteins showed that they can recognize and protect free MT minus ends by decorating stretches of MT lattice formed by minus end polymerization (Goodwin and Vale, 2010; Hendershott and Vale, 2014; Jiang et al., 2014), thus demonstrating that MT minus end growth is a physiologically important process.

Growing MT ends accumulate a rich collection of proteins that are termed MT plus end tracking proteins, or +TIPs (Schuyler and Pellman, 2001; Akhmanova and Steinmetz, 2008). The core components of +TIP complexes are the members of end-binding (EB) family, which recognize growing MT ends by sensing the nucleotide state of tubulin through their N-terminal calponin homology (CH) domains (Maurer et al., 2012). The C-terminal part of EBs consists of a dimeric parallel coiled coil, which ends with a four-helix bundle, and an acidic tail similar to the tail of α-tubulin (Akhmanova and Steinmetz, 2008). The C-terminal EB domain is responsible for binding to numerous partners, which fall into two major structural classes: cytoskeleton-associated protein glycine-rich (CAP-Gly) domain proteins and proteins containing SxIP (Ser-any amino acid-Ile-Pro) motifs (Kumar and Wittmann, 2012; Akhmanova and Steinmetz, 2015). EB partners can either promote or restrict MT growth and regulate MT interactions with different cell components (Kumar and Wittmann, 2012; Akhmanova and Steinmetz, 2015).

Mammalian cells typically coexpress three members of the EB family, EB1, EB2, and EB3, and although these proteins have been knocked down individually or in combinations (Straube and Merdes, 2007; Toyoshima and Nishida, 2007; Komarova et al., 2009; Nakamura et al., 2012; Ferreira et al., 2013; Yue et al., 2014), the impact of disruption of all three EBs on MT organization and dynamics has not been described. Here, we made use of the CRISPR/Cas9 technology to stably mutate all three mammalian EB-encoding genes. These mutations

*C. Yang and J. Wu contributed equally to this paper.

Correspondence to Anna Akhmanova: a.akhmanova@uu.nl

Abbreviations used: CAMSAP, calmodulin-regulated spectrin-associated protein; CH, calponin homology; EB, end-binding; FA, focal adhesion; HEK, human embryonic kidney; MMG, myomegalin; MT, microtubule; MTOC, MT organizing center; PCM, pericentriolar material; RPE, retinal pigment epithelium.

disrupted the CH domains of EB2 and EB3 and abrogated C-terminal partner-binding half of EB1. The EB mutant cell lines displayed only minor defects in cell division and MT plus end polymerization but had strongly perturbed organization of noncentrosomal MTs. In the studied cell lines, MT minus ends that are not attached to the centrosome are stabilized by CAMSAP2, and many of them are tethered to the Golgi apparatus. Disruption of EB1 and EB3 led to shortening of CAM SAP2-decorated MT minus end stretches, their detachment from the Golgi, and Golgi compaction. Furthermore, we found that the mutation of EB1 and EB3 affected cell migration on 2D substrates and invasion in 3D matrix. Our results thus show that EB proteins control different aspects of interphase mammalian cell architecture and have an unexpectedly large impact on the organization of MT minus ends.

Results

Human cell lines with disrupted EB1 and EB3 are viable

To generate triple EB mutant cells, we first tested the efficiency of individual gRNAs targeting EB-encoding genes in HeLa cells using staining with antibodies against the C-terminal halves of EBs (Stepanova et al., 2003; Komarova et al., 2005). Complete loss of EB2 and EB3 reactivity was found with gRNA constructs targeting the N-terminal extension preceding the CH domain of EB2 and the N-terminal part of the CH domain of EB3 (Fig. 1 A and Table S1). In contrast, the EB1-specific gRNA constructs targeting the CH domain were not effective, and we therefore used a construct with a target site after the CH domain (Fig. 1 A and Table S1). We then simultaneously transfected the three EB-targeting constructs into HeLa cells; among 51 clones, we obtained four stable lines that were negative for all three EBs (termed EB1/2/3mut) and analyzed further two of these lines (Fig. 1, B and C). Sequencing showed the presence of deletions or frameshift mutations close to the gRNA targeting sites in all EB-encoding genes (Table S1). The disruption of EB1-encoding gene occurred downstream of the CH domain, thus deleting the C-terminal half of the protein, which is responsible for dimerization, partner binding, and reactivity with the existing EB1-specific antibodies, while the residual CH-domain-containing EB1 fragment might still be expressed and exert some MT-dependent or independent functions. When examined as a GFP fusion, this fragment displayed weak MT binding (Fig. S1 A). Mutations that perturbed EB2 and EB3 sequences were located upstream or within the N-terminal part of the CH domain and can be expected to prevent MT localization (see Fig. S1 A for the illustration of a diffuse distribution of an N-terminal EB3 fragment with an incomplete CH domain). Because the antibodies we used react with the C-terminal EB regions, these clones likely completely lack EB2 and EB3 function.

We have also attempted to simultaneously perturb all three EB-encoding genes in retinal pigment epithelium (RPE1) and HT1080 fibrosarcoma cells but obtained no triple mutants. From 39 clones, we obtained a single RPE1 line lacking both EB1 and EB3 reactivity (termed EB1/3mut; Fig. 1 B). Although the expression of MT plus end–associated EB2 was maintained in this cell line (Fig. 1, B and C), both EB2 gene copies contained a single nucleotide insertion (Table S1), and we observed an EB2-specific band of a smaller size (Fig. 1 B). The presence of this band could be explained by translation initiation from the start codon at the N terminus of the CH domain (Fig. 1 A), as the N-terminal EB2-specific extension has no major impact on MT plus end tracking (Komarova et al., 2009). Furthermore, by simultaneously targeting only the EB1 and EB3-encoding genes, we obtained two HT1080 cell lines lacking both EB1 and EB3 reactivity (Fig. 1, B and C). In both RPE1 and HT1080 cells with mutated EB1 and EB3, EB2 was concentrated more strongly at the outmost MT tips (Fig. 1, C and F), in agreement with the data obtained using RNAi (Komarova et al., 2009). These data support the notion that EBs compete for MT plus ends, with EB2 having lower affinity than EB1 and EB3.

Mitotic index was mildly elevated in HeLa EB1/2/3mut and HT1080 EB1/3mut cells but not in EB1/3mut RPE1 cells (Fig. 1 D and Fig. S1 B). siRNA-mediated depletion of EB2 in EB1/3mut RPE1 cells revealed no additional effects on cell proliferation or division (Fig. S1, C–E). We thus have no explanation for our failure to obtain a triple EB mutant in this cell line.

Analysis of the HeLa EB1/2/3mut cells revealed no striking deviations in the morphology of mitotic spindles and showed that the elevation of the mitotic index was likely due to a prometaphase delay (Fig. 1 E and Fig. S2 A). These results are consistent with previous studies, which showed that knockdown or abnormal expression of individual EB proteins can cause spindle abnormalities but does not block mitotic progression (Green et al., 2005; Draviam et al., 2006; Toyoshima and Nishida, 2007; Ban et al., 2009; Xia et al., 2012; Ferreira et al., 2013; Iimori et al., 2016). In our cell lines, we observed some, but not all, of these abnormalities. For example, although we found no delay in cytokinesis, we did observe that the time interval between spreading of two daughter cells after mitotic exit was significantly increased (Fig. S2, B and C), as described previously for EB3 depletion (Ferreira et al., 2013). However, the EB1/2/3mut HeLa cells showed no reduction of Ska1 localization the mitotic spindle (Fig. S2, D and E), in contrast to the phenotype of acute EB1 depletion (Thomas et al., 2016). These differences are likely due to the fact that the isolation of stable cell lines can result in selection for compensatory mutations. Collectively, our results suggest that proliferating mammalian cells can adapt to the loss of function of all three full-length EBs.

EB1 and EB3 regulate +TIP accumulation at MT plus ends

EB proteins are well known to recruit other +TIPs to MT plus ends, with EB1 and EB3 having higher affinity for some partner proteins compared with EB2 (Akhmanova and Steinmetz, 2008; Bjelić et al., 2012; Jiang et al., 2012; Liu et al., 2015). However, because SxIP and CAP-Gly binding sites are conserved in all three EBs, the contribution of EB2 to +TIP localization remained unclear. The generation of a HeLa EB1/2/3mut cells allowed us to address this question unambiguously. In contrast to control cells, EB1/2/3mut cells lacked enrichment of a CAP-Gly domain–containing protein CLIP-170 and an SxIP-containing protein CLASP1 at MT plus ends; this enrichment could be restored by expressing untagged EB1 or EB3, but not EB2, although all three EBs showed nice MT plus end localization (Fig. 2, A–D). EB2 is thus unable to promote localization of canonical EB-dependent +TIPs CLIP-170 and CLASP1 to MT plus ends.

We also investigated the localization of the MT polymerase ch-TOG, which can recognize MT plus ends autonomously but can also be recruited to them by the SxIP protein SLAIN2 (Brouhard et al., 2008; van der Vaart et al., 2011). ch-TOG localizes as dots at the outmost MT plus ends (Nakamura et al., 2012;

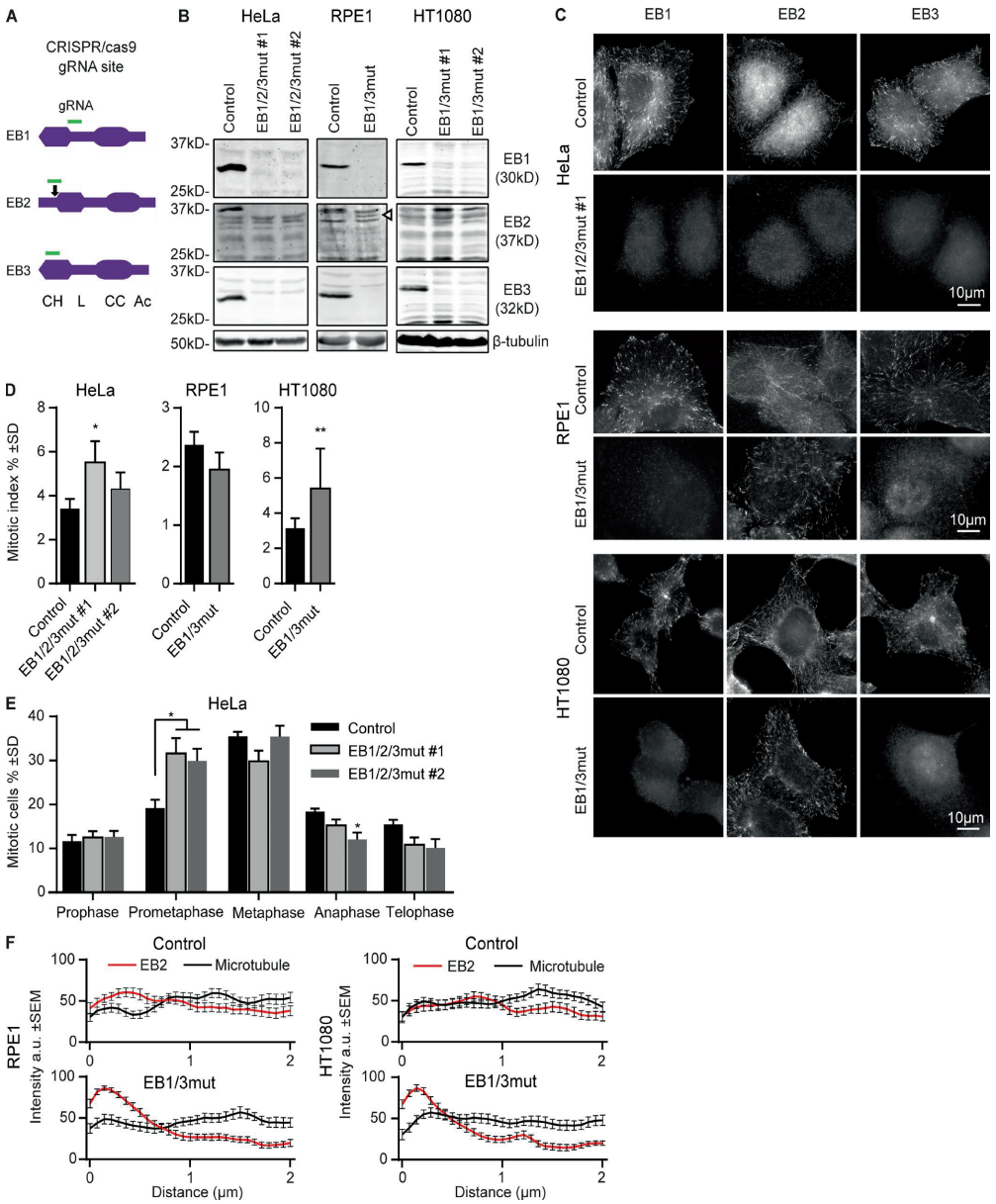

Figure 1. **Characterization of cell lines with disrupted EB-encoding genes.** (A) Schemes of EB1, EB2, and EB3 proteins and the position of gRNA sequences. Arrow indicates the in-frame Met at the beginning of the EB2 CH domain. (B and C) Western blot analysis and immunostaining of control and the EB mutant cells with the indicated antibodies. (D and E) Quantification of the mitotic index and mitotic stages in the indicated cell lines. (D) $n \geq 3$ and (E) $n = 4$ experiments, with 3,000 cells each. (F) Mean intensity of EB2 and α-tubulin staining starting from the MT tip (0); 26–28 MT ends analyzed per condition from 6–10 cells. *, $P < 0.05$; **, $P < 0.01$ (Mann-Whitney *U* test).

Maurer et al., 2014), and this localization is easier to observe when the ch-TOG–GFP fusion is expressed in cells depleted of endogenous ch-TOG (Gutiérrez-Caballero et al., 2015). Using this approach, we found that ch-TOG-GFP can be clearly detected at the plus ends of both control and EB1/2/3mut HeLa cells (Fig. 2, E and F), in agreement with the previous results

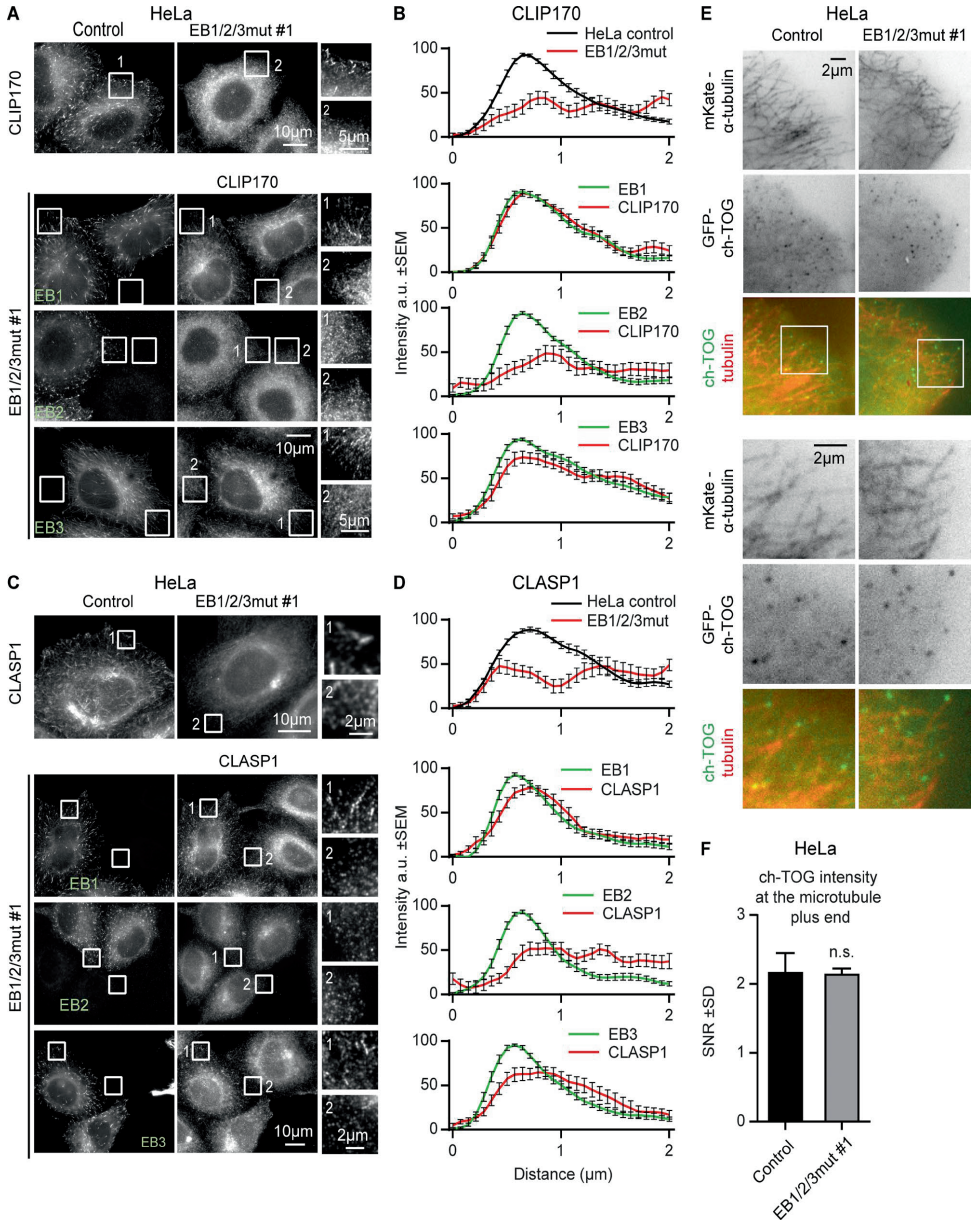

Figure 2. **Effect of EB disruption on +TIP localization.** (A and C) Immunostaining for CLIP170 and CLASP1 in control and EB1/2/3mut HeLa cells expressing the indicated constructs. Enlargements of the boxed areas indicated by numbers are shown on the right. In C, cells were incubated with the GSK3 inhibitor SB415286 (20 µM) for 30 min before fixation. (B and D) Averaged intensities of staining for the indicated +TIP obtained for 20–24 MT ends per condition. MT end position (0) was determined by staining for β-tubulin. (E and F) Live images of the indicated cell lines transfected with ch-TOG-GFP together with mKate-α-tubulin (larger and smaller fields of view shown; E) and quantification of ch-TOG signal-to-noise ratio at MT tips (F). *n* = 30 cells in three independent experiments. Mann-Whitney *U* test.

on EB1 and EB3 depletion (Gutiérrez-Caballero et al., 2015). These data confirm that ch-TOG binding to MT plus ends does not require EB-dependent +TIPs, although the association with SLAIN2 might offer ch-TOG a competitive advantage when MT ends are crowded by EBs and their partners.

EB1 and EB3 support rapid processive MT growth

Previous work in CHO cells showed that simultaneous depletion of EB1 and EB3 had no effect on MT growth rate but increased catastrophe frequency, while in vitro, EBs increase MT growth rate, promote catastrophes, and can strongly synergize with the ch-TOG homologue XMAP215 to increase MT polymerization rate (Komarova et al., 2009; Zanic et al., 2013). Analysis of MT dynamics using β-tubulin–GFP as a marker in HeLa cells partially confirmed our previous observations by showing that the mutation of all three EBs led to increased catastrophe frequency (Fig. 3, A and B). Furthermore, we did observe an ∼25% reduction in MT growth rate (Fig. 3, A and B). Increased MT catastrophe frequency was accompanied by a higher rescue frequency (Fig. 3, A and B), similar to what we previously observed in cells depleted of SLAIN2 or ch-TOG, in which both growth and shortening episodes became more interrupted (van der Vaart et al., 2011). MT depolymerization rate was reduced (Fig. 3, A and B), possibly because the most rapid depolymerization rates are observed during long shrinkage events, and such events were less frequent at higher rescue frequency.

To test which EBs and which domains of EBs are important for regulating MT growth, we performed rescue experiments with EB–GFP fusions and used comets formed by these proteins as readout (Fig. 3, C and D). We observed a good match between the data obtained with fluorescent tubulin and EB1-GFP or EB3-GFP in control cells (Fig. 3 E). MT polymerization rate could be restored by all three EBs, including EB2, as well as by a dimeric EB3 construct, EB3-NL-LZ, in which the whole C-terminal partner-binding domain was substituted with a dimeric coiled coil (leucine zipper) of GCN4 (Fig. 3, C–E). These data suggest that the N-terminal CH domain of EB3 with the adjacent linker region (termed NL), which is sufficient for efficient MT binding (Komarova et al., 2009; Zimniak et al., 2009), can regulate MT growth rate in cells. The protein does need to be in a dimeric configuration, as the monomeric version of the same protein could not fully rescue growth velocity (Fig. 3, C–E), possibly because CH domain dimerization increases protein affinity for MT tips or affects their conformation. It should be noted that because our EB1/2/3mut cells are possibly already expressing monomeric CH domain of EB1, the expression of EB3-NL monomer might have little additional impact.

Strikingly, although EB2 could restore MT growth rate, it could not rescue growth processivity (Fig. 3, C–E), in agreement with our previous data (Komarova et al., 2009). EB3-NL-LZ also failed to suppress catastrophes, and even more interrupted MT growth was observed upon expression of EB3-NL monomer (Fig. 3, C–E). Together, these data suggest that the acceleration of MT growth might mostly depend on the efficient EB binding to the MT tip, whereas catastrophe suppression requires recruitment of EB partners.

EB1 and EB3 are required for coorganization of MTs and the Golgi apparatus

Next, we examined the organization of MT network in EB1/2/3mut cells. Importantly, in HeLa cells the centrosome does not play a dominant role in organizing interphase MTs, except for the G2 phase (Lansbergen et al., 2006; Jeffery et al., 2013), but a high MT density is observed in the Golgi area (Mimori-Kiyosue et al., 2005; Sato et al., 2014). We found that the major impact of the triple EB mutation was on the arrangement of MT minus ends, as the Golgi-associated accumulation of noncentrosomal MTs was lost and the MTs became randomly distributed in the cytoplasm (Fig. 4 A). Loss of MT density at the Golgi could also be clearly observed in RPE1 and HT1080 EB1/3mut cells (Fig. 4 B and Fig. S3, A and B). However, in these cell lines MT disorganization was not as profound, because unlike HeLa cells, they have many centrosomally anchored MTs that were retained in EB1/3mut cells. The loss of Golgi-associated MTs had a strong impact on the area occupied by the Golgi apparatus, which was significantly diminished in both EB1/2/3mut HeLa cells and EB1/3mut RPE1 cells. Both the disorganization of MTs and overcompaction of the Golgi could be fully reversed by expressing EB1-GFP and EB3-GFP but not by EB2-GFP (Fig. 4, C–G; rescue with EB2-GFP was included also in EB1/3mut cells because EB2 gene is mutated in this clone [Fig. 1 B]). To characterize Golgi overcompaction in more detail, we used EM and found that the morphology and size of the individual Golgi stacks were very similar in control and EB1/3mut RPE1 cells, but the area occupied by the Golgi stacks was reduced in the mutant (Fig. 4, H and I; and Fig. S3 C).

Our recent study showed that the attachment of noncentrosomal MTs to the Golgi depends on the interaction of the minus end decorating protein CAMSAP2 with the complex of myomegalin (MMG) and AKAP450 (Wu et al., 2016), a large scaffolding protein recruited to the Golgi membranes by the Golgi matrix protein GM130 (Hurtado et al., 2011). We examined the distribution of CAMSAP2 in EB1/2/3mut cells and found that it was affected in two ways: the stretches of CAMSAP2-decorated MT lattice became significantly shorter and were redistributed from the central part of the cell to the cell periphery (Fig. 5, A, B, and G). A similar phenotype was also observed in RPE1 and HT1080 EB1/3mut cells (Fig. 5, C, D, and H; and Fig. S3 D). Shortening of CAMSAP2-decorated stretches in EB1/3mut cells was not due to the reduction of CAMSAP2 expression (Fig. S3 E) or their detachment from Golgi, because in cells lacking AKAP450 or MMG, two proteins required for MT minus end tethering to Golgi membranes (Wu et al., 2016), CAMSAP2-bound MT segments were even slightly longer than in control (Fig. 5 H). Importantly, both the length and the localization of CAMSAP2 stretches could be fully rescued by expressing EB1-GFP or EB3-GFP, but not by EB2-GFP in both HeLa 1/2/3mut cells and RPE1 EB1/3mut cells (Fig. 5, E–H; and Fig. S3, F and G). EB1 and EB3, but not EB2, thus control the length of CAMSAP2-decorated MT minus ends and their attachment to the Golgi.

Coorganization of the Golgi and noncentrosomal MTs depends on the EB–MMG complex

To test which part of the EBs is required for the attachment of noncentrosomal MTs to the Golgi, we used different EB3 mutants. We found that the localization of CAMSAP2 stretches to the Golgi could be rescued by an EB3 mutant lacking the C-terminal tyrosine, which is essential for EB binding to CAP-Gly domains (Honnappa et al., 2006), but not by EB3 mutants, which were unable to bind to SxIP partners either because of the substitutions in the SxIP-binding pocket (the

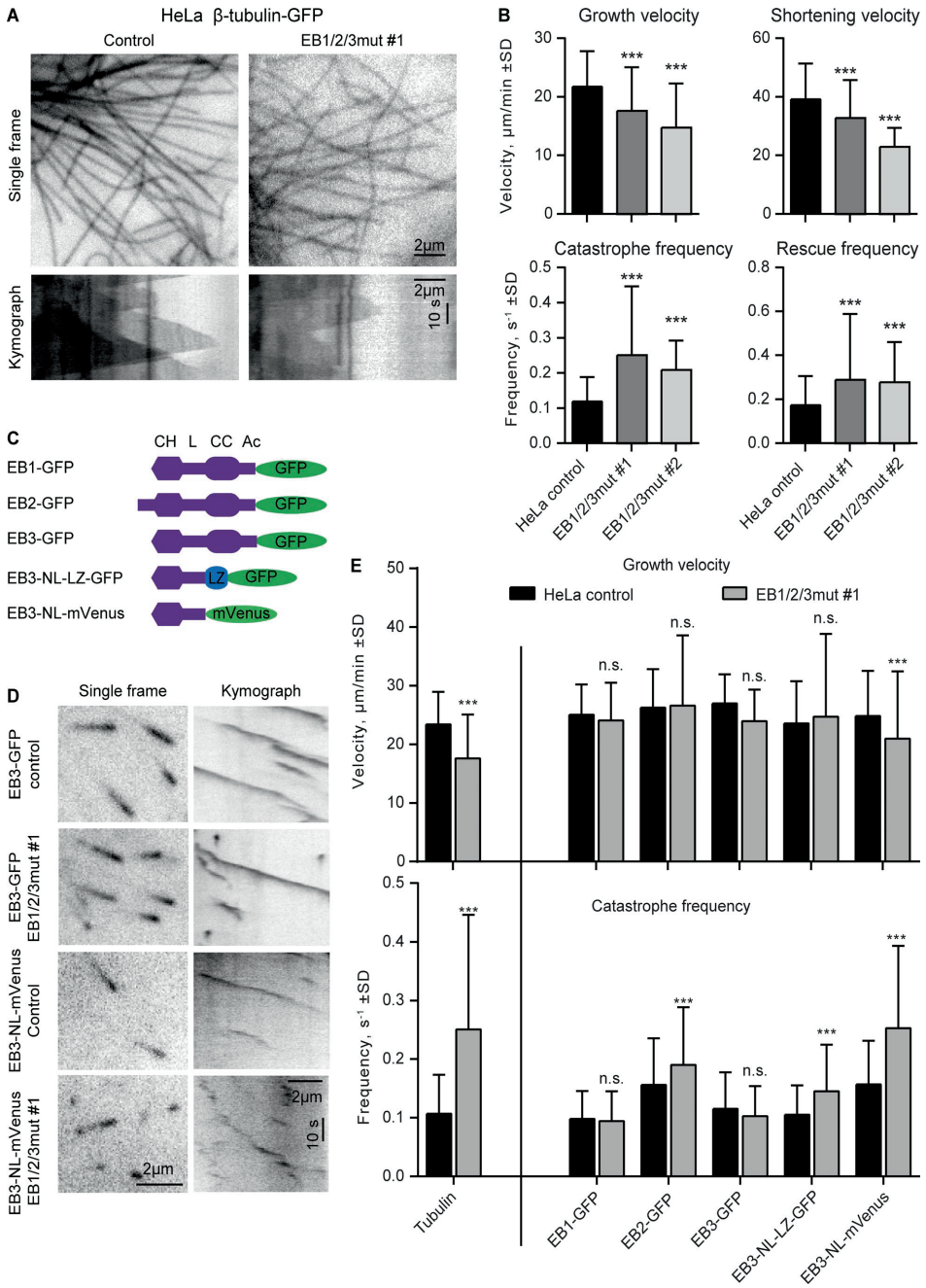

Figure 3. **Effect of EB disruption on MT dynamics.** (A) Single frames and kymographs of MT dynamics in the indicated cell lines transiently transfected with β-tubulin–GFP. (B) Parameters of MT dynamics in the indicated cell lines. 74–240 MT plus ends were analyzed per condition. (C and D) Scheme of the used EB constructs (C) and single frames and kymographs illustrating MT plus end dynamics visualized with the indicated constructs (D). (E) Plots of MT growth velocity and catastrophe frequency. 158–264 MT plus ends were analyzed per condition. ***, P < 0.001 (Mann-Whitney *U* test).

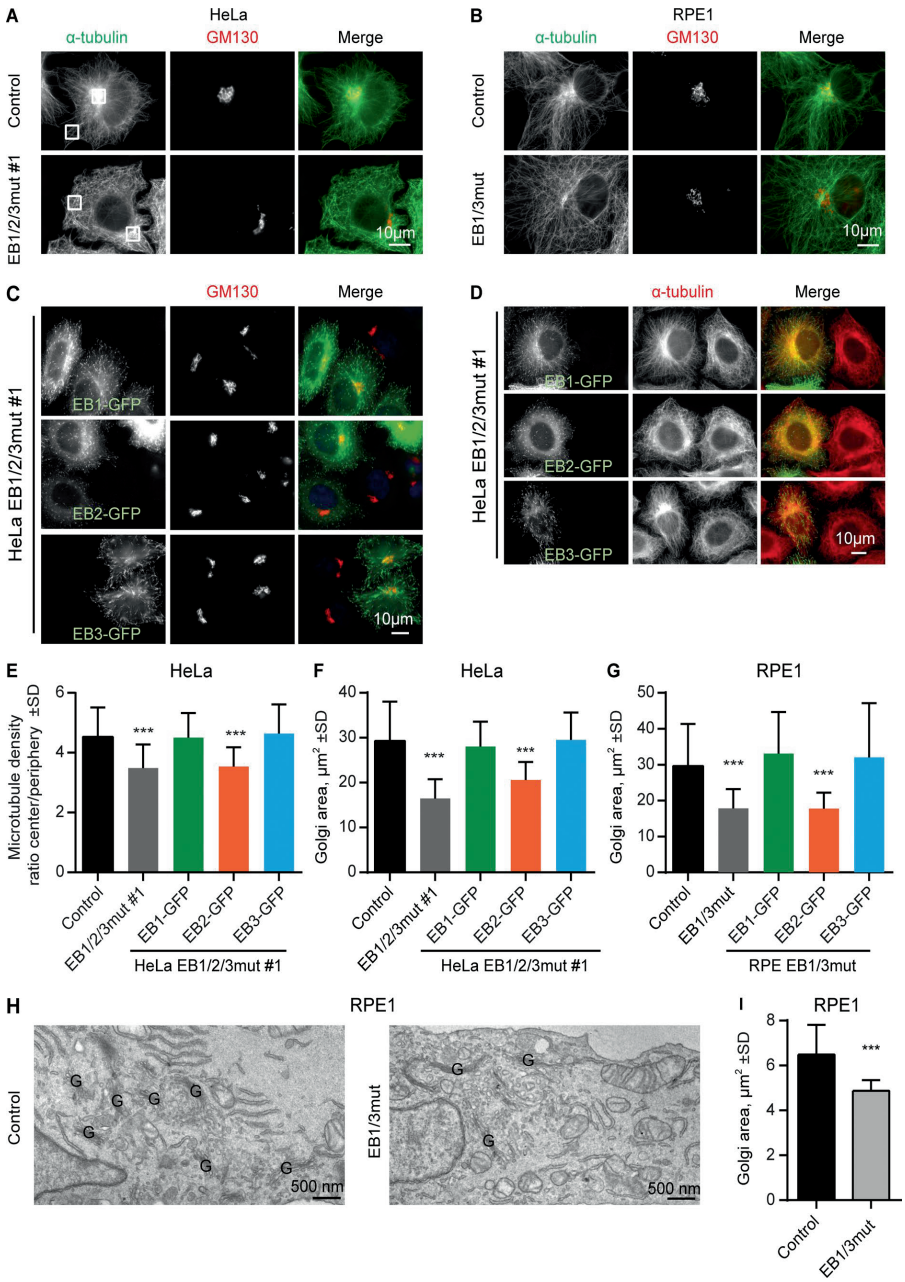

Figure 4. **Effect of EB disruption on MT and Golgi organization.** (A–D) Immunostaining for α-tubulin and GM130 in the indicated cell lines; in C and D, cells were transfected with the indicated EB–GFP fusions. Boxes in A show examples of areas used for quantification in E. (E–G) Quantification of the ratio of MT intensity in the cell center and cell periphery (boxes in A; E) or the Golgi area in the indicated cell lines, transfected with the indicated constructs. *n* = 24–41 cells per condition (E), 31–66 cells (F), and 28–47 cells (G). (H and I) EM images of the Golgi area (Golgi stacks indicated with a G; H) and quantification of the total area occupied by in Golgi stacks (I). *n* = 3 experiments with 50 cells each. ***, P < 0.001 (Mann-Whitney *U* test).

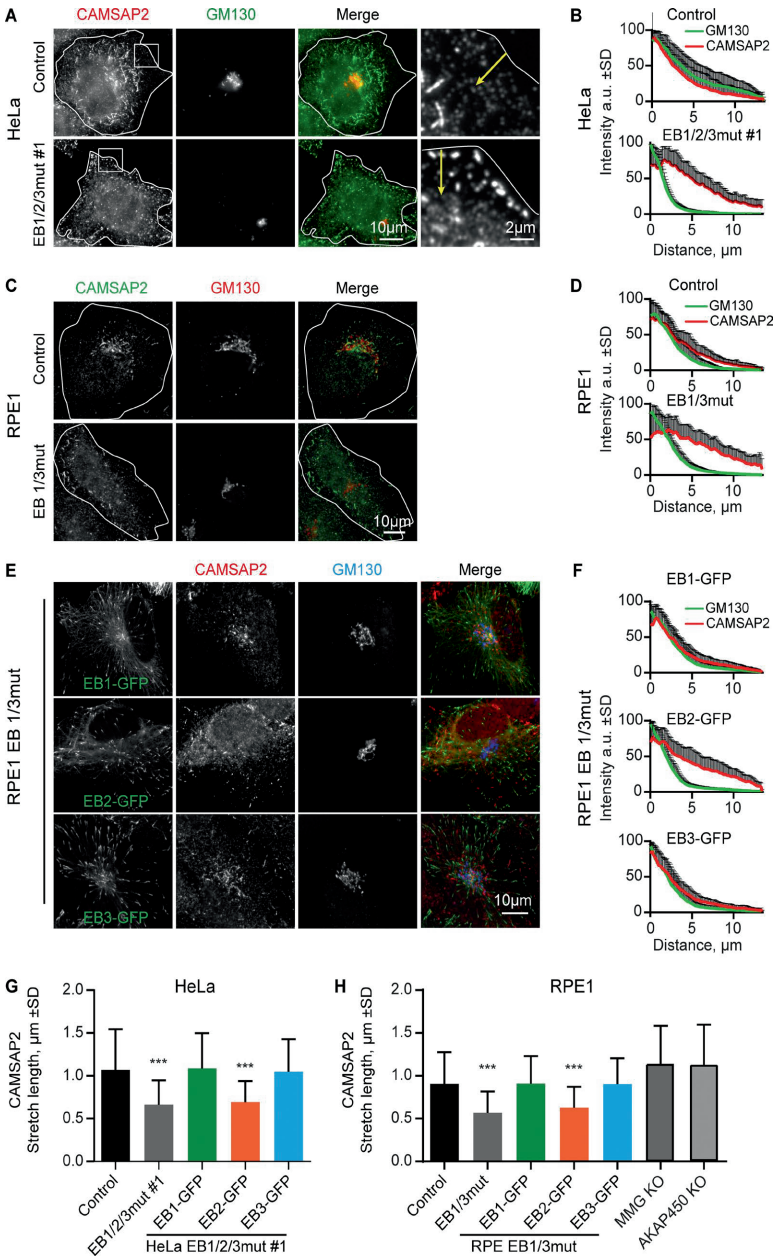

Figure 5. **Distribution of CAMSAP2-decorated MT minus ends in cells with mutated EBs.** (A and C) Immunostaining for CAMSAP2 and GM130 in the indicated cells. Enlargements on the right in A show cell periphery; yellow arrows indicate the 3-µm-broad region used for quantification in Fig. S3 G. (B, D, and F) Averaged intensity distributions for GM130 and CAMSAP2 in the indicated cell lines, either untransfected or transfected with the indicated constructs. Distance from the center of the Golgi is shown on the horizontal axis and normalized fluorescence intensity on the vertical axis. n = 23–43 cells per condition. (E) Immunostaining for CAMSAP2 and GM130 in EB1/3mut RPE1 cells expressing the indicated constructs. (G and H). Quantification of CAMSAP2 stretch length. 1000 stretches in 10 cells were measured per condition, except for MMG and AKAP450 knockout cells (H), for which 200 stretches in 8 and 10 cells were measured. ***, $P < 0.001$ (Mann-Whitney U test).

double Y226A, E234A mutant, termed ΔSxIP) or the deletion of the whole acidic tail region (ΔTail; Montenegro Gouveia et al., 2010; Fig. 6, A and B; and Fig. S4 A). Consistently, GFP-tagged EB1 and EB3, but not EB2, were recruited to Golgi membranes in nocodazole-treated RPE1 EB1/3mut cells in a manner dependent on an intact SxIP- but not the CAP-Gly–binding site (Fig. S4 B).

In vitro binding assays with purified proteins showed that CAMSAP2 does not interact with EBs (Fig. S4 C), excluding direct binding between CAMSAP2 and EBs as the mechanism of MT minus end tethering to the Golgi. We therefore focused our attention on MMG, which is required for MT minus end attachment to the Golgi (Wu et al., 2016), directly interacts with EB1, and recruits it to the Golgi through an SxIP motif SRLP (Roubin et al., 2013; Wang et al., 2014; Fig. 6 C). Knockout of MMG caused detachment of CAMSAP2 stretches from the Golgi, and this defect could be rescued by expressing the N-terminal SRLP-containing portion of MMG (Wu et al., 2016; Fig. 6 D). We disrupted the SRLP site in MMG N terminus by mutating leucine and proline residues to asparagines (LP/NN mutant) and found that these mutations blocked the binding of MMG to EB3 (Fig. 6 E), in agreement with the previously published data on EB1 (Wang et al., 2014). In contrast, the interactions between MMG and AKAP450, which recruits MMG to the Golgi, and the binding of the AKAP450–MMG complex to CAMSAP2 could still occur (Fig. S4, D and E). However, the LP/NN mutant of the MMG N terminus (MMG-1-389-NN) completely failed to rescue localization of CAMSAP2 stretches at the Golgi in MMG knockout cells (Fig. 6, D and F).

We hypothesized that by binding to MMG, EBs create an additional MT-binding site through their CH domain. To prove this idea, we fused either the N- or C-terminal part of EB3 to the MMG N terminus with the mutated SRLP motif (Fig. 6 C). Both fusions localized to the Golgi, and in addition, the N-terminal EB fusion also accumulated at MT plus ends (Fig. 6, A and D; and Fig. S4 A). The Golgi localization of this construct was more obvious in MMG knockout cells, while MT tips were better visible in EB1/3mut cells (Fig. 6, A and D), as could be expected because of the competition with endogenous MMG or EB proteins, respectively. Remarkably, the fusion bearing the N-terminal part of EB3, but not the EB3 C terminus, restored the localization of CAMSAP2 stretches to the Golgi both in MMG knockout and EB1/EB3mut cells (Fig. 6, A, B, D, and F; and Fig. S4 A). Furthermore, a complete rescue of CAMSAP2 stretch localization was also observed by fusing the LP/NN mutant of the MMG N terminus to MT-binding domains of CLIP-115 (a double CAP-Gly motif; Hoogenraad et al., 2000) or the MT-decorating protein MAP7/ensconsin (Faire et al., 1999). Because the latter protein is not a +TIP, these data indicate that the binding of CAMSAP2 stretches to the Golgi requires additional affinity of Golgi membranes for MT shafts but not to their growing ends. This notion was supported by the experiment in which we inhibited MT growth by applying the MT-stabilizing drug paclitaxel and found that the colocalization of CAMSAP2 stretches at the Golgi was preserved (Fig. S5 A). Finally, because EB2 could not be recruited to the Golgi in nocodazole treated cells (Fig. S4 B) and could not restore MT minus end tethering to the Golgi and Golgi morphology in EB knockout cells (Fig. 4, C–G; Fig. 5 E; and Fig. S3, F and G), we hypothesized that EB2 has a lower affinity for MMG compared with EB1 and EB3 and found that this was indeed the case (Fig. 6 G). Collectively, our results indicate that EB1 and EB3 bind to Golgi membranes because their C-terminal domains strongly interact with MMG. At the Golgi, EB1 and EB3 contribute to the tethering of CAMSAP2-decorated MTs, a function that does not strictly depend on the recognition of growing MT ends.

EB-dependent Golgi–MT attachment controls Golgi morphology

The data described above indicate that MT binding of EBs contributes to Golgi–MT tethering. This binding might counteract dynein-mediated Golgi compaction and thus explain why the disruption of EB1 and EB3 leads to reduction of the area occupied by Golgi stacks. In contrast, the Golgi was enlarged in CAMSAP2 knockout cells (Wu et al., 2016), possibly because Golgi-attached free MT minus ends facilitate Golgi self-assembly (Vinogradova et al., 2012). To further explore how EBs and CAMSAP2 regulate Golgi compaction, we generated a triple-mutant line by targeting CAMSAP2 in EB1/3mut RPE1 cells (termed EB1/3/CAMSAP2mut). Also these cells could be stably propagated (Fig. 7 A). They had a centrosomally organized MT system and no MT density in the Golgi area (Fig. 7 B). Interestingly, the centrosome in these cells was surrounded by short compacted MTs (Fig. 7 C), the origin of which is unclear. The Golgi area in EB1/3/CAMSAP2mut cells was smaller than in CAMSAP2 knockout but larger than in EB1/3mut cells (Fig. 7, D and E). The changes in the Golgi area were due to the loss of MT tethering but not because of the inability of Golgi membranes to nucleate MTs, as this function was fully preserved in EB1/3mut and EB1/3/CAMSAP2mut cells (Fig. 7, F and G).

Previously, we observed that MT-dependent extension of Golgi ribbons became more obvious in cells treated with centrinone (Wu et al., 2016), a Plk4 inhibitor that prevents duplication of centrioles and causes centrosome loss (Wong et al., 2015). In RPE1 cells, this drug inhibits cell cycle progression, leading to cell enlargement and Golgi expansion. Centrinone treatment caused centriole loss in >90% of control cells and in 80% of EB1/3mut cells (Fig. 8, A and B). Our previous work showed that centriole depletion led to formation of acentrosomal MT arrays, the organization of which depended on the presence of MT minus end regulators (Wu et al., 2016). In control and CAMSAP2 knockout cells, the Golgi apparatus became the dominant MTOC, likely because of AKAP450-dependent recruitment of γ-tubulin released from the centrosome (Wu et al., 2016). In cells lacking AKAP450 or MMG, loss of centrosomes led to the formation of noncentrosomal MT arrays with the minus ends stabilized by CAMSAP2, while the Golgi was strongly compacted and completely detached from CAMSAP2 stretches and MT density (Wu et al., 2016).

In EB1/3mut cells, a γ-tubulin–positive MTOC was still present in 44% of cells, indicating that a significant part of the cell population had an acentriolar MTOC (Fig. 8, A and B). In the remaining 56% of the cells, a γ-tubulin–positive MTOC was lost, and MTs acquired a semiparallel organization (Fig. 8 C), very similar to what we observed AKAP450 and MMG knockouts (Wu et al., 2016). However, in contrast to AKAP450 and MMG knockouts, Golgi membranes partly overlapped with the area of high MT density (Fig. 8 C). Furthermore, although in centrinone-untreated EB1/3mut cells we observed strong detachment of CAMSAP2 stretches from the Golgi (Fig. 5, A–D), this defect was partially restored after centrinone treatment (Fig. 8, D and E). We noticed that CAMSAP2 stretches became significantly longer after centrinone treatment, and their length

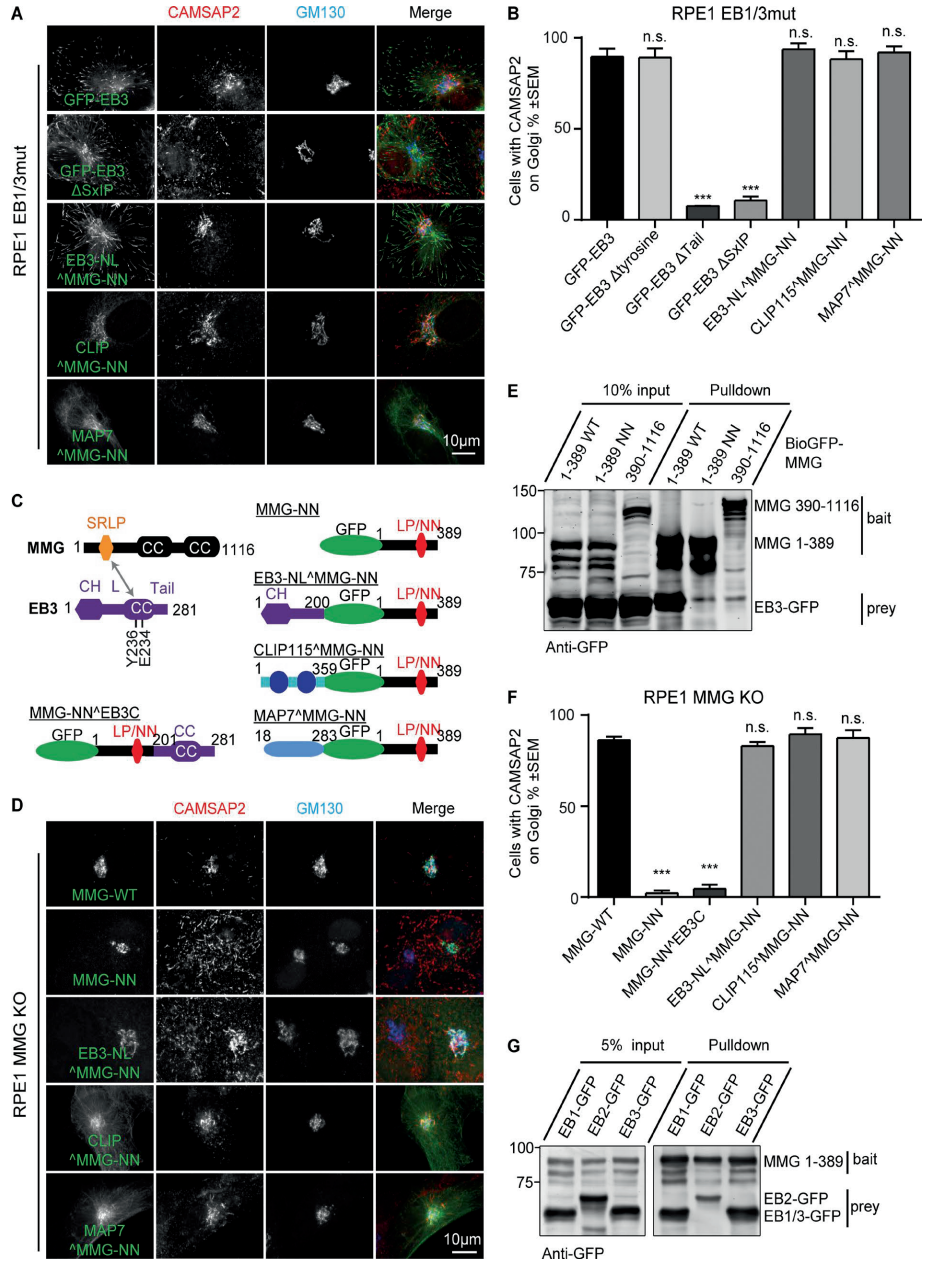

Figure 6. **EB interaction with MMG is required to recruit CAMSAP2 stretches to the Golgi.** (A and D) Immunostaining for CAMSAP2 and GM130 of EB1/3mut (A) or MMG knockout (D) RPE1 cells expressing the indicated constructs. (B and F) Percentage of cells with CAMSAP2 stretches in the Golgi area in EB1/3mut (B) or MMG knockout (F) RPE1 cells expressing the indicated constructs. $n = 77–112$ transfected cells in B and 41–81 transfected cells in F. **, $P < 0.01$; ***, $P < 0.001$ (Student's t test). (C) A scheme of MMG–EB3 interaction and the fusion constructs used. (E and G) Streptavidin pull-down assays with the extracts of HEK293T cells coexpressing the indicated biotinylation tag (Bio)-GFP–MMG fusions, the indicated EB–GFP fusions, and biotin ligase BirA, analyzed by Western blotting with anti-GFP antibodies.

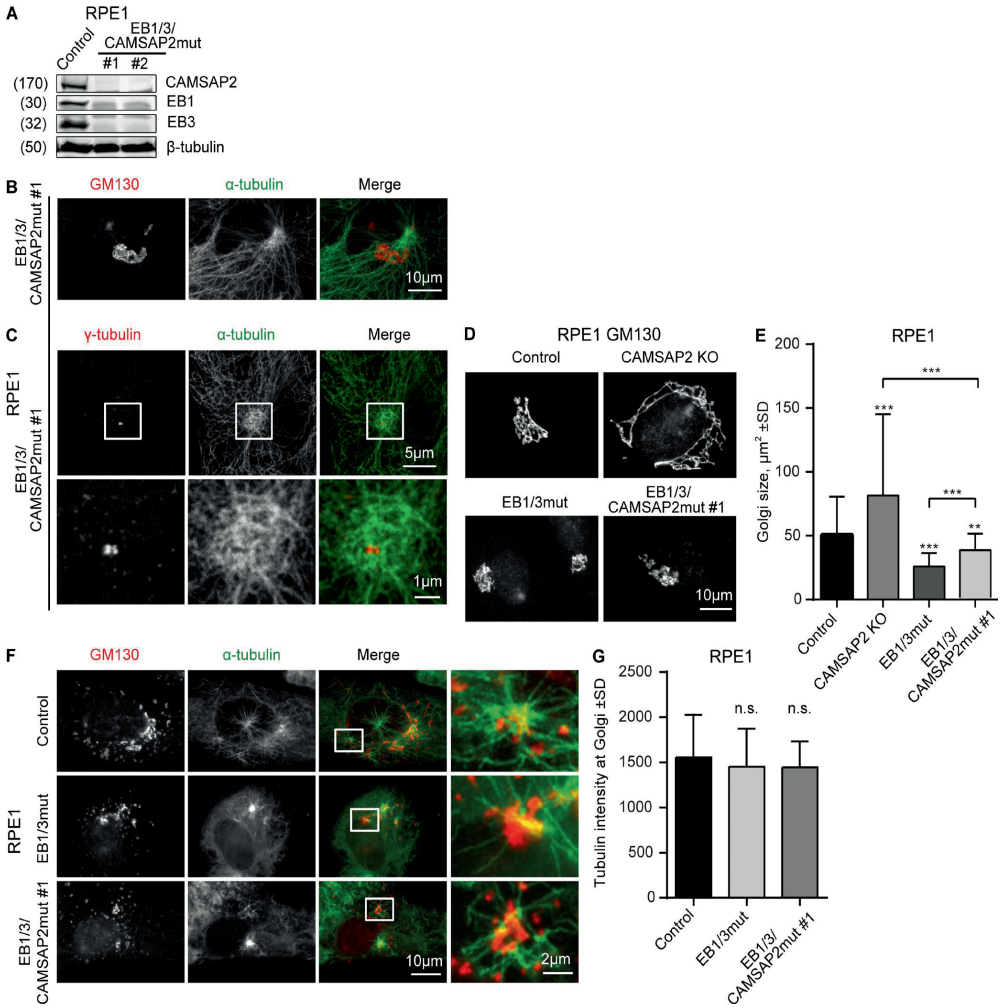

Figure 7. **Effect of EB1, EB3, and CAMSAP2 disruption on Golgi organization and MT nucleation from Golgi.** (A) Western blots of the extracts of EB1/3/CAMSAP2mut RPE1 cells. (B and C) Immunostaining for α-tubulin and GM130 (B) or γ-tubulin (C) in EB1/3/CAMSAP2mut RPE1 cells. In C, enlarged images of the boxed areas are shown below. (D and E) Immunostaining for GM130 and quantification of the Golgi area in the indicated cell lines. $n = 50$ cells per condition. (F) Immunostaining of GM130 and α-tubulin in the indicated cell lines after a 3-min recovery from nocodazole treatment. (G) Tubulin intensity in the vicinity of Golgi membranes in the indicated cell lines treated as in F. $n = 30$ cells per condition. n.s., no significant differences; **, $P < 0.01$; ***, $P < 0.001$ (Mann-Whitney *U* test).

became much less sensitive to the loss of EB1 and EB3 (Fig. 8 F). Such longer CAMSAP2 stretches likely have a higher affinity for the AKAP450/MMG-bound Golgi membranes and may be less dependent on additional interactions provided by EBs.

In the triple EB1/3/CAMSAP2mut cells, the efficiency of centriole depletion was 73%, but most of them still retained a γ-tubulin–positive MTOC (Fig. 8, A and B). Previously, we observed a similar phenomenon in cells simultaneously lacking CAMSAP2 and AKAP450: the majority of surviving centrinone-treated AKAP450/CAMSAP2 knockout cells maintained an acentriolar γ-tubulin–containing MTOC (Wu et al., 2016). The fact that cells with acentriolar MTOCs were also predominant in the centrinone-treated EB1/3/CAMSAP2mut cell population is consistent with the view that, similar to AKAP450, EB1 and EB3 are part of an important link between MTs and the Golgi, and when this link is removed along with CAMSAP2, cell survival depends on the clustering of pericentriolar material (PCM) even though centrioles are absent.

Because centrinone-treated EB1/3/CAMSAP2mut cells retained a γ-tubulin–positive cluster, they had a radial MT array, and the Golgi was organized around the MTOC (Fig. 8 C). In control cells, Golgi stacks were often arranged into linear structures, which were particularly prominent after centrinone

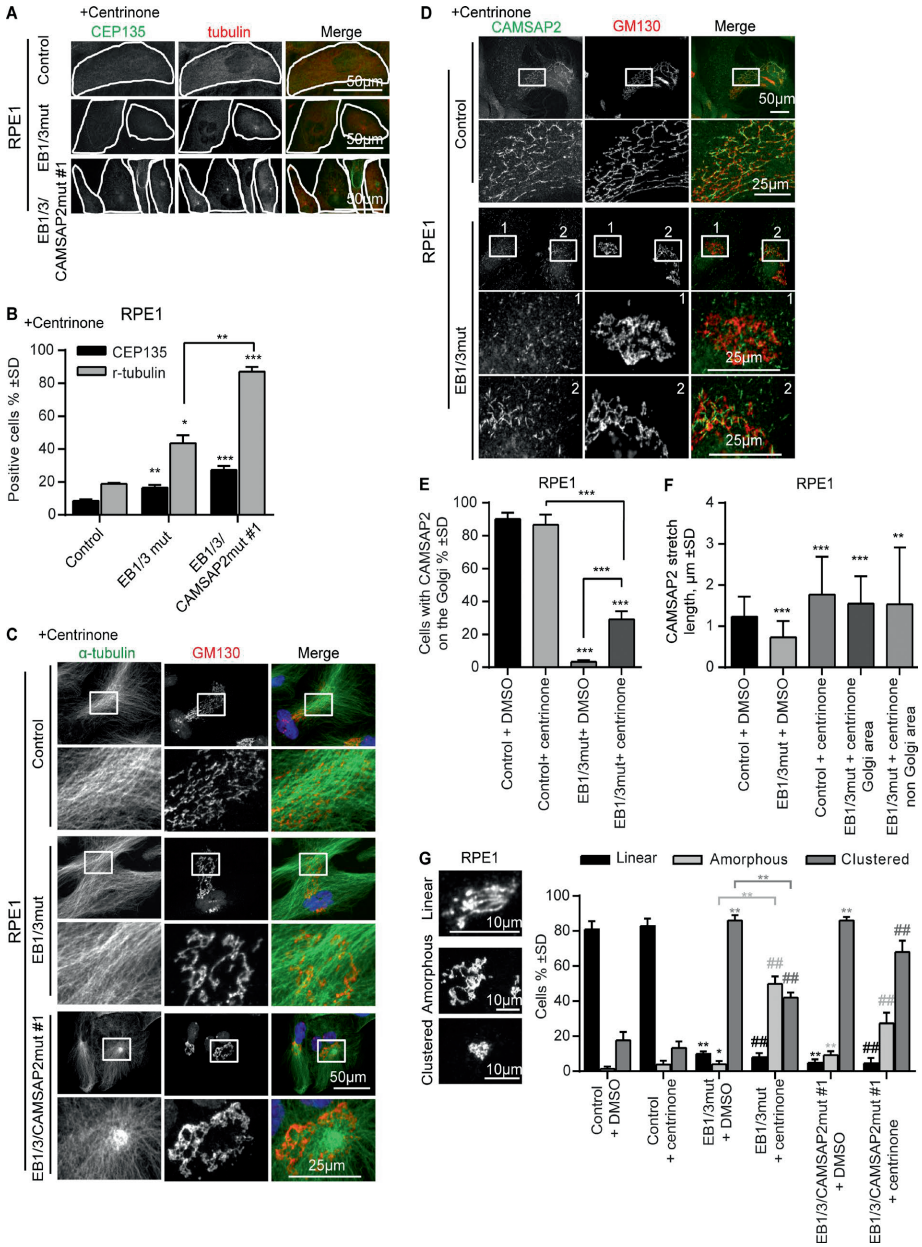

Figure 8. **Effect of EB1, EB3, and CAMSAP2 disruption on MT and Golgi organization after centriole depletion.** (A and B) Immunostaining for CEP135 and γ-tubulin (A) and percentage of γ-tubulin– and CEP135-positive cells in the indicated cell lines after 11 d of treatment with 125 nM centrinone (B). n = 366–391 cells per condition. *, P < 0.05; **, P < 0.01; ***, P < 0.001 (Student's t test). (C and D) Immunostaining for α-tubulin (C) or CAMSAP2 (D) and GM130 in the indicated cell lines treated with centrinone. Enlarged portions of the boxed areas are shown at the bottom. (E and F) Percentage of cells with CAMSAP2 stretches at the Golgi (E) and quantification of the CAMSAP2 stretch length (F) for the indicated cell lines and treatments. n = 248–418 cells per condition in E and 199–260 CAMSAPP2 stretches in F. **, P < 0.01; ***, P < 0.001 (Mann-Whitney U test). (G) Quantification of Golgi morphology for the indicated PRE1 cell lines and treatments. Three types of Golgi organization are shown on the left. 335–642 control and 153–593 centrinone-treated cells were analyzed. Significant differences between values are indicated: *, control (DMSO) treatment; #, centrinone treatment. * or #, P < 0.05; ** or ##, P < 0.01 (Mann-Whitney U test).

treatment (Fig. 8, D and G). In contrast, in all cells with disrupted EB1 and EB3, Golgi elements had a much more amorphous and clustered appearance (Fig. 8 G). Collectively, our data show EB1 and EB3 participate in MT minus end organization and in controlling the extension of Golgi ribbons along MTs, while in the absence of these two EBs, Golgi stacks acquire a more compact arrangement.

EB1 and EB3 are required for cell migration in 2D and 3D

To get further insight into the function of EBs in interphase cells, we next analyzed cell movement. Migration in EB1/2/3mut cells could not be tested, because of the poor motility of the parental HeLa strain. EB1/3mut RPE1 knockout cells moved significantly slower than control cells in monolayer wound healing assays (Fig. 9 A). The ability of cells to polarize by positioning the Golgi in the direction of migration was perturbed in the mutants (Fig. 9 B), similar to what was previously observed for the knockouts of AKAP450 and CAMSAP2, which are also required for Golgi–MT attachment (Rivero et al., 2009; Wu et al., 2016). Also, when RPE1 cell motility was observed in sparse cultures, the velocity of cell movement was significantly reduced, a defect that could be rescued by expressing EB1-GFP and to some extent by EB3-GFP, but not by EB2-GFP (Fig. 9, C and D). However, the ability of cells to move in one direction and the polarized organization of the actin cytoskeleton (i.e., formation of actin-rich lamellae at the leading edge and localization of myosin IIB at the retracting edge) were not significantly affected (Fig. S5, B and C). We reasoned that slower motility could be due to a defect in cell adhesion. Indeed, although the mean size of focal adhesions (FAs) was not affected, EB1/3mut RPE1 cells had more FAs in inner cell regions, and their size was slightly larger (Fig. 9, E–H). We next examined MT-dependent trafficking, focusing on the motility of Rab6-positive exocytotic carriers because they were previously implicated FA remodeling (Stehbens et al., 2014), and found that although the velocity of vesicle motility in EB1/3mut cells was normal, the radial organization of vesicle tracks was strongly perturbed (Fig. S5, D–F). The strong reduction of motility on 2D substrate observed in EB1/3mut cells is thus likely caused by aberrant FA turnover, possibly due to their abnormal regulation by EB-dependent +TIPs or trafficking defects (Stehbens and Wittmann, 2012).

We also examined the ability of EB1/3mut cells to invade 3D collagen matrix using HT1080 cells as a model and found that the velocity of their movement was very strongly reduced (Fig. 9, I and J). This defect was likely due at least partly to the fact that these cells were unable to acquire a polarized morphology with a single long invasive pseudopod at the front and instead extended multiple short protrusions (Fig. 9, K and L). This phenotype was reminiscent of that previously observed for AKAP450, MMG, and CAMSAP2 depletion (Wu et al., 2016), suggesting that the loss of Golgi–MT attachment might affect cell polarity and thus motility in 3D matrix.

Discussion

In this study we showed that some mammalian cell lines, such as HeLa, can survive when all the members of the EB protein family are stably disrupted. This result is not entirely surprising given that loss of EB homologues in other eukaryotes, such as budding yeast, is not lethal (Berlin et al., 1990), and *Arabidopsis thaliana* plants with strongly reduced expression of all three EB homologues have surprisingly mild phenotypes (Bisgrove et al., 2008). However, we were unable to disrupt all three EB-encoding genes in RPE1 and HT1080 background, even though the depletion of EB2 in RPE1 on EB1/3mut background revealed no striking additional defects. Recent work showed that acute simultaneous knockout of EB1 and EB3 in HeLa cells causes very significant spindle abnormalities (McKinley and Cheeseman, 2017). We favor the idea that mammalian cells normally require EBs for different aspects of cell division but can adapt to their absence through compensatory mutations, the selection for which can occur with different efficiency dependent on cell background.

The most striking and unexpected finding of our study is the important role of the EB1 and EB3 in controlling the organization of MT minus ends. This function comprises two effects (Fig. 10). First, EB1 and EB3 promote elongation of CAMSAP2-decorated MT stretches, and this may depend on the binding of EBs to growing MT plus or minus ends, as the elongation of CAMSAP2 stretches requires minus end polymerization, while their disassembly can occur from both ends (Jiang et al., 2014). Second, EBs can directly promote the interaction between MTs and Golgi membranes by binding to the Golgi-associated SxIP protein MMG. In MMG knockout cells, the length of CAMSAP2 stretches is normal, but they are not recruited to the Golgi. CAMSAP2 localization to the Golgi can be restored by directly targeting the MT-binding CH domain of EB3 or other MT-binding domains to Golgi membranes. MT minus end attachment to Golgi membranes does not require the high-affinity binding of EBs to growing, GTP cap-bearing MT tips. Instead, this interaction appears to rely on the weaker EB binding to the GDP-MT lattice, and can be also taken over by a MT-associated protein lacking MT tip preference. Such "zippering" between MT shafts and membranes associated with an EB partner might be similar to MT–cortex interactions in the axon initial segment, which require EBs and the SxIP motif-containing protein ankyrin-G (Fréal et al., 2016). The EB-dependent Golgi–MT connection becomes less important when CAMSAP2 stretches are elongated in centrinone-treated cells. These data support the view that Golgi–MT coorganization is based on the presence of multiple weak interactions and that an increase in CAMSAP2 decoration of MTs can compensate for the absence of EBs. Weak multisite binding also helps explain why other proteins, such as CLASPs and MTCL1, contribute to Golgi–MT association (Efimov et al., 2007; Sato et al., 2014).

The importance of the EBs for connecting Golgi membranes to MTs is supported by the observation that in the absence of EBs, Golgi ribbons are more compact. We think that this is due to the fact that MT attachments to the Golgi do not only allow this membrane structure to serve as an MTOC which promotes its own assembly (Efimov et al., 2007; Miller et al., 2009; Rivero et al., 2009; Zhu and Kaverina, 2013; Rios, 2014; Sanders and Kaverina, 2015) but also prevent membrane overcompaction caused by dynein-mediated minus end directed transport. When the static links between the Golgi membranes and MTs are removed, as is the case when AKAP450, MMG, or EB1/3 is disrupted, individual Golgi stacks, despite maintaining their normal morphology at the ultrastructural level (Wu et al., 2016), are brought together into a compact aggregate. The function of CAMSAP2 in this context is more complex, because although it can promote Golgi membrane spreading along the

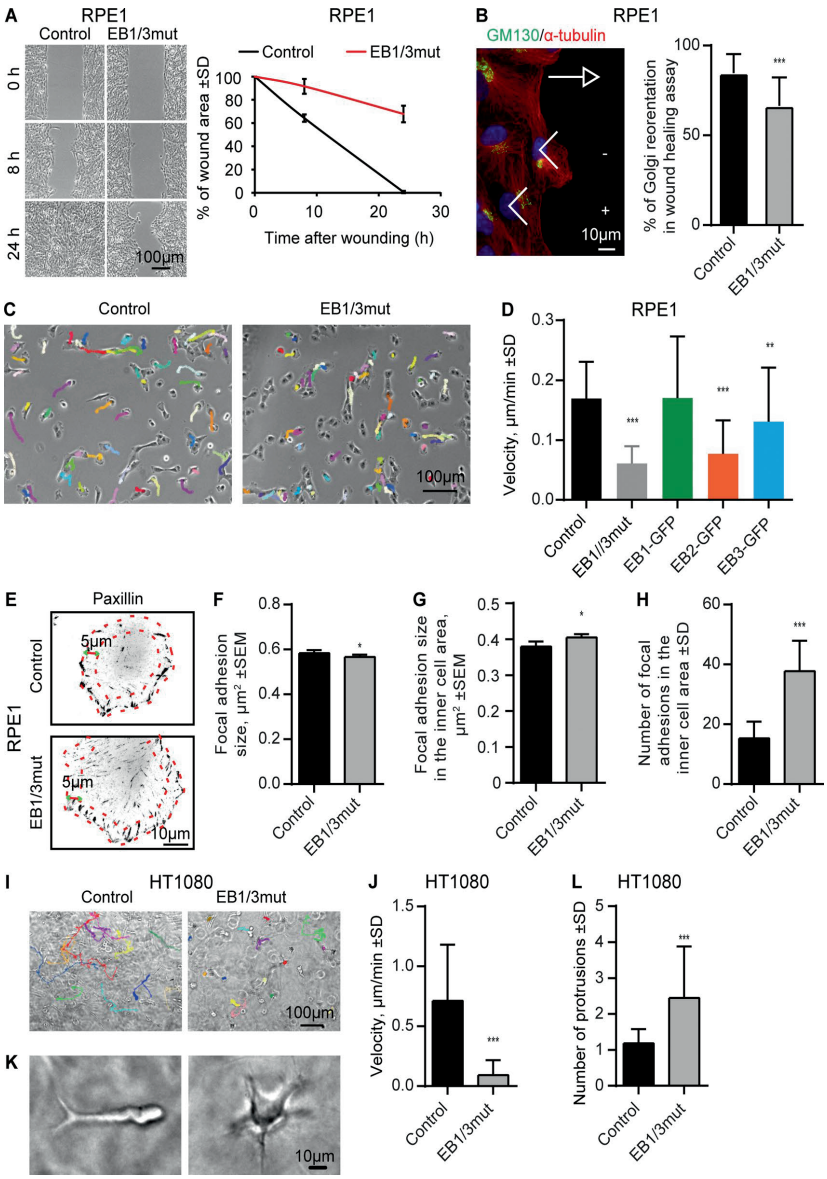

Figure 9. **Effects of EB1 and EB3 disruption on cell migration.** (A) Phase-contrast images of monolayer wound-healing assays in control and EB1/3mut RPE1 cells at the indicated time points and percentage of wound area closure. *n* = 3 independent experiments. (B) Immunostaining for α-tubulin and GM130 in a wound healing assay and the quantification of the Golgi reorientation. *n* = 163 control and 152 EB1/3mut RPE1 cells. (C). Phase contrast images and tracks of control and EB1/3mut cells during 7-h migration in sparse culture (C). (D) Quantification of cell migration velocity in control and EB1/3mut RPE1 cells expressing the indicated constructs. *n* = 30–60 cells. (E–H) Immunostaining for paxillin in the indicated cell lines (E), quantification of FA size in the whole cell (F), and FA size (G) and number (H) in the inner cell area (with 5-µm-broad cell rim excluded, red dotted lines in E). *n* = 44 control and 55 EB1/3mut RPE1 cells; per condition, 3,000 and 1,000 FAs were analyzed in the whole cell and the inner cell area, respectively. (I and J) Phase contrast images and tracks of control and EB1/3mut HT1080 cells in 3D matrix during 24-h migration (I) and quantification of their migration velocity (J). *n* = 24 control and 26 EB1/3mut HT1080 cells. (K and L) Morphology of control and EB1/3mut HT1080 cells in 3D matrix and the mean number of protrusions in these cells. *n* = 65 control and 63 EB1/3mut HT1080 cells. *, P < 0.05; **, P < 0.01; ***, P < 0.001 (Mann-Whitney *U* test).

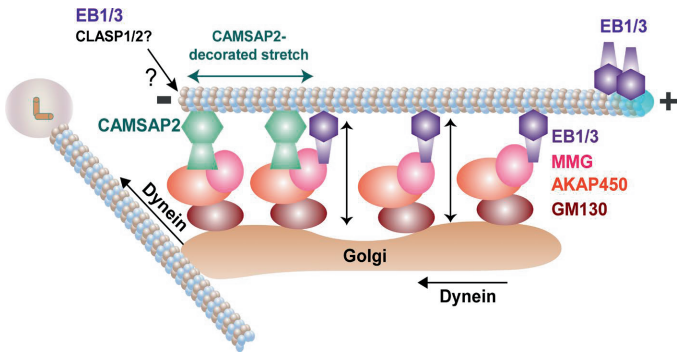

Figure 10. **Model for EB-dependent Golgi–MT coorganization.** MMG associates with Golgi membranes through AKAP450 and GM130 and recruits EB1 and EB3, which bind to MT shafts. CAMSAP2 forms MT minus end-localized stretches, which associate with Golgi membranes by binding to the complex of AKAP450 and MMG. EB1 and EB3 also regulate the length of CAMSAP2-decorated MT stretches, likely by controlling MT end dynamics together with some of their partners such as CLASPs. Association of Golgi membranes with free, CAMSAP2-decorated MT minus ends can promote their clustering through dynein-driven minus end–directed transport. Golgi-associated EB1 and EB3 promote spreading of Golgi ribbons along MTs and counteract their dynein-mediated compaction (double-headed arrows).

MT stretches that it decorates, it can also enhance the overall compaction of the Golgi, because CAMSAP2-bound MT minus are free to be clustered by dynein activity (Fig. 10).

Cells with disrupted AKAP450 and EB1/EB3 display another similarity: when CAMSAP2 is also knocked out, they require an MTOC for survival. Therefore, centriole depletion, which causes formation of nonradial MT networks in control cells, leads to selection of cells with acentriolar but γ-tubulin–positive MTOCs in AKAP450/CAMSAP2 or EB1/3/CAMSAP2 mutants. We propose that while in normal cells, centrioles serve as a high-affinity site for PCM assembly, in centriole-depleted cells, PCM components are recruited to the Golgi, which then serves as an alternative MTOC. When MTs cannot properly attach to the Golgi because of AKAP450 or EB1/3 disruption, semiparallel acentrosomal MT arrays, the minus ends of which are stabilized by CAMSAP2, are formed. However, when CAMSAP2 is also absent, PCM assembles into a single MTOC, likely by dynein-mediated processes (Balczon et al., 1999; Purohit et al., 1999; Young et al., 2000; Dammermann and Merdes, 2002; Kim et al., 2004; Casenghi et al., 2005), and when this fails to happen, MT minus ends become unstable and cell viability is impaired (Wu et al., 2016). This suggests that although CAMSAP2 can stabilize individual MT minus ends, effective minus end stabilization by PCM requires its clustering. Our data also indicate that the interactions between EB1 and EB3 and their C-terminal partners are not essential for interphase centrosome-based MT organization, although we do not exclude the participation of EB2 in this process.

What are the functional consequences of the interactions between MTs and Golgi membranes? First, it is likely that spreading of the Golgi ribbons along MTs facilitates in- and outgoing vesicle trafficking. Consistently, we previously observed that in AKAP450 knockout cells, the overcompacted Golgi located in cell regions with low MT density was surrounded by an abnormally large number of vesicles, suggesting a trafficking defect (Wu et al., 2016). This notion is supported by the observation that ER-to-Golgi trafficking is perturbed in MMG-depleted cells (Wang et al., 2014). Second, detachment of MTs from the Golgi and a complete loss of noncentrosomal MTs impeded cell migration (Hurtado et al., 2011; Vinogradova et al., 2012; Roubin et al., 2013), with a particularly prominent defect observed during cell invasion in 3D matrix (Wu et al., 2016; this study). It is likely that Golgi-anchored MTs are important for cell polarity, for example, by supporting directional vesicle transport to the leading cell edge (Vinogradova et al., 2012) or by promoting cell asymmetry due to concentration of MT density on one side of the nucleus. The defects in MT growth-dependent extension of protrusions that we recently described for SLAIN2-, ch-TOG–, and CLASP1-depleted 3D-cultured mesenchymal cells (Bouchet et al., 2016), as well abnormalities in the turnover of cell–matrix adhesions (Stehbens et al., 2014), likely also contribute to the observed phenotype. Still, it is striking that a major MT-related function of the most abundant and ubiquitous +TIPs in mammalian cells, EB1 and EB3, is to control the organization of MT minus ends, a function that at least partly relies on the association of EBs with the MT shafts and is typically attributed to conventional MT-associated proteins.

Materials and methods

Constructs

Human EB1-GFP, EB2-GFP, and EB3-GFP are described in Stepanova et al. (2003); EB3-NL-LZ-GFP and EB3-NL-mVenus are described in Komarova et al. (2009); and GFP-EB3-Δtyrosine, GFP-EB3-ΔSxIP, and GFP-EB3-ΔTail are described in Montenegro Gouveia et al. (2010). pBrain-chTOGKDP-GFP-shchTOG (Gutiérrez-Caballero et al., 2015) was a gift of S. Royle (University of Warwick, Coventry, England, UK). mKate-α-tubulin was obtained from Evrogen. We used the following previously described constructs: Bio-mCherry-CAMSAP2, GFP-AKAP450 and GFP-MMG (Wu et al., 2016), human βIVb-tubulin-GFP (Bouchet et al., 2016), and GFP-Rab6A (Grigoriev et al., 2007). Truncated GFP-tagged EB1 and EB3, MMG point mutants and MMG–EB3, CLIP-115, and MAP7 chimeras were generated by PCR-based strategies; to generate the two latter clones, cDNAs encoding CLIP-115 (Hoogenraad et al., 2000) and MAP7 (Faire et al., 1999; a gift of C. Bulinski, Columbia University Medical Center, New York, NY) were used. GFP-Ska1 construct was a gift of S. Lens (University Medical Center Utrecht, Utrecht, Netherlands).

A list of primers that were used to generate the DNA constructs is given in Table 1.

The pSpCas9-2A-Puro (PX459) vector that was used for the CRISPR/Cas9 knockout was purchased from Addgene (Ran et al., 2013). Guide RNAs for human EB1, EB2, and EB3 (also known as *MAPRE1*, *MAPRE2*, and *MAPRE3*) were designed using the CRISPR design webpage tool (http://crispr.mit.edu). The targeting sequences for gRNAs were as follows (coding strand sequence indicated): EB1, 5′-TGGAAAAGACTATGACCCTG-3′; EB2, 5′-CCGGAAGCACAC AGTGCGCG-3′; EB3, 5′-TGCACCTCAACTATACCAAG-3′; and CAMSAP2, 5′-CATGATCGATACCCTCATGA-3′ (Wu et al., 2016).

Cell culture, transfection, and rescue experiments

HeLa, human embryonic kidney 239T (HEK293T), HT1080, and RPE1 cell lines were cultured in medium that consisted of 45% DMEM, 45% Ham's F10, and 10% FCS supplemented with penicillin and streptomycin (Akhmanova et al., 2001). The cell lines were routinely checked for mycoplasma contamination using LT07-518 Mycoalert assay (Lonza). For 3D migration experiments, HT1080 cell cultures were set up by cell suspension seeding in 2 mg/ml rat trail collagen I gels (VMR) neutralized according to the manufacturer's protocol, in 8-well chambered cover glasses (Thermo Fisher Scientific).

FuGENE 6 (Promega) was used to transfect HeLa, HT1080, and RPE1 cells with plasmids for generating knockout lines, immunofluorescence, and live cell imaging; polyethylenimine (PEI; Polysciences) was used to transfect HEK293T cells for streptavidin pull-down assays. For rescue experiments, cells were fixed and stained 24–48 h after transfection. Lipofectamine RNAiMAX (Thermo Fisher Scientific) was used to transfect RPE1 cells with siRNA EB2 (target sequence 5′-AATGAACGTTGATAAGGTA-3′) and luciferase (target sequence 5′-CGTACGCGGAATACTTCGA-3′) at 20 nM.

Generation and characterization of EB knockout cell lines

The CRISPR/Cas9-mediated EB1, EB2, and EB3 knockout was performed according to the protocol of Ran et al. (2013). In brief, HeLa, RPE1, and HT1080 cell lines were transfected with the vectors bearing the appropriate targeting sequences using FuGENE 6. 1 d after transfection, RPE1 cells were subjected to selection with 25 µg/ml puromycin for 3 d; HeLa and HT1080 cells were subjected to selection with 2 µg/ml puromycin for 2 d. After selection, cells were allowed to recover in normal medium for ∼7 d, and knockout efficiency was checked by immunofluorescence staining. Depending on the efficiency, 39–51 individual clones were isolated and characterized by Western blotting and immunostaining. EB1/2/3mut HeLa cells and EB1/3mut RPE1 cells were generated by targeting EB1-, EB2-, and EB3-encoding genes simultaneously, and EB1/3mut HT1080 cells were generated by targeting EB1- and EB3-encoding genes simultaneously. EB1/3/CAMSAP2mut RPE1 cells were generated on the basis of the EB1/3mut cell line. MMG and AKAP450 knockout RPE1 cells were described previously (Wu et al., 2016). The mutated portions of the EB-encoding genes were sequenced by PCR using primers located in the vicinity of the corresponding gRNA target sites.

Antibodies, pull down assays and immunofluorescence cell staining

We used rabbit antibodies against CAMSAP2 (NBP1-21402, Novus; 17880-1-AP, Proteintech), EB3 (Stepanova et al., 2003), CLIP170 and CLASP1 (Akhmanova et al., 2001), GM130 (ab52649; Abcam), GFP (ab290; Abcam), CEP135 (SAB4503685-100UG; Sigma-Aldrich), and goat anti–myosin IIB antibody (sc-47205; Santa Cruz). Alexa-Fluor-594-conjugated phalloidin was purchased from Life Technologies (A12381). We used mouse monoclonal antibodies against GM130 and paxillin (610822 and 610823; BD Biosciences), β-tubulin, γ-tubulin (T5201 and T6557; Sigma-Aldrich), and rat monoclonal antibodies against EB2 (Komarova et al., 2005) and α-tubulin YL1/2 (MA1-80017; Pierce). The following secondary antibodies were used: IRDye 800CW/680LT goat anti–rabbit, anti–rat, and anti–mouse and streptavidin IRDye 680RD (Li-Cor Biosciences) and Alexa Fluor 350–, 405–, 488–, and 594–conjugated goat antibodies against rabbit, rat, and mouse IgG (Molecular Probes).

Streptavidin pull-down assays were performed from extracts of HEK293T cells coexpressing biotin ligase BirA, biotinylation- and GFP-tagged constructs used as bait, and GFP-tagged constructs used as prey, as described previously (Lansbergen et al., 2006). In brief, constructs were transfected separately into HEK293 cells by using PEI (Polysciences). After 48 h, protein extracts were prepared using the lysis buffer containing 20 mM Tris-Cl, pH 7.5, 150 mM NaCl, 0.5 mM EDTA, 1 mM DTT, 1% Triton X-100, and a protease inhibitor cocktail (Roche). The pull-down assays were performed using streptavidin beads (Invitrogen).

GST pull-down assays were performed as described previously using EB–GST fusions purified from *Escherichia coli* (Komarova et al., 2005). In brief, individual GST fusion proteins were bound to glutathione Sepharose beads (Amersham Biosciences) in a buffer containing 20 mM Tris HCl, pH 7.5, 300 mM NaCl, and 1% Triton X-100. After incubation for 1 h on a rotating wheel at 4°C, beads were separated from the supernatant by centrifugation and washed four times in the same buffer. The beads were then incubated with purified GFP-CAMSAP2 or GFP-MACF43 and analyzed on Coomassie-stained gels. GFP-CAMSAP2 was purified from HEK293 cells. Cells were transfected using PEI and lysed in the lysis buffer (50 mM Hepes, 300 mM NaCl, and 0.5% Triton X-100, pH 7.4) supplemented with protease inhibitors (Roche). After clearing debris by centrifugation, cell lysates were incubated with StrepTactin beads (28-9355-99; GE Healthcare), and the beads were washed with the lysis buffer without protease inhibitors and with the wash buffer (50 mM Hepes, 300 mM NaCl, and 0.5% Triton X-100, pH 7.4). The proteins were eluted with the elution buffer (50 mM Hepes, 150 mM NaCl, 0.05% Triton X-100, and 2.5 mM desthiobiotin). The N-terminally 6xHis-tagged GFP-MACF43 purified from *E. coli* by immobilized metal-affinity chromatography on Ni-NTA agarose (QIAGEN Benelux) was described previously (Preciado López et al., 2014).

Table 1. **Primers used to generate the DNA constructs**

Construct	Primer Sequence (5′–3′)
GFP-MMG 1-389 WT	CCGGACTCAGATCTCGCGGCCGCATGAAGGAGATTTGCAGGATCTGTG
	GATCAGTTATCTAGATCCGGTGGATCCTTATGAATTCAGCTTTTGTTGTTTCAGC
GFP MMG 1-389 SxNN	AATAACATTCCAGTGAAATCCAGCCTACCTGG
	GCTGGATTTCACTGGAATGTTATTCCTGCTCCCTCGGGGGCTC
GFP-MMG 1-389 SxNN-EB3 201-281	GTTGCTGAAACAACAAAAGCTGAATTCAGGCAGCGGACAAATTCTTGAACTCAACCAACAGCTG
	CTAGATCCGGTGGATCCTTATGATTAGTACTCGTCCTGGTCTTCTTGTTG
EB3-GFP-MMG 1-389 SxNN	CGTCAGATCCGCTAGCGCTACCGGTCATGGCCGTCAATGTGTACTCCAC
	CTTGCTCACCATGGTGGCGACGGATCCGCCTCCAGAACCAGCTCCGGCATCAGTCTCATG
CLIP115 1-359-GFP-MMG 1-389 SxNN	TCAGATCCGCTAGCGCTACCGGTCATGCAGAAGCCCAGTGGC
	CTCACCATGGTGGCGACGGATCCGCCTCCAGAACCAGCTCCGCCTGAGATCTTCCGGGC
MAP7 18-283-GFP-MMG 1-389 SxNN	TCAGATCCGCTAGCGCTACCGGTCATGGTGCGAAGCGAAACAGCAC
	CTCACCATGGTGGCGACGGATCCGCCTCCAGAACCAGCTCCAGAAGAGCCCTCAGGTGGT

For immunofluorescence cell staining, cultured cells were fixed in –20°C methanol for 10 min followed by 4% paraformaldehyde for 10 min in the case of EB1, EB2, EB3, and CLIP170. In the case of CAMSAP2, GM130, and α-tubulin, cells were only fixed with –20°C methanol for 10 min. Cells were then permeabilized with 0.1% Triton X-100 in PBS for 10 min; subsequent washing and labeling steps were performed in PBS supplemented with 2% BSA and 0.05% Tween-20. At the end, slides were rinsed in 70% and 100% ethanol, air-dried, and mounted in Vectashield mounting medium (Vector Laboratories).

Drugs and drug treatments

We used the following drugs: SB 415286 and nocodazole (Sigma-Aldrich), paclitaxel (Enzo Life Sciences), and centrinone (a gift of A. Shiau and T. Gahman, Ludwig Institute for Cancer Research, San Diego, CA). To enhance CLASP1 localization at MT tips, cells were incubated with the GSK3 inhibitor SB415286 at a concentration of 20 µM for 30 min. MT stabilization was performed by treating cells with 5 µM paclitaxel for 30 min at 37°C. MT disassembly was performed by treating the cells with 10 µM nocodazole for 1 h at 37°C, followed by 1 h at 4°C, to achieve both Golgi dispersion and complete disassembly of stable MTs. To deplete centrioles, RPE1 cells were treated with 125 nM centrinone for 11 d, and the drug-containing medium was refreshed every 24 h.

Image acquisition

Images of fixed cells were collected with an Eclipse Ni upright fluorescence microscope and DS-Qi2 CMOS camera (Nikon), using a Plan Apo Lambda 40×, NA 1.30, oil objective (Nikon) or Plan Apo Lambda 100×, NA 1.45, oil objective (Nikon) and Nikon NIS (Br) software. Intensilight C-HGFI (Nikon) was used as a light source. Images of fixed cells were also collected with spinning disk microscopy, which was performed on an inverted research microscope Eclipse Ti-E with the Perfect Focus System (Nikon), equipped with Nikon Apo total internal reflection fluorescence (TIRF) 100×, NA 1.49, oil objective, Yokogawa CSU-X1-A1 confocal head with 405-491-561 triple-band mirror and GFP, mCherry, and GFP/mCherry emission filters (Chroma), ASI motorized stage MS-2000-XYZ with Piezo Top Plate (ASI), a Photometrics Evolve 512 electron-multiplying charge-coupled device (CCD) camera (Photometrics), and controlled by MetaMorph 7.7 software (Molecular Devices). The microscope was equipped with a custom-ordered illuminator (MEY10021; Nikon) modified by Roper Scientific France/PICT-IBiSA, Institut Curie. Cobolt Calypso 491 nm (100 mW) and Cobolt Jive 561 nm (100 mW) lasers (Cobolt) were used as light sources. For simultaneous imaging of green and red fluorescence, we used ET-mCherry/GFP filter set (59022; Chroma) together with the DualView (DV2; Roper) equipped with the dichroic filter 565dcxr (Chroma) and HQ530/30m emission filter (Chroma).

Live-cell fluorescent TIRF imaging was performed on an inverted research microscope Eclipse Ti-E(Nikon) with the Perfect Focus System (Nikon), equipped with Nikon Apo TIRF 100×, NA 1.49, oil objective (Nikon) and iLas^2 system (Dual Laser illuminator for azimuthal spinning TIRF [or Hilo] illumination and Simultaneous Targeted Laser Action) from Roper Scientific. The system was also equipped with ASI motorized stage MS-2000-XY and a Photometrics Evolve Delta 512 electron-multiplying CCD camera and controlled by MetaMorph 7.8 software. Stradus 488 nm (150 mW; Vortran) and OBIS 561 nm (100 mW; Coherent) lasers were used as light sources. For simultaneous imaging of green and red fluorescence, we used Optosplit III (Cairn Research) equipped with the filters from ET-GFP (49002), ET-mCherry (49008), and ET-GFPmCherry (59022) filter sets (Chroma). To keep the cells at 37°C, a stage top incubator model INUBG2E-ZILCS (Tokai Hit) was used. Images were acquired at 15.4 pixels/µm with exposure time 500 ms at 2 frames/s for MT plus end imaging and with exposure 100 ms at 10 frames/s for GFP-Rab6 imaging (in both cases, the total duration of a movie was 50 s). Cells were plated on round 25-mm coverslips, which were mounted in Attofluor Cell Chamber (Thermo Fisher Scientific) and maintained at 37°C.

Live-cell phase contrast imaging was performed on inverted research microscope Eclipse Ti-E with the Perfect Focus System, equipped with Nikon Plan Fluor 10×, NA 0.30, Ph1 and Nikon Plan Apo 20×, NA 0.75, Ph2 Phase Contrast objectives, Lambda SC Smart Shutters (Sutter), motorized stage MS-2000-XY (ASI), and a CoolSNAP HQ2 CCD camera (Photometrics) and controlled with Micro-Manager Open Source Microscopy Software (https://micro-manager.org). To keep the cells at 37°C, a stage top incubator model INUBG2E-ZILCS was used. Images were acquired at 3.1 and 1.6 pixels/µm. Cells were plated on round 25-mm coverslips, which were mounted in Attofluor Cell Chamber and maintained at 37°C and 5% CO_2. Cells were imaged every 5–10 min for 8–24 h.

Preparation and analysis of fluorescence microscopy images

Images were prepared for publication using MetaMorph, ImageJ, and Adobe Photoshop. All images were modified by adjustments of levels and contrast. ImageJ was used for quantification of the immunofluorescence signal intensity. For measurement of parameters of MT dynamics, HeLa EB1/2/3mut cell lines were used for the analysis 24 h after transfection with β-tubulin–GFP or EB–GFP fusions. Parameters of MT growth were analyzed by using kymographs in MetaMorph software (Kymograph function) to distinguish episodes of growth and shortening (in case of imaging of fluorescently labeled tubulin) or the episodes of growth (in case of imaging of fluorescently labeled EB constructs). For measurements of instantaneous rates or transition frequencies, MT end displacements longer than 0.5 µm were taken into account.

The slopes of MT growth and shortening were analyzed in MetaMorph software using Line Region tool and Region Measurements function (Distance and Angle options), resulting in a distance and an angle value per episode of growth or shortening. Velocity of growth and shortening was calculated in SigmaPlot software (version 7.101; SPSS) as the tangent of the episode angle. The duration of growth and shortening was calculated as the distance, multiplied by the cosine of the angle. Transition frequencies were calculated as inverted episode durations.

Analysis of fluorescence intensity distribution of EB2, CLIP170, and CLASP1 along MT ends was performed using ImageJ. In brief, MTs with clearly visible ends at the cell periphery were analyzed. Fixed Line Length tool was used to obtain the profile of MT or +TIP intensity, and the intensity profiles were then normalized and averaged.

For quantification of ch-TOG intensity at the MT plus ends, the mean signal intensity of ch-TOG signal at a MT tip in a free-shaped region of interest was measured in MetaMorph software (Region Measurements function, Average Intensity option), and the mean intensity and SD of ch-TOG signal in cytoplasm were also measured (SD was measured in MetaMorph software using Region Measurements function as Intensity Standard Deviation option). The signal-to-noise ratio was calculated as [(mean intensity at the tip) − (mean intensity in cytoplasm)]/(SD in the cytoplasm).

CAMSAP2 and GM130 distributions were analyzed using the ImageJ Radial Profile plugin. A circle of 13.3 µm was drawn with the center positioned in the center of the Golgi. Golgi size was determined by Quick Selection tool in Photoshop. The Analyze Particles plugin was used to quantify FA size and number. MTrackJ tool was used to extract cell migration tracks and measure their speed and direction.

GFP-Rab6 vesicle movements were analyzed in ImageJ using our previously developed tracking methods (“method 11” in Chenouard et al., 2014). The tracks were then processed using another custom-made

ImageJ plugin, which removes the nonprocessive movements within each track and splits trajectories into multiple segments of processive motion. Finally, the resulting tracks were processed using another published ImageJ plugin (Yao et al., 2017) to quantify the velocities and track radiality with respect to a manually set reference point. For this analysis, we used as the reference point location the center of the Golgi apparatus. The track radiality is the angle between the line connecting the start and end points of this track and the line from the starting point of the track to the reference point. The angle ranges from 0° to 180°, where 0° corresponds to a particle moving along the radius away from the reference point to the cell periphery, and 180° corresponds to a particle moving radially toward the cell center.

Transmission EM sample preparation and analysis

Cells were fixed at room temperature by adding Karnovsky fixative (2.5% glutaraldehyde and 2% formaldehyde [Electron Microscopy Sciences] in 0.2 M cacodylate buffer, pH 7.4) 1:1 to culture medium for 10 min. This was replaced by fresh fixative for 2 h at room temperature. Cells were then postfixed with 1% OsO_4/1.5% $K_3Fe(III)(CN)6$ in 0.065 M phosphate buffer for 2 h at 4°C and finally 1 h with 0.5% uranyl acetate. After fixation, cells were dehydrated and embedded in epon epoxy resin (Polysciences). Ultrathin sections of 60 nm were contrasted with uranyl acetate and lead citrate using the AC20 (Leica) and examined with a 1010 electron microscope (Jeol Europe). Images were taken from three different sets of cells per condition. 50 random images per set were taken (150 per condition).

All measurements were done using ImageJ. For the quantification of the area within which Golgi stacks are confined in the cell, the smallest possible ellipse to enclose all the Golgi stacks was drawn in ImageJ, and then the area of that ellipse was measured. This was done for three different independent sets of cells per condition, and then 50 cells within each set (in total 150 cells were measured per experimental condition). Independently, the length of individual Golgi stacks was measured with the Segmented Line tool, the thickness with the Straight Line tool, and the area with the Freehand Selection tool.

Statistical analysis

Statistical significance was analyzed either using the Mann-Whitney *U* test or two-tailed *t* test, as indicated in figure legends. For the *t* test, data distribution was assumed to be normal, but this was not formally tested. Statistical significance was determined using GraphPad Prism software (version 6.07).

Online supplemental material

Figs. S1 and S2 illustrate analyses of cell division in EB1/3mut RPE1 and EB1/2/3mut HeLa cells. Fig. S3 provides information on MTs, Golgi, and CAMSAP2 stretch organization in different knockout lines. Fig. S4 shows the recruitment of EBs and CAMSAP2 to the Golgi and the biochemical characterization of the interactions between AKAP450, MMG, CAMSAP2, and EB1. Fig. S5 illustrates the distribution of EB1 in paclitaxel-treated cells and shows that disruption of EB1 and EB3 has no significant impact on certain aspects of cell polarity and directionality of cell movement but does affect the organization of tracks of GFP-Rab6–positive exocytotic vesicles. Table S1 provides information on mutations in sequences of EB-encoding genes in different knockout lines.

Acknowledgments

We thank A. Shiau, T. Gahman, S. Royle, C. Bulinski, and S. Lens for gifts of materials.

This study was supported by China Scholarship Council scholarships to C. Yang and J. Wu, a H2020 European Research Council Synergy grant 609822 to A. Akhmanova, and Netherlands Organisation for Scientific Research STW grant OTP13391 to E. Meijering and A. Akhmanova.

The authors declare no competing financial interests.

Author contributions: C. Yang and J. Wu designed and conducted the experiments and wrote the paper. I. Grigoriev performed live cell imaging and image analysis. C. de Heus, N. Liv, and J. Klumperman performed and analyzed EM experiments. Y. Yao, I. Smal, and E. Meijering established live cell imaging analysis procedures and helped with image analysis. R.Z. Qi contributed essential reagents. A. Akhmanova designed and supervised the study and wrote the paper.

Submitted: 4 January 2017
Revised: 8 June 2017
Accepted: 18 July 2017

References

Akhmanova, A., and M.O. Steinmetz. 2008. Tracking the ends: a dynamic protein network controls the fate of microtubule tips. *Nat. Rev. Mol. Cell Biol.* 9:309–322. http://dx.doi.org/10.1038/nrm2369

Akhmanova, A., and M.O. Steinmetz. 2015. Control of microtubule organization and dynamics: two ends in the limelight. *Nat. Rev. Mol. Cell Biol.* 16:711–726. http://dx.doi.org/10.1038/nrm4084

Akhmanova, A., C.C. Hoogenraad, K. Drabek, T. Stepanova, B. Dortland, T. Verkerk, W. Vermeulen, B.M. Burgering, C.I. De Zeeuw, F. Grosveld, and N. Galjart. 2001. Clasps are CLIP-115 and -170 associating proteins involved in the regional regulation of microtubule dynamics in motile fibroblasts. *Cell.* 104:923–935. http://dx.doi.org/10.1016/S0092-8674(01)00288-4

Balczon, R., C.E. Varden, and T.A. Schroer. 1999. Role for microtubules in centrosome doubling in Chinese hamster ovary cells. *Cell Motil. Cytoskeleton.* 42:60–72. http://dx.doi.org/10.1002/(SICI)1097-0169(1999)42:1<60::AID-CM6>3.0.CO;2-7

Ban, R., H. Matsuzaki, T. Akashi, G. Sakashita, H. Taniguchi, S.Y. Park, H. Tanaka, K. Furukawa, and T. Urano. 2009. Mitotic regulation of the stability of microtubule plus-end tracking protein EB3 by ubiquitin ligase SIAH-1 and Aurora mitotic kinases. *J. Biol. Chem.* 284:28367–28381. http://dx.doi.org/10.1074/jbc.M109.000273

Berlin, V., C.A. Styles, and G.R. Fink. 1990. BIK1, a protein required for microtubule function during mating and mitosis in Saccharomyces cerevisiae, colocalizes with tubulin. *J. Cell Biol.* 111:2573–2586. http://dx.doi.org/10.1083/jcb.111.6.2573

Bisgrove, S.R., Y.R. Lee, B. Liu, N.T. Peters, and D.L. Kropf. 2008. The microtubule plus-end binding protein EB1 functions in root responses to touch and gravity signals in *Arabidopsis*. *Plant Cell.* 20:396–410. http://dx.doi.org/10.1105/tpc.107.056846

Bjelić, S., C.O. De Groot, M.A. Schärer, R. Jaussi, K. Bargsten, M. Salzmann, D. Frey, G. Capitani, R.A. Kammerer, and M.O. Steinmetz. 2012. Interaction of mammalian end binding proteins with CAP-Gly domains of CLIP-170 and p150(glued). *J. Struct. Biol.* 177:160–167. http://dx.doi.org/10.1016/j.jsb.2011.11.010

Bouchet, B.P., I. Noordstra, M. van Amersfoort, E.A. Katrukha, Y.C. Ammon, N.D. Ter Hoeve, L. Hodgson, M. Dogterom, P.W.B. Derksen, and A. Akhmanova. 2016. Mesenchymal cell invasion requires cooperative regulation of persistent microtubule growth by SLAIN2 and CLASP1. *Dev. Cell.* 39:708–723. http://dx.doi.org/10.1016/j.devcel.2016.11.009

Brouhard, G.J., J.H. Stear, T.L. Noetzel, J. Al-Bassam, K. Kinoshita, S.C. Harrison, J. Howard, and A.A. Hyman. 2008. XMAP215 is a processive microtubule polymerase. *Cell.* 132:79–88. http://dx.doi.org/10.1016/j.cell.2007.11.043

Casenghi, M., F.A. Barr, and E.A. Nigg. 2005. Phosphorylation of Nlp by Plk1 negatively regulates its dynein-dynactin-dependent targeting to the centrosome. *J. Cell Sci.* 118:5101–5108. http://dx.doi.org/10.1242/jcs.02622

Chenouard, N., I. Smal, F. de Chaumont, M. Maška, I.F. Sbalzarini, Y. Gong, J. Cardinale, C. Carthel, S. Coraluppi, M. Winter, et al. 2014. Objective comparison of particle tracking methods. *Nat. Methods.* 11:281–289. http://dx.doi.org/10.1038/nmeth.2808

Dammermann, A., and A. Merdes. 2002. Assembly of centrosomal proteins and microtubule organization depends on PCM-1. *J. Cell Biol.* 159:255–266. http://dx.doi.org/10.1083/jcb.200204023

Draviam, V.M., I. Shapiro, B. Aldridge, and P.K. Sorger. 2006. Misorientation and reduced stretching of aligned sister kinetochores promote chromosome missegregation in EB1- or APC-depleted cells. *EMBO J.* 25:2814–2827. http://dx.doi.org/10.1038/sj.emboj.7601168

Efimov, A., A. Kharitonov, N. Efimova, J. Loncarek, P.M. Miller, N. Andreyeva, P. Gleeson, N. Galjart, A.R. Maia, I.X. McLeod, et al. 2007. Asymmetric CLASP-dependent nucleation of noncentrosomal microtubules at the trans-Golgi network. *Dev. Cell.* 12:917–930. http://dx.doi.org/10.1016/j.devcel.2007.04.002

Faire, K., C.M. Waterman-Storer, D. Gruber, D. Masson, E.D. Salmon, and J.C. Bulinski. 1999. E-MAP-115 (ensconsin) associates dynamically with microtubules in vivo and is not a physiological modulator of microtubule dynamics. *J. Cell Sci.* 112:4243–4255.

Ferreira, J.G., A.J. Pereira, A. Akhmanova, and H. Maiato. 2013. Aurora B spatially regulates EB3 phosphorylation to coordinate daughter cell adhesion with cytokinesis. *J. Cell Biol.* 201:709–724. http://dx.doi.org/10.1083/jcb.201301131

Fréal, A., C. Fassier, B. Le Bras, E. Bullier, S. De Gois, J. Hazan, C.C. Hoogenraad, and F. Couraud. 2016. Cooperative interactions between 480 kDa ankyrin-G and EB proteins assemble the axon initial segment. *J. Neurosci.* 36:4421–4433. http://dx.doi.org/10.1523/JNEUROSCI.3219-15.2016

Goodwin, S.S., and R.D. Vale. 2010. Patronin regulates the microtubule network by protecting microtubule minus ends. *Cell.* 143:263–274. http://dx.doi.org/10.1016/j.cell.2010.09.022

Green, R.A., R. Wollman, and K.B. Kaplan. 2005. APC and EB1 function together in mitosis to regulate spindle dynamics and chromosome alignment. *Mol. Biol. Cell.* 16:4609–4622. http://dx.doi.org/10.1091/mbc.E05-03-0259

Grigoriev, I., D. Splinter, N. Keijzer, P.S. Wulf, J. Demmers, T. Ohtsuka, M. Modesti, I.V. Maly, F. Grosveld, C.C. Hoogenraad, and A. Akhmanova. 2007. Rab6 regulates transport and targeting of exocytotic carriers. *Dev. Cell.* 13:305–314. http://dx.doi.org/10.1016/j.devcel.2007.06.010

Gutiérrez-Caballero, C., S.G. Burgess, R. Bayliss, and S.J. Royle. 2015. TACC3-ch-TOG track the growing tips of microtubules independently of clathrin and Aurora-A phosphorylation. *Biol. Open.* 4:170–179. http://dx.doi.org/10.1242/bio.201410843

Hendershott, M.C., and R.D. Vale. 2014. Regulation of microtubule minus-end dynamics by CAMSAPs and patronin. *Proc. Natl. Acad. Sci. USA.* 111:5860–5865. http://dx.doi.org/10.1073/pnas.1404133111

Honnappa, S., O. Okhrimenko, R. Jaussi, H. Jawhari, I. Jelesarov, F.K. Winkler, and M.O. Steinmetz. 2006. Key interaction modes of dynamic +TIP networks. *Mol. Cell.* 23:663–671. http://dx.doi.org/10.1016/j.molcel.2006.07.013

Hoogenraad, C.C., A. Akhmanova, F. Grosveld, C.I. De Zeeuw, and N. Galjart. 2000. Functional analysis of CLIP-115 and its binding to microtubules. *J. Cell Sci.* 113:2285–2297.

Howard, J., and A.A. Hyman. 2003. Dynamics and mechanics of the microtubule plus end. *Nature.* 422:753–758. http://dx.doi.org/10.1038/nature01600

Hurtado, L., C. Caballero, M.P. Gavilan, J. Cardenas, M. Bornens, and R.M. Rios. 2011. Disconnecting the Golgi ribbon from the centrosome prevents directional cell migration and ciliogenesis. *J. Cell Biol.* 193:917–933. http://dx.doi.org/10.1083/jcb.201011014

Iimori, M., S. Watanabe, S. Kiyonari, K. Matsuoka, R. Sakasai, H. Saeki, E. Oki, H. Kitao, and Y. Maehara. 2016. Phosphorylation of EB2 by Aurora B and CDK1 ensures mitotic progression and genome stability. *Nat. Commun.* 7:11117. http://dx.doi.org/10.1038/ncomms11117

Jeffery, J.M., I. Grigoriev, I. Poser, A. van der Horst, N. Hamilton, N. Waterhouse, J. Bleier, V.N. Subramaniam, I.V. Maly, A. Akhmanova, and K.K. Khanna. 2013. Centrobin regulates centrosome function in interphase cells by limiting pericentriolar matrix recruitment. *Cell Cycle.* 12:899–906. http://dx.doi.org/10.4161/cc.23879

Jiang, K., G. Toedt, S. Montenegro Gouveia, N.E. Davey, S. Hua, B. van der Vaart, I. Grigoriev, J. Larsen, L.B. Pedersen, K. Bezstarosti, et al. 2012. A proteome-wide screen for mammalian SxIP motif-containing microtubule plus-end tracking proteins. *Curr. Biol.* 22:1800–1807. http://dx.doi.org/10.1016/j.cub.2012.07.047

Jiang, K., S. Hua, R. Mohan, I. Grigoriev, K.W. Yau, Q. Liu, E.A. Katrukha, A.F. Altelaar, A.J. Heck, C.C. Hoogenraad, and A. Akhmanova. 2014. Microtubule minus-end stabilization by polymerization-driven CAMSAP deposition. *Dev. Cell.* 28:295–309. http://dx.doi.org/10.1016/j.devcel.2014.01.001

Kim, J.C., J.L. Badano, S. Sibold, M.A. Esmail, J. Hill, B.E. Hoskins, C.C. Leitch, K. Venner, S.J. Ansley, A.J. Ross, et al. 2004. The Bardet-Biedl protein BBS4 targets cargo to the pericentriolar region and is required for microtubule anchoring and cell cycle progression. *Nat. Genet.* 36:462–470. http://dx.doi.org/10.1038/ng1352

Komarova, Y., G. Lansbergen, N. Galjart, F. Grosveld, G.G. Borisy, and A. Akhmanova. 2005. EB1 and EB3 control CLIP dissociation from the ends of growing microtubules. *Mol. Biol. Cell.* 16:5334–5345. http://dx.doi.org/10.1091/mbc.E05-07-0614

Komarova, Y., C.O. De Groot, I. Grigoriev, S.M. Gouveia, E.L. Munteanu, J.M. Schober, S. Honnappa, R.M. Buey, C.C. Hoogenraad, M. Dogterom, et al. 2009. Mammalian end binding proteins control persistent microtubule growth. *J. Cell Biol.* 184:691–706. http://dx.doi.org/10.1083/jcb.200807179

Kumar, P., and T. Wittmann. 2012. +TIPs: SxIPping along microtubule ends. *Trends Cell Biol.* 22:418–428. http://dx.doi.org/10.1016/j.tcb.2012.05.005

Lansbergen, G., I. Grigoriev, Y. Mimori-Kiyosue, T. Ohtsuka, S. Higa, I. Kitajima, J. Demmers, N. Galjart, A.B. Houtsmuller, F. Grosveld, and A. Akhmanova. 2006. CLASPs attach microtubule plus ends to the cell cortex through a complex with LL5beta. *Dev. Cell.* 11:21–32. http://dx.doi.org/10.1016/j.devcel.2006.05.012

Liu, H., J. Yue, H. Huang, X. Gou, S.Y. Chen, Y. Zhao, and X. Wu. 2015. Regulation of focal adhesion dynamics and cell motility by the EB2 and Hax1 protein complex. *J. Biol. Chem.* 290:30771–30782. http://dx.doi.org/10.1074/jbc.M115.671743

Maurer, S.P., F.J. Fourniol, G. Bohner, C.A. Moores, and T. Surrey. 2012. EBs recognize a nucleotide-dependent structural cap at growing microtubule ends. *Cell.* 149:371–382. http://dx.doi.org/10.1016/j.cell.2012.02.049

Maurer, S.P., N.I. Cade, G. Bohner, N. Gustafsson, E. Boutant, and T. Surrey. 2014. EB1 accelerates two conformational transitions important for microtubule maturation and dynamics. *Curr. Biol.* 24:372–384. http://dx.doi.org/10.1016/j.cub.2013.12.042

McKinley, K.L., and I.M. Cheeseman. 2017. Large-scale analysis of CRISPR/Cas9 cell-cycle knockouts reveals the diversity of p53-dependent responses to cell-cycle defects. *Dev. Cell.* 40:405–420. http://dx.doi.org/10.1016/j.devcel.2017.01.012

Miller, P.M., A.W. Folkmann, A.R. Maia, N. Efimova, A. Efimov, and I. Kaverina. 2009. Golgi-derived CLASP-dependent microtubules control Golgi organization and polarized trafficking in motile cells. *Nat. Cell Biol.* 11:1069–1080. http://dx.doi.org/10.1038/ncb1920

Mimori-Kiyosue, Y., I. Grigoriev, G. Lansbergen, H. Sasaki, C. Matsui, F. Severin, N. Galjart, F. Grosveld, I. Vorobjev, S. Tsukita, and A. Akhmanova. 2005. CLASP1 and CLASP2 bind to EB1 and regulate microtubule plus-end dynamics at the cell cortex. *J. Cell Biol.* 168:141–153. http://dx.doi.org/10.1083/jcb.200405094

Montenegro Gouveia, S., K. Leslie, L.C. Kapitein, R.M. Buey, I. Grigoriev, M. Wagenbach, I. Smal, E. Meijering, C.C. Hoogenraad, L. Wordeman, et al. 2010. In vitro reconstitution of the functional interplay between MCAK and EB3 at microtubule plus ends. *Curr. Biol.* 20:1717–1722. http://dx.doi.org/10.1016/j.cub.2010.08.020

Nakamura, S., I. Grigoriev, T. Nogi, T. Hamaji, L. Cassimeris, and Y. Mimori-Kiyosue. 2012. Dissecting the nanoscale distributions and functions of microtubule-end-binding proteins EB1 and ch-TOG in interphase HeLa cells. *PLoS One.* 7:e51442. http://dx.doi.org/10.1371/journal.pone.0051442

Preciado López, M., F. Huber, I. Grigoriev, M.O. Steinmetz, A. Akhmanova, G.H. Koenderink, and M. Dogterom. 2014. Actin-microtubule coordination at growing microtubule ends. *Nat. Commun.* 5:4778. http://dx.doi.org/10.1038/ncomms5778

Purohit, A., S.H. Tynan, R. Vallee, and S.J. Doxsey. 1999. Direct interaction of pericentrin with cytoplasmic dynein light intermediate chain contributes to mitotic spindle organization. *J. Cell Biol.* 147:481–492. http://dx.doi.org/10.1083/jcb.147.3.481

Ran, F.A., P.D. Hsu, J. Wright, V. Agarwala, D.A. Scott, and F. Zhang. 2013. Genome engineering using the CRISPR-Cas9 system. *Nat. Protoc.* 8:2281–2308. http://dx.doi.org/10.1038/nprot.2013.143

Rios, R.M. 2014. The centrosome-Golgi apparatus nexus. *Philos. Trans. R. Soc. Lond. B Biol. Sci.* 369:369. http://dx.doi.org/10.1098/rstb.2013.0462

Rivero, S., J. Cardenas, M. Bornens, and R.M. Rios. 2009. Microtubule nucleation at the cis-side of the Golgi apparatus requires AKAP450 and GM130. *EMBO J.* 28:1016–1028. http://dx.doi.org/10.1038/emboj.2009.47

Roubin, R., C. Acquaviva, V. Chevrier, F. Sedjaï, D. Zyss, D. Birnbaum, and O. Rosnet. 2013. Myomegalin is necessary for the formation of centrosomal and Golgi-derived microtubules. *Biol. Open.* 2:238–250. http://dx.doi.org/10.1242/bio.20123392

Sanders, A.A., and I. Kaverina. 2015. Nucleation and dynamics of Golgi-derived microtubules. *Front. Neurosci.* 9:431. http://dx.doi.org/10.3389/fnins.2015.00431

Sato, Y., K. Hayashi, Y. Amano, M. Takahashi, S. Yonemura, I. Hayashi, H. Hirose, S. Ohno, and A. Suzuki. 2014. MTCL1 crosslinks and stabilizes non-centrosomal microtubules on the Golgi membrane. *Nat. Commun.* 5:5266. http://dx.doi.org/10.1038/ncomms6266

Schuyler, S.C., and D. Pellman. 2001. Microtubule "plus-end-tracking proteins": the end is just the beginning. *Cell.* 105:421–424. http://dx.doi.org/10.1016/S0092-8674(01)00364-6

Stehbens, S., and T. Wittmann. 2012. Targeting and transport: how microtubules control focal adhesion dynamics. *J. Cell Biol.* 198:481–489. http://dx.doi.org/10.1083/jcb.201206050

Stehbens, S.J., M. Paszek, H. Pemble, A. Ettinger, S. Gierke, and T. Wittmann. 2014. CLASPs link focal-adhesion-associated microtubule capture to localized exocytosis and adhesion site turnover. *Nat. Cell Biol.* 16:561–573. http://dx.doi.org/10.1038/ncb2975

Stepanova, T., J. Slemmer, C.C. Hoogenraad, G. Lansbergen, B. Dortland, C.I. De Zeeuw, F. Grosveld, G. van Cappellen, A. Akhmanova, and N. Galjart. 2003. Visualization of microtubule growth in cultured neurons via the use of EB3-GFP (end-binding protein 3-green fluorescent protein). *J. Neurosci.* 23:2655–2664.

Straube, A., and A. Merdes. 2007. EB3 regulates microtubule dynamics at the cell cortex and is required for myoblast elongation and fusion. *Curr. Biol.* 17:1318–1325. http://dx.doi.org/10.1016/j.cub.2007.06.058

Thomas, G.E., K. Bandopadhyay, S. Sutradhar, M.R. Renjith, P. Singh, K.K. Gireesh, S. Simon, B. Badarudeen, H. Gupta, M. Banerjee, et al. 2016. EB1 regulates attachment of Ska1 with microtubules by forming extended structures on the microtubule lattice. *Nat. Commun.* 7:11665. http://dx.doi.org/10.1038/ncomms11665

Toyoshima, F., and E. Nishida. 2007. Integrin-mediated adhesion orients the spindle parallel to the substratum in an EB1- and myosin X-dependent manner. *EMBO J.* 26:1487–1498. http://dx.doi.org/10.1038/sj.emboj.7601599

van der Vaart, B., C. Manatschal, I. Grigoriev, V. Olieric, S.M. Gouveia, S. Bjelic, J. Demmers, I. Vorobjev, C.C. Hoogenraad, M.O. Steinmetz, and A. Akhmanova. 2011. SLAIN2 links microtubule plus end-tracking proteins and controls microtubule growth in interphase. *J. Cell Biol.* 193:1083–1099. http://dx.doi.org/10.1083/jcb.201012179

Vinogradova, T., R. Paul, A.D. Grimaldi, J. Loncarek, P.M. Miller, D. Yampolsky, V. Magidson, A. Khodjakov, A. Mogilner, and I. Kaverina. 2012. Concerted effort of centrosomal and Golgi-derived microtubules is required for proper Golgi complex assembly but not for maintenance. *Mol. Biol. Cell.* 23:820–833. http://dx.doi.org/10.1091/mbc.E11-06-0550

Wang, Z., C. Zhang, and R.Z. Qi. 2014. A newly identified myomegalin isoform functions in Golgi microtubule organization and ER-Golgi transport. *J. Cell Sci.* 127:4904–4917. http://dx.doi.org/10.1242/jcs.155408

Wong, Y.L., J.V. Anzola, R.L. Davis, M. Yoon, A. Motamedi, A. Kroll, C.P. Seo, J.E. Hsia, S.K. Kim, J.W. Mitchell, et al. 2015. Cell biology. Reversible centriole depletion with an inhibitor of Polo-like kinase 4. *Science.* 348:1155–1160. http://dx.doi.org/10.1126/science.aaa5111

Wu, J., C. de Heus, Q. Liu, B.P. Bouchet, I. Noordstra, K. Jiang, S. Hua, M. Martin, C. Yang, I. Grigoriev, et al. 2016. Molecular pathway of microtubule organization at the Golgi apparatus. *Dev. Cell.* 39:44–60. http://dx.doi.org/10.1016/j.devcel.2016.08.009

Xia, P., Z. Wang, X. Liu, B. Wu, J. Wang, T. Ward, L. Zhang, X. Ding, G. Gibbons, Y. Shi, and X. Yao. 2012. EB1 acetylation by P300/CBP-associated factor (PCAF) ensures accurate kinetochore-microtubule interactions in mitosis. *Proc. Natl. Acad. Sci. USA.* 109:16564–16569. http://dx.doi.org/10.1073/pnas.1202639109

Yao, Y., I. Smal, I. Grigoriev, M. Martin, A. Akhmanova, and E. Meijering. 2017. Automated analysis of intracellular dynamic processes. *Methods Mol. Biol.* 1563:209–228. http://dx.doi.org/10.1007/978-1-4939-6810-7_14

Young, A., J.B. Dictenberg, A. Purohit, R. Tuft, and S.J. Doxsey. 2000. Cytoplasmic dynein-mediated assembly of pericentrin and gamma tubulin onto centrosomes. *Mol. Biol. Cell.* 11:2047–2056. http://dx.doi.org/10.1091/mbc.11.6.2047

Yue, J., M. Xie, X. Gou, P. Lee, M.D. Schneider, and X. Wu. 2014. Microtubules regulate focal adhesion dynamics through MAP4K4. *Dev. Cell.* 31:572–585. http://dx.doi.org/10.1016/j.devcel.2014.10.025

Zanic, M., P.O. Widlund, A.A. Hyman, and J. Howard. 2013. Synergy between XMAP215 and EB1 increases microtubule growth rates to physiological levels. *Nat. Cell Biol.* 15:688–693. http://dx.doi.org/10.1038/ncb2744

Zhu, X., and I. Kaverina. 2013. Golgi as an MTOC: making microtubules for its own good. *Histochem. Cell Biol.* 140:361–367. http://dx.doi.org/10.1007/s00418-013-1119-4

Zimniak, T., K. Stengl, K. Mechtler, and S. Westermann. 2009. Phosphoregulation of the budding yeast EB1 homologue Bim1p by Aurora/Ipl1p. *J. Cell Biol.* 186:379–391. http://dx.doi.org/10.1083/jcb.200901036

Table S1. **Mutations in EB genes from different clones**

Hela EB1/2/3mut EB1 control

EB1

gRNA: TGGAAAAGACTATGACCCTG
AACTATGATGGAAAAGACTATGACCCTGTGGCTGCCAGACAAGGTCAAGAAACTGCAGTGGCTCCTTCCCTTGTTGCTCCAGCTCTGAATAAA
N Y D G K D Y D P V A A R Q G Q E T A V A P S L V A P A L N K

Clone #1 Insertion: C EB1 126AA +21AA after frameshift
AACTATGATGGAAAAGACTATGACCC**C**TGTGGCTGCCAGACAAGGTCAAGAAACTGCAGTGGCTCCTTCCCTTGTTGCTCCAGCTCTGAATAA
N Y D G K D Y D P C G C Q T R S R N C S G S F P C C S S S E Stop

Clone #1 Deletion: C EB1 125AA +20AA after frameshift
AACTATGATGGAAAAGACTATGACC-TGTGGCTGCCAGACAAGGTCAAGAAACTGCAGTGGCTCCTTCCCTTGTTGCTCCAGCTCTGAATAAA
N Y D G K D Y D L W L P D K V K K L Q W L L P L L L Q L Stop

Clone #2 Deletion: TAGC EB1 123AA +21AA after frameshift
AACTATGATGGAAAAGAC----TACCTGTGGCTGCCAGACAAGGTCAAGAAACTGCAGTGGCTCCTTCCCTTGTTGCTCCAGCTCTGAATAAA
N Y D G K D Y L W L P D K V K K L Q W L L P L L L Q L Stop

Clone #2 Deletion: C EB1 125AA +20AA after frameshift
AACTATGATGGAAAAGACTATGACC-TGTGGCTGCCAGACAAGGTCAAGAAACTGCAGTGGCTCCTTCCCTTGTTGCTCCAGCTCTGAATAAA
N Y D G K D Y D L W L P D K V K K L Q W L L P L L L Q L Stop

EB2

gRNA:CCGGAAGCACACAGTGCGCG
ATTCCTTTCCGGAAGCACACAGTGCGCGGGGAGCGTTCCTACAG(intron)
I P F R K H T V R G E R S Y

Clone #1 Deletion: GCGGGGAGCG EB2 34AA +15AA after frameshift
ATTCCTTTCCGGAAGCACACAGTGC----------TTCCTACAG(intron)
I P F R K H T V L P T

Clone #1Deletion: CACACAGTGCGCGGGGAGCGTTCCTACAG EB2 31AA +20AA after frameshift
ATTCCTTTCCGGAAG----------(intron)
I P F R K

Clone #2 Insertion: C EB2 34AA +293 AA after frameshift
ATTCCTTTCCGGAAGCACACAGTGC**C**GCGGGGAGCGTTCCTACAG(intron)
I P F R K H T V P R G A F L Q

Clone #2 Deletion: CAGTGCGCGGGGAGCGTTCCTA EB2 32AA +13AA after frameshift
ATTCCTTTCCGGAAGCACA----------CAG(intron)
I P F R K H T

EB3

gRNA: TGCACCTCAACTATACCAAG
TGGGTCAACGACTCCCTGCACCTCAACTATACCAAGATAGAACAGCTTTGTTCAG(intron)
W V N D S L H L N Y T K I E Q L C S

Clone #1 Deletion: GACTCCCTGCACCTCAAC EB3 Deletion of 6AA in CH domain
TGGGTCAAC----------TATACCAAGATAGAACAGCTTTGTTCAG(intron)
W V N Y T K I E Q L C S

Clone #2 Insertion: A EB3 28AA +59AA after frameshift
TGGGTCAACGACTCCCTGCA**A**CCTCAACTATACCAAGATAGAACAGCTTTGTTCAG(intron)
W V N D S L Q P Q L Y Q D R T A L F

RPE EB1/3mut

EB1

```
  gRNA: TGGAAAAGACTATGACCCTG
AACTATGATGGAAAAGACTATGACCCTGTGGCTGCCAGACAAGGTCAAGAAACTGCAGTGGCTCCTTCCCTTGTTGCTCCAGCTCTGAATAAA
 N  Y  D  G  K  D  Y  D  P  V  A  A  R  Q  G  Q  E  T  A  V  A  P  S  L  V  A  P  A  L  N  K
```

Deletion: C EB1 125AA +20AA after frameshift

```
AACTATGATGGAAAAGACTATGACC-TGTGGCTGCCAGACAAGGTCAAGAAACTGCAGTGGCTCCTTCCCTTGTTGCTCCAGCTCTGAATAAA
 N  Y  D  G  K  D  Y  D   L  W  L  P  D  K  V  K  K  L  Q  W  L  L  P  L  L  L  Q  L  Stop
```

EB2

```
  gRNA: CCGGAAGCACACAGTGCGCG
ATTCCTTTCCGGAAGCACACAGTGCGCGGGGAGCGTTCCTACAG(intron)
 I  P  F  R  K  H  T  V  R  G  E  R  S  Y
```

Insertion: A EB2 34AA +27AA after frameshift

```
ATTCCTTTCCGGAAGCACACAGTGCAGCGGGGAGCGTTCCTACAG(intron)
 I  P  F  R  K  H  T  V  Q  R  G  A  F  L  Q
```

Insertion: C EB2 34AA +27AA after frameshift

```
ATTCCTTTCCGGAAGCACACAGTGCCGCGGGGAGCGTTCCTACAG(intron)
 I  P  F  R  K  H  T  V  P  R  G  A  F  L  Q
```

EB3

```
          gRNA: TGCACCTCAACTATACCAAG
TGGGTCAACGACTCCCTGCACCTCAACTATACCAAGATAGAACAGCTTTGTTCAG(intron)
 W  V  N  D  S  L  H  L  N  Y  T  K  I  E  Q  L  C  S
```

Insertion: A EB3 28AA +59AA after frameshift

```
TGGGTCAACGACTCCCTGCAACCTCAACTATACCAAGATAGAACAGCTTTGTTCAG(intron)
 W  V  N  D  S  L  Q  P  Q  L  Y  Q  D  R  T  A  L  F
```

For each gene, the gRNA target sequence, the WT sequence, and its translation are shown in black, deletions are indicated by dashes, and insertions and amino acids resulting from frameshifts are shown in red. Parentheses indicate start of an intron. Note that in HeLa1/2/3mut clone 1, a small in-frame deletion is present in the EB3 CH domain, but no EB3 reactivity is detected in this clone with anti-EB3 rabbit polyclonal antibodies. All the different allelic variants of EB-encoding genes recovered from each clone are shown.

Supplemental material

JCB

Yang et al., https://doi.org/10.1083/jcb.201701024

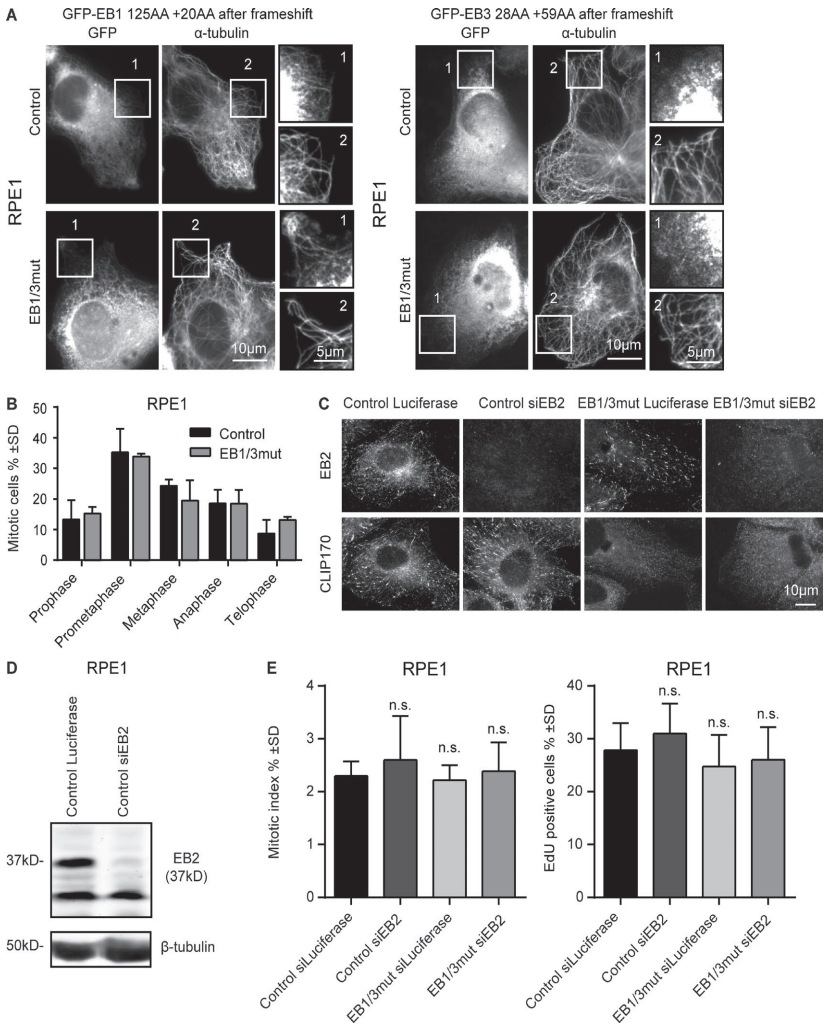

Figure S1. **Characterization of cell division after disruption of EB-encoding genes in RPE1 cells.** (A) Immunostaining for α-tubulin in control and EB1/3mut RPE1 cells expressing EB1 and EB3 fragments, which would result from the missense mutations observed in EB11/3mut RPE1 cells. Enlarged images of the boxed areas indicated by numbers are shown on the right. (B) Quantification of mitotic stages in control and EB1/3mut RPE1cells. Three independent experiments with 3,000 cells per condition were analyzed. No significant differences were detected (Student's *t* test). (C) Immunostaining for EB2 and CLIP170 in control and EB1/3mut RPE1 cells transfected with the indicated siRNAs. (D) Western blot illustrating EB2 expression in RPE1 cells transfected with siRNAs against luciferase (control) or EB2. (E) Quantification of the mitotic index and EdU-positive RPE1 control or EB1/3mut cells transfected with the indicated siRNAs. $n \geq 3$ experiments, with 1,000 cells per experiment. n.s., $P > 0.05$ (Mann-Whitney *U* test).

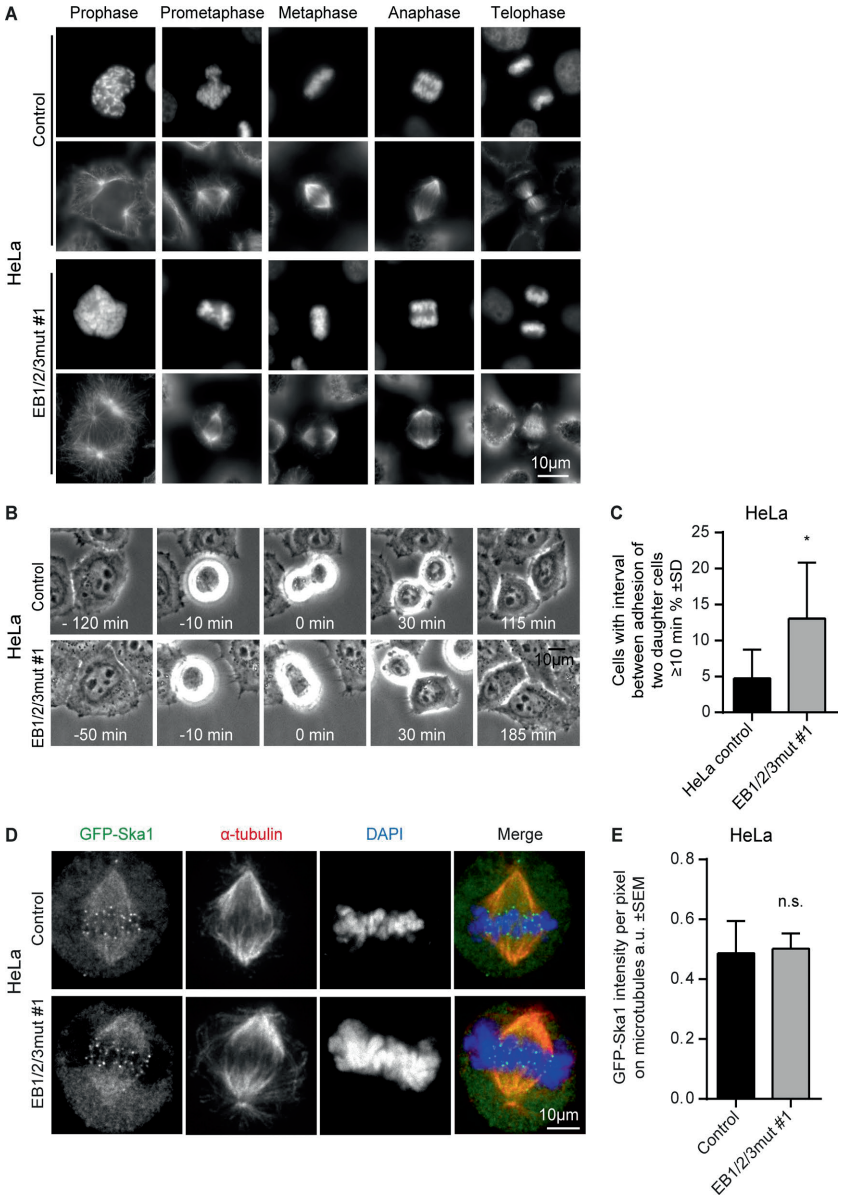

Figure S2. **Characterization of cell division after disruption of EB-encoding genes in HeLa cells.** (A) Immunostaining for α-tubulin and DAPI in control and EB1/2/3mut HeLa cells at different stages of mitosis. (B) Selected frames of phase-contrast live cell imaging of control cells and EB1/2/3mut HeLa cells. 0 min corresponds to the first frame in anaphase. (C) Quantification of the percentage of cells displaying a more than 10 min time interval between the adherence of the two daughter cells after mitosis in control and EB1/2/3mut HeLa cells. 160 and 495 cells were analyzed; *, $P < 0.05$ (Mann-Whitney *U* test). (D) Immunostaining for α-tubulin and DAPI in control and EB1/2/3mut HeLa cells expressing GFP-Ska1 construct. (E) Quantification of intensity of GFP-Ska1 on the spindle microtubules in control and EB1/2/3mut HeLa cells. $n > 30$; n.s., $P > 0.05$ (Mann-Whitney *U* test).

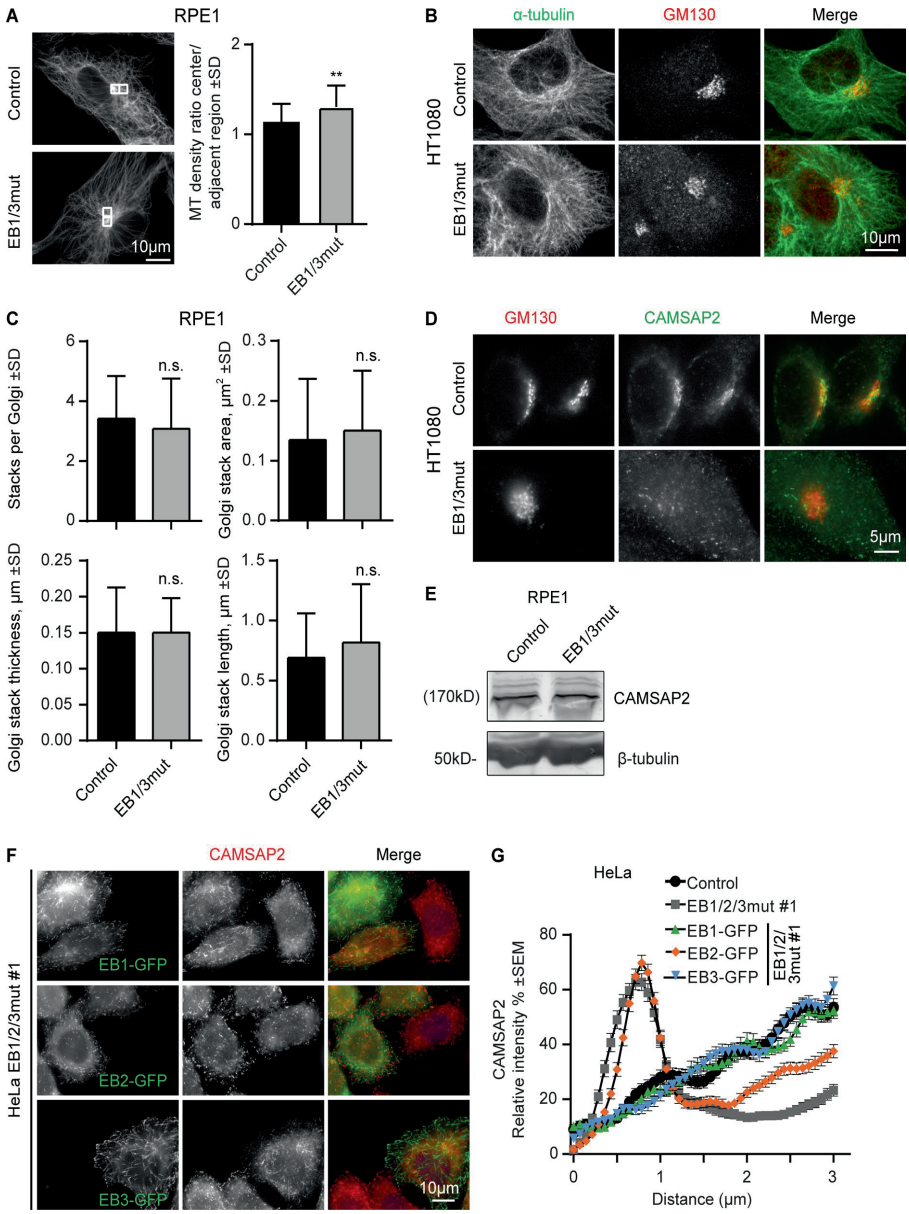

Figure S3. **Effects of EB disruption on MT and Golgi organization and the distribution of CAMSAP2-decorated MT minus ends.** (A) Immunostaining and quantification of the ratio of MT density around the centrosome and an adjacent cell region in the indicated RPE1 cells. 30 control and 35 EB1/3mut cells were analyzed. **, P < 0.01 (Mann-Whitney *U* test). (B and D) Immunostaining for GM130 and α-tubulin (B) or CAMSAP2 (D) in control and EB1/3mut HT1080 cells. (C) Quantification of Golgi stack number, Golgi stack area, thickness and length measured in EM images. 28 images of control and EB1/3mut RPE1 cells were analyzed. (E) Western blot analysis of CAMSAP2 expression in control and EB1/3mut PRE1 cells. (F) Immunostaining for CAMSAP2 in EB1/2/3mut HeLa cells expressing the indicated constructs. (G) Quantification the relative intensity of CAMSAP2 staining within a 3-µm distance from the cell edge (as depicted by yellow arrows in Fig. 5 A) in control and EB1/2/3mut cells expressing the indicated constructs. Ninety to 105 cells were analyzed per condition.

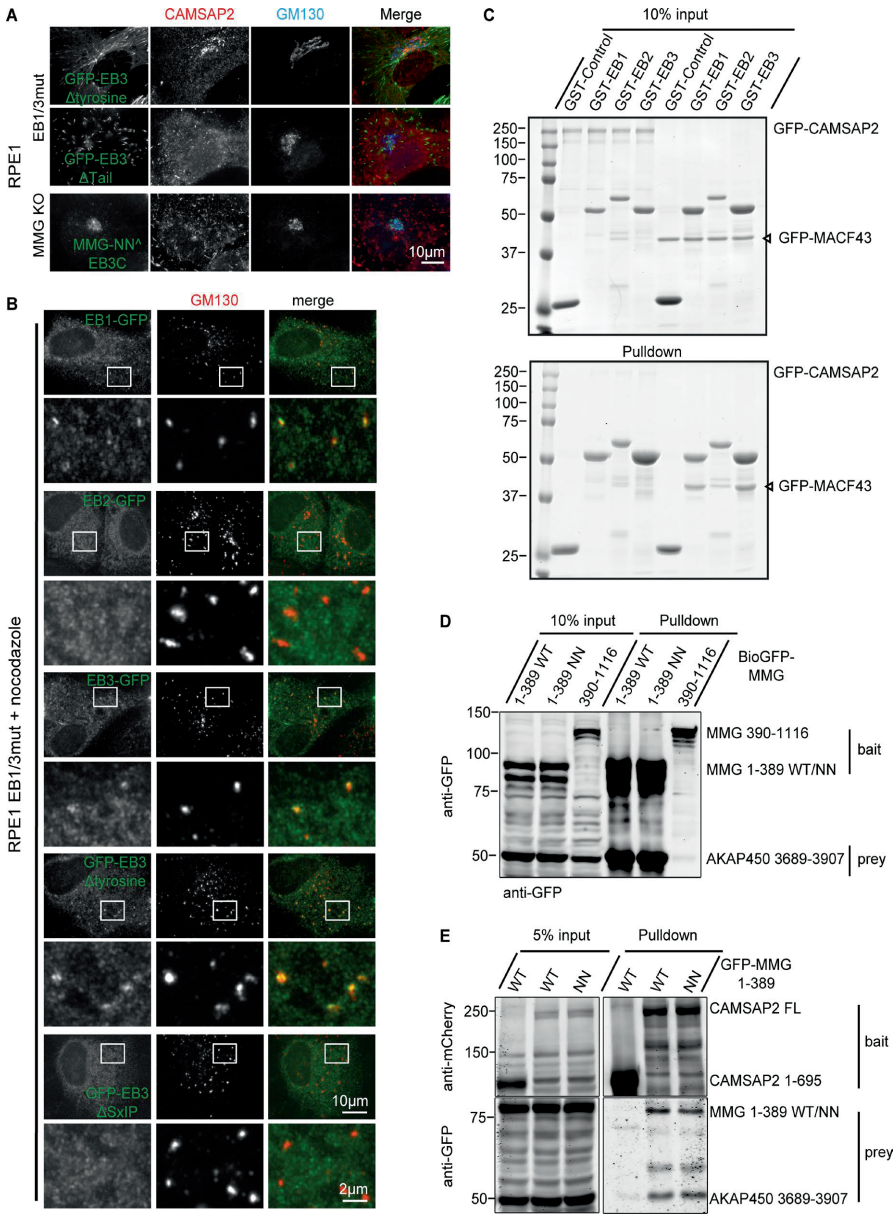

Figure S4. **Recruitment of EBs and CAMSAP2 to the Golgi and biochemical characterization of the interactions between AKAP450, MMG, CAMSAP2, and EB1.** (A) Immunostaining for CAMSAP2 and GM130 in EB1/3mut and MMG knockout RPE1 cells expressing the indicated constructs. (B) Immunostaining for GM130 in EB1/3mut RPE1 cells transfected with the indicated GFP-tagged constructs and treated with 14 μM nocodazole for 3 h. Enlarged portions of the boxed areas are shown below each row of panels. (C) Coomassie blue–stained gel of GST-EB pull down assays with purified GFP-CAMSAP2 and GFP-MACF43. GFP-MACF43 serves here as a positive control; it is the C-terminal 43 amino acid long peptide of MACF2 with a single SxIP motif, dimerized by the addition of a leucine zipper (Honnappa et al., 2009). (D) Streptavidin pull-downs with the extracts of HEK293T cells coexpressing Bio-GFP-myomegalin (MMG) 1–389 WT, Bio-GFP-myomegalin 1–389 NN, or Bio-GFP-myomegalin 390–1116 together with GFP-AKAP450 3689–3907 and BirA, analyzed by Western blotting with anti-GFP antibodies. (E) Streptavidin pull-down with the extracts of HEK293T cells coexpressing Bio-mCherry-CAMSAP2 1–695 or full length (FL) together with GFP-AKAP450 3689–3907, GFP-myomegalin 1–389 WT, or the LP/NN mutant and BirA, analyzed by Western blotting with antibodies against GFP or mCherry.

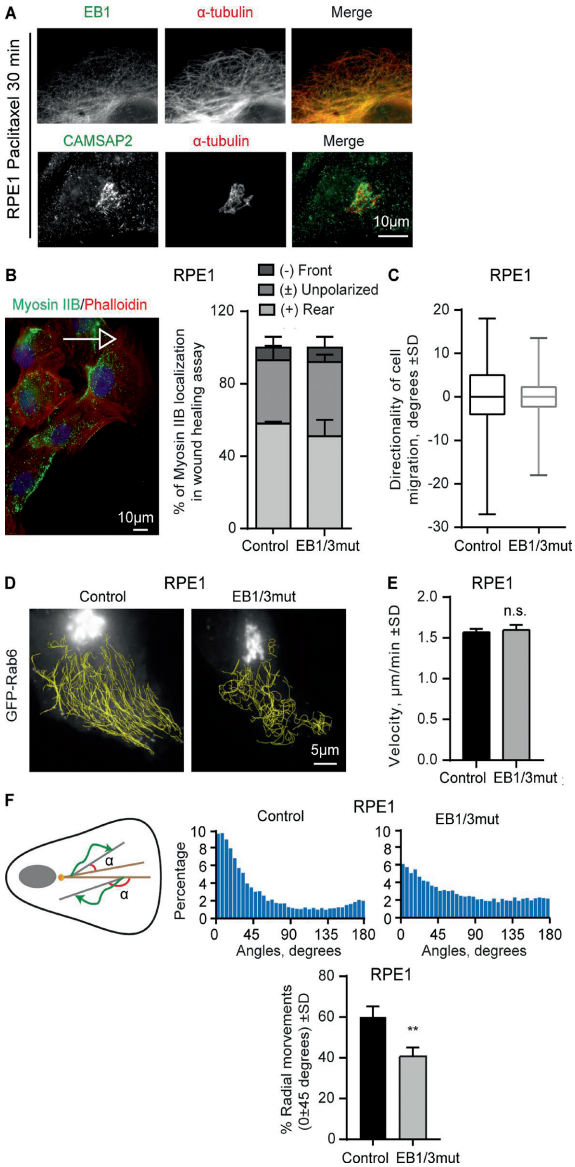

Figure S5. **Polarized distribution of Myosin IIB and the directionality of cell migration are not perturbed in EB1/3mut RPE1 cells.** (A) Immunostaining for EB1 and α-tubulin (top) or CAMSAP2 and GM130 (bottom) in RPE1 cells treated with 5 μM paclitaxel for 30 min. (B) Immunostaining for myosin IIB and F-actin (phalloidin) in a monolayer wound healing assay and quantification of myosin IIB localization relative to the monolayer wound. 196 control and 195 EB1/3mut RPE1 cells were analyzed. No significant differences were observed (Mann-Whitney *U* test). (C) Quantification of movement directionality during migration in sparse control and EB1/3mut RPE1 cultures. The angle between the vectors of cell displacement was measured in three subsequent frames. 0°, movement vectors were parallel between frames 1 and 2, and frames 2 and 3. Positive angle: counterclockwise deviation from 0°; negative angle: clockwise deviation from 0°. 51 control and 60 EB1/3mut RPE1 cells were analyzed. No significant differences were observed (Mann-Whitney *U* test). (D) Representative images of GFP-Rab6A (labeled as GFP-Rab6) vesicle tracks in control and EB1/3mut RPE1 cells. (E) Velocity of GFP-Rab6 vesicle movements. $n = 3$ experiments, representing in total 10,000 vesicle tracks in 10–12 cells per experiment. (F) Quantification of the radiality of GFP-Rab6 tracks in control and EB1/3mut RPE1 cells. Track angles range from 0° to 180°, where 0° corresponds to a particle moving along the radius away from the reference point (from the center of the Golgi to the cell periphery), and 180° corresponds to a particle moving radially toward the cell center. Percentage of tracks with the angle between 0° and 45° is shown on the right. $n = 3$ experiments, with 10–12 cells per experiment. n.s., $P > 0.05$; **, $P < 0.01$ (Mann-Whitney *U* test).

Provided online as a PDF is table S1, which shows mutations in EB genes from different clones.

References

Honnappa, S., S.M. Gouveia, A. Weisbrich, F.F. Damberger, N.S. Bhavesh, H. Jawhari, I. Grigoriev, F.J. van Rijssel, R.M. Buey, A. Lawera, et al. 2009. An EB1-binding motif acts as a microtubule tip localization signal. *Cell*. 138:366–376. http://dx.doi.org/10.1016/j.cell.2009.04.065

3

Investigation of the effects of End Binding proteins on the properties of growing microtubule plus ends

Chao Yang, Ilya Grigoriev, Eugene A. Katrukha, Ruddi Rodríguez García, Cédric Gerwoud van der Ham and Anna Akhmanova

To be submitted

Cell Biology, Department of Biology, Faculty of Science, Utrecht University,

Padualaan 8, 3584 CH Utrecht, The Netherlands

Abstract

Microtubules are cytoskeletal polymers that can rapidly switch between phases of growth and shortening. This dynamic behavior is intimately connected to the hydrolysis of GTP nucleotide by β-tubulin. Newly incorporated tubulin dimers are bound to GTP, and growing microtubules bear at their ends a stabilizing cap of GTP-bound tubulin dimers. When GTP is hydrolyzed, the stabilizing cap is lost, and this leads to rapid microtubule disassembly. End Binding proteins specifically recognize GTP-bound microtubule lattices and accumulate at microtubule plus ends in the region overlapping with the GTP cap. In vitro work has shown that EBs can accelerate GTP hydrolysis by tubulin, thus shortening the length of the stabilizing cap, and this likely explains why in vitro, EBs potentiate microtubule catastrophes. However, in cells, EBs suppress rather than induce catastrophes. This could be due to EB-driven alteration of microtubule tip structure, direct tip occlusion and protection against depolymerases, or recruitment of microtubule stabilizing proteins. Here, we set out to test how EBs and their ability to recruit a broad variety of binding partners affect the properties of growing microtubule ends. We compared EB comet length in cells and in an in vitro assay with purified components, and found that at the same microtubule polymerization rate, their length depended on the fluorescent EB protein used, and for the same EB protein, the comets appeared somewhat longer in vitro than in cells. Based on laser severing experiments, we found that the length of the stable microtubule plus-end proximal zone was not significantly affected by the presence of EBs. However, the behavior of the microtubule plus ends changed in two ways: they became more mobile, and their growth appeared to be more interrupted, with short excursions of growth and disassembly. This effect was apparent with EB versions lacking the C-terminal partner-binding domain of the EBs and could be rescued by recruiting this domain back to microtubule plus ends. While further work is necessary to confirm these findings, our results suggest that the major impact of EBs on growing microtubule ends in cells depends on their microtubule tip-associated binding partners.

INTRODUCTION

Microtubules are dynamic polymers built of dimers of α-tubulin and β-tubulin, which bind to each other in a head-to-tail fashion. Tubulin is a GTPase – when microtubules polymerize, the GTP nucleotide bound to β-tubulin is hydrolyzed with some delay after the next tubulin dimer is added to the microtubule end. As a result, a growing microtubule end bears a cap of GTP-bound tubulin subunits, which stabilize the polymer. When GTP is hydrolyzed and the cap is lost, the microtubule switches to depolymerization (Desai and Mitchison, 1997). Recent work has indicated that the size of the cap correlates with the instantaneous stability of microtubules, and the switching between growth and shrinkage occurs when the number of GTP-bound tubulin subunits at the end of the cap falls beyond a certain threshold (Duellberg et al., 2016).

End Binding proteins associate with a site located between protofilaments at the vertex of four tubulin dimers, close to the structural elements of β-tubulin that are affected by GTP hydrolysis. This binding mode has two important consequences – EBs can distinguish between different nucleotide states of β-tubulin (Maurer et al., 2011; Maurer et al., 2012; Roostalu et al., 2019; Zanic et al., 2009) and can also accelerate GTP hydrolysis and shorten the stabilizing GTP cap (Maurer et al., 2014; Zhang et al., 2015). EB binding to microtubules can thus in principle be used to determine the length of the cap (Seetapun et al., 2012). Furthermore, the addition of EB proteins potentiates catastrophes in assays with purified tubulin and makes microtubules more sensitive to drugs that induce microtubule depolymerization (Bieling et al., 2007); (Komarova et al., 2009; Mohan et al., 2013). Paradoxically, in cells, EBs have an opposite effect – they inhibit rather than promote catastrophes (Komarova et al., 2009). This can be potentially explained by the ability of EBs to concentrate at the growing microtubule plus ends a large variety of microtubule regulators (Akhmanova and Steinmetz, 2015; Kumar and Wittmann, 2012). Interestingly, previous work has also shown that a dimeric version of EB3 containing the microtubule-binding but not the partner-binding domain could also suppress catastrophes in cells to some extent, although not as potently as the full length EB3 (Komarova et al., 2009). These experiments were carried out in cells that were simultaneously depleted of EBs using RNA interference and still likely expressed low levels of endogenous EB proteins. Such residual expression is a major concern, because whereas human cultured cells are thought to express ~100-500 nM EB1, which is typically the most abundant EB isoform in cycling cells (Itzhak et al., 2016; Wisniewski et al., 2014), already 10 nM EB1 is sufficient to significantly shorten the length of GTP cap in vitro (Maurer et al., 2014).

In Chapter 2, we described our efforts to obtain better data on the loss of EBs by using CRISPR-Cas9-mediated gene knockouts. We have generated cells, in which EB1, EB2 and EB3-encoding genes were simultaneously mutated. However, whereas these mutations fully abrogated the expression of EB2 and EB3, the N-terminal microtubule-binding CH-domain of EB1 was likely still expressed. Here, we describe the generation of new HeLa cell lines, in which the three EB-encoding genes were mutated in a way to completely prevent the expression of the three proteins, including their microtubule-binding portions. We used these cells as a tool to compare the length of the GTP cap in cells and in vitro, and to get insight into how EBs alter the properties of growing microtubule plus ends. Our data suggest that EBs affect both the dynamics and the displacement of microtubule tips to which they bind, and that these effects largely depend on the EB partners that interact with the C-terminal regions of the EBs.

RESULTS

Generation of EB1, EB2 and EB3 knockout cells

In Chapter 2, we described the generation of HeLa cells with mutations disrupting EB1, EB2

and EB3-encoding genes by simultaneous transfection of the cells with constructs encoding Cas9 and EB1, EB2 and EB3-specific single-guide RNAs (gRNAs). These gRNAs were positioned within the N-termini of EB2 and EB3 and within the middle part of EB1. The resulting mutant cells (EB1/2/3mut) could still potentially express the microtubule-binding CH domain of EB1. Here, we selected new gRNAs that could efficiently disrupt EB genes and were all positioned within the sequences encoding CH domains in order to abrogate microtubule binding (Figure 1A). Based on our previous experience, we first generated EB2 knockout cell lines and then used them for simultaneous transfection of the EB1 and EB3-specific gRNA constructs, which resulted in generation of three cell lines lacking the expression of EB1, EB2 and EB3, as determined by Western blotting (Figure 1B) and immunofluorescence cell staining (Figure 1C). Sequencing two of these cell lines showed that frameshift mutations were present at the gRNA targeting sites in the CH domains (Table S1). Since for Western blotting, we use antibodies that recognize the C-terminal halves of the EBs, we conclude that these HeLa cell lines lack all three EB proteins and thus termed them EB1/2/3 knockout cells. Similar to the EB1/2/3mut cells described in Chapter 2, these cells had a strongly disorganized microtubule network, consistent with the defect in microtubule minus end attachment to Golgi membranes (data not shown).

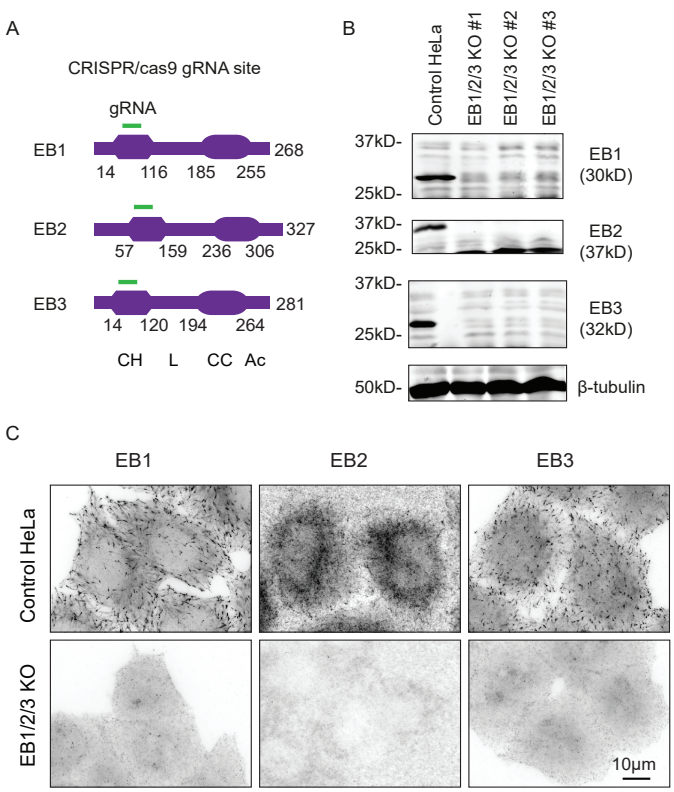

Figure 1. Characterization of EB1/2/3 knockout cell lines

A. Schemes of EB1, EB2 and EB3 proteins and the position of gRNA sequences.

B,C. Western blot analysis and immunofluorescence staining of control HeLa and the EB1/2/3 knockout (KO) cells with the indicated antibodies.

Comparison of the EB comet lengths in cells and in vitro

EB1/2/3 knockout cells represent an excellent system to compare the behavior of individual EBs in cells and in assays with purified proteins, because when they are transfected with a fluorescently tagged EB fusion protein, this fusion is the only EB species present in the cell. Our first goal was to determine whether the size of the GTP cap, as reflected by the length of EB comets, is the same in vitro and in cells. For a fair comparison, it was important to use similar EB concentrations for both measurements and also to compare microtubules growing at a similar rate, because the size of the GTP cap and thus the EB comet length depends on the microtubule polymerization velocity (Duellberg et al., 2016; Mimori-Kiyosue et al., 2000; Roth et al., 2018).

To estimate EB concentration in cells, we used Fluorescence Correlation Spectroscopy (FCS). We used a stable EB3-GFP-expressing MDA-MB-231 breast cancer cell line described previously (Bouchet et al., 2016) , as well as EB1/2/3 knockout cells transiently transfected with EB3-GFP and selected to have clearly detectable comet-like signals at the microtubule plus ends but no labeling along microtubule lattices (Figure 2A). To avoid measurements of signals corresponding to EB comets, we collected data for 10-30 s, and excluded the data with an obvious intensity peak. Next, we calculated the autocorrelation G(t), fitted it using the diffusion model for one fluorescent species (Figure 2B) and calculated protein concentrations as described in Materials and Methods. In both cases, FCS measurements showed that the concentration of EB3-GFP was in the range of 150-300 nM, with an average close to 200 nM (Figure 2C). While in the stable EB3-GFP cell line, EB3-GFP is expressed on the background of endogenous EBs, in the EB1/2/3 knockout cells it is the only EB species present, and its concentration falls within the range of the estimated endogenous EB concentrations.

To obtain dynamic microtubules in vitro, we used previously described assays in which microtubules are grown from GMPCPP-stabilized microtubule seeds and imaged by Total Internal Reflection Fluorescence (TIRF) microscopy (Bieling et al., 2007; Montenegro Gouveia et al., 2010). In the standard version of the assay used in the lab, which is performed at 30°C with 15 µM tubulin in the presence of EB3, the average microtubule growth rate is typically in the range of 3-4 µm/min, whereas in cells, microtubule growth rate is typically 15-20 µm/min (see Chapter 2 and below). To obtain rapidly growing microtubules in vitro, we performed the assays at 37°C in the presence of 15 µM tubulin and 200 nM GFP-EB3, either alone or

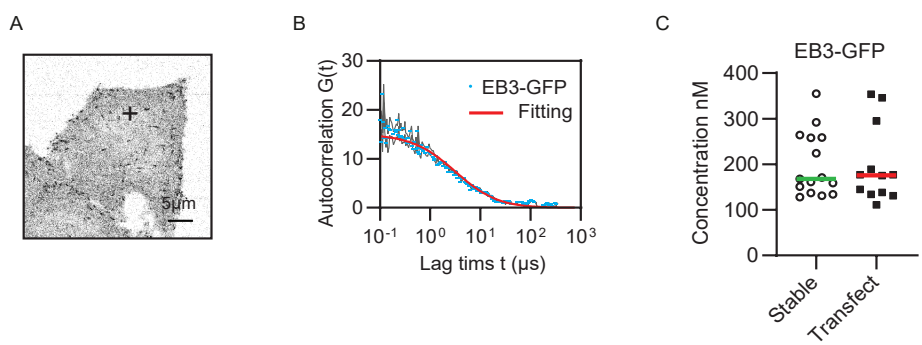

Figure 2. Estimation of EB concentration by FCS

A. A representative single frame of an EB1/2/3 KO cell transfected with EB3-GFP used for FCS measurements.

B. Representative autocorrelation of EB3-GFP signals with fitting. Dots represent experimental data and the red line represents the fitted curve.

C. FCS measurements of EB3-GFP concentration in MDA-MB-231 stable cell line (17 cells) and transiently transfected EB1/2/3 KO cells (12 cells).

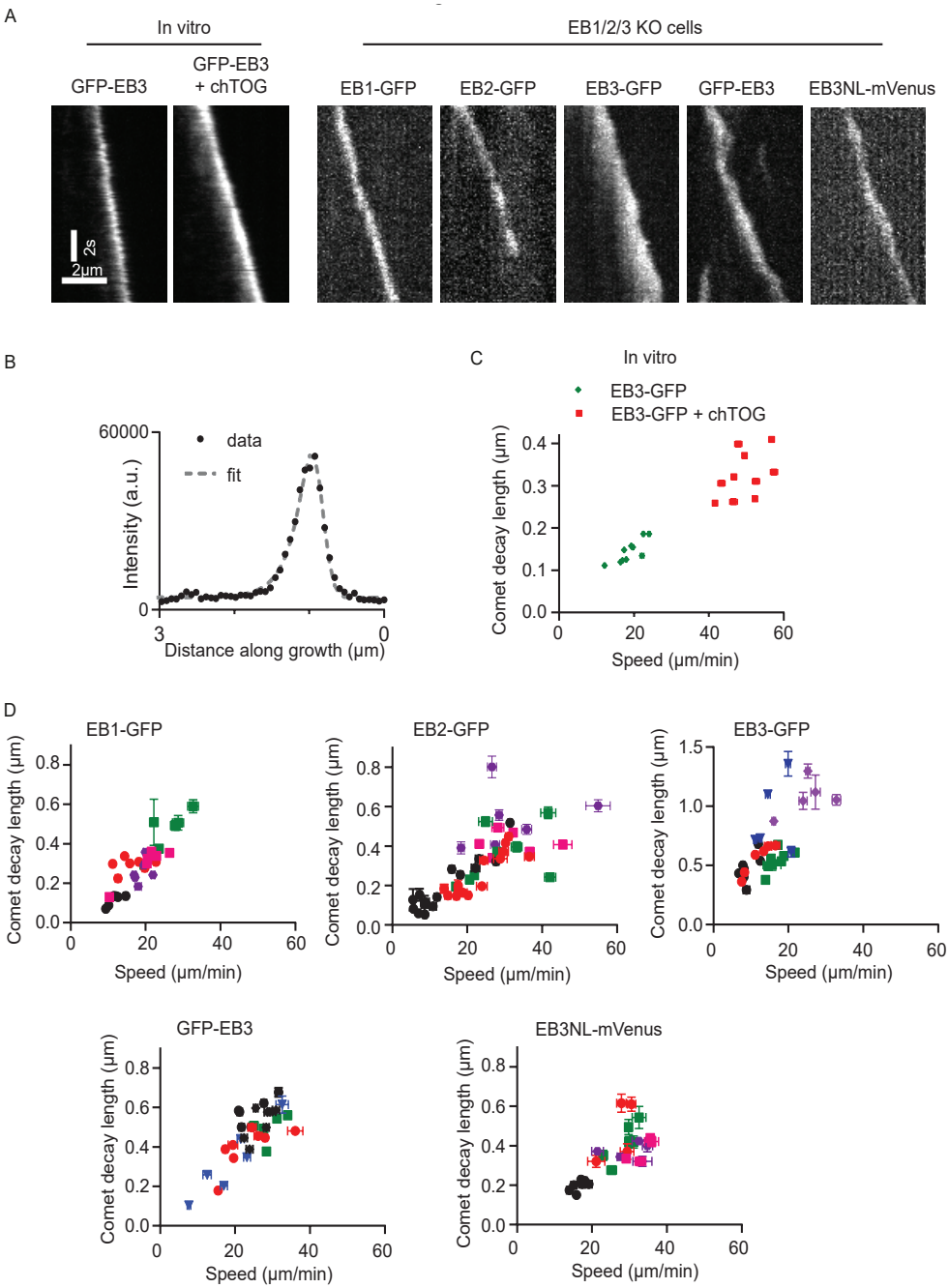

Figure 3. Determination of the EB comet length in cells and in vitro

A. From left to right: representative kymographs showing microtubule plus end growth in the presence of 200 nM GFP-EB3 in vitro, 200 nM GFP-EB3 and mCherry-chTOG in vitro and the indicated fluorescent EB constructs expressed in the EB1/2/3 KO cells.

B. Example of an individual fitting of EB3-GFP fluorescence intensity profile in the EB1/2/3 KO cells. Dots represent

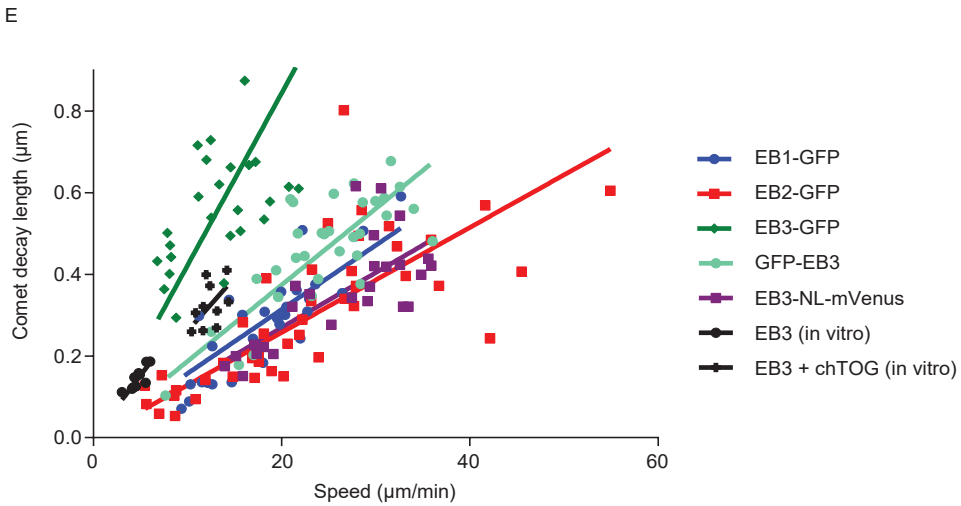

experimental data and dashed line represents the fitted curve.

C. Plot of comet decay length versus microtubule end growth speed for in vitro assays with 200 nM GFP-EB3 (green dots, n=10) and 200 nM GFP-EB3 and mCherry-chTOG (red dots, n=10). Each dot corresponds to a single growth event of an individual microtubule and represents average of fits to 20 (minimum) to 200 timepoints.

D. Plots of comet decay length versus MT end growth speed in the EB1/2/3 KO cells. Each dot corresponds to a single growth event of an individual microtubule and represents average of fits to 20 (minimum) to 200 timepoints. Dots of the same color were measured in the same cell. Measurements counts are: EB1-GFP (5 cells, 32 comets), EB2-GFP (8 cells, 44 comets), EB3-GFP (5 cells, 31 comets), GFP-EB3 (5 cells, 32 comets), EB3-NL-mVenus (5 cells, 26 comets). Error bars represent SEM.

E. The data from Figure 3C and 3D pooled together and fitted with a straight line passing through the origin of coordinates.

together with 200 nM chTOG. chTOG is a microtubule polymerase, which is known to strongly accelerate microtubule growth velocity, particularly when combined with an EB protein (Aher, 2017; Zanic et al., 2013). In these conditions, we could obtain microtubules growing with the velocity of up to 15 µm/min, which is close to the rate observed in cells.

For the analysis of EB comet length, we selected periods of uninterrupted microtubule growth (Figure 3A). At each time frame, we fitted EB comet intensity with a function that exponentially decays away from the tip (convolved with microscope's point spread function) (Figure 3B). As an estimate of comet length, we used the characteristic length of decay. As expected, we observed a strong correlation between microtubule growth rate and the comet decay length (Figure 3C). Next, we performed similar measurements using images of comets obtained by expressing in EB1/2/3 knockout cells different fluorescent EB fusions, including EB1-GFP, EB2-GFP and EB3-GFP; furthermore, we also included in this analysis GFP-EB3, with GFP positioned at the N- and not the C-terminus of the fusion. Comparing differently tagged EB proteins was relevant, because N-terminal tags can affect or even inhibit the interaction of EBs with microtubules, an effect that is particularly strong for EB1 (Skube et al., 2010; Zhu et al., 2009). EB3 can tolerate both the more frequently used C-terminal tag, as well as the N-terminal one, if GFP is connected to the CH domain with a flexible linker (Montenegro Gouveia et al., 2010). We therefore included in our analysis both EB3-GFP and GFP-EB3, because the latter construct corresponds to the recombinant protein used in vitro. Furthermore, we also included in the analysis a monomeric EB3 version, EB3-NL, labeled with monomeric Venus (mVenus) to prevent

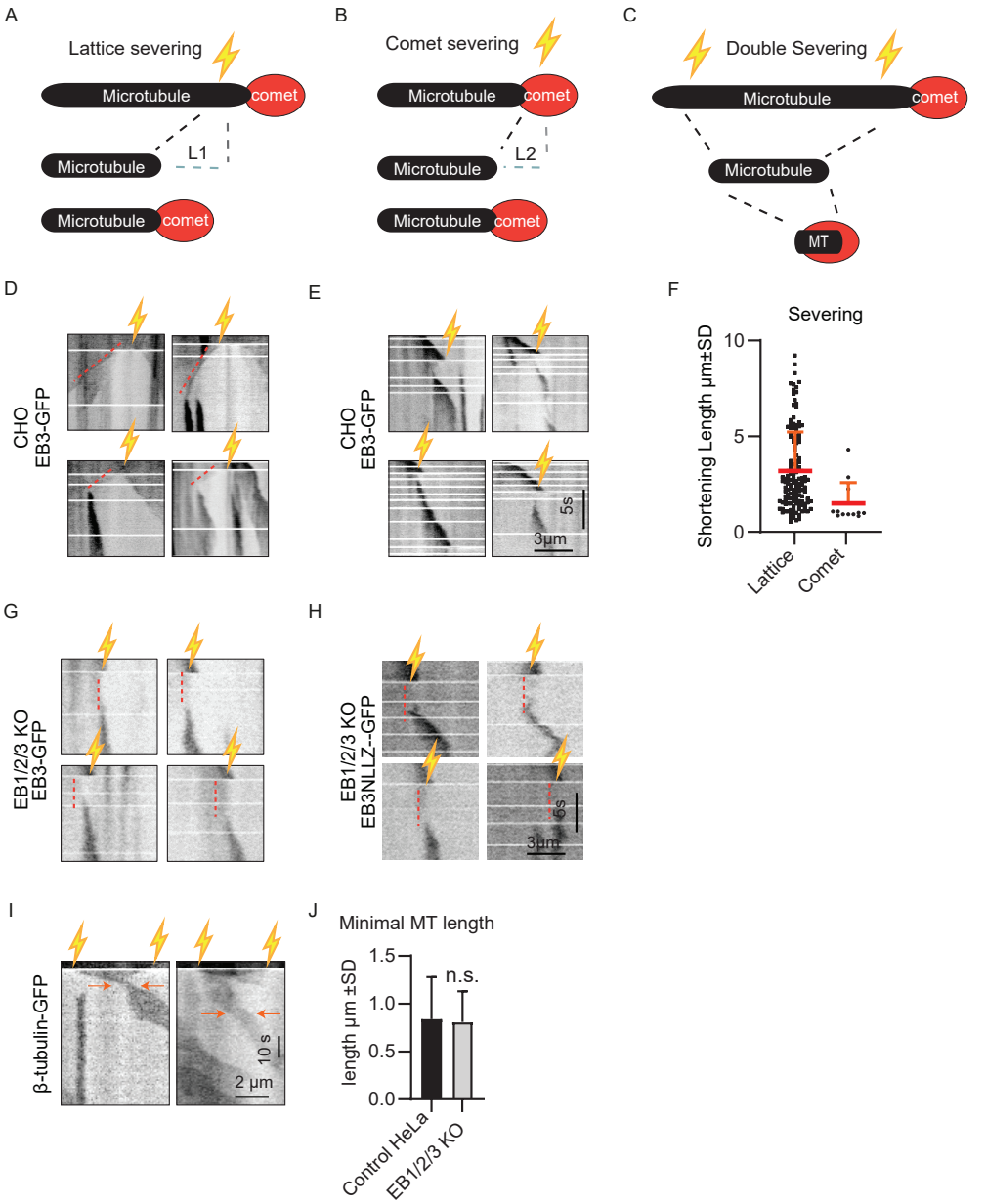

Figure 4. Analysis of the stability of the tip-proximal microtubule lattice region by microtubule severing

A-C. Modes of severing: (A) lattice severing, (B) comet severing and (C) double severing.

D,E. Kymographs of lattice severing and comet severing in CHO cells transfected with EB3-GFP. Microtubule severing was performed either at a distance greater than 2 µm or within 2 µm away from the outermost microtubule tip. After microtubule severing (shown with an orange lightning bolt), the behavior of the newly generated microtubule plus end was observed over time, and the shortening length (red stippled line) was measured until the first rescue event, which was detected as reappearance of the EB3-GFP signal. White horizontal lines across the kymographs represent the moments of photoablation, as multiple microtubules were severed during the

potential dimerization caused by the fluorescent tag. This fusion contains the CH domain and the intrinsically disordered linker region of EB3 but not the C-terminal domain responsible for dimerization and partner binding (Komarova et al., 2009). Similar to observations in vitro, also in cells, we observed a clear correlation between the comet decay length for all the EB constructs and microtubule growth rate (Figure 3D).
When all the data were combined and compared with each other (Figure 3E), it became clear that the linear fits of the correlation between comet decay length and microtubule growth rate were very similar for EB2-GFP and EB3-NL-mVenus, whereas EB1-GFP comets were slightly longer at the same growth rates, and EB3-GFP comets were significantly longer, while the growth rates observed with EB3-GFP in this dataset were slower. GFP-EB3 comets were slightly longer than the ones with EB1-GFP, but significantly shorter than the ones obtained with EB3-GFP. GFP-EB3 comets observed in our in vitro assays were longer than GFP-EB3 comets in cells, but shorter than EB3-GFP comets observed in cells. To conclude, the measurements of EB comet length in cells and in vitro indicate that they depend on the nature of the EB protein used and its dimerization status, and the comets might be slightly shorter in cells than in vitro. In particular, dimeric EB3 appears to be different from EB1 and EB2, displaying longer comets, especially if the CH domain is not preceded by a fluorescent tag. Since it is unclear whether these differences reflect the changes in GTP cap length, the differences between EBs in their ability to recognize binding sites with mixed nucleotides or their dissociation kinetics, further analyses that would include different combinations of EBs with fluorescent tags of different colors would be needed.

Analysis of the stability of the tip-proximal microtubule lattice region by microtubule severing
Another way of addressing the properties of the GTP cap is by probing its stability. Previous work has shown that microtubules shorten significantly slower and undergo rescue more frequently in the vicinity of the microtubule tip as compared to microtubule regions located more than 2 µm away from the tip (Seetapun et al., 2012). To extend these observations and probe microtubule tip stability, we performed photoablation experiments, in which microtubules were severed within the internal shaft region or within the tip-proximal 2 µm region (Figure 4A,B). These two types of severing events had clearly different outcomes – whereas microtubules cut within the ~2 µm vicinity of the tip underwent only very short depolymerization excursions, these excursions were much longer when the severing event took place at a distance longer than 2 µm from the tip (Figure 4D-F). These experiments were initially performed in control cells expressing endogenous EBs and EB3-GFP as a plus end

acquisition of one movie.

F. Quantification of microtubule shortening length after lattice and comet severing. N=3 experiments, for lattice severing, 139 microtubules in 47 cells; for comet severing, 12 microtubules in 9 cells.

G,H. Kymographs of comet severing in EB1/2/3 KO cells transfected with EB3-GFP or EB3-NL-LZ-GFP. Red dashed lines represent stable microtubule plus ends before they were rescued.

I,J Kymographs of double severing in control HeLa and EB1/2/3 KO cells transfected with β-tubulin-GFP. To allow visualization of both microtubule ends, microtubules were rapidly severed at two spots separated by ~1-5 micrometers (shown with two orange lightning bolts) and the behavior of newly generated minus and plus ends was observed over time. In control cells, minus ends were either stable or depolymerized, whereas plus ends underwent dynamic instability. If a plus end (and/or minus end) depolymerized and reached the opposite end, the microtubule disappeared. However, often the depolymerizing end was rescued (or paused) before complete microtubule disappearance. The length of the shortest microtubule segments (orange arrows) observed in such situations was measured and shown in (J). N=4 experiments, 57 microtubules in 27 control HeLa cells and 58 microtubules in 29 EB1/2/3 KO cells.

marker (Figure 4D-F), but similar increased tip stability was also observed in EB1/2/3 knockout cells expressing EB3-GFP (Figure 4G). The same result was obtained in EB1/2/3 knockout cells with a dimeric EB3 version, EB3-NL-LZ-GFP, in which the C-terminal dimerization and partner-binding domain was substituted for the leucine zipper of GCN4 (Komarova et al., 2009) (Figure 4H). Since no endogenous EBs were present in the latter experiment, these data show that the stability of the tip-proximal microtubule region in cells does not depend on the EB-dependent plus end accumulation of microtubule-stabilizing EB partners.

It is however possible that EB3-NL-LZ-GFP makes microtubule plus-end proximal lattice more stable by simply by occluding it. To address this possibility, we tried to perform laser severing experiments in the absence of an EB marker, using microtubules labeled with β-tubulin-GFP. Since the tubulin signal is weaker than that of the EBs and selecting growing microtubule plus ends in the tubulin channel is more challenging, it was difficult to obtain conclusive data by cutting GFP-tubulin-positive tips. We instead performed severing of β-tubulin-GFP-labeled microtubules at two sites to obtain a free microtubule fragment (Figure 4C). In the majority of cases, the plus end of such a fragment first significantly shortened and then was rescued and started growing, whereas the minus end typically shortened (Figure 4I). Interestingly, when the plus end was growing, the shortening of the minus often slowed down when the fragment reached the length of 0.8-1 μm. We reasoned that the minimal "surviving" fragment length corresponded to the microtubule part which contained sufficiently high concentration of GTP tubulin to inhibit microtubule depolymerization from the minus end. Interestingly, such measurements yielded very similar results in control and EB1/2/3 knockout cells (Figure 4J). These data might suggest that the absence of EBs does not significantly affect the stability of the microtubule lattice proximal to the growing end and thus the length of the stabilizing cap.

Effect of EBs and their individual domains on microtubule tip behavior

Although the length of the plus-end-proximal microtubule fragment that "survives" after severing was similar in control and EB1/2/3 knockout cells, we also observed an interesting difference in their behavior: the severed microtubule fragments displayed rapid motility more frequently in the EB1/2/3 knockout than in control cells (Figure 5A-D). In control cells, the velocity of the microtubule fragment movement, measured as minus end displacements, was comparable to microtubule growth and depolymerization rates (10-15 μm/min), suggesting that the displacement was caused by microtubule disassembly, while rapid movements were rare. However, movements with the velocity in the range of 36-100 μm/min, which resembles the velocity of microtubule-based motors, became more frequent in EB1/2/3 knockout cells. Among the rapidly moving microtubules, approximately half (5 out of 12) moved with their minus end forward, while 6 moved in the opposite direction, and for one fragment the direction was difficult to determine. We therefore think that this behavior does not reflect microtubule dynamics, but rather microtubule displacement driven by motors positioned at the cell cortex or other structures, such as the ER, which are larger than the microtubule fragment.

To get further insight into microtubule tip motility, we turned to rescue experiments with different EB fusions in control and EB1/2/3 knockout cells, as these fusions allow higher quality of detection of the microtubule plus end. In control cells, EB3-GFP as well as EB3-NL-LZ-GFP and other EB markers tested showed characteristic microtubule tip dynamics: periods of processive growth with occasional short interruptions, which terminated in signal disappearance corresponding to microtubule catastrophe (see kymographs illustrating the behavior of the individual comets, Figure 6A,B). Similar behavior was observed when EB1-GFP, EB3-GFP or GFP-EB3 were expressed in EB1/2/3 knockout cells (Figure 6C, E, F). In contrast, a much more irregular tip behavior was observed in EB1/2/3 knockout cells expressing GFP-

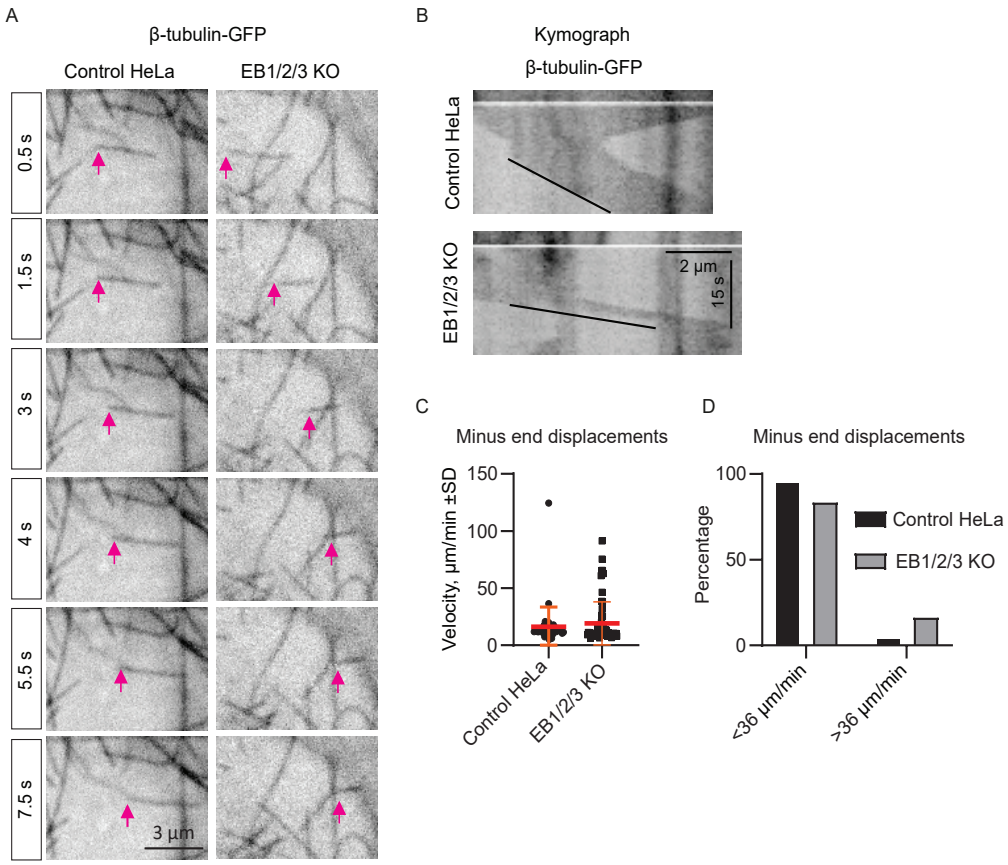

Figure 5. Analysis of the microtubule displacement after lattice severing

A. Time lapse imaging illustrating microtubule displacements after microtubule severing at the indicated time point. The minus end of the severed microtubule is indicated with an arrow.

B. Kymograph illustrating microtubule displacements after lattice severing in control and EB1/2/3 KO cells. The black line highlights the displacement of the minus end.

C. Quantification of speed of microtubule minus end displacements after lattice severing in control HeLa and EB1/2/3 KO cells. N=2 experiments, 45 events of movement for 24 microtubules in 12 control HeLa cells and 73 events of movements for 36 microtubules in 18 EB1/2/3 KO cells.

D. Quantification of microtubule minus end displacements below and above 36 µm/min in control HeLa and EB1/2/3 KO cells.

EB2, EB3-NL-LZ-GFP and EB3-NL-mVenus (Figure 6D,G H). Two main features of this behavior were rapid back-and-forth movements with a short amplitude (1-2 µm), as well as occasional fast longer displacements (Figure 6D,G, H). Importantly, the signals of these EB proteins were present not only during forward, but also during backward movements; such signals were most obvious with EB3-NL-LZ-GFP and least visible with EB3-NL-mVenus. Back-and-forth movements of EB-positive microtubule ends can be interpreted in two ways. First, they might represent microtubule growth and depolymerization excursions during which the EB signal persists, perhaps because the GTP cap is not completely lost or because the EB protein tracks a depolymerizing microtubule end. Second, microtubule plus end can keep growing but be displaced by the activity of microtubule motors. Very rapid displacements are likely caused by

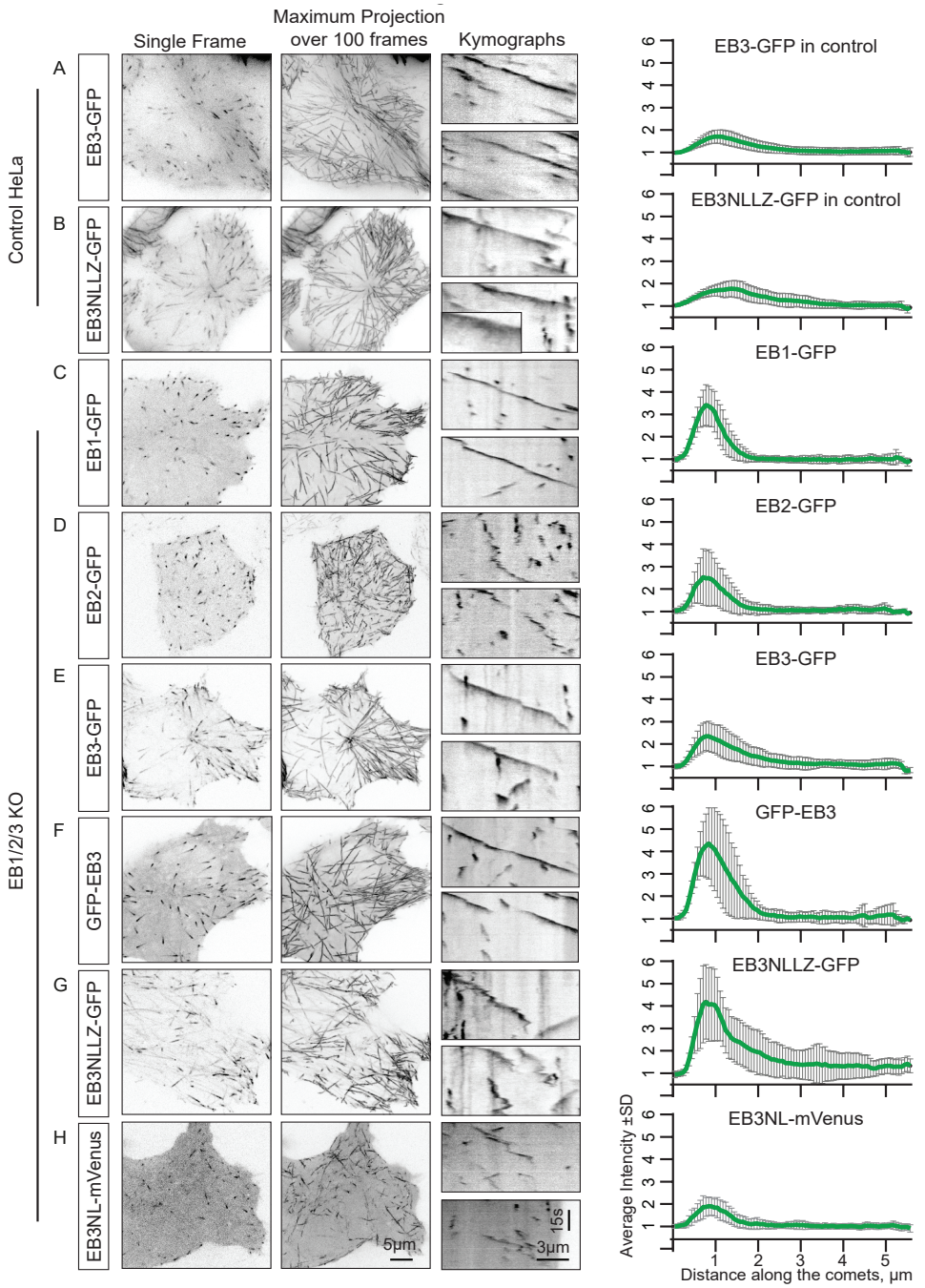

Figure 6. Effect of EBs and their individual domains on microtubule tip behavior

A-H. Single frame and maximum intensity projections of 100 frames of control HeLa cells (A, B) or EB1/2/3 KO cells (C-G) transfected with the indicated fluorescent EB fusion constructs, their representative kymographs and averaged comet intensity profiles. To obtain averaged profiles, 5 µm long (84 pixels) and 3 pixel wide lines were placed horizontally across the trace of the growing microtubule end, starting ~5 pixels in front of the comet and

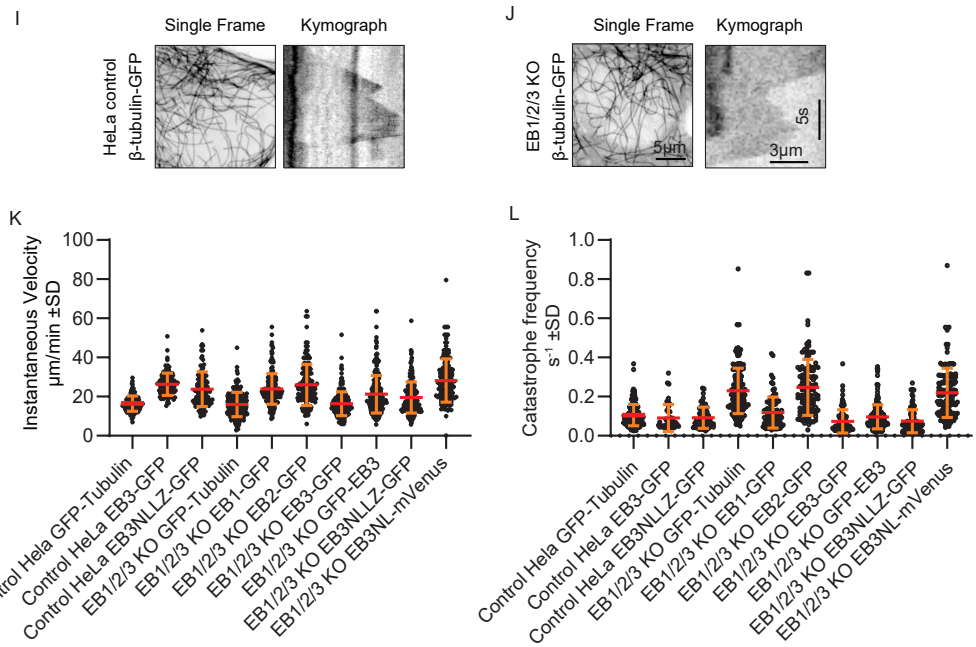

ending behind the comet. The average intensity has been measured along this line using the Linescan option of MetaMorph software. Intensities along each line were normalized to the background in front of the comet (divided to the average values of the first 5 pixels). n= 19-26 comets measured in 5 cells. The inset in kymograph of EB3-NL-LZ-GFP illustrates the irregularity of comet decay observed with this construct.

I-J. Single frames and kymographs of β-tubulin-GFP-labeled microtubules in control HeLa and EB1/2/3 KO cells.

K-L. Quantification of instantaneous microtubule growth rate and catastrophe frequencies in control HeLa and EB1/2/3 KO cells transfected with the indicated constructs.

the second phenomenon; however, short oscillations with the range of 1-2 μm can be explained by frequent catastrophes followed by rescues that occur within the stabilizing cap. It is also important to note that EB3-NL-LZ-GFP accumulations at microtubule tips differed from those observed with the other EB-GFP fusions – instead of the comet-like shape with the highest intensity close to microtubule tip, they often had internal densities or appeared to split into two, and this was reflected in the more irregular "tail" in their averaged profile (Figure 6G).

Analysis of microtubule growth parameters showed that the growth rate measured using β-tubulin-GFP as readout was similar (~16 μm/min) in control and EB1/2/3 knockout cells, whereas catastrophe frequency was strongly elevated in cells lacking the EBs, as described previously for the cells depleted of EB1 and EB3 (Figure 6I-L) (Komarova et al., 2009) and EB1/2/3mut cells (Chapter 2). Measurement of instantaneous microtubule growth rate with the EB fusions resulted in values that varied between ~26-28 μm/min for EB2 and EB3-NL-mVenus and ~16 μm/min for EB3-GFP (Figure 6K). Catastrophe frequency was elevated in EB2-GFP and EB3-NL-mVenus-expressing EB1/2/3 knockout cells, in line with previous observations (Figure 6L) (Chapter 2, (Komarova et al., 2009)). It should be noted that the growth rates measured with EBs and fluorescent tubulin can be different, because the brighter EB signals allow easier detection of growing microtubule ends, but also complicate the definition of growth episodes in cases of frequent tip oscillations. Furthermore, whereas EB-positive microtubule ends can be detected throughout the cell volume, reliable detection of tubulin-GFP-labeled microtubule

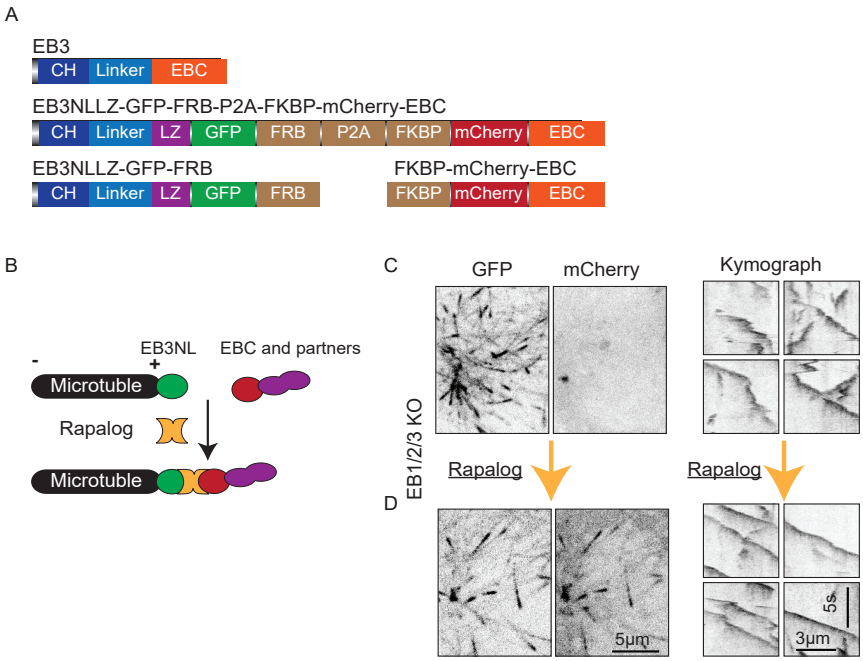

Figure 7. Rescue of microtubule plus end dynamics by the partner-binding domain of EB3

A. Scheme of the chimeric protein design of EB3-NL-LZ-GFP-FRB-P2A-FKBP-mCherry-EBC, which is split into the GFP-tagged and mCherry-tagged parts at the P2A site after it is expressed.

B. Scheme of the chemical dimerization-based rescue of microtubule growth EB3 C-terminus. Without rapalog, the EB3-NL-LZ-GFP (green) accumulates at microtubule plus ends, while the mCherry-EBC (red) together with its interaction partners (purple) is diffusely present in the cytoplasm; upon the addition of rapalog (yellow), EBC and its partners are recruited to plus ends.

C,D. Single frames of the GFP and mCherry channels and representative kymographs of the GFP channel before and after rapalog addition.

ends is only possible at the cell edge or under the cell nucleus, where microtubule dynamics can be different from the internal cytoplasm due to the vicinity of the cell cortex (Mimori-Kiyosue et al., 2005). It should also be noted that catastrophe frequency values measured with EB3-NL-LZ-GFP should be interpreted with caution, because in this analysis, we assumed that occurrence of a catastrophe coincided with the loss of the EB signal. However, this might not be the case if this construct does not efficiently dissociate from depolymerizing microtubule ends.

Finally, we examined whether we could reverse the “erratic” behavior of EB3-NL-LZ-GFP-decorated plus ends in EB1/2/3 knockout cells by recruiting to them the C-terminal partner-binding domain of EB3. To achieve this, we employed an inducible protein heterodimerization system, in which two protein domains, FRB and FKBP, stably bind to each other upon the addition of a rapamycin analog (rapalog) (Hoogenraad et al., 2003; Pollock et al., 2000). The EB3-NL-LZ-GFP protein was fused to FRB, and a mCherry-tagged C-terminal part of EB3 (EBC) was fused to FKBP (Figure 7A). The two proteins were expressed from the same open reading frame within a single plasmid but were separated by a self-cleaving 2A peptide (Liu et al., 2017), allowing their equimolar expression (Figure 7B). Before rapalog addition, EB3-NL-LZ-GFP-FRB associated with microtubule plus ends and displayed a behavior very similar

to that of EB3-NL-LZ-GFP, whereas FKBP-mCherry-EBC was diffuse (Figure 7C). Upon rapalog addition, FKBP-mCherry-EBC was efficiently recruited to microtubule plus ends and blocked their oscillatory behavior, making growth episodes more processive and "smooth" (Figure 7D). These data suggest that the irregular growth observed in EB1/2/3 knockout cells with an EB3 version lacking the ability to bind its normal partners can be acutely rescued by restoring partner binding.

DISCUSSION

In this Chapter, we described the generation of HeLa cells completely lacking the expression of EB proteins. This cell line is a very useful tool to address the common and distinct functions of different EB isoforms and their domains by performing rescue experiments. Endogenous expression levels of EB proteins are quite high (in the range of 100-500 nM for EB1 (Itzhak et al., 2016; Wisniewski et al., 2014)), and we found that the expression levels of GFP-tagged EB fusions we normally use for imaging experiments fall within this range.

Since EBs specifically bind to the stabilizing cap at growing microtubule ends, our main goal was to investigate how they affect the properties of this cap. We confirmed previous observations showing that EB comet decay length, which is thought to reflect the length of the GTP cap, correlates with the microtubule growth rate. However, it is not possible to make straightforward conclusions about the absolute length of the cap, because the comet length depends on the EB probe used, with EB3-GFP making the longest comets. This is not an intrinsic property of the EB3 CH domain alone, but rather depends on the high affinity binding specific for the dimer, as monomeric EB3-NL-mVenus does not make long comets. Longer comets were less obvious with GFP-EB3 than with EB3-GFP, possibly because an N-terminal GFP tag reduces the affinity of the protein for microtubules (Skube et al., 2010; Zhu et al., 2009). By immunofluorescence staining of endogenous proteins, the longest comets are observed for EB2, but this effect depends on the presence of EB1 and/or EB3 (Komarova et al., 2009; Roth et al., 2018)(Chapter 2). In the experiments described here, in the absence of EB1 and EB3, EB2-GFP comets did not have a longer “tail”, which one could expect if this protein indeed had preference for a binding site with mixed GTP and GDP nucleotides, as proposed recently (Roth et al., 2018). To better understand the differences between the EB constructs in terms of plus end decoration, it would be important to perform FRAP assays to investigate EB turnover.

We also attempted to compare EB comet length in cells and in vitro at the same microtubule growth rate using GFP-EB3 as a marker and found that this length was somewhat longer in the in vitro assays. However, due to the differences between comet lengths observed with different fluorescent EB fusions, these data should be interpreted with caution, and additional data using different EB proteins in vitro should be included for comparison.

Do EBs affect the length of the stabilizing cap? In the absence of a completely independent probe for GTP tubulin, this question is impossible to address. We tried to get some insight into this problem by performing laser severing experiments. We found that growing microtubules showed some resistance to depolymerization from the minus end, with short plus-end proximal fragments being able to “survive” for significant time periods. This experiment obviously does not conclusively demonstrate that we are indeed studying the stability of GTP cap, because minus end stability can be affected by different factors. In particular, it would be important to rule out the impact of CAMSAP2, the major minus-end stabilizing protein in HeLa cells.

Surprisingly, we found that microtubule tip-proximal fragments generated by photoablation showed more frequent motility in EB1/2/3 knockout cells than in control cells. Specifically, in EB1/2/3 knockout cells, we more frequently observed microtubule fragments that moved with the velocity of 36-100 μm/min, which suggests displacement by a motor protein. It is tempting to speculate that in the absence of decoration by EBs and their partners, such microtubule pieces become more accessible to motor proteins. Kinesin-1 represents an attractive candidate, because it is an abundant motor which might have preference for expanded microtubule lattice characteristic of GTP-tubulin (Shima et al., 2018). Indeed, approximately half of the rapidly moving fragments moved with their minus end forward, as could be expected for a kinesin-driven displacement.

Using EBs as probes for microtubule tip behavior, we found that there was a big difference

between EB1 and EB3, which can bind with high affinity to various partner proteins, and EB2, which shows only a low affinity to many EB partners, as well as EB3 deletion mutants EB3-NL and EB3-NL-LZ that lack the partner-binding domain altogether. Whereas full-length EB1 and EB3 could restore "smooth" microtubule growth observed in control cells, EB2, EB3-NL and EB3-NL-LZ showed much more irregular growth pattern, which could be interpreted as a combination of alternating growth and shortening excursions and rapid displacements of the microtubule tip. The relative input of these two potential components requires detailed analysis, possibly after collecting data at a higher frame rate. Such irregular microtubule growth correlated with increased catastrophe frequency, calculated based on the loss of the EB signal and direct microtubule labeling. It is important to note that in case of EB3-NL-LZ, the actual catastrophe frequency might be underestimated if the protein tends to persist at depolymerizing microtubule tips. Further analysis would be necessary to understand the nature of EB3-NL-LZ behavior at the microtubule plus ends.

Importantly, the irregular dynamics of microtubule ends in EB1/2/3 knockout cells in the presence of EB3-NL-LZ could be acutely rescued by recruiting the partner-binding C-terminus of EB3. This raises an important question – which EB partners are responsible for this effect? Since EB1-GFP and EB3-GFP, bearing a C-terminal GFP tag, can restore microtubule growth, CAP-Gly domain-containing EB partners such as CLIP170 or the dynein assessor complex dynactin are unlikely to be involved, because a CAP-Gly domain requires for binding a free C-terminal tyrosine residue (Steinmetz and Akhmanova, 2008; Weisbrich et al., 2007). In contrast, linear motifs such as SxIP or LxxPTPh can bind to EBs irrespective of the presence of a C-terminal tag (Akhmanova and Steinmetz, 2008; Honnappa et al., 2009; Kumar et al., 2017). An interesting candidate is the protein SLAIN2, which has multiple SxIP and SxIP-like EB-binding motifs and can concentrate at the EB-positive plus ends the microtubule polymerase chTOG (van der Vaart et al., 2011). The depletion of SLAIN2 in mammalian cells also increases catastrophe and rescue frequencies and shows a similar interrupted growth pattern as the one observed with EB2 or the N-terminal EB3 constructs (van der Vaart et al., 2011). Other explanations are also possible – for example, the increased motility of the plus ends and their perturbed growth could be mechanistically linked, as rapid movements of microtubule tips could potentially create pushing forces on the outermost microtubule extremities causing a catastrophe.

In future, it would be important to find out whether the irregular microtubule growth observed with the fluorescent fusions of EB2, EB3-NL and EB3-NL-LZ in EB1/2/3 knockout cells can also be detected with fluorescent tubulin. The data we have obtained so far did not allow us to either prove or rule out this possibility, because better detection of growing microtubule ends in the tubulin channel would be necessary to draw definitive conclusions. If microtubule tips indeed undergo rapid growth and depolymerization excursions in the complete absence of EBs, this would indicate that EBs, likely with aid of some SxIP partners, stabilize microtubule growth. If this turns out not be the case, it would mean that EBs play a dual role – through the microtubule-binding domain, they destabilize the tip, but this activity is counteracted by EB partners. The increase in microtubule catastrophe frequency measured with fluorescent tubulin in EB1/2/3 knockout cells argues in favor of the first possibility, but more careful analysis is needed. Taken together, our results indicate that EBs have a profound effect on several features of microtubule plus end dynamics, and the EB1/2/3 knockout cells described here will be instrumental to unravel the underlying mechanisms.

Materials and Methods

Cell culture and transfection

HeLa, MDA-MB-231 and HEK 293T cell lines were cultured in medium which consisted of 45% DMEM, 45% Ham's F10, and 10% fetal calf serum supplemented with penicillin and streptomycin (Akhmanova et al., 2001). CHO-K1 cells were cultured in DMEM medium with 10% fetal calf serum supplemented with penicillin and streptomycin (Komarova et al., 2005). FuGENE 6 (Promega) was used to transfect both HeLa and CHO-K1 cells, for live cell imaging experiments, cells were transfected for 24 hrs; polyethylenimine (PEI, Polysciences) was used to transfect HEK293T cells for protein purification. For measurement of parameters of microtubule dynamics, control HeLa and EB1/2/3 knockout cell lines were used for the analysis at 24h after transfection with indicated constructs.

Constructs and gRNAs

Human EB1-GFP, EB2-GFP and EB3-GFP was described by (Stepanova et al., 2003); EB3-NL-LZ-GFP, EB3-NL-mVenus and GFP-EB3 were described by (Komarova et al., 2009). chTOG-mCherry were described by (Gutierrez-Caballero et al., 2015), a kind gift of S. Royle (University of Warwick, UK); the EB3-NL-LZ-GFP-FRB-P2A-FKBP-mCherry-EBC fused construct was generated by PCR-based strategies using previously described constructs (Liu et al., 2017; van Bergeijk et al., 2015).

The pSpCas9-2A-Puro (PX459) vector that was used for the CRISPR/Cas9 knockout was purchased from Addgene (Ran et al., 2013). The targeting sequences of 20 nucleotides that were cloned into pSpCas9 -2A-Puro (PX459) for different knockouts were as follows: EB1, 5' CCAGCATGTCATGTCGACTT; EB2, 5'-CAGACATGACATCATTGCAT; EB3, 5'-TGCACCTCAACTATACCAAG.

Generation of EB1/2/3 KO cell lines

Guide RNAs for human EB1, EB2 and EB3 (also known as MAPRE1,2,3) were designed using the CRISPR design webpage tool (http://crispor.tefor.net/crispor.py), and cloned into a mammalian expression vector, pSpCas9-2A-Puro (PX459v2). The CRISPR/Cas9 mediated EB1, EB2 and EB3 KO was performed according to the protocol by (Ran et al., 2013). In brief, HeLa cell lines were transfected with the vector bearing the appropriate targeting sequences using Fugene 6. One day after transfection, HeLa cells were subjected to selection with 2 µg/ml puromycin for 2 days. After selection, cells were allowed to recover in normal medium for ~ 3 days, and knockout efficiency was checked by immunofluorescence staining. EB1/2/3 knockout cells were generated using a two-step procedure. We first generated, confirmed and characterized EB2 knockout cell lines, and then simultaneously transfected these with EB1 and EB3-specific gRNA constructs. From the isolated clones, three clones were further characterized by Western blotting and immunostaining, and two clones were characterized by sequencing (Table S1).

Antibodies and immunofluorescence cell staining

We used rabbit antibody against EB3 (Stepanova et al., 2003), rat monoclonal antibody against EB2 (Komarova et al., 2005) and mouse monoclonal antibody against EB1 (BD, 610535). The following secondary antibodies were used: IRDye 800CW/ 680LT goat anti-rabbit, anti-rat and anti-mouse (Li-Cor Biosciences); Alexa-350, Alexa-405, Alexa-488 and Alexa-594 conjugated goat antibodies against rabbit, rat and mouse IgG (Molecular Probes).

Cultured cells were fixed with –20 °C methanol for 10 min followed by 4% paraformaldehyde for 10 min. Cells were then permeabilized with 0.1% Triton X-100 in phosphate buffered saline

(PBS) for 10 min; subsequent washing and labelling steps were carried out in PBS supplemented with 2% bovine serum albumin and 0.05% Tween-20. At the end, slides were rinsed in 70% and 100% ethanol, air-dried and mounted in Vectashield mounting medium (Vector laboratories).

Drugs and drug treatments

To generate EB1/2/3 KO cells, HeLa cells were subjected for selection with puromycin for 2 days at the concentration of 2 µg/ml. For chemical heterodimerization assays, rapalog (AP21967, ARIAD) was dissolved to 0.1 mM in ethanol and used at a final concentration of 100 nM; images were acquired 40 min after the initiation of drug treatment.

In vitro reconstitution assays

In vitro assays were performed as described previously (Aher et al., 2018). chTOG-mCherry protein was purified from HEK293T cells and GFP-EB3 (Montenegro Gouveia et al., 2010) was a gift of Dr. M. Steinmetz (Paul Scherrer Institute, Switzerland). Microtubules were grown from GMPCPP-stabilized microtubule seeds in reaction mixtures containing 15 µM porcine brain tubulin, 75 mM KCl, 1 mM guanosine triphosphate, 0.1% methylcellulose, 0.2 mg/ml κ-casein and oxygen scavenger mixture (50 mM glucose, 400 µg/ ml glucose oxidase, 200 µg/ ml catalase, and 4 mM DTT in MRB80 buffer). The reaction mix was added to the flow chamber after centrifugation in an Airfuge for 5 minutes at 119,000 x g. The flow chamber was sealed with vacuum grease, and dynamic microtubules were imaged immediately at 37 °C with a TIRF microscope. All tubulin products were from Cytoskeleton Inc.

Fluorescence Correlation Spectroscopy (FCS)

To measure the cytoplasmic concentration of EB3, we performed FCS with a Leica SP8 STED 3X microscope driven by LAS X and SymPhoTime (PicoQuant) software using a HC PLAPO 63x 1.2 NA water immersion objective. The sample was excited at 488 nm and time correlation was calculated at the time frequency of 600 kHz. Confocal imaging was used to localize the MDA-MB-231 cells and EB3-GFP transfected EB1/2/3 knockout cells. To avoid the measurement of EB comets or other unrelated rare events, we collected data for 10 to 30s, and exclude the data with an obvious intensity peak. We fitted the autocorrelation function G(t) with pure diffusion model for one species fluorescent species (Chen et al., 2002) as follows:

$$G(t) = \sum_{n=1}^{n_{Diff}-1} \frac{\rho[i]}{\left[1+\frac{t}{\tau_{Diff}[i]}\right]\left[1+\frac{t}{\tau_{Diff}[i]\kappa^2}\right]^{0.5}}$$

where n_{Diff} is the number of independently diffusing species, ρ is the contribution of the i^{th} diffusing species, τ_{Diff} is the diffusion time of the i^{th} diffusing species, and κ is the length to diameter ratio of the focal volume set to 4, estimated by calibration measurements. We calculated the cytoplasmic concentration as $C = \frac{1/G(0)}{V_{eff}N_A}$, where V_{eff} is the effective excitation volume that was estimated at 0.3fl by a calibration measurement and N_A is the Avogadro constant. For calibration, we used Rhodamine 6G (Sigma, 989-38-8), which has a known diffusion coefficient of 4.14 x 10^{-6} cm^2s^{-1}, and we calibrated the V_{eff} according the protocol provided by PicoQuant.

Image acquisition

Images of fixed cells were collected with a Nikon Eclipse Ni upright fluorescence microscope and a Nikon DS-Qi2 CMOS camera (Nikon), using a Plan Apo Lambda 60x N.A. 1.40 oil objective (Nikon) or Plan Apo Lambda 100x N.A. 1.45 oil objective (Nikon) and a Nikon NIS (Br) software

(Nikon). Nikon Intensilight C-HGFI has been used as a light source to get fluorescent image. Live cell imaging was collected with spinning disk microscopy, which was performed on an inverted research microscope Nikon Eclipse Ti-E (Nikon) with the perfect focus system (PFS) (Nikon), equipped with Nikon Apo TIRF 100x N.A. 1.49 oil objective (Nikon), Yokogawa CSU-X1-A1 confocal head (Yokogawa) with 405-491-561 triple band mirror and ET-GFP, ET-mCherry and ET-GFP/mCherry emission filters (Chroma), ASI motorized stage MS-2000-XYZ with Piezo Top Plate (ASI), a Photometrics Evolve 512 EMCCD camera (Photometrics) and controlled by the MetaMorph 7.8 software (Molecular Devices). The microscope was equipped with a custom-ordered illuminator (Nikon, MEY10021) modified by Roper Scientific France/PICT-IBiSA, Institut Curie. Vortran Stradus 488 (100 mW) and Cobolt Jive 561 nm (100 mW) lasers (Cobolt) have been used as the light sources to get fluorescent image. Images were collected with 100 ms and 500 ms exposure time at 10 and 2 frames per second. To keep the samples at 37°C for live cell imaging, we used a stage top incubator model INUBG2E-ZILCS (Tokai Hit).
For the photoablation experiments, we used the same ILas system (Roper Scientific France/PICT-IBiSA, Institut Curie) mounted on Nikon Eclipse microscope described above. A 355 nm passively Q-switched pulsed laser (Teem Photonics) was used for the photoablation together with the CFI S Fluor 100x 0.5-1.3 N.A. oil objective (Nikon). Duration of laser pulse was around ~0.3 s in one diffraction limited spot across one individual microtubule. To cut several microtubules simultaneously the same laser beam has been moved along the line positioned perpendicular to several microtubules; in this case the total laser beam exposure was ~1.3 s. To introduce free microtubule segments, two cuts along the lattice of the same microtubule has been applied positioned 5-7 micrometers one from another, or several several microtubules were cut simultaneously using two lines arranged perpendicular those microtubules.
In vitro reconstitution assays were imaged using Total Internal Reflection Fluorescence (TIRF) microscopy using an inverted research microscope Nikon Eclipse Ti-E (Nikon) with the perfect focus system (Nikon), equipped with Nikon Apo TIRF 100x N.A. 1.49 oil objective (Nikon) and iLas² system (Dual Laser illuminator for azimuthal spinning TIRF (or Hilo) illumination and Simultaneous Targeted Laser Action) from Roper Scientific (Evry, FRANCE) with a custom modification for targeted Photoablation using a 532 nm pulsed laser. The system was also equipped with ASI motorized stage MS-2000-XY (ASI), Photometrics Evolve Delta 512 EMCCD camera (Photometrics) and controlled by the MetaMorph 7.8 software (Molecular Devices). Stradus 488 nm (150 mW, Vortran) and OBIS 561 nm (100 mW, Coherent) lasers were used as the light sources. Images were collected at 10 frames/s with 100 ms exposure time. Images were projected onto the CCD chip at a magnification of 0.065 µm/pixel.

Quantification of EB comets decay length and speed

EB comet intensity analysis was performed as described earlier (Aher et al., 2018). Stream microscopy recordings were used to create kymographs by drawing segmented lines of 12 pixel width (0.8 µm) along growing MTs using KymoResliceWide plugin with maximum transverse intensity (http://fiji.sc/KymoResliceWide). Using kymograph images, we traced the growing MT tips with the "Segmented Line" ROI tool from ImageJ to mark the approximate position of the growing tip used for initial fitting position estimate later. The fitting of fluorescent intensity profiles was performed using a custom-written MATLAB script. Individual intensity profiles were extracted from kymographs at each time point within a range from 2.5 µm behind till 1 µm ahead from the approximate growing tip position marked earlier.

For the fitting of the EB comet intensity profile we assumed that the density distribution of EBs in the comet decays exponentially from its maximum value close to the MT tip. To represent its convolution with microscope's PSF, we used a sum of the complimentary error function (lattice binding) and an exponential decay function convoluted with Gaussian distribution:

$$I(x) = I_{BG} + \frac{1}{2} I_{lattice} \cdot \mathrm{erfc}\left(\frac{x - x_c}{\sqrt{2}\sigma_{PSF}}\right) +$$
$$+ \frac{1}{2} I_{EB} \cdot \exp\left(\frac{\lambda}{2}(\sigma_{PSF}^2 \lambda + 2(x - x_c))\right) \cdot \left(1 - \mathrm{erf}\left(\frac{\sigma_{PSF}^2 \lambda + x - x_c}{\sqrt{2}\sigma_{PSF}}\right)\right)$$

where fitting parameter I_{BG} corresponds to the intensity of background, $I_{lattice}$ to the amplitude of the fluorescent intensity fraction associated with the lattice binding, I_{EB} to the amplitude of convolved exponential decay, x_c to the position of the maximum number of molecules in the molecules distribution (start of exponential decay position), σ_{PSF} to the standard deviation of microscope's point spread function and λ to the comet's exponential decay constant. The value of σ_{PSF} was measured using immobilized 100 nm diameter fluorescent Tetraspeck beads on the same microscope and filter sets as the movies of EB-labeled comets and was equal to 112 nm.

Image preparation and analysis

Images were prepared for publication using MetaMorph, ImageJ and Adobe Photoshop. All images were modified by adjustments of levels and contrast. ImageJ was used for quantification of the immunofluorescence signal intensity. Instantaneous rates of microtubule plus end growth and the frequencies of catastrophes were measured using kymographs, which were generated in MetaMorph software along the 12 pixel-wide line. Only microtubule plus end displacements longer than 0.5 µm were taken into account. Displacements of free microtubules generated by photoablation were also measured using kymographs.

Acknowledgements

This work was supported by the European Research Council Synergy grant 609822 to A.A.

References

Aher, A. 2017. Tipping microtubule polymerization: Insights from in vitro reconstitution.

Aher, A., M. Kok, A. Sharma, A. Rai, N. Olieric, R. Rodriguez-Garcia, E.A. Katrukha, T. Weinert, V. Olieric, L.C. Kapitein, M.O. Steinmetz, M. Dogterom, and A. Akhmanova. 2018. CLASP Suppresses Microtubule Catastrophes through a Single TOG Domain. *Dev Cell*. 46:40-58.

Akhmanova, A., C.C. Hoogenraad, K. Drabek, T. Stepanova, B. Dortland, T. Verkerk, W. Vermeulen, B.M. Burgering, C.I. De Zeeuw, F. Grosveld, and N. Galjart. 2001. Clasps are CLIP-115 and -170 associating proteins involved in the regional regulation of microtubule dynamics in motile fibroblasts. *Cell*. 104:923-935.

Akhmanova, A., and M.O. Steinmetz. 2008. Tracking the ends: a dynamic protein network controls the fate of microtubule tips. *Nat Rev Mol Cell Biol*. 9:309-322.

Akhmanova, A., and M.O. Steinmetz. 2015. Control of microtubule organization and dynamics: two ends in the limelight. *Nat Rev Mol Cell Biol*. 16:711-726.

Bieling, P., L. Laan, H. Schek, E.L. Munteanu, L. Sandblad, M. Dogterom, D. Brunner, and T. Surrey. 2007. Reconstitution of a microtubule plus-end tracking system in vitro. *Nature*. 450:1100-1105.

Bouchet, B.P., I. Noordstra, M. van Amersfoort, E.A. Katrukha, Y.C. Ammon, N.D. Ter Hoeve, L. Hodgson, M. Dogterom, P.W. Derksen, and A. Akhmanova. 2016. Mesenchymal Cell Invasion Requires Cooperative Regulation of Persistent Microtubule Growth by SLAIN2 and CLASP1. *Dev Cell*. 39:708-723.

Chen, Y., J.D. Muller, Q. Ruan, and E. Gratton. 2002. Molecular brightness characterization of EGFP in vivo by fluorescence fluctuation spectroscopy. *Biophys J*. 82:133-144.

Desai, A., and T.J. Mitchison. 1997. Microtubule polymerization dynamics. *Annu Rev Cell Dev Biol*. 13:83-117.

Duellberg, C., N.I. Cade, D. Holmes, and T. Surrey. 2016. The size of the EB cap determines instantaneous microtubule stability. *Elife*. 5.

Gutierrez-Caballero, C., S.G. Burgess, R. Bayliss, and S.J. Royle. 2015. TACC3-ch-TOG track the growing tips of microtubules independently of clathrin and Aurora-A phosphorylation. *Biol Open*.

Honnappa, S., S.M. Gouveia, A. Weisbrich, F.F. Damberger, N.S. Bhavesh, H. Jawhari, I. Grigoriev, F.J. van Rijssel, R.M. Buey, A. Lawera, I. Jelesarov, F.K. Winkler, K. Wuthrich, A. Akhmanova, and M.O. Steinmetz. 2009. An EB1-binding motif acts as a microtubule tip localization signal. *Cell*. 138:366-376.

Hoogenraad, C.C., P. Wulf, N. Schiefermeier, T. Stepanova, N. Galjart, J.V. Small, F. Grosveld, C.I. de Zeeuw, and A. Akhmanova. 2003. Bicaudal D induces selective dynein-mediated microtubule minus end-directed transport. *Embo J*. 22:6004-6015.

Itzhak, D.N., S. Tyanova, J. Cox, and G.H. Borner. 2016. Global, quantitative and dynamic mapping of protein subcellular localization. *Elife*. 5.

Komarova, Y., C.O. De Groot, I. Grigoriev, S.M. Gouveia, E.L. Munteanu, J.M. Schober, S. Honnappa, R.M. Buey, C.C. Hoogenraad, M. Dogterom, G.G. Borisy, M.O. Steinmetz, and A. Akhmanova. 2009. Mammalian end binding proteins control persistent microtubule growth. *J Cell Biol*. 184:691-706.

Komarova, Y., G. Lansbergen, N. Galjart, F. Grosveld, G.G. Borisy, and A. Akhmanova. 2005. EB1 and EB3 control CLIP dissociation from the ends of growing microtubules. *Mol Biol Cell*. 16:5334-5345.

Kumar, A., C. Manatschal, A. Rai, I. Grigoriev, M.S. Degen, R. Jaussi, I. Kretzschmar, A.E. Prota, R. Volkmer, R.A. Kammerer, A. Akhmanova, and M.O. Steinmetz. 2017. Short Linear Sequence Motif LxxPTPh Targets Diverse Proteins to Growing Microtubule Ends. *Structure*. 25:924-932.

Kumar, P., and T. Wittmann. 2012. +TIPs: SxIPping along microtubule ends. *Trends Cell Biol*. 22:418-428.

Liu, Z., O. Chen, J.B.J. Wall, M. Zheng, Y. Zhou, L. Wang, H. Ruth Vaseghi, L. Qian, and J. Liu. 2017. Systematic comparison of 2A peptides for cloning multi-genes in a polycistronic vector. *Sci Rep*. 7:2193.

Maurer, S.P., P. Bieling, J. Cope, A. Hoenger, and T. Surrey. 2011. GTPgammaS microtubules mimic the growing microtubule end structure recognised by end-binding proteins (EBs). *Proc Natl Acad Sci U S A*. 109:3988-3993.

Maurer, S.P., N.I. Cade, G. Bohner, N. Gustafsson, E. Boutant, and T. Surrey. 2014. EB1 accelerates two

conformational transitions important for microtubule maturation and dynamics. *Curr Biol*. 24:372-384.

Maurer, S.P., F.J. Fourniol, G. Bohner, C.A. Moores, and T. Surrey. 2012. EBs recognize a nucleotide-dependent structural cap at growing microtubule ends. *Cell*. 149:371-382.

Mimori-Kiyosue, Y., I. Grigoriev, G. Lansbergen, H. Sasaki, C. Matsui, F. Severin, N. Galjart, F. Grosveld, I. Vorobjev, S. Tsukita, and A. Akhmanova. 2005. CLASP1 and CLASP2 bind to EB1 and regulate microtubule plus-end dynamics at the cell cortex. *J Cell Biol*. 168:141-153.

Mimori-Kiyosue, Y., N. Shiina, and S. Tsukita. 2000. The dynamic behavior of the APC-binding protein EB1 on the distal ends of microtubules. *Curr Biol*. 10:865-868.

Mohan, R., E.A. Katrukha, H. Doodhi, I. Smal, E. Meijering, L.C. Kapitein, M.O. Steinmetz, and A. Akhmanova. 2013. End-binding proteins sensitize microtubules to the action of microtubule-targeting agents. *Proc Natl Acad Sci U S A*. 110:8900-8905.

Montenegro Gouveia, S., K. Leslie, L.C. Kapitein, R.M. Buey, I. Grigoriev, M. Wagenbach, I. Smal, E. Meijering, C.C. Hoogenraad, L. Wordeman, M.O. Steinmetz, and A. Akhmanova. 2010. In Vitro Reconstitution of the Functional Interplay between MCAK and EB3 at Microtubule Plus Ends. *Curr Biol*. 20:1717-1722.

Pollock, R., R. Issner, K. Zoller, S. Natesan, V.M. Rivera, and T. Clackson. 2000. Delivery of a stringent dimerizer-regulated gene expression system in a single retroviral vector. *Proc Natl Acad Sci U S A*. 97:13221-13226.

Ran, F.A., P.D. Hsu, J. Wright, V. Agarwala, D.A. Scott, and F. Zhang. 2013. Genome engineering using the CRISPR-Cas9 system. *Nat Protoc*. 8:2281-2308.

Roostalu, J., C. Thomas, N.I. Cade, S. Kunzelmann, I.A. Taylor, and T. Surrey. 2019. The speed of GTP hydrolysis determines GTP cap size and controls microtubule stability. *bioRxiv* 779108.

Roth, D., B.P. Fitton, N.P. Chmel, N. Wasiluk, and A. Straube. 2018. Spatial positioning of EB family proteins at microtubule tips involves distinct nucleotide-dependent binding properties. *J Cell Sci*. 132.

Seetapun, D., B.T. Castle, A.J. McIntyre, P.T. Tran, and D.J. Odde. 2012. Estimating the microtubule GTP cap size in vivo. *Curr Biol*. 22:1681-1687.

Shima, T., M. Morikawa, J. Kaneshiro, T. Kambara, S. Kamimura, T. Yagi, H. Iwamoto, S. Uemura, H. Shigematsu, M. Shirouzu, T. Ichimura, T.M. Watanabe, R. Nitta, Y. Okada, and N. Hirokawa. 2018. Kinesin-binding-triggered conformation switching of microtubules contributes to polarized transport. *J Cell Biol*. 217:4164-4183.

Skube, S.B., J.M. Chaverri, and H.V. Goodson. 2010. Effect of GFP tags on the localization of EB1 and EB1 fragments in vivo. *Cytoskeleton (Hoboken)*. 67:1-12.

Steinmetz, M.O., and A. Akhmanova. 2008. Capturing protein tails by CAP-Gly domains. *Trends Biochem Sci*. 33:535-545.

Stepanova, T., J. Slemmer, C.C. Hoogenraad, G. Lansbergen, B. Dortland, C.I. De Zeeuw, F. Grosveld, G. van Cappellen, A. Akhmanova, and N. Galjart. 2003. Visualization of microtubule growth in cultured neurons via the use of EB3-GFP (end-binding protein 3-green fluorescent protein). *J Neurosci*. 23:2655-2664.

van Bergeijk, P., M. Adrian, C.C. Hoogenraad, and L.C. Kapitein. 2015. Optogenetic control of organelle transport and positioning. *Nature*. 518:111-114.

van der Vaart, B., C. Manatschal, I. Grigoriev, V. Olieric, S.M. Gouveia, S. Bjelic, J. Demmers, I. Vorobjev, C.C. Hoogenraad, M.O. Steinmetz, and A. Akhmanova. 2011. SLAIN2 links microtubule plus end-tracking proteins and controls microtubule growth in interphase. *J Cell Biol*. 193:1083-1099.

Weisbrich, A., S. Honnappa, R. Jaussi, O. Okhrimenko, D. Frey, I. Jelesarov, A. Akhmanova, and M.O. Steinmetz. 2007. Structure-function relationship of CAP-Gly domains. *Nat Struct Mol Biol*. 14:959-967.

Wisniewski, J.R., M.Y. Hein, J. Cox, and M. Mann. 2014. A "proteomic ruler" for protein copy number and concentration estimation without spike-in standards. *Mol Cell Proteomics*. 13:3497-3506.

Zanic, M., J.H. Stear, A.A. Hyman, and J. Howard. 2009. EB1 recognizes the nucleotide state of tubulin in the microtubule lattice. *PLoS One*. 4:e7585.

Zanic, M., P.O. Widlund, A.A. Hyman, and J. Howard. 2013. Synergy between XMAP215 and EB1 increases microtubule growth rates to physiological levels. *Nat Cell Biol*. 15:688-693.

Zhang, R., G.M. Alushin, A. Brown, and E. Nogales. 2015. Mechanistic Origin of Microtubule Dynamic Instability and Its Modulation by EB Proteins. *Cell*. 162:849-859.

Zhu, Z.C., K.K. Gupta, A.R. Slabbekoorn, B.A. Paulson, E.S. Folker, and H.V. Goodson. 2009. Interactions between EB1 and microtubules: dramatic effect of affinity tags and evidence for cooperative behavior. *J Biol Chem*. 284:32651-32661.

Table S1

Sequencing Hela EB1/2/3KO clones

EB1

```
                                                                gRNA:    3’ TTCAGCTGTACTGTACGACC  5’
ATGGCAGTGAACGTATACTCAACGTCAGTGACCAGTGATAACCTAAGTCGACATGACATGCTGGCCTGGATCAATGAGTCT
 M  A  V  N  V  Y  S  T  S  V  T  S  D  N  L  S  R  H  D  M  L  A  W  I  N  E  S

Clone #1  Insertion: A   EB1  15AA +3AA after frameshift
ATGGCAGTGAACGTATACTCAACGTCAGTGACCAGTGATAACCTAAGATCGACATGA
 M  A  V  N  V  Y  S  T  S  V  T  S  D  N  L  R  S  T  *

Clone #1 Deletion:  CGACATGA   EB1 16AA +6AA after frameshift
ATGGCAGTGAACGTATACTCAACGTCAGTGACCAGTGATAACCTAAGT--------CATGCTGGCCTGGATCAATGA
 M  A  V  N  V  Y  S  T  S  V  T  S  D  N  L  S          H  A  G  L  D  Q  *
Clone #1 Deletion: AG   EB1 15AA +2AA after frameshift
ATGGCAGTGAACGTATACTCAACGTCAGTGACCAGTGATAACCTA--TCGACATGA
 M  A  V  N  V  Y  S  T  S  V  T  S  D  N  L    S  T  *

Clone #2 Deletion: TAAG   EB1 15AA +13AA after frameshift
ATGGCAGTGAACGTATACTCAACGTCAGTGACCAGTGATAACC----TCGACATGACATGCTGGCCTGGATCAATGAGTCTCTGCAGTTGA
 M  A  V  N  V  Y  S  T  S  V  T  S  D  N      L  D  M  T  C  W  P  G  S  M  S  L  C  S  *
Clone #2 Deletion: T  EB1   AA 16AA +13AA after frameshift
ATGGCAGTGAACGTATACTCAACGTCAGTGACCAGTGATAACCTAAG-CGACATGACATGCTGGCCTGGATCAATGAGTCTCTGCAGTTGA
 M  A  V  N  V  Y  S  T  S  V  T  S  D  N  L  S   D  M  T  C  W  P  G  S  M  S  L  C  S  *
Clone #2 Deletion: AGATCGAC   EB1   AA 15AA +1AA after frameshift
ATGGCAGTGAACGTATACTCAACGTCAGTGACCAGTGATAACCT--------ATGA
 M  A  V  N  V  Y  S  T  S  V  T  S  D  N  L          *
```

EB2

```
                                                gRNA: CAGACATGACATCATTGCAT
TGGGGAATGGCGGTCAATGTGTATTCTACCTCGATAACCCAAGAGACTATGAGCAGACATGACATCATTGCATGGGTTAATGACATA
 W  G  M  A  V  N  V  Y  S  T  S  I  T  Q  E  T  M  S  R  H  D  I  I  A  W  V  N  D I V

Clone #1 Deletion: CATTGCATGG  EB2 62AA +3AA after frameshift
TGGGGAATGGCGGTCAATGTGTATTCTACCTCGATAACCCAAGAGACTATGAGCAGACATGACAT---------GTTAATGACATAG
 W  G  M  A  V  N  V  Y  S  T  S  I  T  Q  E  T  M  S  R  H  D  M           L  M  T  *
Clone #1 Deletion: CATTG EB2 63AA +2AA after frameshift
TGGGGAATGGCGGTCAATGTGTATTCTACCTCGATAACCCAAGAGACTATGAGCAGACATGACAT-----CATGGGTTAA
 W  G  M  A  V  N  V  Y  S  T  S  I  T  Q  E  T  M  S  R  H  D  I       M  G  *
Clone #2 Deletion: CATTGCATGG  EB2 62AA +3AA after frameshift
TGGGGAATGGCGGTCAATGTGTATTCTACCTCGATAACCCAAGAGACTATGAGCAGACATGACAT----------GTTAATGACATAG
 W  G  M  A  V  N  V  Y  S  T  S  I  T  Q  E  T  M  S  R  H  D  M           L  M  T  *
Clone #2 Deletion: CATTG EB2 63AA +2AA after frameshift
TGGGGAATGGCGGTCAATGTGTATTCTACCTCGATAACCCAAGAGACTATGAGCAGACATGACAT-----CATGGGTTAA
 W  G  M  A  V  N  V  Y  S  T  S  I  T  Q  E  T  M  S  R  H  D  I       M  G  *
```

EB3

```
          gRNA: TGCACCTCAACTATACCAAG
TGGGTCAACGACTCCCTGCACCTCAACTATACCAAGATAGAACAGCTTTGTTCAG(intron)
 W  V  N  D  S  L  H  L  N  Y  T  K  I  E  Q  L  C  S

Clone #1 Deletion: CCTCAACTATACC   EB3 28AA +2AA after frameshift
TGGGTCAACGACTCCCTGCA-------------AAGATAG
 W  V  N  D  S  L  Q              R  *

Clone #2 Insertion: A    EB3 28AA +59AA after frameshift
TGGGTCAACGACTCCCTGCAACCTCAACTATACCAAGATAGAACAGCTTTGTTCAG(intron)
 W  V  N  D  S  L  Q  P  Q  L  Y  Q  D  R  T  A  L  F
Clone #2 Deletion: CCTCAACTATACCAAG    EB3 28AA +1AA after frameshift
TGGGTCAACGACTCCCTGCA----------------ATAG
 W  V  N  D  S  L  Q                 *
```

4

Probing the role of SLAIN2 as a scaffold for phase separation of +TIPs at growing microtubule ends

Chao Yang, Ankit Rai, Amol Aher, Ilya Grigoriev and Anna Akhmanova

In preparation

Cell Biology, Department of Biology, Faculty of Science, Utrecht University,

Padualaan 8, 3584 CH Utrecht, The Netherlands

Abstract

Microtubules are dynamic polymers that can switch between phases of growth and shortening. This behavior can be observed in solutions of purified tubulin; however, in cells, microtubule dynamics is regulated by numerous factors. Some of these factors, termed microtubule plus end tracking proteins (+TIPs), control the dynamics of growing microtubule ends and their connections to other cellular structures. End Binding (EB) proteins are abundant and conserved +TIPs, which recognize the stabilizing cap at growing microtubule ends and recruit many other proteins. EB-binding +TIPs can also interact with each other and form a dynamic network. Recent work has shown that proteins participating in multivalent interaction networks can be prone to liquid-liquid phase separation (LLPS). Whether LLPS plays a role in +TIP function is an open question. SLAIN1/2 proteins are interesting candidates to be involved in LLPS at microtubule plus ends in mammalian cells. Similar to other proteins shown to undergo in LLPS in other cellular contexts, SLAINs have extended intrinsically disordered regions, which contain multiple linear motifs involved in partner binding. SLAINs can directly interact with other major +TIPs, such as EBs, chTOG, CLASPs and CLIPs. Here, we explore the propensity of SLAINs to form condensates in cells and in vitro. We show that SLAIN2 readily forms liquid droplet-like structures when overexpressed in cells, although not at the endogenous expression level, and that EBs and chTOG, but not CLASPs or CLIP170 can participate in formation of these droplets and their interactions with microtubules. We further show that SLAIN2 and chTOG, but not EB3, can form liquid droplets in vitro in the presence of crowing agents in conditions that are compatible with microtubule polymerization. Droplets containing chTOG promote spontaneous microtubule nucleation and formation of microtubule asters. We discuss the implications of our findings for the SLAIN2-mediated control of microtubule dynamics and further steps that need to be taken to understand this process.

INTRODUCTION

Microtubules are essential cytoskeletal filaments that participate in a broad variety of cellular functions, such as control of cell shape, chromosome separation during cell division, intracellular transport and cell motility. Microtubules can rapidly switch between phases of growth and shortening, a process termed dynamic instability (Desai and Mitchison, 1997). This process is tightly controlled in cells by numerous microtubule associated proteins (MAPs), which can increase or decrease microtubule growth rate or affect the frequencies of transitions between growth and shortening, termed catastrophes and rescues (Akhmanova and Steinmetz, 2015). Many factors controlling microtubule dynamics can specifically accumulate at growing microtubule plus ends; such proteins are termed microtubule plus end tracking proteins, or +TIPs (Akhmanova and Steinmetz, 2008; Schuyler and Pellman, 2001).

End Binding proteins are highly conserved +TIPs, which can autonomously track growing microtubule plus ends by sensing the nucleotide state of tubulin through their CH domains (Maurer et al., 2012; Zhang et al., 2015). At their C-termini, EBs contain binding sites for two other types of +TIPs – proteins with globular CAP-Gly motifs and proteins with intrinsically disordered regions bearing linear motifs such as SxIP or LxxPTPh (Akhmanova and Steinmetz, 2008; Honnappa et al., 2009; Kumar et al., 2017). The latter group of proteins is particularly numerous, because short linear motifs can easily arise during evolution. Importantly, some EB-interacting +TIPs can also bind to each other directly: for example, CLIP170 can bind to EBs through its N-terminal CAP-Gly domains (Akhmanova et al., 2001), whereas the coiled coil region located in the middle of the CLIP170 binds to CLASPs (Mimori-Kiyosue et al., 2005). CLASPs, in turn, bind to EBs through their two centrally located SxIP motifs (Mimori-Kiyosue et al., 2005).

Another interesting example of a +TIP with multiple interaction sites is represented by SLAIN1/2. SLAINs have dimeric helical N-termini followed by a long intrinsically disordered region that contains multiple SxIP or LxxPTPh-like binding sites for the EBs and can also directly interact with CLASPs as well as the CAP-Gly domains of CLIPs (Kumar et al., 2017; Liu et al., 2017; van der Vaart et al., 2011)(Figure 1A). Moreover, the N-terminal part of SLAINs binds to chTOG (colonic and hepatic tumor overexpressed gene, known in XMAP215 in *Xenopus*, Mini spindles (Msps) in *Drosophila*, and Dis 1, Alp14 or Stu2 in different yeast species) (van der Vaart et al., 2011). XMAP215/chTOG is a microtubule polymerase that can bind to tubulin dimers through its TOG domains and accelerate tubulin addition to microtubule plus ends (Brouhard et al., 2008). Based on the biochemical data, SLAINs can potentially form multivalent assemblies with multiple +TIPs and regulate microtubule polymerization through chTOG. Previous work has established that SLAINs indeed promote rapid and persistent microtubule growth (Bouchet et al., 2016; van der Vaart et al., 2012; van der Vaart et al., 2011). The phenotype of SLAIN2 depletion in mammalian cells is similar to that of chTOG depletion – in both cases, microtubule growth rate is moderately affected but growth episodes are frequently interrupted by catastrophes (Bouchet et al., 2016; van der Vaart et al., 2011). Although XMAP215 family proteins can autonomously track growing plus ends in different species (Al-Bassam et al., 2012; Brouhard et al., 2008; Li et al., 2012; Roostalu et al., 2015), SLAIN1/2 contribute to the accumulation of chTOG at microtubule plus ends (van der Vaart et al., 2011), and the same is true for the functional counterpart of SLAINs, sentin, in *Drosophila* (Li et al., 2011). It was thus proposed that the complexes of SLAINs and EBs regulate microtubule plus end dynamics by enhancing chTOG binding to microtubule plus ends (van der Vaart et al., 2011).

Although this model appears straightforward, understanding how EBs, chTOG and SLAINs work together to regulate microtubule growth is not trivial. In vitro work has shown that EBs and chTOG, which do not interact with each other directly, display distinct localization

at growing microtubule plus ends: chTOG binds to the outermost microtubule extremities, where curved tubulin dimers are exposed, whereas EBs show enhanced accumulation in the region behind the microtubule tip (Maurer et al., 2014). Also in cells, chTOG localizes as a dot at the outermost tip of an EB comet (Gutierrez-Caballero et al., 2015; Nakamura et al., 2012) (see Chapter 2). Importantly, although EBs and XMAP215/chTOG do not interact and appear to be spatially separated at microtubule ends, they can cooperatively accelerate microtubule growth rate to physiological levels (Zanic et al., 2013), possibly because EB binding allosterically affects XMAP215 activity by modifying the structure of the microtubule tip. Furthermore, there is a significant discrepancy between the effect of EBs and chTOG on microtubule plus end dynamics in vitro and in cells: EBs, chTOG and their combination increase both the growth rate and catastrophe frequency in vitro, whereas in cells, the loss of these proteins promotes catastrophes but has only a mild effect on the instantaneous growth rate (Komarova et al., 2009; van der Vaart et al., 2011; Yang et al., 2017; Zanic et al., 2013). To test whether this discrepancy is due to the activity of SLAINs, which can connect EBs and chTOG, Aher et al. have reconstituted microtubule growth in vitro in the presence of chTOG, EB3 and SLAIN2 (Aher, 2017). This work confirmed that EB3 and chTOG indeed cooperatively increase microtubule growth rate and catastrophe frequency. The addition of SLAIN2 caused a further, albeit mild increase in the growth rate but did not block catastrophes. These results thus provided no explanation for the ability of EBs, chTOG and SLAIN2 to suppress catastrophes in cells.

One obvious reason for the discrepancy between the results obtained in vitro and in cells is the contribution of additional cellular MAPs, which are absent in the in vitro assays. Furthermore, macromolecular crowding of the cytoplasm could potentially affect the properties and interactions of different +TIPs, for example, by causing liquid-liquid phase separation (LLPS). Recent work has shown that phase separation might be a process relevant for the understanding of microtubule organization: in the presence of crowding agents in vitro, centrosomal proteins from *C. elegans* as well as mammalian neuronal MAP tau were shown to form condensates, concentrate free tubulin and induce microtubule nucleation (Hernandez-Vega et al., 2017; Woodruff et al., 2017). SLAINs are potentially interesting candidates to participate in condensate formation, because they have extended intrinsically disordered low-complexity sequence regions (Figure 1A), and such regions have been reported to be present in proteins driving LLPS in other systems (Alberti et al., 2019). Due to these sequence features and the abundance of binding sites for other +TIPs, SLAINs could potentially serve as condensate "scaffolds" (Alberti et al., 2019), that would help to recruit "client" proteins such as chTOG, which, through its tubulin-binding TOG domains, could locally concentrate free tubulin around microtubule tips and shift microtubule dynamics towards polymerization.

To start testing such a possibility, we explored the ability of SLAIN2 to form condensates in cells and in vitro and to concentrate different +TIPs. Further, we have defined conditions for in vitro experiments, in which macromolecular crowding agents are combined with tubulin to obtain dynamic microtubules. These assays can be explored in future to study the effects of molecular crowding on microtubule growth.

RESULTS

SLAIN2 forms liquid-like droplets when overexpressed in cells

To test the ability of SLAIN2 to form condensates, we have overexpressed GFP-SLAIN2 in HeLa cells. As we have described previously, at low expression levels SLAIN2 specifically labeled growing microtubule plus ends (van der Vaart et al., 2011), while at higher expression levels it formed round droplet-like structures (Figure 1C). The formation of these structures was not dependent on EBs, as it was also observed in HeLa cells completely lacking EB1, EB2 and

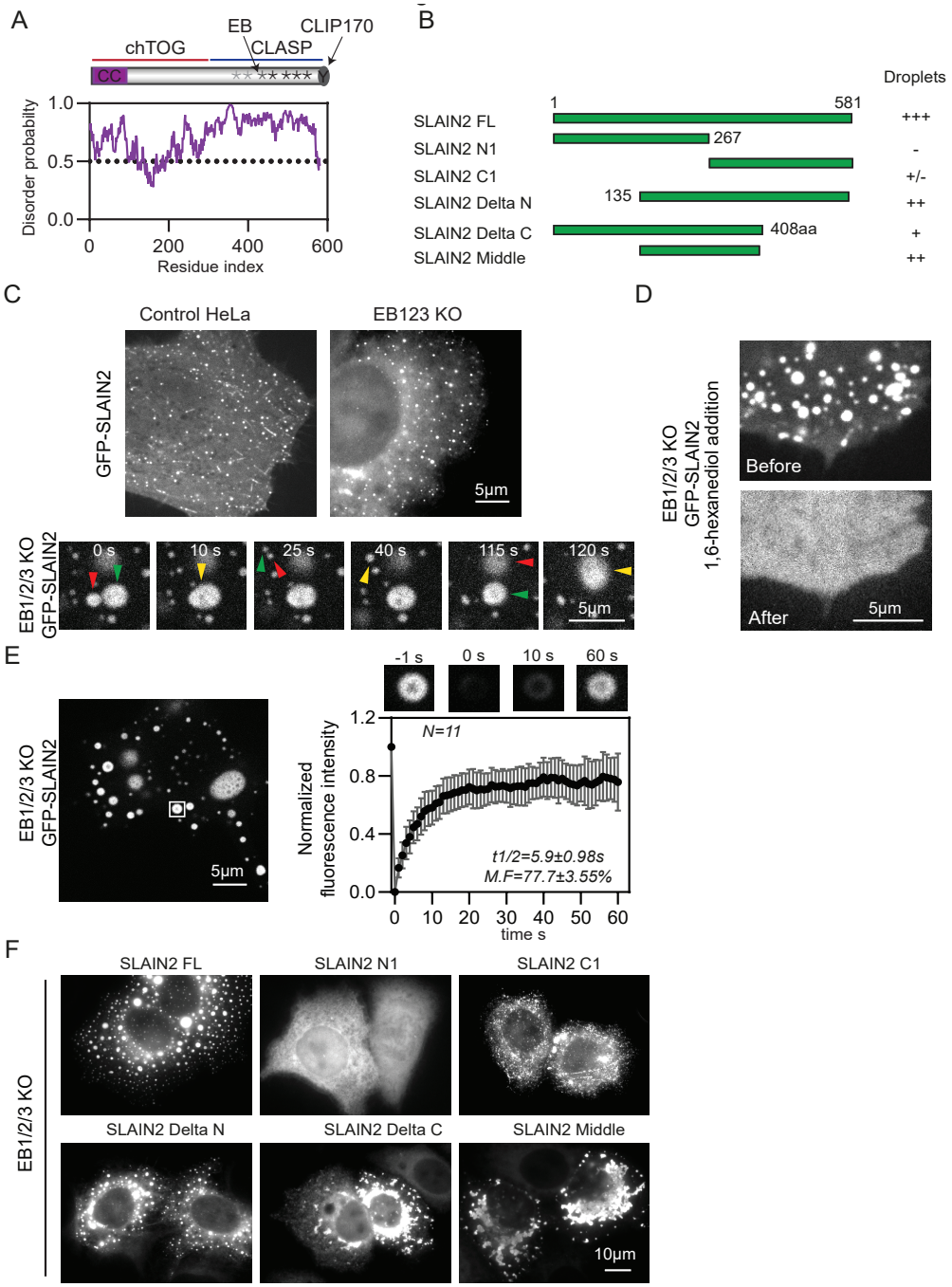

Figure 1. Characterization of SLAIN2 droplets

(A) A scheme of SLAIN2 protein and its partner-binding sites, and the prediction of intrinsically disordered regions using https://iupred2a.elte.hu/ website.

(B) A scheme of SLAIN2 deletion constructs used and a summary of their ability to form droplets when overexpressed with a GFP tag in cells.

(C) Representative fixed images of control HeLa cells and EB1/2/3 knockout (KO) cell lines transiently transfected with GFP-SLAIN2. Enlarged live images of SLAIN2 droplets in HeLa EB1/2/3 KO cells at different time points are shown below.
(D) Representative single frames of GFP-SLAIN2-overexpressing HeLa EB1/2/3 KO cells before and after the addition of 3.5% 1,6-hexanediol.
(E) (Left) Representative image of a FRAP experiment. Photobleaching was performed in the boxed area of a GFP-SLAIN2-overexpressing HeLa EB1/2/3 KO cell. Right, top – images of the photobleached droplet at the indicated time points. Right, bottom – analysis of recovery curves for 11 droplets from 4 cells. The half-time of recovery and the mobile fraction (M.F.) are indicated.
(F) Representative fixed images of GFP-SLAIN2 deletion constructs overexpressed in HeLa EB1/2/3 KO cells.

EB3 (EB1/2/3 knockout cells, see Chapter 3 for the description of this cell line) (Figure 1C). SLAIN2-positive structures disappeared when cells were treated with 1,6 hexanediol (Figure 1D), a cell-permeable compound that can effectively interfere with LLPS of many intrinsically disordered proteins and cause dissolution of protein condensates because it acts as a mild inhibitor of hydrophobic interactions (Alberti et al., 2019; Ribbeck and Gorlich, 2002). GFP-SLAIN2-positive structures displayed other features characteristic of liquid-like droplets: they underwent random movements throughout the cell and readily fused after making contact with each other (Figure 1C). Furthermore, Fluorescence Recovery after photobleaching (FRAP) experiments revealed that SLAIN2 droplets showed fast, though typically not complete recovery when they were individually photobleached (Figure 1E). It should be noted that GFP-SLAIN2 droplets did not appear completely homogeneous, and larger droplets contained inclusions with low fluorescence (Figure 1E), possibly because the droplets were nucleated around some cytoplasmic structures.
We next used deletion mutants of SLAIN2 to identify the part of the protein responsible for condensate formation. Interestingly, the middle part of SLAIN2 (residues 135-408), which contains low-complexity sequences, was sufficient for the formation of droplet-like structures (Figure 1B and F). The N-terminal part, which includes the chTOG binding site, showed no self-association, whereas the C-terminal part bearing the interaction sites for EBs, CLASPs and CLIP170 showed significant binding to microtubules and also formed some droplet-like structures, but this occurred less efficiently compared to the middle part of SLAIN2. We conclude that in conditions of overexpression, SLAIN2 can form structures that resemble liquid droplets, and this property depends on the centrally located intrinsically disordered low-complexity sequence region. SLAIN2-positive structures will be termed “SLAIN2 droplets” in the text below, although we are aware of the fact that the data above do not conclusively prove that SLAIN2-positive structures indeed represent liquid droplets.

SLAIN2 droplets accumulate EB1 and chTOG, but not CLASPs or CLIP170

To investigate whether SLAIN2-scaffolded droplets can accumulate different “client” +TIPs, we performed immunofluorescence staining experiments and co-expression of GFP-SLAIN2 with +TIPs bearing a red fluorescent tag. We found that endogenous EB1 was strongly enriched in SLAIN2 droplets (Figure 2A). Interestingly, when GFP-SLAIN2 was co-expressed together with mRFP-EB3, both proteins strongly colocalized and redistributed along microtubule bundles (Figure 2A). It appears that EBs can promote spreading of SLAIN2 condensates along microtubule surface. In line with this idea, GFP-SLAIN2 droplets appeared to be somewhat more tightly associated with microtubules and their tips in control HeLa cells than in EB1/2/3 knockout cells (Figure 2B), although due to the very dense microtubule system in HeLa cells, the difference was difficult to prove.
Furthermore, we found that endogenous chTOG, but not CLASP1 and CLASP2 or CLIP170

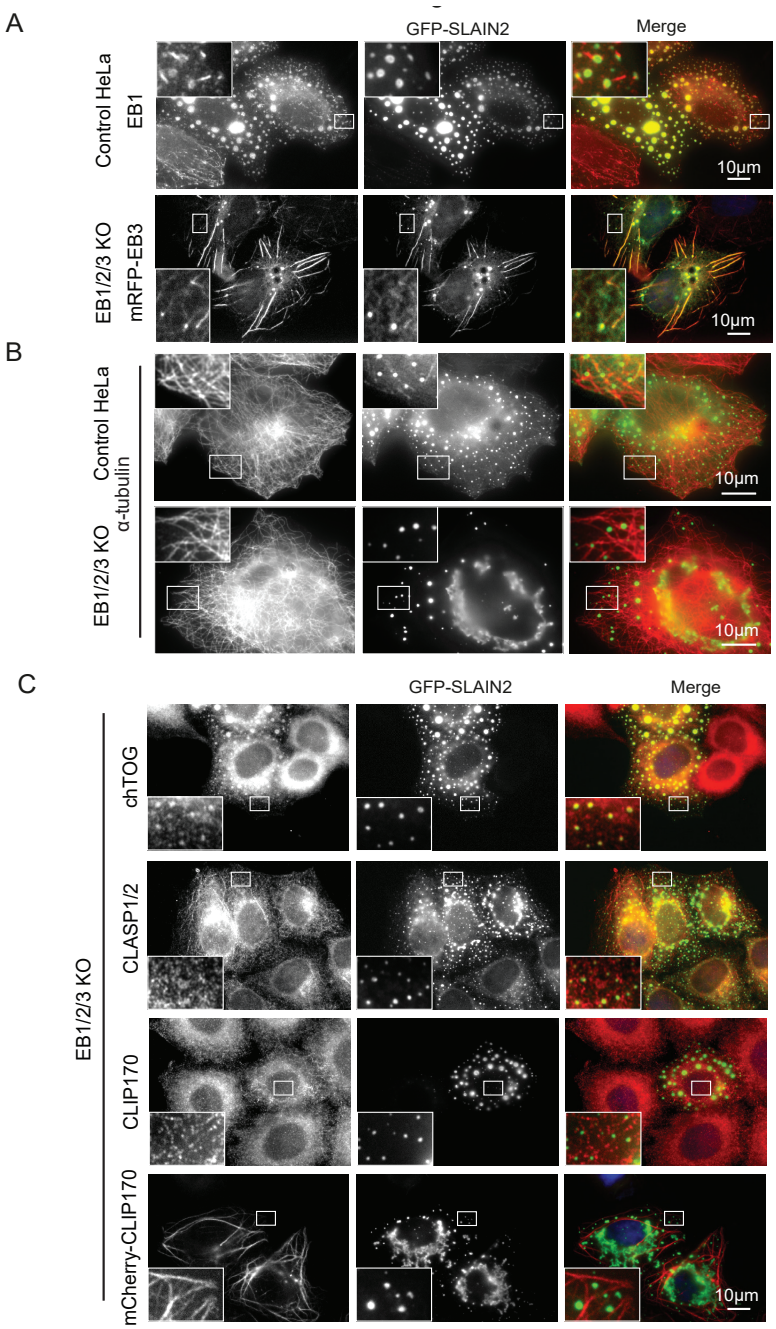

Figure 2. Analysis of the colocalization of SLAIN2-interacting +TIPs with SLAIN2 droplets

(A) Immunofluorescence cell staining for endogenous EB1 in control HeLa cells and overexpression of mRFP-EB3 in EB1/2/3 KO cells transiently transfected with GFP-SLAIN2.

(B) Immunofluorescence cell staining for α-tubulin (red) in control and EB1/2/3 KO HeLa cells transiently transfected with GFP-SLAIN2.

(C) Immunofluorescence cell staining for endogenous chTOG, CLASP1/2 and CLIP170 and overexpression of mCherry-CLIP170 in HeLa EB1/2/3 KO cells transiently transfected with GFP-SLAIN2. Insets show enlargements of boxed areas.

strongly colocalized with GFP-SLAIN2 droplets in EB1/2/3 knockout HeLa cells (Figure 2C). In contrast to mRFP-EB3, which caused redistribution of GFP-SLAIN2 to microtubules, mCherry-CLIP170 had no effect on the appearance GFP-SLAIN2 droplets, and no colocalization between these droplets and CLIP170-decorated microtubule bundles was observed (Figure 2C). We conclude that among the direct binding partners of SLAIN2, EB1 and chTOG but not CLASPs and CLIP170 can behave as "clients" that partition into condensates formed by SLAIN2.

SLAIN2 does not form droplets in cells at endogenous expression levels

Formation of GFP-SLAIN2 droplets could be a protein overexpression artifact. Since the antibodies against SLAIN2 do not work well for immunofluorescence cell staining in HeLa cells, in order to detect endogenous SLAIN2 (SLAIN1 is not expressed in HeLa cells (van der Vaart et al., 2011)), we have generated knock-in lines of control and EB1/2/3 knockout HeLa cells, in which endogenous SLAIN2 was fused to HaloTag (Figure 3A). We performed staining with HaloTag TMRDirect ligand followed by Fluorescence-Activated Cell Sorting, isolated individual fluorescent clones and characterized four control and three EB1/2/3 knockout HeLa cell lines in more detail. Using Western blotting with anti-SLAIN2 antibodies, we found that all these clones were heterozygous for the HaloTag insertion (Figure 3B). The intensity ratios between the wild type and HaloTag-fused SLAIN2 bands varied between different clones (Figure 3B). HeLa cells are known to be triploid, which could explain this variation, although additional sources of variability between the clones, such as presence of additional gene copies or differences in expression levels between different alleles, cannot be ruled out.

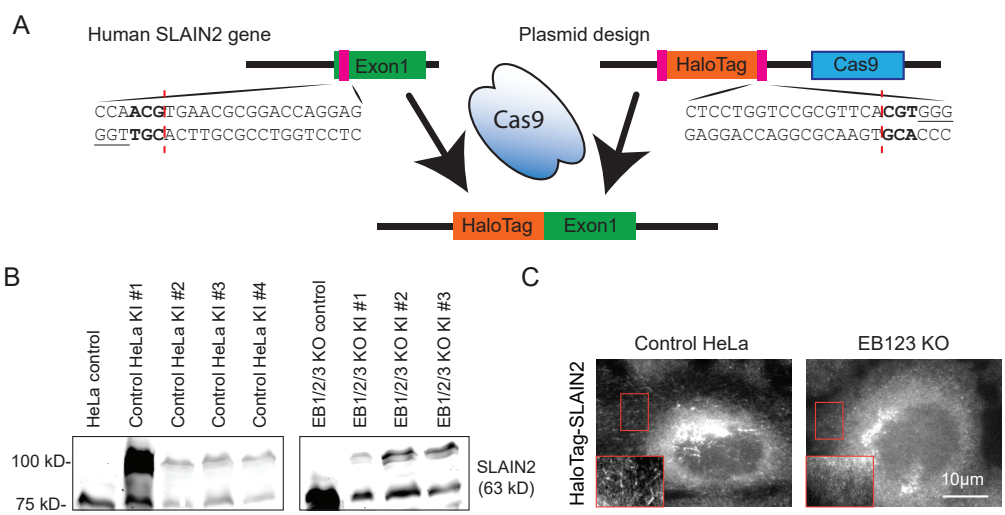

Figure 3. Generation of HaloTag-SLAIN2 knock-in cell lines

(A) A scheme of the HaloTag-SLAIN2 knock-in generation; the guide RNA sequence and the sequences flanking the HaloTag are shown. The sites recognized and cut by Cas9 are underlined and indicated with red dotted lines, respectively.

(B) Western blot analysis of HaloTag-SLAIN2 knock-in control and EB1/2/3 knockout HeLa cells.

(C) Representative images of fixed HaloTag-SLAIN2 knock-in control and EB1/2/3 knockout HeLa cells. Insets show enlargements of the boxed areas.

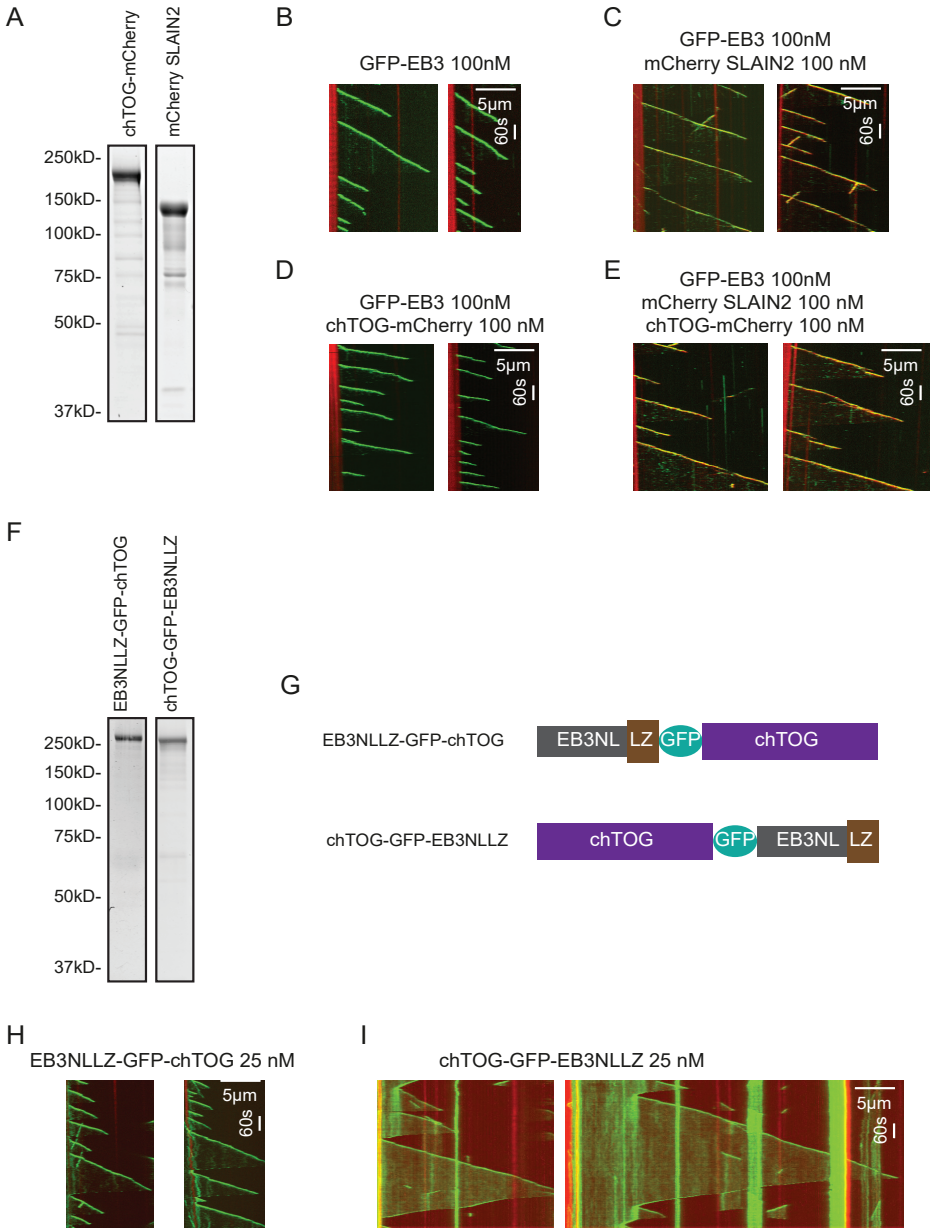

Figure 4. Regulation of microtubule dynamics by EB3, chTOG, SLAIN2 and EB3-chTOG fusions.

(A) Coomassie blue stained gels with mCherry-SLAIN2 and chTOG-mCherry purified from HEK293 cells.

(B-E) Kymographs illustrating microtubule plus end growth in the presence of the indicated protein combinations.

(F, G) Coomassie blue stained gels (F) and schemes (G) of the EB3-chTOG chimeric proteins purified from HEK293 cells.

(H-I) Kymographs illustrating microtubule plus end growth in the presence of the EB3-chTOG chimeras depicted in (F).

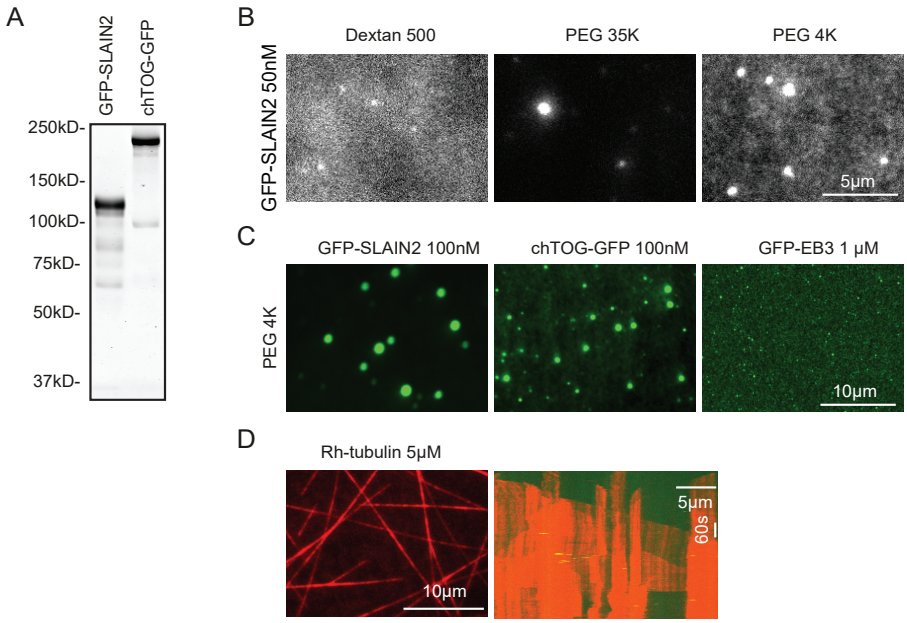

Figure 5. Purified GFP-SLAIN2 and chTOG form condensates in vitro in the presence of crowding agents
(A) Coomassie blue stained gels with GFP-SLAIN2 and chTOG-GFP purified from HEK293 cells.
(B) Images of 50 nM GFP-SLAIN2 incubated in a buffer with 5% Dextan 500, PEG 35000 and PEG 4000.
(C) Images of GFP-SLAIN2, chTOG-GFP and GFP-EB3 incubated in a buffer with 5% PEG 4000.
(D) Spontaneous microtubule nucleation in a 5 μM solution of porcine rhodamine-labeled tubulin in the presence of 5% PEG 4000.

Imaging of fixed HaloTag-SLAIN2 cells showed the presence of clear microtubule plus end labeling in control cells and mostly a diffuse staining in EB1/2/3 knockout cells, while no obvious droplets were observed (Figure 3C). However, this does not exclude the possibility that when SLAIN2 is concentrated by EBs at the microtubule tips, weak interactions between SLAIN2 molecules promote formation of small condensates in microtubule tip vicinity.

Regulation of microtubule dynamics by EB3, chTOG, SLAIN2 and EB3-chTOG fusions
To further explore the ability of SLAIN2 to form liquid droplets, we turned to in vitro experiments. We purified mCherry-SLAIN2 and chTOG-mCherry from HEK293 cells by using the StrepII tag that can specifically bind to StrepTactin beads; since endogenous chTOG readily co-purifies with SLAIN2 (Aher, 2017), after binding the proteins to the beads, we washed them with a buffer containing 1.5 M NaCl to improve protein purity (Figure 4A). We first tested the properties of the purified GFP-SLAIN2 and chTOG-GFP using in vitro assays with dynamic microtubules grown from GMPCPP-stabilized seeds in the presence of 15 μM tubulin in the absence of crowding agents (Aher et al., 2018; Montenegro Gouveia et al., 2010). As described previously (Aher, 2017), the combination of SLAIN2 and EB3 caused some increase in microtubule growth rate compared to microtubules grown in the presence of EB3 alone (as could be seen from the slope of the kymographs), possibly due to the presence of some co-purified chTOG (Figure 4B,C). When chTOG and EB3 were combined, both the growth rate and catastrophe frequency were increased (Figure 4D). The addition of SLAIN2 mildly suppressed catastrophes as compared to the EB3-chTOG combination (Figure 4E).
To further test whether a physical connection between EB3 and chTOG can alter their effect on

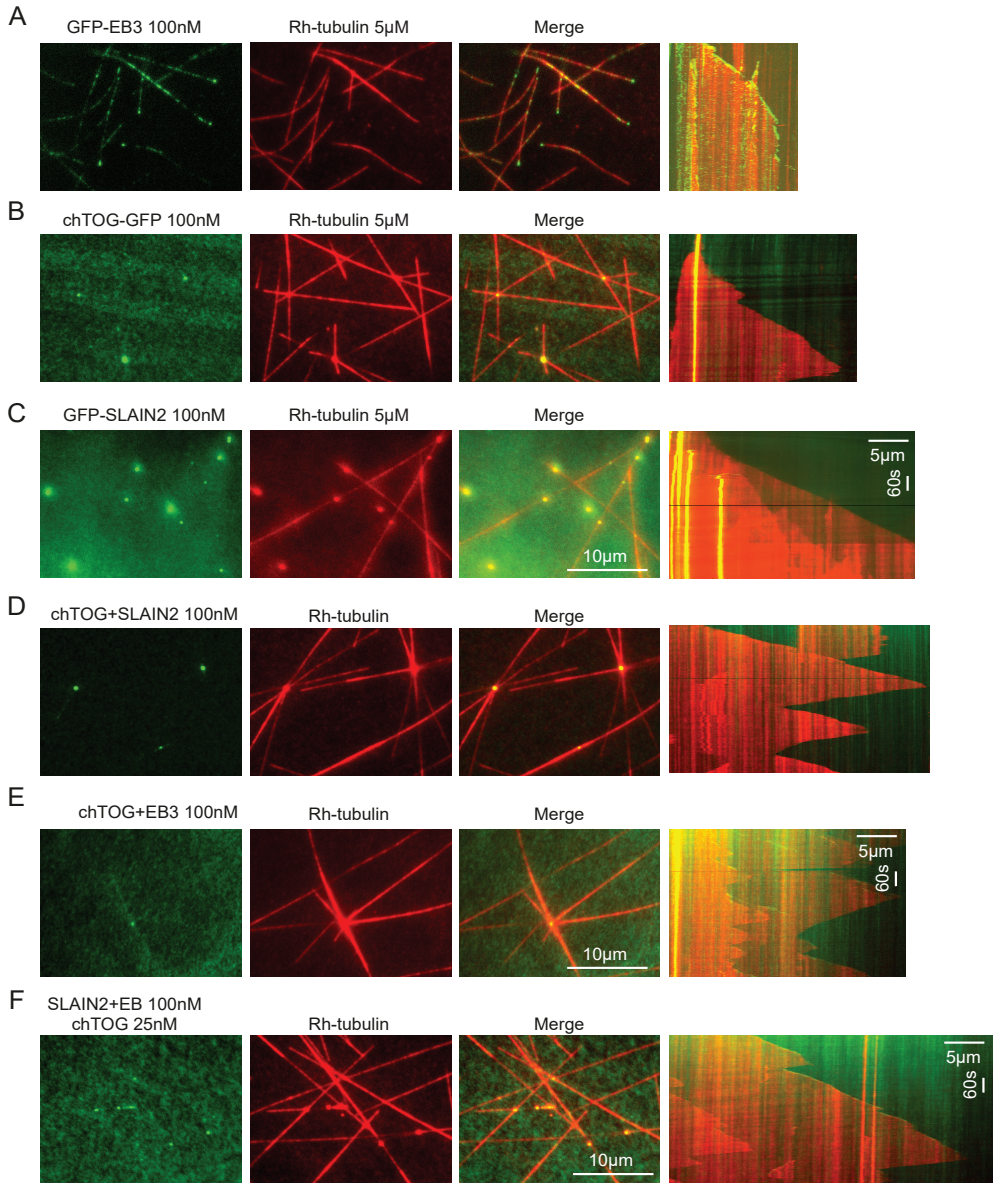

Figure 6. Microtubule dynamics in the presence of +TIPs and a crowding agent

GFP-EB3, chTOG-GFP and GFP-SLAIN2 at the indicated concentrations were incubated singly or in the indicated combinations in the presence of 5 µM porcine rhodamine-labeled tubulin and 5% PEG 4000. Single frames from time-lapse imaging and representative kymographs illustrating the dynamics of microtubule plus ends are shown.

microtubule dynamics, we generated two alternative tandem fusions of full-length chTOG and the N-terminal microtubule-binding part of EB3, which was dimerized with a leucine zipper (EB3-NL-LZ) (Figure 4F,G). Interestingly, when these fusions were tested even at quite low concentrations (25 nM, compared to 100 nM concentrations of EB3, chTOG and SLAIN2 described above), the two proteins had distinct effects on microtubule growth. The fusion protein in

which chTOG was positioned at the C-terminus of EB3 increased catastrophes without strongly affecting microtubule growth rate (Figure 4H). In contrast, when EB3 was fused to the chTOG C-terminus, the resulting fusion increased microtubule growth rate and reduced catastrophe frequency (Figure 4I). These data indicate that a direct connection of chTOG to EB3, and/or the dimerization of chTOG in a molecular context where its TOG domains are positioned at the N-terminus of the protein can promote rapid and processive microtubule growth. These data suggest that the oligomerization of chTOG by dimers of SLAIN2 and EB2 could potentially alter the properties of this microtubule polymerase, so that it could accelerate microtubule growth without inducing catastrophes, and perhaps even cause catastrophe suppression.

SLAIN2 and chTOG form droplets in vitro in the presence of macromolecular crowding agents
Our next step was to investigate the effect of different macromolecular crowding agents on the behavior of SLAIN2, chTOG and EB3. For these experiments, we purified GFP-tagged SLAIN2 and chTOG (Figure 5A), so that they could be combined with tubulin bearing a red fluorescent label. We found that 50 nM GFP-SLAIN2 readily formed droplet-like structures in vitro in the presence of 5% Dextan 500, PEG 35000 and PEG 4000 (Figure 5B). For subsequent experiments, 5% PEG 4000 was used. Whereas 50-100 nM GFP-SLAIN2 and chTOG-GFP made large droplet-like structures in these conditions, this was not observed for GFP-EB3 even at a 1 µM concentration (Figure 5C). We also tested different tubulin concentrations in the presence of crowding agents and found that while the concentration we normally use for in vitro assays, 15 µM, lead to extensive spontaneous microtubule nucleation, making the assay impossible to interpret, only moderate microtubule nucleation was observed at 5 µM tubulin in the presence of 5% PEG 4000 (Figure 5D). This concentration was used for subsequent assays.

Reconstitution of microtubule dynamics in the presence of +TIPs and crowding agents
Next, we explored the behavior of GFP-tagged EB3, SLAIN2 and chTOG in the presence of 5 µM tubulin and 5% PEG 4000. Compared to the conditions without PEG 4000 (Figure 4B), GFP-EB3 showed binding not only to growing microtubule tips but also along the lattice (Figure 6A). EB3 induces catastrophes in our in vitro assays (Komarova et al., 2009; Mohan et al., 2013; Montenegro Gouveia et al., 2010), and this also occurred in the presence of PEG 4000. However, while no microtubule rescues are observed in our assays in the presence of EB3 alone (Komarova et al., 2009; Mohan et al., 2013; Montenegro Gouveia et al., 2010) (Figure 4B), these became quite frequent in the presence of PEG 4000. chTOG promoted nucleation of microtubules, which formed aster-like structures centered at chTOG condensates (Figure 6B). This observation fits well with previously published data showing that chTOG can promote microtubule nucleation in the absence of crowding agents (Roostalu et al., 2015; Wieczorek et al., 2015). In contrast, the condensates formed by GFP-SLAIN2 did not form microtubule nucleation centers, even though they did concentrate some tubulin (Figure 6C).
When chTOG-GFP and GFP-SLAIN2 were combined, all GFP-labeled condensates abundantly nucleated microtubules, suggesting that the two proteins co-segregated into the same structures (Figure 6D). We note that the proteins would need to be labeled with tags of different colors to prove that this is indeed the case. A similar result was observed with the combination of chTOG-GFP and GFP-EB3, although the condensates appeared smaller than with chTOG-GFP alone, and some green signal was present at microtubule plus ends (Figure 6E). When all three proteins were combined, we did not observe formation of microtubule asters originating from condensates, but we did see clear labeling at growing microtubule plus ends and some irregular signals along microtubule lattices (Figure 6F). This suggests that similar to the results in cells (Figure 2A), EB3 promotes redistribution of SLAIN2 and chTOG along the

microtubule lattice. Importantly, in all cases when EB3 or chTOG were present, we observed catastrophes, which were particularly frequent when the EB3 and chTOG were combined, in line with previous results without crowding agents (Aher, 2017). The addition of SLAIN2 had no major effect on microtubule plus end dynamics in these conditions (Figure 6F), although a quantification of the parameters of microtubule dynamics would be needed to make firm conclusions. We have not performed such a quantification because due to time limitations, our data were obtained only with a single set of protein concentrations, and we think that it would make more sense to explore a broader concentration range of the three proteins before collecting quantitative data.

DISCUSSION

Extensive previous work has identified a variety of MAPs and characterized their effects on microtubule dynamics in cells and in vitro. In some cases, a good match was found between in vitro and cellular data: for example, the kinesin-13 MCAK drives microtubule disassembly and induces catastrophes, whereas CLASPs suppress catastrophes and promote rescues both in cells and in vitro (Aher et al., 2018; Al-Bassam et al., 2010; Hunter et al., 2003; Lawrence et al., 2018; Maney et al., 2001; Mimori-Kiyosue et al., 2005; Montenegro Gouveia et al., 2010). However, in other cases, there are discrepancies between the effects of particular MAPs observed in cells and in systems with purified components. One potential source of such discrepancies is the molecular crowding of the cytoplasm, which is not recapitulated in standard in vitro reconstitutions of microtubule dynamics.

Here, we made some steps towards exploring the effects of molecular crowding on the regulation of microtubule plus end growth by EB3, SLAIN2 and chTOG. Based on the sequences of the three proteins, we hypothesized that SLAIN2, which contains long intrinsically disordered low-complexity sequence regions, could serve as a scaffold for LLPS. We found that this was indeed the case in SLAIN2-overexpressing cells and also in vitro in the presence of crowding agents. Interestingly, SLAIN2 scaffolds were selective – EB1 and chTOG partitioned into GFP-SLAIN2 droplets, while other direct partners of SLAIN2, CLIP170 and CLASPs, did not. It should be noted, however, that since many different proteins are subject to LLPS in such conditions (Alberti et al., 2019; McSwiggen et al., 2019), our results do not prove that SLAIN2, either alone or together with its binding partners indeed forms condensates in cells at physiologically relevant concentrations. Using CRISPR/Cas9 mediated knock-in technology, we have labeled endogenous SLAIN2 in control and EB1/2/3 knockout HeLa cells with a HaloTag and confirmed that it does not form obvious droplet-like structures at endogenous expression levels. However, it is well established that local enrichment of proteins prone to LLPS can nucleate condensates, even if the average cellular concentration is not sufficient for partitioning into two phases (Alberti et al., 2019; Bracha et al., 2018; Snead and Gladfelter, 2019). EB-dependent concentration of SLAIN2 at growing microtubule ends could thus potentially lead to local condensate formation of SLAIN2 on microtubule plus ends. Dynamic condensation on microtubule surface has been described for other MAPs, such as, for example, the neuronal protein tau (Siahaan et al., 2019; Tan et al., 2019).

One way to examine this possibility would be to introduce into SLAIN2 either deletions or point mutations that would specifically disrupt its self-association without perturbing the binding sites for different +TIPs. One could then test whether such mutants can still form droplet-like structures when overexpressed and whether they can substitute for the endogenous SLAIN2 in controlling processive microtubule growth. Given that formation of SLAIN2 droplets mostly depends on the middle part of the protein, which may not be directly involved in interactions with other +TIPs, such an approach would likely be feasible. However, introducing such

mutations would require careful controls – simply reducing the length of the middle part of SLAIN2 might bring the chTOG and EB-binding sites into close proximity and might cause steric hindrance at microtubule tips or affect the interactions of the EBs and chTOG with microtubules in other ways. Mutation of the low-complexity regions of SLAIN2, on the other hand, might require introduction of multiple substitutions. LLPS of proteins can be mediated by different types of non-covalent bonds, including cation-pi, pi-pi, electrostatic, hydrophobic and dipole interactions (Alberti et al., 2019; Vernon et al., 2018). Systematic multisite substitution of different types of residues such as arginines (e.g. (Wang et al., 2018)) or prolines, which are enriched in the middle part of SLAIN2, might be needed to achieve a significant effect. One potential argument in favor of starting this avenue of investigation is the observation that SLAIN2 is specifically inactivated in mitosis through extensive multisite phosphorylation. An increase in negative charges can inhibit the ability of proteins to undergo phase separation (Snead and Gladfelter, 2019; Wang et al., 2018), and the presence of multiple phosphorylation sites in the middle of SLAIN2 might suggest that they have a regulatory function by affecting the tendency of the protein for LLPS.

Another way of testing the potential importance of LLPS in SLAIN2 function is by reconstituting its effect on microtubules in vitro in conditions of molecular crowding. We purified SLAIN2 and chTOG and performed some preliminary tests. We found that SLAIN2 could form condensates in vitro, and that these condensates had little affinity for microtubules. In combination with chTOG, which by itself could also form condensates in the presence of crowding agents, SLAIN2 appeared to be able to participate in chTOG-containing structures that nucleated microtubules, but it did not seem to have any major additional effects. In the presence of EB3, which can partition into SLAIN2 droplets in cells and promote their spreading along microtubules, SLAIN2 and chTOG redistributed along microtubule lattices. Although some signal was present at microtubule ends, in the conditions that we used, there was no strong enrichment of the proteins at microtubule tips compared to normal plus end tracking observed in the absence of crowding agents, likely because a significant protein pool was captured along microtubule shafts. Further adjustment of the buffer conditions might be necessary to optimize these assays. For example, increasing the ionic strength of the buffer could suppress the interaction EB3 with microtubule lattices in favor of tip localization (Buey et al., 2011) and might help to enrich both SLAIN2 and chTOG at microtubule plus ends.

One argument in favor of pursuing this line of research is our observation that the chTOG-EB3-NL-LZ-GFP fusion seemed to be able to accelerate microtubule polymerization and also suppress catastrophes. While careful quantification of microtubule dynamics at different protein concentrations would be needed to prove this conclusion, these results could suggest that whereas chTOG and XMAP215 are monomers (Al-Bassam and Chang, 2011), their oligomerization and/or direct linkage to EBs could alter their properties. Since both EB3 and SLAIN2 are dimers, their assemblies could potentially bind to two chTOG molecules, and further oligomerisation could be achieved through the formation of condensates of SLAIN2.

Additional tools and information would be needed to optimize the assays aimed at testing the properties of SLAIN2-chTOG-EB3 condensates. First, in our experiments, all proteins were labeled with a GFP tag, and it would be important to introduce the three proteins with tags of different colors in order to determine their effects on each other's behavior in the system. Since we have already generated chTOG and SLAIN2 with green and red fluorescent tags, such experiments would certainly be feasible. Second, an obvious parameter to be varied is the concentration of each protein and their relative ratios. In cells, EB concentration is thought to be in the range of several hundred nM (EB1 has a concentration of ~300 nM in *Xenopus* egg extracts and ~100-500 nM in different cell lines), while the concentrations of various +TIPs

were estimated to be ~10-100 nM (15-40 nM for SLAIN2 and 20-50 nM for chTOG (Tirnauer et al., 2002; Itzhak et al., 2016; Liu et al., 2019; Wisniewski et al., 2014). The endogenous concentrations of chTOG and SLAIN2 thus appear lower, and the concentration of EB3 appears higher than in the in vitro assays we used. However, since the measurements based on mass spectrometry may be imprecise, determining the exact concentrations of EBs, SLAIN2 and chTOG in a particular cell type, such as HeLa cells, by alternative methods would be needed for informing further reconstitution efforts.

It is of course possible that the differences in the effects of EBs, SLAIN2 and chTOG on microtubule growth in cells and in vitro are explained by the presence of additional cellular components. Although CLIP170 and CLASPs do not partition into SLAIN2 droplets, their interactions with SLAIN2 could contribute to SLAIN2 function, especially as CLASPs are potent anti-catastrophe factors (Aher et al., 2018; Lawrence et al., 2018). Another interesting candidate is TACC3, a protein the effect of which on microtubules is not clear, but which is known to bind to chTOG and colocalize together with chTOG at the outermost microtubule plus ends in cells (Gutierrez-Caballero et al., 2015). It is interesting to note that TACC3 was also shown to have a tendency for LLPS in cells and in vitro: TACC3 is essential for the formation of a liquid-like spindle domain, which participates in acentrosomal spindle assembly in mammalian oocytes (So et al., 2019). Inclusion of purified TACC3 in the in vitro reconstitution assays, with and without crowding agents, would be an important future goal. Furthermore, it is possible and even likely that we are currently overlooking some molecular players that could affect microtubule growth or +TIP behavior in cells. For example, RNA molecules are well known to play an important role in forming membraneless cell organelles by LLPS-related processes (Alberti et al., 2019; Snead and Gladfelter, 2019). RNA was shown to concentrate in granules that localized in the vicinity of microtubule plus ends in cell protrusions; these granules contained another EB-binding +TIP, APC (Mili et al., 2008), and the potential role of RNA in +TIP-mediated control of microtubule dynamics might thus deserve investigation.

To summarize, our experiments have not yet provided conclusive evidence that would allow us to either prove or reject a potential role of LLPS in the regulation of microtubule plus end dynamics by SLAIN2 and its binding partners. We expect that the tools described in this chapter will help future progress within this research area, which, based on the insights obtained so far, appears promising enough to be further pursued.

Materials and Methods

DNA constructs, cell lines and cell culture

Human GFP-SLAIN2 (van der Vaart et al., 2011), mRFP-EB3 (Grigoriev et al., 2008) and mCherry-CLIP170 (Lansbergen et al., 2006) were described previously. SLAIN2 deletion constructs, mCherry-SLAIN2, chTOG-mCherry and EB3-chTOG chimeric constructs were made by PCR-based strategies in modified pEGFP-C1 or N1 with a StrepII tag. chTOG construct (Gutierrez-Caballero et al., 2015) was a gift of S. Royle (University of Warwick, UK).

The CRISPR/Cas9 pORANGE vector (Willems et al., 2019) that was used for generating SLAIN2 HeLa knock-in cells was a kind gift from J. Willems and H. MacGillavry (Utrecht University, the Netherlands). Guide RNA for human SLAIN2 (5'- CTCCTGGTCCGCGTTCACGT -3') was designed using the CRISPR design webpage tool (http://crispor.tefor.net/crispor.py) and inserted into pORANGE. The sequence encoding HaloTag (a gift from N. Bovenschen, University Medical Center Utrecht, the Netherlands) was inserted into the same vector at the Hind III and Xhol I restriction sites using Gibson Assembly.

HeLa (Kyoto) and human embryonic kidney 239T (HEK293T) cell lines were cultured in medium that consisted of 45% DMEM, 45% Ham's F10, and 10% fetal calf serum supplemented with penicillin and streptomycin (Akhmanova et al., 2001). HeLa cells with a triple knockout of EB1, EB2 and EB3 (EB1/2/3 KO) are described in Chapter 3. The cell lines were routinely checked for mycoplasma contamination using LT07-518 Mycoalert assay (Lonza). FuGENE 6 (Promega) was used to transfect HeLa cells with plasmids for CRISPR/Cas9 knock-in, immunofluorescence staining and live cell imaging; polyethylenimine (PEI, Polysciences) was used to transfect HEK293T cells for protein purification. 1,6-hexanediol (Sigma) was prepared as a 10× stock in medium and used at a final concentration of 3.5%.

Generation of SLAIN2 knock-in cell lines

SLAIN2 knock-in cells were generated using CRISPR/Cas9 pORANGE vector (Willems et al., 2019), according to the protocol described by (Ran et al., 2013). In brief, control and EB1/2/3 knockout HeLa cells were transfected with the vector bearing the appropriate targeting sequences and the HaloTag sequence using Fugene 6. One day after transfection, cells were subjected to selection with 2 µg/ml puromycin for 2 days. After selection, cells were allowed to recover in normal medium for 2 days, and knock-in efficiency was determined by immunofluorescence staining. Cells were subsequently sorted by flow cytometry. 61 and 58 individual clones were isolated in control and EB 1/2/3 knockout HeLa cells, respectively, and 4 control and 3 EB1/2/3 knockout HeLa cell lines were characterized by Western blotting and immunostaining.

Antibodies and immunofluorescence cell staining

We used rabbit antibodies against SLAIN1/2 (van der Vaart et al., 2011), chTOG (a gift from L. Cassimeris, Lehigh University, Bethelehem, PA; (Charrasse et al., 1998)), EB3 (Stepanova et al., 2003), CLIP170 and CLASP1/2 (Akhmanova et al., 2001), and rat monoclonal antibodies against α-tubulin YL1/2 (Pierce, MA1-80017). The following secondary antibodies were used: IRDye 800CW/ 680LT goat anti-rabbit, and anti-mouse (Li-Cor Biosciences); Alexa-594 conjugated goat antibodies against rabbit and rat IgG (Molecular Probes).

Cultured cells were fixed in –20 °C methanol for 10 min followed by 4% paraformaldehyde for 10 min in the case of EB1, CLIP170 and SLAIN2. For HaloTag staining, 0.01 µM HaloTag TMRDirect ligand (Promega) was added to cell culture medium and incubated overnight. In the case of α-tubulin and CLASP1/2 staining, cells were fixed with –20 °C methanol for 10 min. Cells were then permeabilized with 0.1% Triton X-100 in phosphate buffered saline (PBS) for 10

min; subsequent washing and labelling steps were carried out in PBS supplemented with 2% bovine serum albumin and 0.05% Tween-20. At the end, slides were rinsed in 70% and 100% ethanol, air-dried and mounted in Vectashield mounting medium (Vector laboratories).

Protein expression and purification for in vitro assays

Human mCherry-SLAIN2, GFP-SLAIN2, chTOG-GFP, chTOG-mCherry and EB-chTOG chimeras were prepared as described previously (Aher et al., 2018). Briefly, both proteins were expressed in HEK293T cells using a modified pTT5 expression vector (Addgene no. 44006). Cells were collected from one 15-cm dish after 48 h transfection and lysed in 500 µl lysis buffer (50 mM HEPES, 300 mM NaCl and 0.5% Triton X-100, pH 7.4) supplemented with protease inhibitors (Roche) on ice for 15 minutes. The supernatant obtained from the cell lysate after centrifugation was incubated with 40 µl of StrepTactin beads (GE Healthcare) for 45 min. After incubation, the beads were washed five times with high salt wash buffer (50 mM HEPES, 1.5 M NaCl and 0.01% Triton X-100). The proteins were eluted with 40 µl of elution buffer (50 mM HEPES, 150 mM NaCl, 1 mM $MgCl_2$, 1 mM EGTA, 1 mM dithiothreitol (DTT), 2.5 mM d-Desthiobiotin and 0.05% Triton X-100, pH 7.4). Purified proteins were snap-frozen and stored at 80 °C. GFP-EB3 (Montenegro Gouveia et al., 2010) was a gift of Dr. M. Steinmetz (Paul Scherrer Institute, Switzerland).

In vitro assays

In vitro assays without crowding agents were performed as described previously (Aher et al., 2018) Microtubules were grown from GMPCPP stabilized microtubule seeds in reaction mixtures containing 15 µM porcine brain tubulin that is some cases was supplemented with 3% rhodamine-tubulin, 75 mM KCl, 1 mM guanosine triphosphate, 0.1% methylcellulose, 0.2 mg/ml κ-casein and oxygen scavenger mixture (50 mM glucose, 400 µg/ ml glucose oxidase, 200 µg/ml catalase, and 4 mM DTT in MRB80 buffer) and indicated proteins. The flow chamber was sealed with vacuum grease, and dynamic microtubules were imaged immediately at 30 °C with a TIRF microscope. All tubulin products were from Cytoskeleton.

For in vitro assays with crowding agents, polyethylene glycol (PEG) 4000 (Invitrogen), Dextran 500 (Sigma) and PEG 35.000 (Sigma) were used as crowding agents. 5% PEG 4000 was used for the later experiments with or without porcine tubulin. Tubulin concentration was reduced to 5 µM in the presence of PEG 4000.

Image acquisition

Images of fixed cells were collected with a Nikon Eclipse Ni upright fluorescence microscope and a Nikon DS-Qi2 CMOS camera (Nikon), using a Plan Apo Lambda 100x N.A. 1.45 oil objective (Nikon) and Nikon NIS (Br) software (Nikon). Nikon Intensilight C-HGFI has been used as a light source. Images of live cells were collected with spinning disk microscopy, which was performed on an inverted research microscope Nikon Eclipse Ti-E (Nikon) with the perfect focus system (PFS) (Nikon), equipped with Nikon Apo TIRF 100x N.A. 1.49 oil objective (Nikon), Yokogawa CSU-X1-A1 confocal head (Yokogawa) with 405-491-561 triple band mirror and GFP, mCherry and GFP/mCherry emission filters (Chroma), ASI motorized stage MS-2000-XYZ with Piezo Top Plate (ASI), a Photometrics Evolve 512 EMCCD camera (Photometrics) and controlled by the MetaMorph 7.7 software (Molecular Devices). The microscope was equipped with a custom-ordered illuminator (Nikon, MEY10021) modified by Roper Scientific France/PICT-IBiSA, Institut Curie and Cobolt Calypso 491 nm (100 mW) and Cobolt Jive 561 nm (100 mW) lasers (Cobolt). For analysis of SLAIN2 droplets dynamics, HeLa EB1/2/3 knockout cell line was transfected

with GFP-SLAIN2 for 24 h, and live images were collected at 5 s per frame. For FRAP analysis, live cell images were collected 1 s per frame.
In vitro reconstitution assays were imaged using Total Internal Reflection Fluorescence (TIRF) microscopy using an inverted research microscope Nikon Eclipse Ti-E (Nikon) with the perfect focus system (Nikon), equipped with Nikon Apo TIRF 100x N.A. 1.49 oil objective (Nikon) and iLas^2 system (Dual Laser illuminator for azimuthal spinning TIRF (or Hilo) illumination and Simultaneous Targeted Laser Action) from Roper Scientific (Evry, FRANCE) with a custom modification for targeted Photoablation using a 532 nm pulsed laser. System was also equipped with ASI motorized stage MS-2000-XY (ASI), Photometrics Evolve Delta 512 EMCCD camera (Photometrics) and controlled by the MetaMorph 7.8 software (Molecular Devices). Stradus 488 nm (150 mW, Vortran) and OBIS 561 nm (100 mW, Coherent) lasers were used as the light sources. Images were projected onto the CCD chip at a magnification of 0.065 µm/pixel. To keep the samples at 37°C for live cell imaging and 30°C for in vitro assays, we used a stage top incubator model INUBG2E-ZILCS (Tokai Hit).

Image preparation and analysis
Images were prepared for publication using MetaMorph and ImageJ. All images were modified by adjustments of levels and contrast. ImageJ was used for quantification of the immunofluorescence signals. Analysis of recovery half time (t1/2) and mobile fraction was performed by using ImageJ and Prism GraphPad. In brief, SLAIN2 droplets were photobleached and mean fluorescence was measured and exported to Prism GraphPad, and t1/2 and mobile fraction was analyzed by a nonlinear fit. ImageJ plugin KymoResliceWide v.0.4 (https://github.com/ekatrukha/KymoResliceWide (Katrukha, 2015)) was used for generating kymographs illustrating microtubule life histories.

Acknowledgements
We thank S. Royle for the gift of chTOG construct, J.Willems and H. MacGillavry for the gift of pORANGE vector and Dr. M. Steinmetz for the gift of GFP-EB3, and N. Bovenschen for the HaloTag vector. This work was supported by the European Research Council Synergy grant 609822 to A.A.

References

Aher, A. 2017. Tipping microtubule polymerization: Insights from in vitro reconstitution. PhD thesis.

Aher, A., M. Kok, A. Sharma, A. Rai, N. Olieric, R. Rodriguez-Garcia, E.A. Katrukha, T. Weinert, V. Olieric, L.C. Kapitein, M.O. Steinmetz, M. Dogterom, and A. Akhmanova. 2018. CLASP Suppresses Microtubule Catastrophes through a Single TOG Domain. *Dev Cell*. 46:40-58.

Akhmanova, A., C.C. Hoogenraad, K. Drabek, T. Stepanova, B. Dortland, T. Verkerk, W. Vermeulen, B.M. Burgering, C.I. De Zeeuw, F. Grosveld, and N. Galjart. 2001. Clasps are CLIP-115 and -170 associating proteins involved in the regional regulation of microtubule dynamics in motile fibroblasts. *Cell*. 104:923-935.

Akhmanova, A., and M.O. Steinmetz. 2008. Tracking the ends: a dynamic protein network controls the fate of microtubule tips. *Nat Rev Mol Cell Biol*. 9:309-322.

Akhmanova, A., and M.O. Steinmetz. 2015. Control of microtubule organization and dynamics: two ends in the limelight. *Nat Rev Mol Cell Biol*. 16:711-726.

Al-Bassam, J., and F. Chang. 2011. Regulation of microtubule dynamics by TOG-domain proteins XMAP215/Dis1 and CLASP. *Trends Cell Biol*. 21:604-614.

Al-Bassam, J., H. Kim, G. Brouhard, A. van Oijen, S.C. Harrison, and F. Chang. 2010. CLASP promotes microtubule rescue by recruiting tubulin dimers to the microtubule. *Dev Cell*. 19:245-258.

Al-Bassam, J., H. Kim, I. Flor-Parra, N. Lal, H. Velji, and F. Chang. 2012. Fission yeast Alp14 is a dose-dependent plus end-tracking microtubule polymerase. *Mol Biol Cell*. 23:2878-2890.

Alberti, S., A. Gladfelter, and T. Mittag. 2019. Considerations and Challenges in Studying Liquid-Liquid Phase Separation and Biomolecular Condensates. *Cell*. 176:419-434.

Bouchet, B.P., I. Noordstra, M. van Amersfoort, E.A. Katrukha, Y.C. Ammon, N.D. Ter Hoeve, L. Hodgson, M. Dogterom, P.W. Derksen, and A. Akhmanova. 2016. Mesenchymal Cell Invasion Requires Cooperative Regulation of Persistent Microtubule Growth by SLAIN2 and CLASP1. *Dev Cell*. 39:708-723.

Bracha, D., M.T. Walls, M.T. Wei, L. Zhu, M. Kurian, J.L. Avalos, J.E. Toettcher, and C.P. Brangwynne. 2018. Mapping Local and Global Liquid Phase Behavior in Living Cells Using Photo-Oligomerizable Seeds. *Cell*. 175:1467-1480.

Brouhard, G.J., J.H. Stear, T.L. Noetzel, J. Al-Bassam, K. Kinoshita, S.C. Harrison, J. Howard, and A.A. Hyman. 2008. XMAP215 is a processive microtubule polymerase. *Cell*. 132:79-88.

Buey, R.M., R. Mohan, K. Leslie, T. Walzthoeni, J.H. Missimer, A. Menzel, S. Bjelic, K. Bargsten, I. Grigoriev, I. Smal, E. Meijering, R. Aebersold, A. Akhmanova, and M.O. Steinmetz. 2011. Insights into EB structure and the role of its C-terminal domain in discriminating microtubule tips from lattice. *Mol Biol Cell*. 22:2912-2923.

Charrasse, S., M. Schroeder, C. Gauthier-Rouviere, F. Ango, L. Cassimeris, D.L. Gard, and C. Larroque. 1998. The TOGp protein is a new human microtubule-associated protein homologous to the Xenopus XMAP215. *J Cell Sci*. 111:1371-1383.

Desai, A., and T.J. Mitchison. 1997. Microtubule polymerization dynamics. *Annu Rev Cell Dev Biol*. 13:83-117.

Grigoriev, I., S.M. Gouveia, B. van der Vaart, J. Demmers, J.T. Smyth, S. Honnappa, D. Splinter, M.O. Steinmetz, J.W. Putney, Jr., C.C. Hoogenraad, and A. Akhmanova. 2008. STIM1 is a MT-plus-end-tracking protein involved in remodeling of the ER. *Curr Biol*. 18:177-182.

Gutierrez-Caballero, C., S.G. Burgess, R. Bayliss, and S.J. Royle. 2015. TACC3-ch-TOG track the growing tips of microtubules independently of clathrin and Aurora-A phosphorylation. *Biol Open*.

Hernandez-Vega, A., M. Braun, L. Scharrel, M. Jahnel, S. Wegmann, B.T. Hyman, S. Alberti, S. Diez, and A.A. Hyman. 2017. Local Nucleation of Microtubule Bundles through Tubulin Concentration into a Condensed Tau Phase. *Cell Rep*. 20:2304-2312.

Honnappa, S., S.M. Gouveia, A. Weisbrich, F.F. Damberger, N.S. Bhavesh, H. Jawhari, I.

Grigoriev, F.J. van Rijssel, R.M. Buey, A. Lawera, I. Jelesarov, F.K. Winkler, K. Wuthrich, A. Akhmanova, and M.O. Steinmetz. 2009. An EB1-binding motif acts as a microtubule tip localization signal. *Cell*. 138:366-376.

Hunter, A.W., M. Caplow, D.L. Coy, W.O. Hancock, S. Diez, L. Wordeman, and J. Howard. 2003. The kinesin-related protein MCAK is a microtubule depolymerase that forms an ATP-hydrolyzing complex at microtubule ends. *Mol Cell*. 11:445-457.

Itzhak, D.N., S. Tyanova, J. Cox, and G.H. Borner. 2016. Global, quantitative and dynamic mapping of protein subcellular localization. *Elife*. 5.

Komarova, Y., C.O. De Groot, I. Grigoriev, S.M. Gouveia, E.L. Munteanu, J.M. Schober, S. Honnappa, R.M. Buey, C.C. Hoogenraad, M. Dogterom, G.G. Borisy, M.O. Steinmetz, and A. Akhmanova. 2009. Mammalian end binding proteins control persistent microtubule growth. *J Cell Biol*. 184:691-706.

Kumar, A., C. Manatschal, A. Rai, I. Grigoriev, M.S. Degen, R. Jaussi, I. Kretzschmar, A.E. Prota, R. Volkmer, R.A. Kammerer, A. Akhmanova, and M.O. Steinmetz. 2017. Short Linear Sequence Motif LxxPTPh Targets Diverse Proteins to Growing Microtubule Ends. *Structure*. 25:924-932.

Lansbergen, G., I. Grigoriev, Y. Mimori-Kiyosue, T. Ohtsuka, S. Higa, I. Kitajima, J. Demmers, N. Galjart, A.B. Houtsmuller, F. Grosveld, and A. Akhmanova. 2006. CLASPs attach microtubule plus ends to the cell cortex through a complex with LL5beta. *Dev Cell*. 11:21-32.

Lawrence, E.J., G. Arpag, S.R. Norris, and M. Zanic. 2018. Human CLASP2 specifically regulates microtubule catastrophe and rescue. *Mol Biol Cell*. 29:1168-1177.

Li, W., T. Miki, T. Watanabe, M. Kakeno, I. Sugiyama, K. Kaibuchi, and G. Goshima. 2011. EB1 promotes microtubule dynamics by recruiting Sentin in Drosophila cells. *J Cell Biol*. 193:973-983.

Li, W., T. Moriwaki, T. Tani, T. Watanabe, K. Kaibuchi, and G. Goshima. 2012. Reconstitution of dynamic microtubules with Drosophila XMAP215, EB1, and Sentin. *J Cell Biol*. 199:849-862.

Liu, Q., S. Remmelzwaal, A.J.R. Heck, A. Akhmanova, and F. Liu. 2017. Facilitating identification of minimal protein binding domains by cross-linking mass spectrometry. *Sci Rep*. 7:13453.

Liu, Y., Y. Mi, T. Mueller, S. Kreibich, E.G. Williams, A. Van Drogen, C. Borel, M. Frank, P.L. Germain, I. Bludau, M. Mehnert, M. Seifert, M. Emmenlauer, I. Sorg, F. Bezrukov, F.S. Bena, H. Zhou, C. Dehio, G. Testa, J. Saez-Rodriguez, S.E. Antonarakis, W.D. Hardt, and R. Aebersold. 2019. Multi-omic measurements of heterogeneity in HeLa cells across laboratories. *Nat Biotechnol*. 37:314-322.

Maney, T., M. Wagenbach, and L. Wordeman. 2001. Molecular dissection of the microtubule depolymerizing activity of mitotic centromere-associated kinesin. *J Biol Chem*. 276:34753-34758.

Maurer, S.P., N.I. Cade, G. Bohner, N. Gustafsson, E. Boutant, and T. Surrey. 2014. EB1 accelerates two conformational transitions important for microtubule maturation and dynamics. *Curr Biol*. 24:372-384.

Maurer, S.P., F.J. Fourniol, G. Bohner, C.A. Moores, and T. Surrey. 2012. EBs recognize a nucleotide-dependent structural cap at growing microtubule ends. *Cell*. 149:371-382.

McSwiggen, D.T., M. Mir, X. Darzacq, and R. Tjian. 2019. Evaluating phase separation in live cells: diagnosis, caveats, and functional consequences. *Genes Dev*.

Mili, S., K. Moissoglu, and I.G. Macara. 2008. Genome-wide screen reveals APC-associated RNAs enriched in cell protrusions. *Nature*. 453:115-119.

Mimori-Kiyosue, Y., I. Grigoriev, G. Lansbergen, H. Sasaki, C. Matsui, F. Severin, N. Galjart, F. Grosveld, I. Vorobjev, S. Tsukita, and A. Akhmanova. 2005. CLASP1 and CLASP2 bind to EB1 and regulate microtubule plus-end dynamics at the cell cortex. *J Cell Biol*. 168:141-153.

Mohan, R., E.A. Katrukha, H. Doodhi, I. Smal, E. Meijering, L.C. Kapitein, M.O. Steinmetz, and

A. Akhmanova. 2013. End-binding proteins sensitize microtubules to the action of microtubule-targeting agents. *Proc Natl Acad Sci U S A*. 110:8900-8905.

Montenegro Gouveia, S., K. Leslie, L.C. Kapitein, R.M. Buey, I. Grigoriev, M. Wagenbach, I. Smal, E. Meijering, C.C. Hoogenraad, L. Wordeman, M.O. Steinmetz, and A. Akhmanova. 2010. In Vitro Reconstitution of the Functional Interplay between MCAK and EB3 at Microtubule Plus Ends. *Curr Biol*. 20:1717-1722.

Nakamura, S., I. Grigoriev, T. Nogi, T. Hamaji, L. Cassimeris, and Y. Mimori-Kiyosue. 2012. Dissecting the nanoscale distributions and functions of microtubule-end-binding proteins EB1 and ch-TOG in interphase HeLa cells. *PLoS One*. 7:e51442.

Ran, F.A., P.D. Hsu, J. Wright, V. Agarwala, D.A. Scott, and F. Zhang. 2013. Genome engineering using the CRISPR-Cas9 system. *Nat Protoc*. 8:2281-2308.

Ribbeck, K., and D. Gorlich. 2002. The permeability barrier of nuclear pore complexes appears to operate via hydrophobic exclusion. *EMBO J*. 21:2664-2671.

Roostalu, J., N.I. Cade, and T. Surrey. 2015. Complementary activities of TPX2 and chTOG constitute an efficient importin-regulated microtubule nucleation module. *Nat Cell Biol*. 17:1422-1434.

Schuyler, S.C., and D. Pellman. 2001. Microtubule "plus-end-tracking proteins": The end is just the beginning. *Cell*. 105:421-424.

Siahaan, V., J. Krattenmacher, A.A. Hyman, S. Diez, A. Hernandez-Vega, Z. Lansky, and M. Braun. 2019. Kinetically distinct phases of tau on microtubules regulate kinesin motors and severing enzymes. *Nat Cell Biol*. 21:1086-1092.

Snead, W.T., and A.S. Gladfelter. 2019. The Control Centers of Biomolecular Phase Separation: How Membrane Surfaces, PTMs, and Active Processes Regulate Condensation. *Mol Cell*. 76:295-305.

So, C., K.B. Seres, A.M. Steyer, E. Monnich, D. Clift, A. Pejkovska, W. Mobius, and M. Schuh. 2019. A liquid-like spindle domain promotes acentrosomal spindle assembly in mammalian oocytes. *Science*. 364.

Stepanova, T., J. Slemmer, C.C. Hoogenraad, G. Lansbergen, B. Dortland, C.I. De Zeeuw, F. Grosveld, G. van Cappellen, A. Akhmanova, and N. Galjart. 2003. Visualization of microtubule growth in cultured neurons via the use of EB3-GFP (end-binding protein 3-green fluorescent protein). *J Neurosci*. 23:2655-2664.

Tan, R., A.J. Lam, T. Tan, J. Han, D.W. Nowakowski, M. Vershinin, S. Simo, K.M. Ori-McKenney, and R.J. McKenney. 2019. Microtubules gate tau condensation to spatially regulate microtubule functions. *Nat Cell Biol*. 21:1078-1085.

Tirnauer, J.S., S. Grego, E.D. Salmon, and T.J. Mitchison. 2002. EB1-microtubule interactions in Xenopus egg extracts: role of EB1 in microtubule stabilization and mechanisms of targeting to microtubules. *Mol Biol Cell*. 13:3614-3626.

van der Vaart, B., M.A. Franker, M. Kuijpers, S. Hua, B.P. Bouchet, K. Jiang, I. Grigoriev, C.C. Hoogenraad, and A. Akhmanova. 2012. Microtubule plus-end tracking proteins SLAIN1/2 and ch-TOG promote axonal development. *J Neurosci*. 32:14722-14728.

van der Vaart, B., C. Manatschal, I. Grigoriev, V. Olieric, S.M. Gouveia, S. Bjelic, J. Demmers, I. Vorobjev, C.C. Hoogenraad, M.O. Steinmetz, and A. Akhmanova. 2011. SLAIN2 links microtubule plus end-tracking proteins and controls microtubule growth in interphase. *J Cell Biol*. 193:1083-1099.

Vernon, R.M., P.A. Chong, B. Tsang, T.H. Kim, A. Bah, P. Farber, H. Lin, and J.D. Forman-Kay. 2018. Pi-Pi contacts are an overlooked protein feature relevant to phase separation. *Elife*. 7.

Wang, J., J.M. Choi, A.S. Holehouse, H.O. Lee, X. Zhang, M. Jahnel, S. Maharana, R. Lemaitre, A. Pozniakovsky, D. Drechsel, I. Poser, R.V. Pappu, S. Alberti, and A.A. Hyman. 2018. A Molecular Grammar Governing the Driving Forces for Phase Separation of Prion-like RNA Binding Proteins. *Cell*. 174:688-699.

Wieczorek, M., S. Bechstedt, S. Chaaban, and G.J. Brouhard. 2015. Microtubule-associated proteins control the kinetics of microtubule nucleation. *Nat Cell Biol*. 17:907-916.

Willems, J., A.P.H. de Jong, N. Scheefhals, and H.D. MacGillavry. 2019. ORANGE: A CRISPR/Cas9-based genome editing toolbox for epitope tagging of endogenous proteins in neurons. *bioRxiv preprint*:700187.

Wisniewski, J.R., M.Y. Hein, J. Cox, and M. Mann. 2014. A "proteomic ruler" for protein copy number and concentration estimation without spike-in standards. *Mol Cell Proteomics*. 13:3497-3506.

Woodruff, J.B., B. Ferreira Gomes, P.O. Widlund, J. Mahamid, A. Honigmann, and A.A. Hyman. 2017. The Centrosome Is a Selective Condensate that Nucleates Microtubules by Concentrating Tubulin. *Cell*. 169:1066-1077.

Yang, C., J. Wu, C. de Heus, I. Grigoriev, N. Liv, Y. Yao, I. Smal, E. Meijering, J. Klumperman, R.Z. Qi, and A. Akhmanova. 2017. EB1 and EB3 regulate microtubule minus end organization and Golgi morphology. *J Cell Biol*. 216:3179-3198.

Zanic, M., P.O. Widlund, A.A. Hyman, and J. Howard. 2013. Synergy between XMAP215 and EB1 increases microtubule growth rates to physiological levels. *Nat Cell Biol*. 15:688-693.

Zhang, R., G.M. Alushin, A. Brown, and E. Nogales. 2015. Mechanistic Origin of Microtubule Dynamic Instability and Its Modulation by EB Proteins. *Cell*. 162:849-859.

5

Exploring mechanisms controlling microtubule catastrophe and rescue using combinations of microtubule-binding domains

Chao Yang, Ankit Rai, Ilya Grigoriev, Amol Aher, Fangrui Chen, Jacob Hepkema and Anna Akhmanova

In preparation

Cell Biology, Department of Biology, Faculty of Science, Utrecht University,

Padualaan 8, 3584 CH Utrecht, The Netherlands

Abstract

Microtubules are dynamic cytoskeletal polymers that form by head-to-tail addition of tubulin dimers. The dynamic instability of microtubules can be observed in solutions of purified tubulin, however, in cells, microtubule growth and disassembly are tightly controlled by numerous factors. Previous work has shown that artificial targeting of specific protein domains to the plus ends of microtubules can strongly alter their dynamics. Here, we set out to explore such a strategy more systematically by generating fusion proteins between different microtubule-binding domains (MBDs) and testing their effects on microtubule polymerization in vitro. In particular, we wanted to investigate how easy it is to alter catastrophe frequency by recruiting different MBDs to microtubule tips or to modulate microtubule rescues by targeting MBD combinations to microtubule shafts. We found that different TOG domains of chTOG fused to the C-terminus of the microtubule plus-end tracking part of EB3 induced catastrophes, whereas similar fusions of the TOG2 and TOG3 domains of CLASP2 suppressed catastrophes and promoted rescues. EB3 fusions of the GAR domain of spectraplakin and the CAP-Gly domain of CLIP170 could also induce rescues. However, this was not the case for the EB3 fused to the MBD of MAP7 and using MAP7 MBD as a microtubule-tethering moiety inhibited the rescue activity of CLASP2 TOG3 and CLIP170 CAP-Gly domains. We conclude that microtubule dynamics can be readily modulated by MBD combinations, but MBD activities strongly depend on the molecular context in which they interact with microtubules. We have also tested whether any of the artificial tip-tracking factors can restore normal microtubule tip behavior in EB1, EB2 and EB3 triple knockout cells, but found that this is not the case. We expect that some of the generated artificial fusions will be useful for dissecting the molecular details of the mechanisms governing microtubule polymerization dynamics.

INTRODUCTION

Microtubules are dynamic cytoskeletal polymers, and their dynamics can be reconstituted in vitro in solutions of purified tubulin. In cells, microtubule dynamics is tightly regulated by an array of dedicated factors, which display diverse and, in some cases, opposing activities. For example, microtubule polymerase XMAP215/chTOG promotes tubulin addition to microtubule ends, whereas kinesin-13 MCAK induces catastrophes and drives microtubule disassembly (Brouhard et al., 2008; Howard and Hyman, 2007; Kinoshita et al., 2001; Maney et al., 2001; Widlund et al., 2011).

Recent work from our lab has shown that useful insights into the activities of single microtubule-binding domains (MBDs) can be obtained by targeting them to microtubule plus end. This approach was used to uncover the molecular mechanisms underlying the ability of the microtubule plus-end-tracking protein CLASP2 to inhibit catastrophes and induce rescues (Aher et al., 2018). CLASP2 has three conserved TOG domains (TOG1, TOG2 and TOG3), the function of which was unknown. By fusing the individual domains of CLASP2 to the positively charged SxIP-containing polypeptide that interacts with End Binding proteins (EBs) and microtubules, it was shown that the first TOG domain (TOG1) had no effect on microtubule polymerization, while TOG2 efficiently suppressed catastrophes and TOG3 promoted rescues (Aher et al., 2018). Interestingly, a direct fusion of CLASP2 TOG2 to the EB3 N-terminus was sufficient to suppress catastrophes. Whereas these results helped to dissect the activity of CLASP2, they also raised an important question: how unique are the observed effects of CLASP2 TOG2 and TOG3? For example, TOG3 of CLASP2 can weakly interact with microtubule lattice, so would an EB3 fusion with another lattice-binding domain be sufficient to generate an autonomous microtubule rescue factor? Furthermore, as described in the preceding chapters, we have generated cells completely lacking all three EBs, and it would be interesting to know whether tip-tracking protein fusions would have the same effects on microtubule growth in cells as they do in a system with purified components.

To address these questions, we generated a series of fusion proteins containing the N-terminal part of EB3, followed by a dimerization motif and microtubule- or tubulin-binding domains from different microtubule-associated proteins (MAPs) and examined their effects on microtubule dynamics in vitro. We found that the ability to induce rescues was displayed by several very different fusions that had microtubule lattice affinity, indicating that the transition from microtubule shortening to growth can be triggered by widely different types of MBDs. Interestingly, the ability to slow down microtubule polymerization was not directly linked to the capacity to induce rescues, although both effects are related to the regulation of microtubule depolymerization. We also tested whether rescue-inducing domains have similar activities when tethered to microtubules by two different MBDs and found that this was not the case. Our data suggest that the molecular context in which a particular domain is placed can have a strong influence on the effect of this domain on microtubule dynamics. Finally, we have investigated whether the tip-binding fusions generated here could restore the erratic microtubule growth observed in cells lacking all three EBs (Chapter 3) but found that this was not the case.

RESULTS

In vitro analysis of MBD fusions

To generate a series of artificial regulators of microtubule dynamics, we used as a basis the construct EB3-NL-LZ-GFP (Komarova et al., 2009), which contains the N-terminal part of EB3 with the calponin homology (CH) domain followed by the linker region, is dimerized by the addition of the leucine zipper from GCN4 and includes a C-terminal GFP tag. This protein, as

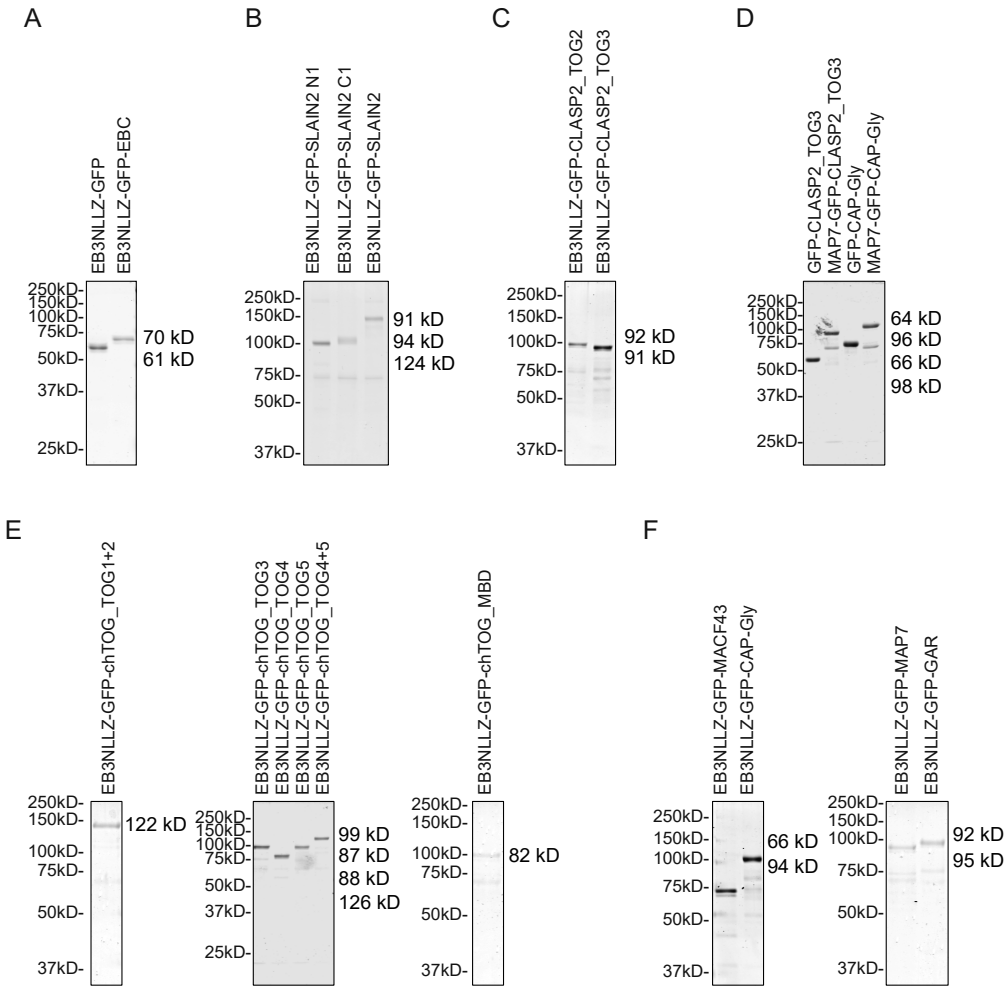

Figure 1. Protein purification of indicated constructs

(A-F) Coomassie blue stained gels with the indicated proteins purified from HEK293 cells.

5

well as the other fusion proteins described in this chapter, was purified from HEK293 cells using a StrepII tag and StrepTactin beads and was subjected to washes with a buffer containing 1.5 M NaCl to improve protein purity (Figure 1A). We tested the effect of this protein, as well as all other proteins described in this chapter, at the concentration of 25 nM using in vitro assays, in which microtubules are grown from GMPCPP-stabilized seeds and observed by Total Internal Reflection Fluorescence (TIRF) microscopy (Aher et al., 2018; Bieling et al., 2007). Since previous work in the lab has shown that the addition of almost any factor can cause mild alterations in microtubule polymerization and depolymerization, here we only focused on strong changes in microtubule dynamics.

Microtubule dynamics observed in the presence of EB3-NL-LZ-GFP was quite similar to that found in the presence of the full length EB3 purified from bacteria (Figure 1, Figure 2A, B, C): the slope of the kymographs as well as the number of catastrophes observed within a 10 min movie were similar. As a control, we fused to the C-terminus of EB3-NL-LZ-GFP the C-terminal part of EB3 (EBC), which is known to bind to numerous EB partners but not to microtubules. We

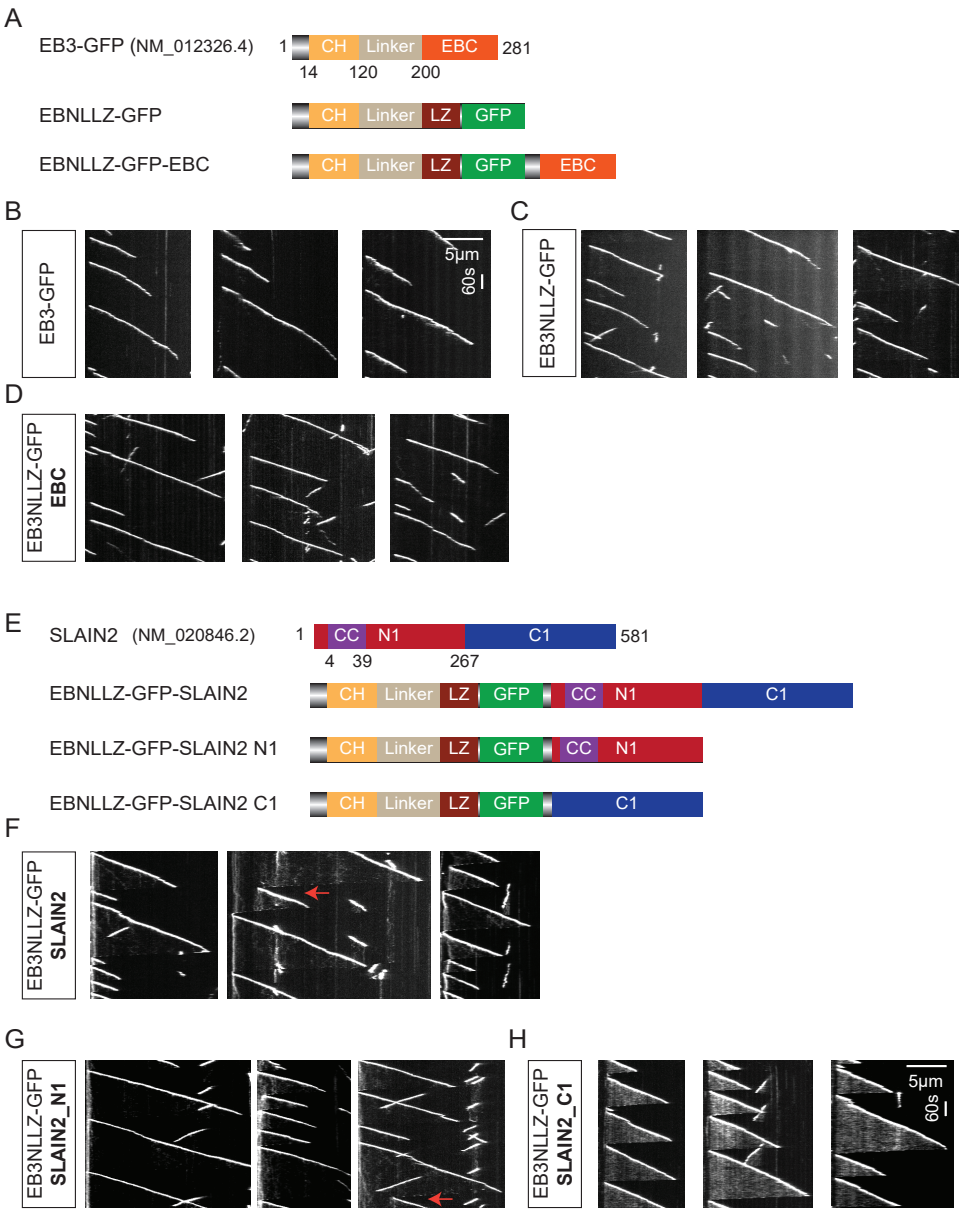

Figure 2. Microtubule dynamics in vitro in the presence of EB3 constructs and EB3-SLAIN2 fusions

(A) Schemes of the EB3 protein constructs.

(B-D) Kymographs illustrating microtubule plus end growth in vitro in the presence of EB3 protein contructs depicted in (A). Only the plus end part of the microtubule is shown.

(E) Schemes of the SLAIN2 and EB3-NL-LZ-GFP-SLAIN2 chimeric proteins.

(B-D) Kymographs illustrating microtubule plus end growth in the presence of EB3-SLAIN2 chimeric proteins depicted in (E).

found that the addition of this domain had no major effect on microtubule dynamics (Figure 1A, Figure 2A-D). We note that hardly any rescues were observed with any of these proteins,

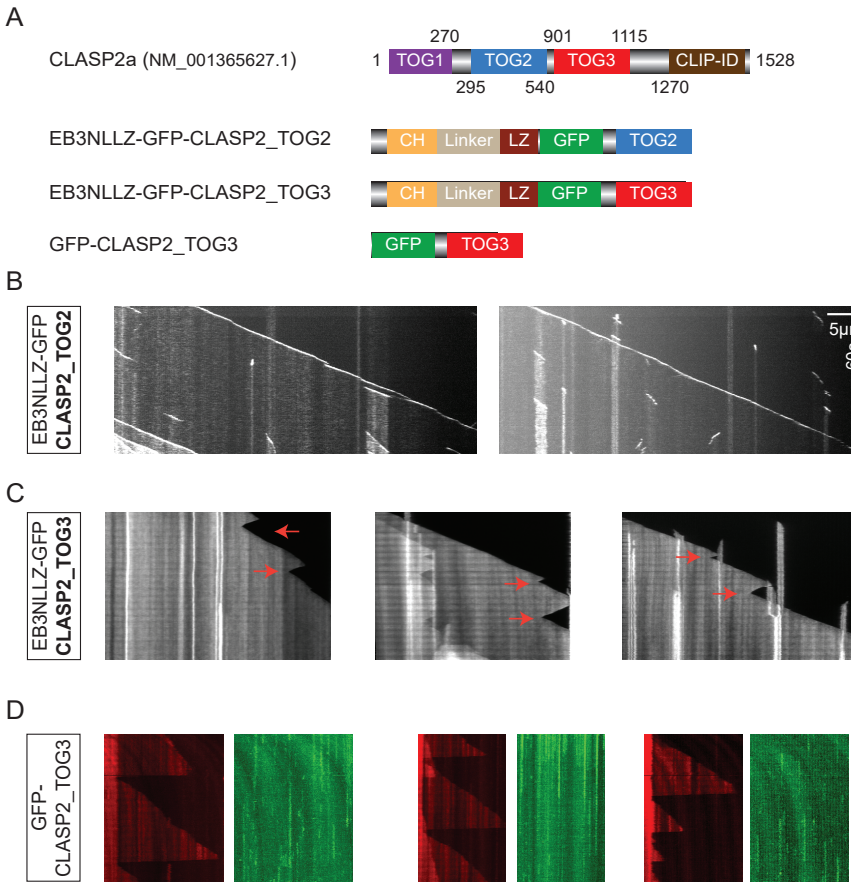

Figure 3. Microtubule dynamics in vitro in the presence of CLASP2-derived fusion proteins

(A) Schemes of the CLASP2α and different CLASP2-derived fusion proteins.

(B-D) Kymographs illustrating microtubule plus end growth in vitro in the presence of the fusion proteins depicted in (A). Only the plus end part of the microtubule is shown.

5

as described for EB3 previously (Aher et al., 2018; Komarova et al., 2009; Mohan et al., 2013), indicating that EB3 displays no autonomous rescue activity.

As an additional control, we used a fusion of EB3-NL-LZ to the full-length SLAIN2 or its N- and C-terminal parts (Figure 1B, Figure 2E-G). SLAIN2 consists of short dimeric coiled coil followed by a long intrinsically disordered region and displays no strong affinity for microtubules (Chapter 4). In line with these data, EB3-NL-LZ-GFP-SLAIN2 fusions behaved similarly to EB3-NL-LZ-GFP alone.

We next set out to probe the effects exerted on microtubule growth by tip-targeted TOG domains of CLASP2. As indicated above, a monomeric version of CLASP2_TOG2-EB3-NL could autonomously suppress catastrophes when included in the assays at 100 nM, though not at lower concentrations (Aher et al., 2018). Here, we tested the dimeric version of this fusion with a C-terminally positioned TOG2 domain (EB3-NL-LZ- GFP-CLASP2_TOG2) (Figure 1C, Figure 3A), and found that it fully blocked catastrophes already at 25 nM (Figure 3B). The higher potency of this chimeric construct compared to TOG2-EB3-NL was likely due to the fact that EB3 dimer has a higher affinity to microtubules compared to EB3 monomer (Komarova et al., 2009; Sen et al., 2013). These data indicate that the catastrophe-suppressing activity of TOG2

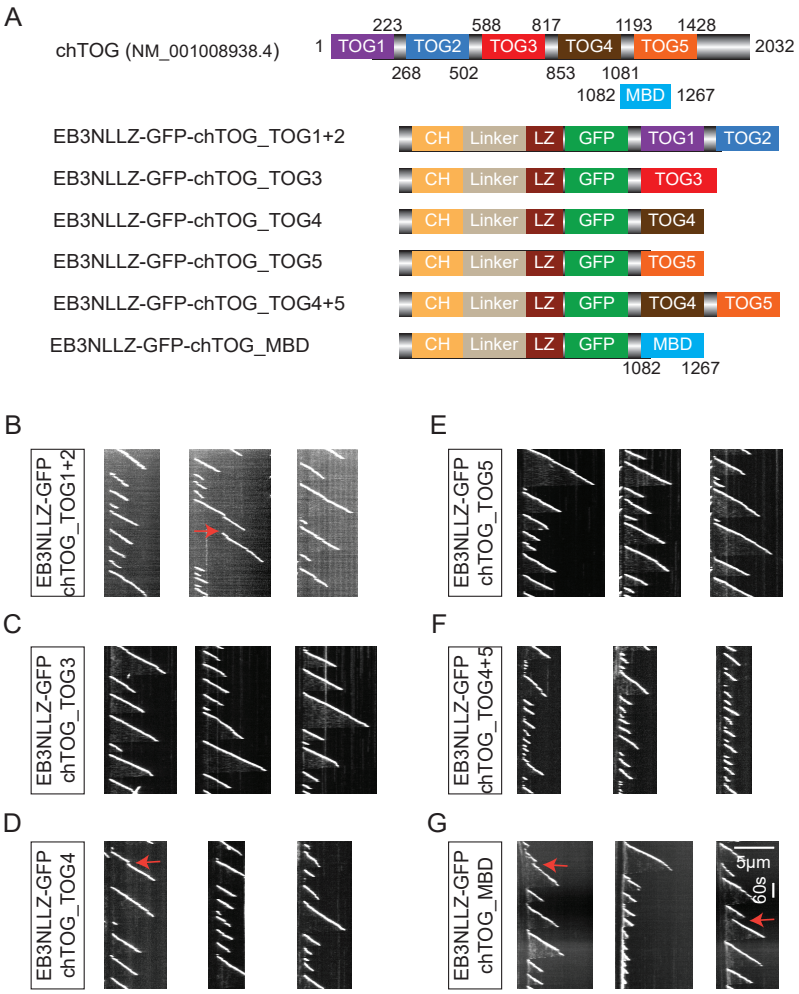

Figure 4. Microtubule dynamics in vitro in the presence of chTOG-derived fusion proteins

(A) Schemes of the chTOG and different chTOG -derived fusion proteins. For chTOG MTBD used (blue), the amino acid region used does not coincide with the domain boundaries and is indicated in the corresponding scheme.

(B-G) Kymographs illustrating microtubule plus end growth in vitro in the presence of the fusion proteins depicted in (A). Only the plus end part of the microtubule is shown.

is not sensitive to its position within the fusion protein. This is not surprising, because TOG2 is located at the N-terminus of some CLASP2 splice isoforms, such as CLASP2β and CLASP2γ, but is in the middle of another splice variant, CLASP2α (Akhmanova et al., 2001).

We also generated an EB3-NL-LZ-GFP fusion of the CLASP2 TOG3 domain and found that, in contrast to all fusion proteins described above, EB3-NL-LZ-GFP-CLASP2_TOG3 did not preferentially track growing microtubule plus ends but decorated the whole microtubule lattice (Figure 1C, Figure 3A, C). This is in line with the previous observation that, unlike CLASP2_TOG2, CLASP2_TOG3 has some affinity for microtubule lattices in microtubule-pelleting assays (Aher et al., 2018). EB3-NL-LZ-CLASP2_TOG3 visibly reduced microtubule depolymerization rate and induced rescues (Figure 3C). Importantly, by itself, 25 nM GFP-CLASP2_TOG3 of CLASP2 showed no strong microtubule decoration or rescue induction in our assays (Figure

1D, Figure 3D). The affinity of this domain alone for microtubules is thus insufficient to have an autonomous effect on microtubule growth in the conditions of our in vitro experiments. To induce an effect, it must be tethered to microtubules by positively charged polypeptide (Aher et al., 2018) or by the N-terminal part of EB3 (Figure 3C).

To test the specificity of the effects induced by EB3-NL-LZ fusions of the TOG2 and TOG3 domains of CLASP2, we next generated similar fusions with the various parts of another TOG-domain containing protein, chTOG. As described in Chapter 4, a combination of chTOG and EB3 strongly accelerated microtubule growth and induced catastrophes, while the direct fusion of chTOG to the N-terminus of EB3 increased microtubule growth rate, reduced catastrophe frequency and induced rescues. Importantly, the fusion of chTOG and EB3 was sensitive to the position of chTOG within the protein – it could only increase microtubule growth rate when chTOG was positioned at the N-terminus, whereas EB3-NL-LZ-GFP-chTOG, with chTOG placed at the C-terminus of the fusion, had little effect on microtubule growth rate but increased catastrophe frequency (Chapter 4).

Here, we fused individual chTOG TOG domains or their combinations to the C-terminus of EB3-NL-LZ-GFP (Figure 1E, Figure 4A). The ability of all these TOG domains to bind to tubulin was previously shown to make some contribution to the polymerase activity of XMAP215 (Widlund et al., 2011). We therefore reasoned that such fusions would allow us to test whether tethering to microtubules of a domain that can bind to free tubulin can induce rescues. In line with the results obtained with the full length EB3-NL-LZ-GFP-chTOG fusion, all these constructs had no strong effect on microtubule polymerization rate but increased catastrophe frequency (Figure 4B-F). Since the TOG1-TOG2 tandem of XMAP215 is by itself sufficient to increase microtubule polymerization rate in vitro (Widlund et al., 2011), these data provide further support for the notion that TOG1-TOG2 domains of chTOG must be present at the N-terminus of the protein to promote tubulin incorporation at microtubule tips. The effects exerted on catastrophes by chTOG TOG4 and TOG5, which were tested individually and as a tandem, appeared to be additive – the EB3-NL-LZ-GFP-chTOG_TOG4-TOG5 fusion caused stronger inhibition of microtubule growth processivity than the separate fusions of TOG4 and TOG5 (Figure 4D-F). We have also tested a fusion construct containing the proposed microtubule binding domain of chTOG (MTBD), located between TOG4 and TOG5 (Figure 4A). Surprisingly, this construct showed no enhanced microtubule lattice binding and increased catastrophe frequency (Figure 4A,G). We also observed occasional rescues, although these were difficult to detect because all these fusion proteins strongly promoted catastrophes and significantly limited the length of microtubule depolymerization episodes and thus the time when rescues can be detected. It should be noted that all EB3-NL-LZ-GFP fusions to chTOG domains robustly tracked growing microtubule plus ends and showed only low accumulation along the microtubule lattice. These data suggest that individual TOG domains of chTOG have no clear microtubule lattice affinity, at least not in the context of an EB fusion. In case of TOG5, this is somewhat surprising, because TOG5 on the fly homolog of chTOG, mini spindles (Msps) was shown to engage with microtubule lattice-incorporated tubulin (Byrnes and Slep, 2017). Importantly, since rescues occur at depolymerizing microtubule ends, they are dependent on protein targeting to microtubule shafts, and it is possible that the rescue activity of the TOG domains of chTOG would be stronger if they were tethered to microtubule lattice and not just to the tip.

The data described above indicate that the TOG3 domain of CLASP2 is functionally distinct from the other TOG domains tested here, because of its ability to interact with microtubule lattice and potently promote rescues. We next set out to investigate whether other microtubule lattice-binding domains could induce rescues in the same fusion context. Four different types of molecules were analyzed – the positively charged intrinsically disordered C-terminal region

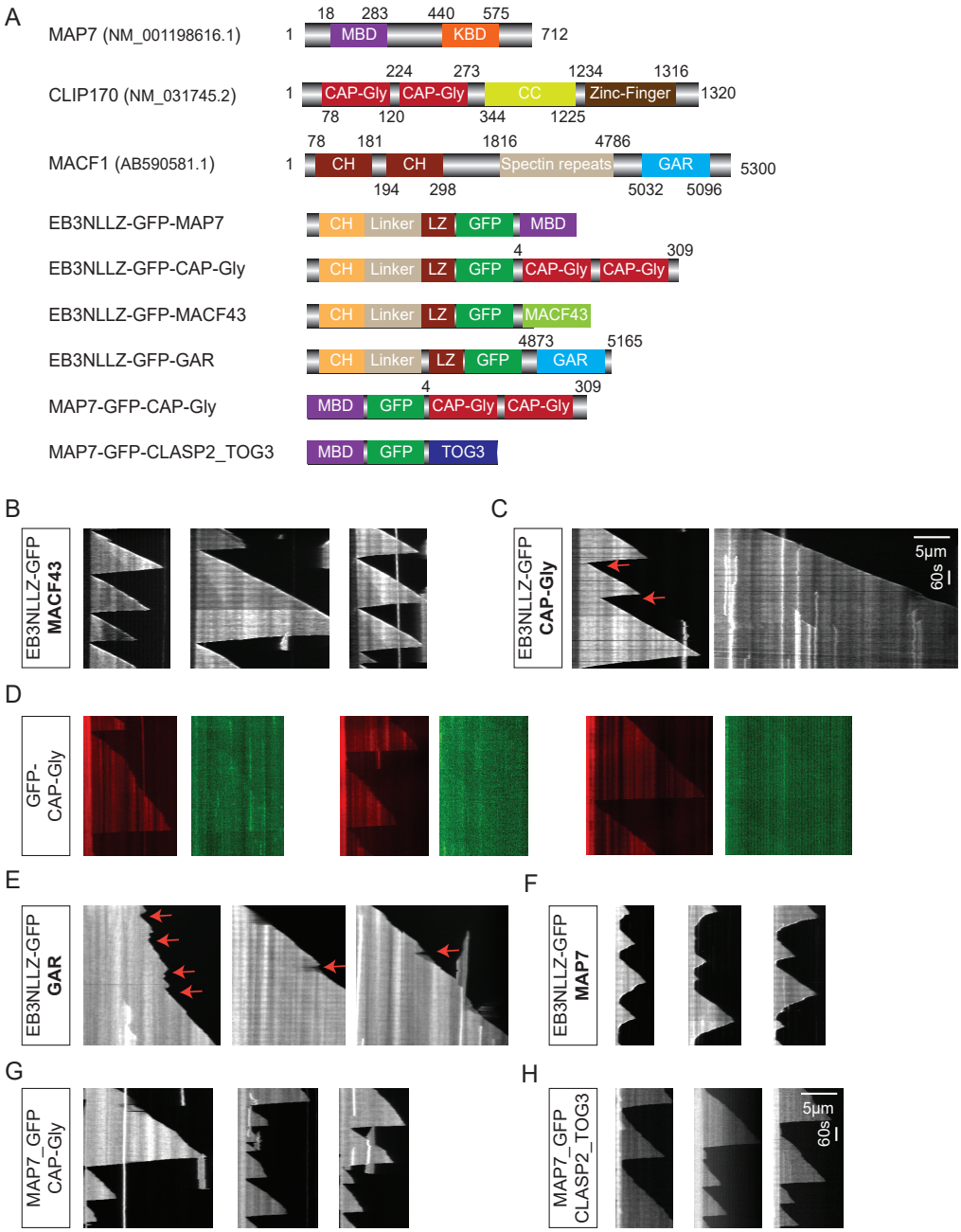

Figure 5. Microtubule dynamics in vitro in the presence of fusions between different MBDs

(A) Schemes of MAP7, CLIP170 and MACF1 and chimeric proteins derived from their domains. The amino acid regions used in different fusions are indicated if they do not coincide with the domain boundaries indicated in the protein schemes.

(B-H) Kymographs illustrating microtubule plus end growth in vitro in the presence of the fusion proteins depicted in (A). Only the plus end part of the microtubule is shown.

of MACF2 (termed MACF43), the globular microtubule- and tubulin-binding CAP-Gly domains of CLIP-170, the MBD of MAP7 that is predicted to be helical, and the globular microtubule binding GAR domain derived from the spectraplakin MACF1 (Figure 1F, Figure 5A).
As expected, all four domains, when fused to EB3-NL-LZ-GFP, displayed prominent microtubule lattice association. Interestingly, their effects on microtubule dynamics were different. EB3-NL-LZ-MACF43 fusion seemed to mildly suppress catastrophes but induced no rescues and did not inhibit microtubule depolymerization (Figure 5B), indicating that simply increasing the affinity of EB3-NL-LZ to microtubule shafts is insufficient to promote rescues. EB3-NL-LZ-CAP-Gly fusion also caused some increase in growth processivity and induced rescues, without significantly slowing down microtubule depolymerization rate (Figure 5C). It should be noted that similar to CLASP2 TOG3, the CAP-Gly domain-containing fragment of CLIP170 used here showed weak microtubule binding affinity on its own (Figure 1D, Figure 5D).
EB3-NL-LZ-GAR fusion strongly increased microtubule rescue frequency – the depolymerization episodes became very short, catastrophes were suppressed and microtubule depolymerization rate was reduced (Figure 5E). The reduction of microtubule growth rate was also apparent with the EB3-NL-LZ-GFP-MAP7 fusion – this protein strongly bound along microtubules, accumulated at depolymerizing microtubule ends and strongly slowed down their disassembly (Figure 5F). We also sometimes observed rescues with EB3-NL-LZ-GFP-MAP7, but these corresponded to events of strong accumulation of the fusion protein at depolymerizing ends (arrows in Figure 5F). Among the proteins tested, the fusions of EB3-NL-LZ to CLASP2_TOG3, GAR and MAP7 domains were the only ones that inhibited microtubule depolymerization, but only two of them were potent rescue factors, indicating that ability to slow down microtubule depolymerization does not directly correlate with the capacity to induce rescues.
Finally, we wanted to investigate whether rescue-promoting domains retain their activity when tethered to the microtubules with a protein other than EB3-NL-LZ. We therefore generated MAP7-GFP-CAP-Gly and MAP7-GFP-CLASP2_TOG3 fusions (Figure 1D, Figure 5A). To our surprise, although both fusions nicely decorated microtubules, they did not increase rescue frequency and had no strong effect on microtubule depolymerization. This result cannot be simply due to the fact that these constructs are monomers in contrast to the EB3-NL-LZ-GFP-fusions that are dimeric, because the monomeric microtubule-tethered TOG3-SxIP fusion did show frequent rescues (Aher et al., 2018). The molecular context in which a particular domain acts can thus have significant consequences for its activity.

Analysis of the effects of MBD fusions in cells
One of our motivations to generate microtubule tip-tracking proteins with different properties was to test their effects in cells lacking the three EBs (EB1/2/3 knockout cells) in order to compare the impact of the same microtubule regulator on microtubule growth in cells and in an in vitro system with purified components. In Chapter 3, we showed that EB3-NL-LZ-GFP fusion did not perturb microtubule growth in control cells but, unlike full length EB1 and EB3, could not rescue microtubule tip dynamics in EB1/2/3 knockout cells, because the growth episodes observed with this fusion were highly irregular, with frequent back-and-forth movements. Here, we tested whether normal microtubule polymerization dynamics could be rescued by different tip-tracking fusions of EB3-NL-LZ. Proteins showing microtubule lattice decoration were not included in this analysis, because we found that they also decorated microtubule shafts in cells, making the analysis of their behavior quite challenging due to the rather dense microtubule system in HeLa cells.
In agreement with the data shown in Chapter 3, highly irregular growth episodes were observed with EB3-NL-LZ-GFP, whereas the EB3-NL-LZ-GFP-EBC fusion containing the complete

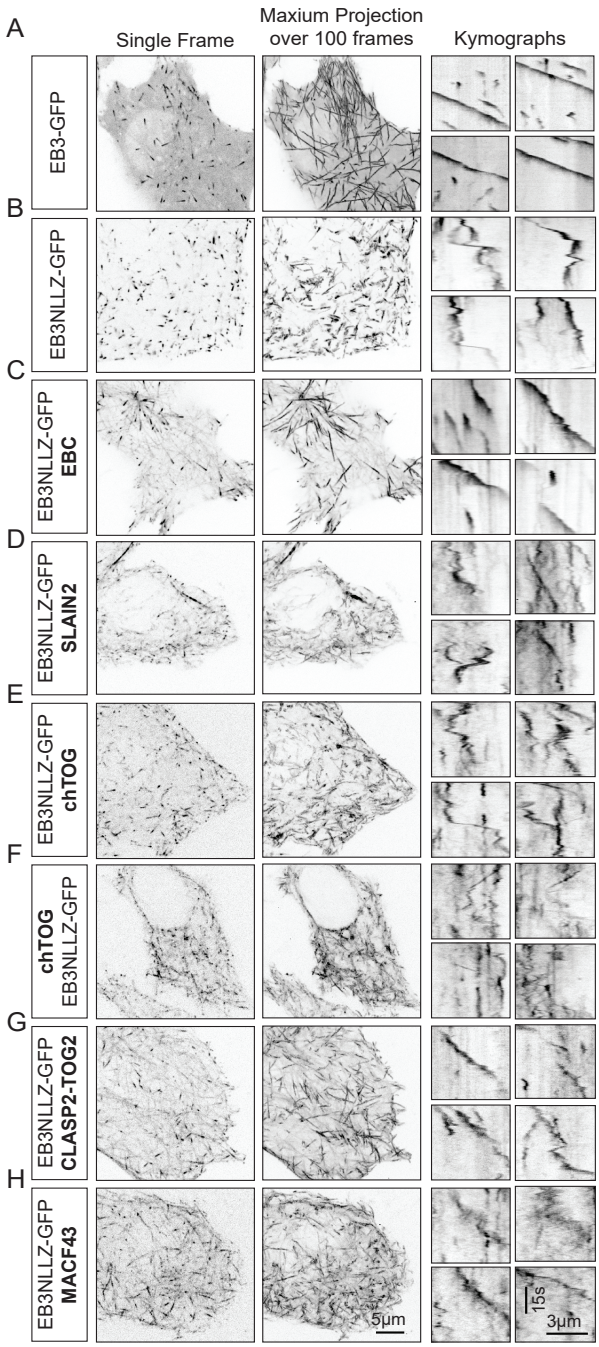

Figure 6. Microtubule plus end dynamics in EB1/2/3 knockout cells expressing different fusions of EB3 to CLASP2, SLAIN2 or chTOG.

(A-H) EB1/2/3 knockout cells HeLa cells were transfected with the indicated EB3 fusions and imaged using spinning disk microscopy. Sigle frames (left), maximum intensity projections of 100 frames (middle) and representative kymographs depicting the behavior of individual microtubule plus ends are shown.

EB3 C-terminus showed normal behavior, which was similar to that of full length EB3-GFP (Figure 6A-C). In contrast, none of the other tested chimeric proteins, which included EB3-NL-LZ-GFP fused to SLAIN2, chTOG, CLASP2_TOG2 or MACF43 peptide could restore the normal, smooth and continuous advancement of microtubule tips (Figure 6D-H). Because of the complex dynamics of microtubule plus ends, the definition of parameters of microtubule dynamics became challenging, and in many cases, microtubule tip movements were difficult to distinguish from growth and depolymerization episodes. Therefore, as already mentioned in Chapter 3, additional efforts would be needed to analyze and understand the complex microtubule tip dynamics observed in these conditions.

DISCUSSION

In this chapter, we set out to examine how well the activities of individual MBDs can be dissected by fusing them to microtubule tip- or lattice tethering domains. Previous experiments exploiting such a strategy have been encouraging – it was possible to identify the catastrophe-suppressing and rescue-promoting domains of CLASPs (Aher et al., 2018). Here, using dimeric EB3-NL-LZ fusions we could confirm previous observations showing that CLASP2_TOG2 domain has a potent catastrophe-suppressing activity, whereas CLASP2_TOG3 domain can induce rescues. We also found that when we added to the C-terminus of EB3-NL-LZ some domains that were not expected to bind to microtubules, such as the C-terminal part of EB3 or SLAIN2, no strong alteration of microtubule dynamics was observed. An obvious caveat of our analysis so far is that we focused only on strong effects, which are visible by visual inspection of kymographs, while milder effects could certainly escape our attention and would require quantification.

We then went on and tested an array of different fusion proteins for their capacity to alter microtubule dynamics and found that some of them could potentiate rescues. Importantly, we observed rescues with EB3-NL-LZ-GFP-CAP-Gly fusion, although previous work in our lab showed that CLIP170, despite of being a well-known microtubule rescue factor in cells (Komarova et al., 2002a), does not induce rescues in vitro either alone or in combination with EB3 (Aher, 2017). In Chapter 4, we also showed that whereas a combination of EB3 and chTOG does not induce rescues, the chTOG-EB3-NL-LZ-GFP fusion does. These results can be interpreted in two ways: one could argue that the results obtained with the fusions are artifacts that do not reflect the activities of endogenous proteins. Alternatively, one could argue that the observations with the fusions reflect the activities that could potentially be observed with +TIP oligomers or clusters, in which several different domains are brought together. For example, when CLIP170 and EB3 are combined as separate proteins, the CAP-Gly domains of CLIP170 most likely interact with the tails of EB3 and thus cannot bind to the tails of α-tubulin (Chen et al., 2019; Weisbrich et al., 2007). In contrast, in the EB3-NL-LZ-GFP-CAP-Gly fusion, CAP-Gly domain can interact with tubulin tails, and this likely explains the relatively high microtubule lattice affinity of this fusion protein. Interestingly, in vitro work of Aher et al. showed CLIP170 does potentiate rescues induced by CLASPs in vitro (Aher, 2017). The interaction between CLIPs and CLASPs does not involve CAP-Gly domains (Akhmanova et al., 2001), leaving these domains free to interact with tubulin, potentially explaining how could CLIP170 could contribute to rescue when complexed with CLASPs.

We also observed frequent rescues induced by the EB3-NL-LZ-GFP-GAR fusion. The GAR domain is part of the very large microtubule-actin cross-linking factor, spectraplakin, and the ability to induce microtubule rescues could, in principle, fit with its role in actin-mediated microtubule regulation (Kodama et al., 2003; Wu et al., 2008).

Altogether, it turned out that it is relatively easy to generate an artificial rescue factor by making MBD fusions. What do our results tell us about the mechanisms of rescue? First, our data suggest that clustering of certain types of MAPs could in principle readily promote rescues.

The current literature is strongly focused on the mechanisms of rescue induction caused by microtubule damage, repair and incorporation into microtubule GDP-bound lattices of GTP-bound tubulin dimers that can generate GTP-islands inhibit microtubule depolymerization (Aumeier et al., 2016; de Forges et al., 2016; Dimitrov et al., 2008; Schaedel et al., 2019; Vemu et al., 2018). While such processes are certainly possible, it seems that, given the abundance of different MAPs, rescue induction by MAP clusters in the absence of microtubule repair deserves further attention.

The actual mechanism of microtubule rescues by MAPs remains unclear. Previous work in the lab has shown that one or two CLASP2α molecules can be sufficient to induce rescues (Aher et al., 2018). It should be noted that CLASP2α includes two potent rescue-inducing TOG domains, TOG2 and TOG3, as well as positively-charged microtubule-binding regions, so the underlying mechanism can still be quite complex. TOG3 domain alone, when tethered to microtubule lattices through EB3 or a positively charged polypeptide, is sufficient to induce rescues (Figure 3C) (Aher et al., 2018). Interestingly, both fusions slow down microtubule depolymerization, and the same is true for the EB3-NL-LZ-GFP-GAR fusion. However, there is no simple relationship between the reduction of the microtubule disassembly rate and rescue induction. First, EB3-NL-LZ-GF-MAP7 fusion strongly reduces microtubule shortening rate, yet it only induces rescues when it forms large clusters at depolymerizing microtubule plus ends (Figure 5F). Second, although full-length CLASP2α is a potent microtubule rescue factor, it accelerates rather than slows down microtubule shortening (Aher et al., 2018; Lawrence et al., 2018), and the ability of TOG3 to slow down microtubule shortening is thus not observed with the full length protein.

Another interesting observation is that two domains that induce microtubule rescue when fused to EB3 N-terminus, do not show the same activity when attached to another MBD, that of MAP7, although abundant microtubule decoration is observed in both cases. Based on competition experiments with tau, the MBD of MAP7 might interact with protofilament crest (Monroy et al., 2018), a position very distinct from the groove between the protofilaments, where the EBs bind (Maurer et al., 2012; Zhang et al., 2015). It is thus possible and even likely that the exact positioning of a rescue domain on the microtubule polymer can affect its properties. Of notice, the relatively low potency of the MAP7 MBD to alter microtubule dynamics in vitro fits well with observations in cells, where it is frequently used as a microtubule dynamics reporter lacking a strong dominant effect of its own (Faire et al., 1999).

Microtubule rescues could potentially be induced by proteins that bind to microtubule lattices and recruit to them free tubulin dimers to promote their incorporation into shortening microtubule ends. Such a mechanism has been proposed for the CLASP homologue from fission yeast (Al-Bassam et al., 2010). We tried to test this idea by using EB3 fusions with the tubulin binding domains of chTOG. The obtained results were not entirely conclusive for two reasons. First, the fusions potentiated catastrophes and thus limited the length of microtubule growth and depolymerization episodes, making it more difficult to detect rescues unless their frequency would be very high. Second, the EB3-chTOG fusions strongly associated with growing microtubule ends rather than microtubule lattices, and from the results above, it is clear that significant binding of a protein to microtubule shafts can promote its rescue activity. Tethering of the TOG domains of chTOG to the microtubules with a positively charged polypeptide might provide more conclusive results.

The generation of EB3-based tip-tracking proteins with different effects on microtubule polymerization in vitro gave us the opportunity to test their effects in cells lacking all three EBs. We confirmed that the addition of EB3 C-terminus to EB3-NL-LZ-GFP restores normal microtubule tip growth in cells. Since in vitro, EB3-NL-LZ-GFP-EBC fusion behaved very

similarly to EB3-NL-LZ-GFP alone, this result shows that restoring normal microtubule tip behavior depends on recruitment of some EB partners. Which partners these are remains to be determined. As discussed in Chapter 3, the irregular dynamics of growing microtubule tips observed with EB3-NL-LZ-GFP in EB1/2/3 knockout cells could be caused by two, not necessarily mutually exclusive types of mechanisms: increased susceptibility to pushing and pulling forces exerted, for example, by motor proteins, or the irregular elongation of whole microtubule tips and/or protofilament subsets. The two microtubule growth regulators, chTOG, which is connected to the EBs indirectly, though SLAIN2, and CLASP2, which binds to EBs directly through the SxIP motifs, were the most obvious candidates for playing a role in the second mechanism. However, the tested fusions of EB3 with chTOG, SLAIN2 or the catastrophe-suppressing domain of CLASP2, TOG2, were unable to rescue plus end dynamics. It is possible that "smooth" microtubule growth depends on a combination of several EB-binding proteins and thus cannot be restored by a single fusion. This option could in principle be tested by co-transfecting cells with several different fusions at the same time. It is also certainly possible that direct fusions do not mimic the domain arrangements present in the native complexes of EBs and their partners. Using inducible protein heterodimerization systems (such as the rapalog-based protein heterodimerization system described in Chapter 3 or optically controlled protein interaction system (van Haren et al., 2018)) could potentially be employed to try to address this issue.

Because of the complex plus end dynamics observed with all the fusions tested, we were also unable to determine whether these fusions increase or decrease catastrophe frequency in EB1/2/3 knockout cells in a way similar to that observed in vitro. Careful analysis of the data collected with different time intervals would be needed to obtain reliable values for the parameters of microtubule dynamics in these conditions. In future, it would also be interesting to test whether the artificial rescue constructs generated here are able to induce rescue in cells. Since high-quality imaging of tubulin would be needed for such measurements, this question should be addressed in a cell type which has a sparse microtubule system and a low rescue frequency, such as CHO cells (Komarova et al., 2002a; Komarova et al., 2002b), rather than HeLa, which display very dense microtubules and frequent rescues. In conclusion, we expect that the constructs generated and characterized here will be useful for future studies of the mechanisms controlling microtubule dynamics.

Materials and Methods

DNA constructs and cell culture

The constructs encoding EB3 (MAPRE3) (Stepanova et al., 2003), SLAIN2 (van der Vaart et al., 2011) , chTOG (Gutierrez-Caballero et al., 2015), CLASP2α (Aher et al., 2018), MAP7 (Hooikaas et al., 2019), MACF1 (Noordstra et al., 2016), and CLIP170 (Akhmanova et al., 2001) were described previously. EB3-NL-LZ chimeric constructs and single domain constructs were made by PCR-based strategies in modified pEGFP-C1 or N1 with a StrepII tag. Human embryonic kidney 239T (HEK293T) cell lines were cultured in medium that consisted of 45% DMEM, 45% Ham's F10, and 10% fetal calf serum supplemented with penicillin and streptomycin. HeLa cells with a triple knockout of EB1, EB2 and EB3 (EB1/2/3 KO) were described in Chapter 3. The cell lines were routinely checked for mycoplasma contamination using LT07-518 Mycoalert assay (Lonza). FuGENE 6 (Promega) was used to transfect HeLa cells for live cell imaging; polyethylenimine (PEI, Polysciences) was used to transfect HEK293T cells for protein purification.

Protein expression and purification for in vitro assays

EB3-NL-LZ chimeras and single domain proteins were prepared as described previously (Aher et al., 2018). Briefly, proteins were expressed in HEK293T cells. Cells were collected from one 15-cm dish after 48 h transfection and lysed in 500 µl lysis buffer (50 mM HEPES, 300 mM NaCl and 0.5% Triton X-100, pH 7.4) supplemented with protease inhibitors (Roche) on ice for 15 minutes. The supernatant obtained from the cell lysate after centrifugation was incubated with 40 µl of StrepTactin beads (GE Healthcare) for 45 min. After incubation, the beads were washed five times with high salt wash buffer (50 mM HEPES, 1.5 M NaCl and 0.01% Triton X-100). The proteins were eluted with 40 µl of elution buffer (50 mM HEPES, 150 mM NaCl, 1 mM $MgCl_2$, 1 mM EGTA, 1 mM dithiothreitol (DTT), 2.5 mM d-Desthiobiotin and 0.05% Triton X-100, pH 7.4). Purified proteins were snap-frozen and stored at 80 °C. GFP-EB3 (Montenegro Gouveia et al., 2010) was a gift of Dr. M. Steinmetz (Paul Scherrer Institute, Switzerland).

In vitro assays

In vitro assays were performed as described previously (Aher et al., 2018). Microtubules were grown from GMPCPP-stabilized microtubule seeds in reaction mixtures containing 15 µM porcine brain tubulin that is some cases was supplemented with 3% rhodamine-tubulin, 75 mM KCl, 1 mM guanosine triphosphate, 0.1% methylcellulose, 0.2 mg/ml κ-casein and oxygen scavenger mixture (50 mM glucose, 400 µg/ ml glucose oxidase, 200 µg/ml catalase, and 4 mM DTT in MRB80 buffer). The reaction mix was added to the flow chamber after centrifugation in an Airfuge for 5 minutes at 119,000 x g. The flow chamber was sealed with vacuum grease, and dynamic microtubules were imaged immediately at 30 °C with a TIRF microscope. All tubulin products were from Cytoskeleton Inc.

Image acquisition

In vitro reconstitution assays were imaged using Total Internal Reflection Fluorescence (TIRF) microscopy using an inverted research microscope Nikon Eclipse Ti-E (Nikon) with the perfect focus system (Nikon), equipped with Nikon Apo TIRF 100x N.A. 1.49 oil objective (Nikon) and iLas² system (Dual Laser illuminator for azimuthal spinning TIRF (or Hilo) illumination and Simultaneous Targeted Laser Action) from Roper Scientific (Evry, FRANCE) with a custom modification for targeted Photoablation using a 532 nm pulsed laser. The system was also equipped with ASI motorized stage MS-2000-XY (ASI), Photometrics Evolve Delta 512 EMCCD

camera (Photometrics) and controlled by the MetaMorph 7.8 software (Molecular Devices). Stradus 488 nm (150 mW, Vortran) and OBIS 561 nm (100 mW, Coherent) lasers were used as the light sources. Images were projected onto the CCD chip at a magnification of 0.065 µm/pixel.

Live cell imaging was performed on an inverted research microscope Nikon Eclipse Ti-E (Nikon) with the perfect focus system (PFS) (Nikon), equipped with Nikon Apo TIRF 100x N.A. 1.49 oil objective (Nikon), Yokogawa CSU-X1-A1 confocal head (Yokogawa) with 405-491-561 triple band mirror and GFP, mCherry and GFP/mCherry emission filters (Chroma), ASI motorized stage MS-2000-XYZ with Piezo Top Plate (ASI), a Photometrics Evolve 512 EMCCD camera (Photometrics) and controlled by the MetaMorph 7.7 software (Molecular Devices). The microscope was equipped with a custom-ordered illuminator (Nikon, MEY10021) modified by Roper Scientific France/PICT-IBiSA, Institut Curie and Cobolt Calypso 491 nm (100 mW) and Cobolt Jive 561 nm (100 mW) lasers (Cobolt). Images were collected with 100 ms exposure time at 2 frames per second. To keep the samples at 37°C for live cell imaging and 30°C for in vitro assays, we used a stage top incubator model INUBG2E-ZILCS (Tokai Hit).

Image preparation and analysis

Images were prepared for publication using MetaMorph and ImageJ. All images were modified by adjustments of levels and contrast. ImageJ plugin KymoResliceWide v.0.4 (https://github.com/ekatrukha/KymoResliceWide (Katrukha, 2015)) was used for generating kymographs illustrating microtubule life histories.

Acknowledgements

We thank Dr. M. Steinmetz for the gift of GFP-EB3. This work was supported by the European Research Council Synergy grant 609822 to A.A.

References

Aher, A. 2017. Tipping microtubule polymerization: Insights from in vitro reconstitution.

Aher, A., M. Kok, A. Sharma, A. Rai, N. Olieric, R. Rodriguez-Garcia, E.A. Katrukha, T. Weinert, V. Olieric, L.C. Kapitein, M.O. Steinmetz, M. Dogterom, and A. Akhmanova. 2018. CLASP Suppresses Microtubule Catastrophes through a Single TOG Domain. *Dev Cell*. 46:40-58.

Akhmanova, A., C.C. Hoogenraad, K. Drabek, T. Stepanova, B. Dortland, T. Verkerk, W. Vermeulen, B.M. Burgering, C.I. De Zeeuw, F. Grosveld, and N. Galjart. 2001. Clasps are CLIP-115 and -170 associating proteins involved in the regional regulation of microtubule dynamics in motile fibroblasts. *Cell*. 104:923-935.

Al-Bassam, J., H. Kim, G. Brouhard, A. van Oijen, S.C. Harrison, and F. Chang. 2010. CLASP promotes microtubule rescue by recruiting tubulin dimers to the microtubule. *Dev Cell*. 19:245-258.

Aumeier, C., L. Schaedel, J. Gaillard, K. John, L. Blanchoin, and M. Thery. 2016. Self-repair promotes microtubule rescue. *Nat Cell Biol*. 18:1054-1064.

Bieling, P., L. Laan, H. Schek, E.L. Munteanu, L. Sandblad, M. Dogterom, D. Brunner, and T. Surrey. 2007. Reconstitution of a microtubule plus-end tracking system in vitro. *Nature*. 450:1100-1105.

Brouhard, G.J., J.H. Stear, T.L. Noetzel, J. Al-Bassam, K. Kinoshita, S.C. Harrison, J. Howard, and A.A. Hyman. 2008. XMAP215 is a processive microtubule polymerase. *Cell*. 132:79-88.

Byrnes, A.E., and K.C. Slep. 2017. TOG-tubulin binding specificity promotes microtubule dynamics and mitotic spindle formation. *J Cell Biol*. 216:1641-1657.

Chen, Y., P. Wang, and K.C. Slep. 2019. Mapping multivalency in the CLIP-170-EB1 microtubule plus-end complex. *J Biol Chem*. 294:918-931.

de Forges, H., A. Pilon, I. Cantaloube, A. Pallandre, A.M. Haghiri-Gosnet, F. Perez, and C. Pous. 2016. Localized Mechanical Stress Promotes Microtubule Rescue. *Curr Biol*. 26:3399-3406.

Dimitrov, A., M. Quesnoit, S. Moutel, I. Cantaloube, C. Pous, and F. Perez. 2008. Detection of GTP-tubulin conformation in vivo reveals a role for GTP remnants in microtubule rescues. *Science*. 322:1353-1356.

Faire, K., C.M. Waterman-Storer, D. Gruber, D. Masson, E.D. Salmon, and J.C. Bulinski. 1999. E-MAP-115 (ensconsin) associates dynamically with microtubules in vivo and is not a physiological modulator of microtubule dynamics. *J Cell Sci*. 112 (Pt 23):4243-4255.

Gutierrez-Caballero, C., S.G. Burgess, R. Bayliss, and S.J. Royle. 2015. TACC3-ch-TOG track the growing tips of microtubules independently of clathrin and Aurora-A phosphorylation. *Biol Open*.

Hooikaas, P.J., M. Martin, T. Muhlethaler, G.J. Kuijntjes, C.A.E. Peeters, E.A. Katrukha, L. Ferrari, R. Stucchi, D.G.F. Verhagen, W.E. van Riel, I. Grigoriev, A.F.M. Altelaar, C.C. Hoogenraad, S.G.D. Rudiger, M.O. Steinmetz, L.C. Kapitein, and A. Akhmanova. 2019. MAP7 family proteins regulate kinesin-1 recruitment and activation. *J Cell Biol*. 218:1298-1318.

Howard, J., and A.A. Hyman. 2007. Microtubule polymerases and depolymerases. *Curr Opin Cell Biol*. 19:31-35.

Kinoshita, K., I. Arnal, A. Desai, D.N. Drechsel, and A.A. Hyman. 2001. Reconstitution of physiological microtubule dynamics using purified components. *Science*. 294:1340-1343.

Kodama, A., I. Karakesisoglou, E. Wong, A. Vaezi, and E. Fuchs. 2003. ACF7: an essential integrator of microtubule dynamics. *Cell*. 115:343-354.

Komarova, Y., C.O. De Groot, I. Grigoriev, S.M. Gouveia, E.L. Munteanu, J.M. Schober, S.

Honnappa, R.M. Buey, C.C. Hoogenraad, M. Dogterom, G.G. Borisy, M.O. Steinmetz, and A. Akhmanova. 2009. Mammalian end binding proteins control persistent microtubule growth. *J Cell Biol*. 184:691-706.

Komarova, Y.A., A.S. Akhmanova, S. Kojima, N. Galjart, and G.G. Borisy. 2002a. Cytoplasmic linker proteins promote microtubule rescue in vivo. *J Cell Biol*. 159:589-599.

Komarova, Y.A., I.A. Vorobjev, and G.G. Borisy. 2002b. Life cycle of MTs: persistent growth in the cell interior, asymmetric transition frequencies and effects of the cell boundary. *J Cell Sci*. 115:3527-3539.

Lawrence, E.J., G. Arpag, S.R. Norris, and M. Zanic. 2018. Human CLASP2 specifically regulates microtubule catastrophe and rescue. *Mol Biol Cell*. 29:1168-1177.

Maney, T., M. Wagenbach, and L. Wordeman. 2001. Molecular dissection of the microtubule depolymerizing activity of mitotic centromere-associated kinesin. *J Biol Chem*. 276:34753-34758.

Maurer, S.P., F.J. Fourniol, G. Bohner, C.A. Moores, and T. Surrey. 2012. EBs recognize a nucleotide-dependent structural cap at growing microtubule ends. *Cell*. 149:371-382.

Mohan, R., E.A. Katrukha, H. Doodhi, I. Smal, E. Meijering, L.C. Kapitein, M.O. Steinmetz, and A. Akhmanova. 2013. End-binding proteins sensitize microtubules to the action of microtubule-targeting agents. *Proc Natl Acad Sci U S A*. 110:8900-8905.

Monroy, B.Y., D.L. Sawyer, B.E. Ackermann, M.M. Borden, T.C. Tan, and K.M. Ori-McKenney. 2018. Competition between microtubule-associated proteins directs motor transport. *Nat Commun*. 9:1487.

Montenegro Gouveia, S., K. Leslie, L.C. Kapitein, R.M. Buey, I. Grigoriev, M. Wagenbach, I. Smal, E. Meijering, C.C. Hoogenraad, L. Wordeman, M.O. Steinmetz, and A. Akhmanova. 2010. In Vitro Reconstitution of the Functional Interplay between MCAK and EB3 at Microtubule Plus Ends. *Curr Biol*. 20:1717-1722.

Noordstra, I., Q. Liu, W. Nijenhuis, S. Hua, K. Jiang, M. Baars, S. Remmelzwaal, M. Martin, L.C. Kapitein, and A. Akhmanova. 2016. Control of apico-basal epithelial polarity by the microtubule minus-end-binding protein CAMSAP3 and spectraplakin ACF7. *J Cell Sci*. 129:4278-4288.

Schaedel, L., S. Triclin, D. Chrétien, A. Abrieu, C. Aumeier, J. Gaillard, L. Blanchoin, M. Théry, and K. John. 2019. Lattice defects induce microtubule self-renewal. *Nature Physics*. 15:830-838.

Sen, I., D. Veprintsev, A. Akhmanova, and M.O. Steinmetz. 2013. End binding proteins are obligatory dimers. *PLoS One*. 8:e74448.

Stepanova, T., J. Slemmer, C.C. Hoogenraad, G. Lansbergen, B. Dortland, C.I. De Zeeuw, F. Grosveld, G. van Cappellen, A. Akhmanova, and N. Galjart. 2003. Visualization of microtubule growth in cultured neurons via the use of EB3-GFP (end-binding protein 3-green fluorescent protein). *J Neurosci*. 23:2655-2664.

van der Vaart, B., C. Manatschal, I. Grigoriev, V. Olieric, S.M. Gouveia, S. Bjelic, J. Demmers, I. Vorobjev, C.C. Hoogenraad, M.O. Steinmetz, and A. Akhmanova. 2011. SLAIN2 links microtubule plus end-tracking proteins and controls microtubule growth in interphase. *J Cell Biol*. 193:1083-1099.

van Haren, J., R.A. Charafeddine, A. Ettinger, H. Wang, K.M. Hahn, and T. Wittmann. 2018. Local control of intracellular microtubule dynamics by EB1 photodissociation. *Nat Cell Biol*. 20:252-261.

Vemu, A., E. Szczesna, E.A. Zehr, J.O. Spector, N. Grigorieff, A.M. Deaconescu, and A. Roll-Mecak. 2018. Severing enzymes amplify microtubule arrays through lattice GTP-tubulin incorporation. *Science*. 361:eaau1504.

Weisbrich, A., S. Honnappa, R. Jaussi, O. Okhrimenko, D. Frey, I. Jelesarov, A. Akhmanova, and M.O. Steinmetz. 2007. Structure-function relationship of CAP-Gly domains. *Nat Struct Mol Biol*. 14:959-967.

Widlund, P.O., J.H. Stear, A. Pozniakovsky, M. Zanic, S. Reber, G.J. Brouhard, A.A. Hyman, and J. Howard. 2011. XMAP215 polymerase activity is built by combining multiple tubulin-binding TOG domains and a basic lattice-binding region. *Proc Natl Acad Sci U S A*. 108:2741-2746.

Wu, X., A. Kodama, and E. Fuchs. 2008. ACF7 regulates cytoskeletal-focal adhesion dynamics and migration and has ATPase activity. *Cell*. 135:137-148.

Zhang, R., G.M. Alushin, A. Brown, and E. Nogales. 2015. Mechanistic Origin of Microtubule Dynamic Instability and Its Modulation by EB Proteins. *Cell*. 162:849-859.

6

Gerneral Discussion

Chao Yang

In this thesis, we have combined experiments in cells and in vitro to investigate how End Binding (EB) proteins and their partners control microtubule polymerization dynamics and the architecture of microtubule networks. Our main goal was to generate human cells completely lacking the EBs as a tool to study the importance and impact of these highly conserved microtubule plus end tracking proteins (+TIPs) on different aspects of microtubule behavior and dynamics. Below, we discuss our findings and put them in context of the current scientific literature.

End Binding proteins – highly conserved, but not essential microtubule regulators?

EBs are among the most conserved microtubule regulators, which target to growing microtubule ends a broad variety of proteins and form the core of +TIP complexes. EBs recognize the growing ends of microtubules by binding to the stabilizing cap formed during polymerization (Maurer et al., 2012). There is still some discussion about the preferred state of tubulin (e.g. GTP or GDP-Pi)(Maurer et al., 2014; Maurer et al., 2012; Zanic et al., 2009; Zhang et al., 2015) and the preferred structural state to which the EBs bind (Guesdon et al., 2016; Reid et al., 2019). Recent work using recombinant tubulin with a mutation in the GTPase site of β-tubulin showed that EB proteins bind with high affinity to the GTP conformation of microtubules (Roostalu et al., 2019). While there are other proteins, for example, some kinesins, which appear to show preference for GTP-bound microtubules (Jiang et al., 2019; Shima et al., 2018; van Riel et al., 2017), and some other microtubule-regulating proteins, such as XMAP215/chTOG or TPX2, which can target growing microtubule plus ends autonomously (Brouhard et al., 2008; Roostalu et al., 2015), a significant part of the microtubule tip-associated proteome is EB-dependent (Akhmanova and Steinmetz, 2010; Akhmanova and Steinmetz, 2015; Jiang et al., 2012). This means that a complete loss of EBs will significantly alter the composition of proteins associated with growing microtubule ends. Using our EB1, EB2 and EB3 (EB1/2/3) knockout cells, we have confirmed the loss of several major EB-binding +TIPs from growing microtubule plus ends (Chapter 2).

Taking these considerations into account, it is quite surprising that EBs are not essential in several different species. For example, *Arabidopsis* plants with strongly reduced expression of the three EB homologs show relatively mild growth phenotypes (Bisgrove et al., 2008). Mutations of the budding and fission yeast EB homologues affects cell division and, in the case of fission yeast, also the cell shape, but are not lethal (Beinhauer et al., 1997; Schwartz et al., 1997). Furthermore, recent work showed that it is possible to generate *C. elegans* worms completely lacking all EB isoforms (Schmidt et al., 2017). Therefore, it is not surprising that we were successful in generating mammalian cell lines in which the three mammalian EB isoforms, EB1, EB2 and EB3, were mutated (Chapter 2) or knocked out (Chapter 3). It is important to note that while this approach worked with HeLa cells, we were not able to obtain a similar triple EB knockout in RPE1 cells, although it was possible to stably mutate in this cell line both EB1- and EB3-encoding genes. An important question is whether various mutants and cells adapt to the lack of EBs by altering the expression of other proteins. We think that such an explanation is quite likely, because while our EB1/2/3 knockout cells have only mild mitotic phenotypes (Chapter 2 and our unpublished data), acute simultaneous knockout of EB1 and EB3 did induce strong mitotic perturbations (McKinley and Cheeseman, 2017), a result that we could confirm (our unpublished data). These data indicate that HeLa cells likely undergo some compensatory changes that allow them to survive without EBs. How do cells cope with the absence of EBs? No systematic analysis addressing this question has been performed to our knowledge in animal cells. It would be interesting to perform RNA sequence and proteomics analysis of EB1/2/3 knockout cell lines to identify the factors that are up- or down regulated in

these cells to allow them to survive.
While the loss of EBs did not cause lethality in the systems described above, it did lead to strong defects in the interphase and mitotic microtubule networks. Even if mutations in EB-encoding genes are not lethal, they would likely sensitize the cells to the absence of other microtubule regulators. For example, EB1 was shown to be essential for the viability of mammalian cells deficient in proteins required for the spindle assembly checkpoint (Raaijmakers et al., 2018). In budding yeast, the EB homolog Bim1 is known to be required for one of the partially redundant pathways of spindle positioning (reviewed in (Geymonat and Segal, 2017)). A similar situation was uncovered in spindle positioning in *C. elegans*, where EB1 contributes to generating a robust cortical force generation mechanism, and this contribution can be uncovered in mutants with partially perturbed dynein function (Schmidt et al., 2017).
To understand how cells deal with the absence of EBs, it is important to know whether their binding partners can still exert some activity at microtubule ends. For some proteins, this seems very likely. For example, microtubule-depolymerizing kinesin-13 MCAK can reach microtubule plus ends by diffusion in the absence of other microtubule-associated proteins (Helenius et al., 2006). Binding to EBs can improve its access to microtubule plus ends crowded by other microtubule regulators (Lee et al., 2008; Montenegro Gouveia et al., 2010); however, if, in the absence of EBs, microtubule tips become less crowded, MCAK can likely perform its catastrophe-inducing function autonomously. The same may apply to other microtubule tip-binding factors, leading to a situation where in the absence of EBs the absolute numbers of specific microtubule-associated proteins located in the close vicinity of the microtubule tips are reduced, but the balance of their activities might remain similar. To test this idea, it would be interesting to examine whether knockout or depletion of some prominent EB-dependent +TIPs still have some effect on microtubule plus end dynamics when EBs are absent. Our preliminary unpublished data show that the depletion of CLASP1 and CLASP2, which are targeted to microtubule plus ends by EB1 and EB3, indeed affect microtubule dynamics not only in wild type but also in EB1/2/3 knockout cells.

Similarities, differences and redundancy between EB family members
Generation of EB knockouts allowed us to perform rescue experiments and thus critically test the similarities and differences between the three mammalian EB family members, EB1, EB2 and EB3. Previous work has shown that EB1 is ubiquitously expressed and is the predominant EB protein in dividing cells, while EB3 can be upregulated in differentiating cells (Jaworski et al., 2009; Nakagawa et al., 2000; Straube and Merdes, 2007; Su and Qi, 2001). EB3 has a higher affinity to microtubules compared to EB1 (Roth et al., 2018; Stepanova et al., 2003). In vitro, the patterns of EB1 and EB3 binding to microtubules coincide, whereas in cells, the peaks of EB1 and EB3 accumulation appear to be very slightly shifted (EB1 is ~140 nm closer to the outermost microtubule end compared to EB3)(Roth et al., 2018). EB1 and EB3 were shown to perform common and distinct functions during cell division and ciliogenesis and to display some distinct post-translational modifications (Ban et al., 2009; Ferreira et al., 2013; Schroder et al., 2011). In terms of partner binding, EB1 and EB3 appear quite similar (Jiang et al., 2012); moreover, the two proteins efficiently heterodimerize (De Groot et al., 2010), and therefore, in cells where one of them is low in abundance (like EB3 is cycling mammalian cells), the other one is likely to be present in heterodimers with the more abundant EB isoform (Komarova et al., 2009). In line with all these data, in our experiments, both EB1 and EB3 could rescue the phenotypes that we were studying (microtubule minus-end organization and microtubule plus end growth) equally well (Chapter 2 and Chapter 3). This was in contrast to EB2, which could not rescue these phenotypes. Since in our rescue experiments we used immunofluorescence

cell staining or live cell imaging with EB-GFP fusions to ensure that the expression levels of the three EB proteins are similar, this difference was due to the biochemical properties of EB2.
EB2 differs from EB1 and EB3 in several significant ways. First, it does not heterodimerize with EB1 and EB3 (De Groot et al., 2010). Second, EB2 has a lower affinity for outermost microtubule tips and is displaced from them by the other two EB family members (Komarova et al., 2009; Roth et al., 2018). Unlike EB1 and EB3, which have a strong preference for GTP or GTPγS-bound microtubules in vitro, EB2 appears to prefer microtubule lattices with a mixture of different nucleotides (Maurer et al., 2011; Roostalu et al., 2019; Roth et al., 2018). Third, EB2 has a lower affinity to many of the EB binding partners (Jiang et al., 2012) (Chapter 2), and thus cannot recruit them to the microtubule plus ends (Chapter 2). EB2 also lacks the catastrophe suppressing activity common for EB1 and EB3 (Komarova et al., 2009)(Chapter 2 and 3).
The exact role of EB2 requires further investigation. Several studies reported distinct post-translational modifications of EB2, for example, during cell division and neuronal development, but their functional significance requires further clarification (Baltussen et al., 2018; Iimori et al., 2016; Stenner et al., 2013). Precise regulation of EB2 levels has been reported to be important for epithelial differentiation (Goldspink et al., 2013), whereas the interaction between MAP4K4 and EB2 was suggested to be required for cell adhesion dynamics (Yue et al., 2014). We have tried to confirm the latter interaction, but without success (our unpublished data). EB2 has also been implicated in a congenital disorder characterized by circumferential skin creases, intellectual disability, craniofacial and other developmental abnormalities (Isrie et al., 2015), but the mechanistic basis of these developmental defects is currently unclear. Our studies of EB knockout cells have shed no light on the function of EB2, and it seems that further research on this rather enigmatic EB family member should be continued in other, possibly differentiated cell types.

Regulation of microtubule plus end dynamics by the EBs

As indicated above, EB proteins are generally thought to interact with the GTP cap at growing microtubule ends (Maurer et al., 2011; Maurer et al., 2012; Roostalu et al., 2019; Zanic et al., 2009; Zhang et al., 2015). This interaction can have several consequences. First, both fluorescence imaging in vitro and cryo-EM analysis support the notion that EBs can accelerate GTP hydrolysis by tubulin, making the stabilizing cap at the microtubule end shorter (Maurer et al., 2014; Zhang et al., 2015). This observation is consistent with the in vitro data showing that EBs promote catastrophes and also sensitize microtubules to the action of microtubule-depolymerizing drugs (Bieling et al., 2007; Komarova et al., 2009; Mohan et al., 2013). Importantly, the shortening of EB-binding region at the microtubule plus end is observed already at 10 nM EB1 (Maurer et al., 2014). Second, binding of the EBs can alter the state of microtubule plus ends by inducing some conformational changes and/or directly affecting their stability. For example, although EBs bind between protofilaments with a peak at ~100 nm behind the outermost microtubule tip (Maurer et al., 2014; Maurer et al., 2012), they do accelerate microtubule polymerization, with EB3 being more potent than the other EB homologs (Komarova et al., 2009; Roth et al., 2018). How EBs increase microtubule growth rate is currently unclear; altering protofilament conformations at microtubule tips in a way that promotes tubulin addition or potentiates tubulin sheet closure (Vitre et al., 2008) can be possible explanations. It is interesting that EB1 can allosterically cooperate with XMAP215 in accelerating microtubule growth, and a similar effect has been observed with the combination of XMAP215 and microtubule stabilizing drug taxol, which interacts with a luminal site on β-tubulin (Zanic et al., 2013). It has also been proposed that the EB1 homolog from fission yeast, Mal3, binds and stabilizes the microtubule lattice seam, a site of lateral contacts

between α- and β-tubulin (Sandblad et al., 2006), though this idea did not find confirmation in subsequent cryo-EM studies (Maurer et al., 2012; Zhang et al., 2015). It should be noted that these results might depend on how such structural analyses are performed, because Mal3 has been shown to promote formation of A-lattice protofilament contacts when added in excess during microtubule assembly (des Georges et al., 2008). In addition to such direct effects on the microtubule itself, EBs can also exert indirect effects. For example, occlusion of microtubule tips can potentially protect them against depolymerases (Montenegro Gouveia et al., 2010). Furthermore, recruitment of EB partners can affect microtubule growth in different and sometimes opposing ways (Akhmanova and Steinmetz, 2015; Kumar and Wittmann, 2012). One of our goals was to test how EB proteins affect the properties of the stabilizing cap at microtubule tips. Using microtubule-severing experiments, we found that the ~0.8-1 µm-long region proximal to a growing microtubule plus end indeed shows increased stability, which was similar between control and EB1/2/3 knockout cells. However, in these cells, we did find evidence of increased motility of microtubule plus ends, which might point towards the idea that EBs inhibit, directly or indirectly, the interactions of microtubule tips with molecular motors. Consistent with previous work (Komarova et al., 2009), we found that EBs suppress catastrophes, an effect that appears to depend on the interactions with EB-binding partners containing SxIP or LxxPTPh motifs. This is consistent with the ability of EBs to serve as hubs for protein recruitment to microtubule plus ends.

The hub function of the EBs and their partners: from dimers and oligomers to phase separation?

One of the most exciting properties of EBs is their capacity to interact with numerous binding partners. These include the CAP-Gly domain-containing proteins CLIP170, CLIP115 and p150^{Glued}, the large subunit of dynactin (Akhmanova and Steinmetz, 2008), as well as numerous proteins containing SxIP or LxxPTPh motifs (Akhmanova and Steinmetz, 2015; Honnappa et al., 2009; Kumar et al., 2017; Kumar and Wittmann, 2012). Since quite a few of these proteins can also bind to each other, together, they can potentially form an extended protein interaction network (Akhmanova and Steinmetz, 2015; Gupta et al., 2014). Whereas individual binding nodes of this network have been characterized in detail, in some cases including crystal structures and affinity measurements, the properties of the network as a whole as well as the behavior of the individual proteins within this network are still insufficiently understood.

EB1 proteins are dimers and can in principle interact with either a single dimeric partner or two monomeric ones. Are EB interactions with microtubule tips influenced by their partners? To address this question, one can try to compare the dwell times of EB proteins at microtubule tips in cells and in assays with purified proteins, where they are the only +TIPs present. In vitro, the reported dwell time values were shown to vary between as 0.05 s for EB1 (Bieling et al., 2008), 0.3-0.7 s for EB1, EB2 and EB3 (Montenegro Gouveia et al., 2010; Roth et al., 2018) and up to 5 s for EB3, although in the latter case, careful measurements demonstrated an affinity gradient, with longest dwell times observed at the outermost microtubule plus ends (Roostalu et al., 2019). This variability could be due to the variation in the in vitro assay conditions, such as ionic strength, because electrostatic interactions play an important role in EB binding to microtubule lattice (Buey et al., 2011). Indeed, a buffer with 80 mM PIPES and 50 mM KCl was used in the studies by Montenegro Gouveia et al. (2010) and Roth et al. (2018), where shorter dwell times were reported, whereas a buffer with 80 mM PIPES and 30 mM KCl was used by Roostalu et al. (2019), where longer dwell times were observed. In cells, the half-life of EB3-GFP association with growing microtubule plus ends was shown to be ~0.3 s (Dragestein et al., 2008), whereas a value of 0.4 s was obtained for CLIP170, for which 0.25 s

mean dwell time was reported in the presence of EB1 in vitro (Bieling et al., 2008). In spite of the variability of the exact measurement conditions, these data suggest that the interactions with protein partners do not have a strong inhibitory effect on the turnover of EBs or CLIP170 on microtubule tips. In this thesis, we obtained tools that will allow performing more precise measurements: by transfecting fluorescently tagged EB constructs into EB1/2/3 knockout cells, it will be possible to perform measurements of EB turnover on the same microscope setup with the same concentrations of EBs in cells and in vitro. Such measurement might provide insight into whether the participation in the +TIP network affects EB turnover. It is important to mention though that if the concentration of EBs at the microtubule plus ends is significantly higher than of their binding partners, FRAP assays may not be very revealing, because most of EB molecules will not be partner-bound. Detailed comparison of the turnover of wild type EBs and point mutants in which the SxIP binding pocket is mutated (Montenegro Gouveia et al., 2010) and/or the C-terminal CAP-Gly binding tyrosine residue occluded or removed (Steinmetz and Akhmanova, 2008; Weisbrich et al., 2007) might help to shed light on this question.

In Chapter 4, we have taken some steps to explore the hypothesis that +TIP complexes could undergo liquid-liquid phase separation (LLPS), with SLAIN2 playing a role of LLPS scaffold. This question appeared relevant for two reasons. First, SLAIN2 resembles other LLPS-prone proteins (Alberti et al., 2019), because it contains extended intrinsically disordered regions and can undergo interactions with multiple +TIPs, some of which can also bind to each other. Second, the depletion of SLAIN2 and its major binding partners, EB1/EB3 and chTOG, has a similar cellular phenotype – increased frequency of microtubule catastrophes accompanied by an increased frequency of rescues (Chapter 2)(Komarova et al., 2009; van der Vaart et al., 2011). A potentially attractive explanation of this effect is the formation of liquid-like droplets of these +TIPs at microtubule plus ends (Figure 1). Such droplets could prevent catastrophes by concentrating tubulin in the microtubule tip vicinity, similar to what has been proposed for microtubule nucleation at the centrosome (Woodruff et al., 2017). Indications that +TIPs can form condensates also exists in fission yeast, where +TIPs form multivalent interaction networks that can lead to formation of particles that are delivered to the cell cortex (Dodgson et al., 2013; Taberner and Dogterom, 2019).

The obtained results were not conclusive. It became clear that SLAIN2 can form liquid-like droplets when overexpessed in cells and in the presence of crowding agents in vitro, and that the major partners of SLAIN2, EBs and chTOG, but not the other SLAIN2-binding +TIPs, CLIP170 and CLASPs, can partition into these droplets (Chapter 4). However, the endogenous concentration of SLAIN2 appears too low for the spontaneous droplet formation. Whether SLAIN2 undergoes condensation on microtubule plus ends is currently unclear. Since microtubule growth becomes irregular in the absence of full-length EB1 and/or EB3, we examined whether concentrating SLAIN2 or chTOG at the microtubule tips through a direct fusion with EB3 would rescue this phenotype (Chapter 4 and Chapter 5), but found this not to be the case. There are of course many reasons why artificial fusion proteins may not be functional, and this result thus does not allow us to draw any firm conclusions. We also tried to obtain conditions where liquid droplets of EB3, SLAIN2 and chTOG would form at the tips of growing microtubules in vitro, but these experiments were not successful so far. As discussed in Chapter 4, further optimization of these in vitro experiments combined with attempts to inhibit self-association of SLAIN2 without preventing its binding to EBs and chTOG could be a potential way forward to address this question. Measurement of SLAIN2 turnover at microtubule tips in cells and comparing it to its turnover in the presence of EBs and chTOG at different concentrations in vitro could also potentially be informative. We have generated stable HeLa cell lines with endogenous SLAIN2 linked to HaloTag and established an in vitro reconstitution with EB2, SLAIN2 and chTOG,

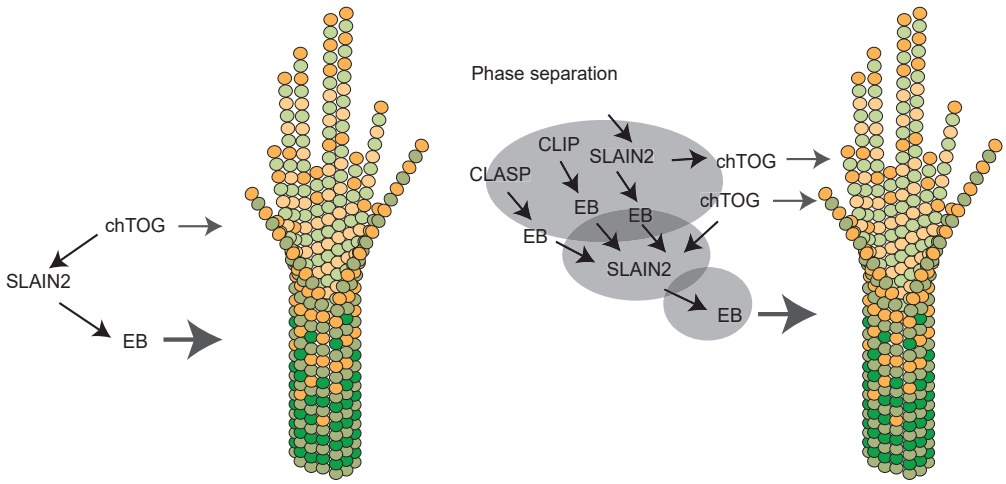

Figure 1. A potential model of SLAIN2-dependent phase separation at growing microtubule plus ends.

SLAIN2 can bind to EBs and chTOG, and SLAIN2 condensates could promote +TIP recruitment to growing microtubule plus ends.

making such experiments possible. Further work is thus needed to resolve whether LLPS plays a role in +TIP function in mammalian cells.

EBs at the minus ends of microtubules: control of microtubule network architecture

The most unexpected outcome of our work was our finding that the knockout of EB1 and EB3 affects the organization of non-centrosomal microtubule minus ends. Previous work from different labs has shown that in cultured mammalian cells studied here, the minus ends of non-centrosomal microtubules are stabilized by the members of CAMSAP family (Akhmanova and Hoogenraad, 2015; Martin and Akhmanova, 2018). Importantly, CAMSAP proteins bind to and are deposited at growing microtubule ends, thus generating stretches of stabilized microtubule lattice (Hendershott and Vale, 2014; Jiang et al., 2014). EBs are expected to be recruited to microtubule minus ends during their growth, because they associate with the GTP-bound microtubule lattice and do not distinguish between plus- and minus-ends (Akhmanova and Steinmetz, 2015). EBs and CAMSAPs can in principle bind to the same growing microtubule minus ends without interfering with each other: the signature domain of CAMSAPs, CKK, binds in the groove between protofilaments to a site that is located between two tubulin dimers (Atherton et al., 2017) and does not overlap with the EB CH-domain binding site, which is situated at the vertex of four tubulin dimers (Maurer et al., 2012). The CH-domain and CKK-binding sites on the microtubule are thus shifted by ~4 nm. We found that in the absence of EBs, CAMSAP2-decorated parts of microtubule minus ends became shorter. Previous work has established that the length of CAMSAP2 stretches is negatively regulated by the microtubule-severing protein katanin, which directly interacts with CAMSAP2 (Jiang et al., 2018; Jiang et al., 2014). It is possible that EB1 and EB3 counteract katanin either directly, by occluding the growing minus end, or indirectly, by bringing in some additional microtubule-stabilizing +TIPs, such as CLASPs.

Furthermore, we found that EB1/3-mutated cells, CAMSAP2-decorated microtubule minus ends become disconnected from the Golgi membranes. Previous work has shown that this

connection is mediated by the binding of CAMSAP2 to the complex of two Golgi-associated proteins, AKAP450 and myomegalin (Wu et al., 2016). This interaction is important for generating semi-radial microtubule networks, in which microtubule minus ends that are concentrated in the central part of the cell but are not all anchored at the centrosome (Martin and Akhmanova, 2018; Wu et al., 2016). Surprisingly, we found that the CAMSAP2-AKAP450-myomegalin interaction alone is not sufficient for this anchoring process – EB1 or EB3 are also required. The EBs directly bind to myomegalin through the SxIP motif (Roubin et al., 2013; Wang et al., 2014) and appear to provide an additional connection between membranes and microtubule shafts. Importantly, this connection seems to depend on the weak affinity of the EBs to GDP-bound tubulin lattices, because it does not require microtubule growth and can be replaced by a direct link of myomegalin to the microtubule lattice-binding domain of MAP7 (Chapter 2). The interactions of Golgi membranes with microtubules thus appear to depend on multiple weak interactions. Such association mode likely ensures the appropriate relative positioning of the Golgi complex and the microtubule network without causing excessive spreading of Golgi membranes along microtubules.

The lack of EB1 and EB3 in HeLa and RPE1 cells leads to the detachment of microtubules from the Golgi and disorganization of the microtubule network (Chapter 2). Similar defects are observed in cells lacking the Golgi membrane associated components of the minus-end anchoring complex, AKAP450 and myomegalin (Gavilan et al., 2017; Martin et al., 2018; Rios, 2014; Rivero et al., 2009; Wu et al., 2016). Such microtubule disorganization has severe consequences for intracellular transport, which becomes less directional, as well as for cell polarity and motility. It should be noted that perturbed microtubule plus end growth and increased motility of microtubule plus ends, described in Chapter 3, can also contribute to microtubule disorganization in cells lacking EB1 and EB3. The relative contribution of the EB-dependent plus- and minus-end pathways to the overall microtubule network architecture requires further analysis.

An interesting question is whether EBs have similar GDP-microtubule binding functions in other cellular contexts. Our results suggest that EBs are not required for microtubule anchoring at the centrosome, and their presence also does not seem to be necessary for microtubule nucleation (Chapter 2). This seems to fit with the absence of strong data supporting direct interplay between γ-tubulin ring complexes and EBs, although such interplay cannot be excluded, because the expression of the components of the gamma-tubulin ring complex was shown to affect microtubule plus-end dynamics (Raynaud-Messina and Merdes, 2007).

An example where the ability of EBs to bind to microtubule shafts has been shown to have clear biological implications is the formation of axon initial segment (AIS) in neurons. AIS is a membrane domain near the proximal end of the axon, where ion channels are concentrated and where the action potential is generated and shaped before it is propagated along the axon. In AIS, EB1 and EB3 serve as a part of the molecular link between stabilized and bundled microtubules and a large cortical scaffolding protein Ankyrin G, which contains multiple SxIP motifs (Freal et al., 2016; Freal et al., 2019; Leterrier et al., 2011). The multisite connections formed between AIS microtubules and plasma membrane formed by Ankyrin G, EB1 and EB3 are reminiscent of those formed between microtubule minus ends and the Golgi complex.

To summarize, the work described in this thesis revealed new important functions of one of the most conserved and well-studied families of +TIPs, the EBs. Furthermore, we expect that the tools that we have generated in the course of our work will be a useful addition to the field that will allow it to move forward.

References

Akhmanova, A., and C.C. Hoogenraad. 2015. Microtubule Minus-End-Targeting Proteins. *Curr Biol*. 25:R162-R171.

Akhmanova, A., and M.O. Steinmetz. 2008. Tracking the ends: a dynamic protein network controls the fate of microtubule tips. *Nat Rev Mol Cell Biol*. 9:309-322.

Akhmanova, A., and M.O. Steinmetz. 2010. Microtubule +TIPs at a glance. *J Cell Sci*. 123:3415-3419.

Akhmanova, A., and M.O. Steinmetz. 2015. Control of microtubule organization and dynamics: two ends in the limelight. *Nat Rev Mol Cell Biol*. 16:711-726.

Alberti, S., A. Gladfelter, and T. Mittag. 2019. Considerations and Challenges in Studying Liquid-Liquid Phase Separation and Biomolecular Condensates. *Cell*. 176:419-434.

Atherton, J., K. Jiang, M.M. Stangier, Y. Luo, S. Hua, K. Houben, J.J.E. van Hooff, A.P. Joseph, G. Scarabelli, B.J. Grant, A.J. Roberts, M. Topf, M.O. Steinmetz, M. Baldus, C.A. Moores, and A. Akhmanova. 2017. A structural model for microtubule minus-end recognition and protection by CAMSAP proteins. *Nat Struct Mol Biol*. 24:931-943.

Baltussen, L.L., P.D. Negraes, M. Silvestre, S. Claxton, M. Moeskops, E. Christodoulou, H.R. Flynn, A.P. Snijders, A.R. Muotri, and S.K. Ultanir. 2018. Chemical genetic identification of CDKL5 substrates reveals its role in neuronal microtubule dynamics. *EMBO J*. 37.

Ban, R., H. Matsuzaki, T. Akashi, G. Sakashita, H. Taniguchi, S.Y. Park, H. Tanaka, K. Furukawa, and T. Urano. 2009. Mitotic regulation of the stability of microtubule plus-end tracking protein EB3 by ubiquitin ligase SIAH-1 and Aurora mitotic kinases. *J Biol Chem*. 284:28367-28381.

Beinhauer, J.D., I.M. Hagan, J.H. Hegemann, and U. Fleig. 1997. Mal3, the fission yeast homologue of the human APC-interacting protein EB-1 is required for microtubule integrity and the maintenance of cell form. *J Cell Biol*. 139:717-728.

Bieling, P., S. Kandels-Lewis, I.A. Telley, J. van Dijk, C. Janke, and T. Surrey. 2008. CLIP-170 tracks growing microtubule ends by dynamically recognizing composite EB1/tubulin-binding sites. *J Cell Biol*. 183:1223-1233.

Bieling, P., L. Laan, H. Schek, E.L. Munteanu, L. Sandblad, M. Dogterom, D. Brunner, and T. Surrey. 2007. Reconstitution of a microtubule plus-end tracking system in vitro. *Nature*. 450:1100-1105.

Bisgrove, S.R., Y.R. Lee, B. Liu, N.T. Peters, and D.L. Kropf. 2008. The microtubule plus-end binding protein EB1 functions in root responses to touch and gravity signals in Arabidopsis. *Plant Cell*. 20:396-410.

Brouhard, G.J., J.H. Stear, T.L. Noetzel, J. Al-Bassam, K. Kinoshita, S.C. Harrison, J. Howard, and A.A. Hyman. 2008. XMAP215 is a processive microtubule polymerase. *Cell*. 132:79-88.

Buey, R.M., R. Mohan, K. Leslie, T. Walzthoeni, J.H. Missimer, A. Menzel, S. Bjelic, K. Bargsten, I. Grigoriev, I. Smal, E. Meijering, R. Aebersold, A. Akhmanova, and M.O. Steinmetz. 2011. Insights into EB structure and the role of its C-terminal domain in discriminating microtubule tips from lattice. *Mol Biol Cell*. 22:2912-2923.

De Groot, C.O., I. Jelesarov, F.F. Damberger, S. Bjelic, M.A. Scharer, N.S. Bhavesh, I. Grigoriev, R.M. Buey, K. Wuthrich, G. Capitani, A. Akhmanova, and M.O. Steinmetz. 2010. Molecular insights into mammalian end-binding protein heterodimerization. *J Biol Chem*. 285:5802-5814.

des Georges, A., M. Katsuki, D.R. Drummond, M. Osei, R.A. Cross, and L.A. Amos. 2008. Mal3, the Schizosaccharomyces pombe homolog of EB1, changes the microtubule lattice. *Nat Struct Mol Biol*. 15:1102-1108.

Dodgson, J., A. Chessel, M. Yamamoto, F. Vaggi, S. Cox, E. Rosten, D. Albrecht, M. Geymonat, A. Csikasz-Nagy, M. Sato, and R.E. Carazo-Salas. 2013. Spatial segregation of polarity factors into distinct cortical clusters is required for cell polarity control. *Nat Commun*. 4:1834.

Dragestein, K.A., W.A. van Cappellen, J. van Haren, G.D. Tsibidis, A. Akhmanova, T.A. Knoch, F. Grosveld, and N. Galjart. 2008. Dynamic behavior of GFP-CLIP-170 reveals fast protein

turnover on microtubule plus ends. *J Cell Biol*. 180:729-737.
Ferreira, J.G., A.J. Pereira, A. Akhmanova, and H. Maiato. 2013. Aurora B spatially regulates EB3 phosphorylation to coordinate daughter cell adhesion with cytokinesis. *J Cell Biol*. 201:709-724.
Freal, A., C. Fassier, B. Le Bras, E. Bullier, S. De Gois, J. Hazan, C.C. Hoogenraad, and F. Couraud. 2016. Cooperative Interactions between 480 kDa Ankyrin-G and EB Proteins Assemble the Axon Initial Segment. *Journal of Neuroscience*. 36:4421-4433.
Freal, A., D. Rai, R.P. Tas, X. Pan, E.A. Katrukha, D. van de Willige, R. Stucchi, A. Aher, C. Yang, A.F.M. Altelaar, K. Vocking, J.A. Post, M. Harterink, L.C. Kapitein, A. Akhmanova, and C.C. Hoogenraad. 2019. Feedback-Driven Assembly of the Axon Initial Segment. *Neuron*. 104:305-321 e308.
Gavilan, M.P., P. Gandolfo, F.R. Balestra, F. Francisco Arias, M. Bornens, and R.M. Rios. 2017. The Centrosome Controls the Number and Spatial Distribution of Microtubules by Negatively Regulating Alternative MTOCs. *BioRxiv*:153304.
Geymonat, M., and M. Segal. 2017. Intrinsic and Extrinsic Determinants Linking Spindle Pole Fate, Spindle Polarity, and Asymmetric Cell Division in the Budding Yeast S. cerevisiae. *Results Probl Cell Differ*. 61:49-82.
Goldspink, D.A., J.R. Gadsby, G. Bellett, J. Keynton, B.J. Tyrrell, E.K. Lund, P.P. Powell, P. Thomas, and M.M. Mogensen. 2013. The microtubule end-binding protein EB2 is a central regulator of microtubule reorganisation in apico-basal epithelial differentiation. *J Cell Sci*. 126:4000-4014.
Guesdon, A., F. Bazile, R.M. Buey, R. Mohan, S. Monier, R.R. Garcia, M. Angevin, C. Heichette, R. Wieneke, R. Tampe, L. Duchesne, A. Akhmanova, M.O. Steinmetz, and D. Chretien. 2016. EB1 interacts with outwardly curved and straight regions of the microtubule lattice. *Nat Cell Biol*. 18:1102-1108.
Gupta, K.K., E.O. Alberico, I.S. Nathke, and H.V. Goodson. 2014. Promoting microtubule assembly: A hypothesis for the functional significance of the +TIP network. *Bioessays*. 36:818-826.
Helenius, J., G. Brouhard, Y. Kalaidzidis, S. Diez, and J. Howard. 2006. The depolymerizing kinesin MCAK uses lattice diffusion to rapidly target microtubule ends. *Nature*. 441:115-119.
Hendershott, M.C., and R.D. Vale. 2014. Regulation of microtubule minus-end dynamics by CAMSAPs and Patronin. *Proc Natl Acad Sci U S A*. 111:5860-5865.
Honnappa, S., S.M. Gouveia, A. Weisbrich, F.F. Damberger, N.S. Bhavesh, H. Jawhari, I. Grigoriev, F.J. van Rijssel, R.M. Buey, A. Lawera, I. Jelesarov, F.K. Winkler, K. Wuthrich, A. Akhmanova, and M.O. Steinmetz. 2009. An EB1-binding motif acts as a microtubule tip localization signal. *Cell*. 138:366-376.
Iimori, M., S. Watanabe, S. Kiyonari, K. Matsuoka, R. Sakasai, H. Saeki, E. Oki, H. Kitao, and Y. Maehara. 2016. Phosphorylation of EB2 by Aurora B and CDK1 ensures mitotic progression and genome stability. *Nat Commun*. 7:11117.
Isrie, M., M. Breuss, G. Tian, A.H. Hansen, F. Cristofoli, J. Morandell, Z.A. Kupchinsky, A. Sifrim, C.M. Rodriguez-Rodriguez, E.P. Dapena, K. Doonanco, N. Leonard, F. Tinsa, S. Moortgat, H. Ulucan, E. Koparir, E. Karaca, N. Katsanis, V. Marton, J.R. Vermeesch, E.E. Davis, N.J. Cowan, D.A. Keays, and H. Van Esch. 2015. Mutations in Either TUBB or MAPRE2 Cause Circumferential Skin Creases Kunze Type. *Am J Hum Genet*. 97:790-800.
Jaworski, J., L.C. Kapitein, S.M. Gouveia, B.R. Dortland, P.S. Wulf, I. Grigoriev, P. Camera, S.A. Spangler, P. Di Stefano, J. Demmers, H. Krugers, P. Defilippi, A. Akhmanova, and C.C. Hoogenraad. 2009. Dynamic microtubules regulate dendritic spine morphology and synaptic plasticity. *Neuron*. 61:85-100.
Jiang, K., L. Faltova, S. Hua, G. Capitani, A.E. Prota, C. Landgraf, R. Volkmer, R.A. Kammerer, M.O. Steinmetz, and A. Akhmanova. 2018. Structural Basis of Formation of the Microtubule Minus-End-Regulating CAMSAP-Katanin Complex. *Structure*. 26:375-382 e374.
Jiang, K., S. Hua, R. Mohan, I. Grigoriev, K.W. Yau, Q. Liu, E.A. Katrukha, A.F. Altelaar, A.J. Heck, C.C. Hoogenraad, and A. Akhmanova. 2014. Microtubule minus-end stabilization by

polymerization-driven CAMSAP deposition. *Dev Cell*. 28:295-309.
Jiang, K., G. Toedt, S. Montenegro Gouveia, N.E. Davey, S. Hua, B. van der Vaart, I. Grigoriev, J. Larsen, L.B. Pedersen, K. Bezstarosti, M. Lince-Faria, J. Demmers, M.O. Steinmetz, T.J. Gibson, and A. Akhmanova. 2012. A Proteome-wide screen for mammalian SxIP motif-containing microtubule plus-end tracking proteins. *Curr Biol*. 22:1800-1807.
Jiang, S., N. Mani, E.M. Wilson-Kubalek, P.I. Ku, R.A. Milligan, and R. Subramanian. 2019. Interplay between the Kinesin and Tubulin Mechanochemical Cycles Underlies Microtubule Tip Tracking by the Non-motile Ciliary Kinesin Kif7. *Dev Cell*. 49:711-730 e718.
Komarova, Y., C.O. De Groot, I. Grigoriev, S.M. Gouveia, E.L. Munteanu, J.M. Schober, S. Honnappa, R.M. Buey, C.C. Hoogenraad, M. Dogterom, G.G. Borisy, M.O. Steinmetz, and A. Akhmanova. 2009. Mammalian end binding proteins control persistent microtubule growth. *J Cell Biol*. 184:691-706.
Kumar, A., C. Manatschal, A. Rai, I. Grigoriev, M.S. Degen, R. Jaussi, I. Kretzschmar, A.E. Prota, R. Volkmer, R.A. Kammerer, A. Akhmanova, and M.O. Steinmetz. 2017. Short Linear Sequence Motif LxxPTPh Targets Diverse Proteins to Growing Microtubule Ends. *Structure*. 25:924-932.
Kumar, P., and T. Wittmann. 2012. +TIPs: SxIPping along microtubule ends. *Trends Cell Biol*. 22:418-428.
Lee, T., K.J. Langford, J.M. Askham, A. Bruning-Richardson, and E.E. Morrison. 2008. MCAK associates with EB1. *Oncogene*. 27:2494-2500.
Leterrier, C., H. Vacher, M.P. Fache, S.A. d'Ortoli, F. Castets, A. Autillo-Touati, and B. Dargent. 2011. End-binding proteins EB3 and EB1 link microtubules to ankyrin G in the axon initial segment. *Proc Natl Acad Sci U S A*. 108:8826-8831.
Martin, M., and A. Akhmanova. 2018. Coming into Focus: Mechanisms of Microtubule Minus-End Organization. *Trends Cell Biol*. 28:574-588.
Martin, M., A. Veloso, J. Wu, E.A. Katrukha, and A. Akhmanova. 2018. Control of endothelial cell polarity and sprouting angiogenesis by non-centrosomal microtubules. *Elife*. 7.
Maurer, S.P., P. Bieling, J. Cope, A. Hoenger, and T. Surrey. 2011. GTPgammaS microtubules mimic the growing microtubule end structure recognised by end-binding proteins (EBs). *Proc Natl Acad Sci U S A*. 109:3988-3993.
Maurer, S.P., N.I. Cade, G. Bohner, N. Gustafsson, E. Boutant, and T. Surrey. 2014. EB1 accelerates two conformational transitions important for microtubule maturation and dynamics. *Curr Biol*. 24:372-384.
Maurer, S.P., F.J. Fourniol, G. Bohner, C.A. Moores, and T. Surrey. 2012. EBs recognize a nucleotide-dependent structural cap at growing microtubule ends. *Cell*. 149:371-382.
McKinley, K.L., and I.M. Cheeseman. 2017. Large-Scale Analysis of CRISPR/Cas9 Cell-Cycle Knockouts Reveals the Diversity of p53-Dependent Responses to Cell-Cycle Defects. *Dev Cell*. 40:405-420 e402.
Mohan, R., E.A. Katrukha, H. Doodhi, I. Smal, E. Meijering, L.C. Kapitein, M.O. Steinmetz, and A. Akhmanova. 2013. End-binding proteins sensitize microtubules to the action of microtubule-targeting agents. *Proc Natl Acad Sci U S A*. 110:8900-8905.
Montenegro Gouveia, S., K. Leslie, L.C. Kapitein, R.M. Buey, I. Grigoriev, M. Wagenbach, I. Smal, E. Meijering, C.C. Hoogenraad, L. Wordeman, M.O. Steinmetz, and A. Akhmanova. 2010. In Vitro Reconstitution of the Functional Interplay between MCAK and EB3 at Microtubule Plus Ends. *Curr Biol*. 20:1717-1722.
Nakagawa, H., K. Koyama, Y. Murata, M. Morito, T. Akiyama, and Y. Nakamura. 2000. EB3, a novel member of the EB1 family preferentially expressed in the central nervous system, binds to a CNS-specific APC homologue. *Oncogene*. 19:210-216.
Raaijmakers, J.A., R. van Heesbeen, V.A. Blomen, L.M.E. Janssen, F. van Diemen, T.R. Brummelkamp, and R.H. Medema. 2018. BUB1 Is Essential for the Viability of Human Cells in which the Spindle Assembly Checkpoint Is Compromised. *Cell Rep*. 22:1424-1438.
Raynaud-Messina, B., and A. Merdes. 2007. Gamma-tubulin complexes and microtubule

organization. *Curr Opin Cell Biol*. 19:24-30.
Reid, T.A., C. Coombes, S. Mukherjee, R.R. Goldblum, K. White, S. Parmar, M. McClellan, M. Zanic, N. Courtemanche, and M.K. Gardner. 2019. Structural state recognition facilitates tip tracking of EB1 at growing microtubule ends. *Elife*. 8.
Rios, R.M. 2014. The centrosome-Golgi apparatus nexus. *Philos Trans R Soc Lond B Biol Sci*. 369.
Rivero, S., J. Cardenas, M. Bornens, and R.M. Rios. 2009. Microtubule nucleation at the cis-side of the Golgi apparatus requires AKAP450 and GM130. *EMBO J*. 28:1016-1028.
Roostalu, J., N.I. Cade, and T. Surrey. 2015. Complementary activities of TPX2 and chTOG constitute an efficient importin-regulated microtubule nucleation module. *Nat Cell Biol*. 17:1422-1434.
Roostalu, J., C. Thomas, N.I. Cade, S. Kunzelmann, I.A. Taylor, and T. Surrey. 2019. The speed of GTP hydrolysis determines GTP cap size and controls microtubule stability. *bioRxiv* 779108.
Roth, D., B.P. Fitton, N.P. Chmel, N. Wasiluk, and A. Straube. 2018. Spatial positioning of EB family proteins at microtubule tips involves distinct nucleotide-dependent binding properties. *J Cell Sci*. 132.
Roubin, R., C. Acquaviva, V. Chevrier, F. Sedjai, D. Zyss, D. Birnbaum, and O. Rosnet. 2013. Myomegalin is necessary for the formation of centrosomal and Golgi-derived microtubules. *Biol Open*. 2:238-250.
Sandblad, L., K.E. Busch, P. Tittmann, H. Gross, D. Brunner, and A. Hoenger. 2006. The Schizosaccharomyces pombe EB1 homolog Mal3p binds and stabilizes the microtubule lattice seam. *Cell*. 127:1415-1424.
Schmidt, R., L.E. Fielmich, I. Grigoriev, E.A. Katrukha, A. Akhmanova, and S. van den Heuvel. 2017. Two populations of cytoplasmic dynein contribute to spindle positioning in C. elegans embryos. *J Cell Biol*. 216:2777-2793.
Schroder, J.M., J. Larsen, Y. Komarova, A. Akhmanova, R.I. Thorsteinsson, I. Grigoriev, R. Manguso, S.T. Christensen, S.F. Pedersen, S. Geimer, and L.B. Pedersen. 2011. EB1 and EB3 promote cilia biogenesis by several centrosome-related mechanisms. *J Cell Sci*. 124:2539-2551.
Schwartz, K., K. Richards, and D. Botstein. 1997. BIM1 encodes a microtubule-binding protein in yeast. *Mol Biol Cell*. 8:2677-2691.
Shima, T., M. Morikawa, J. Kaneshiro, T. Kambara, S. Kamimura, T. Yagi, H. Iwamoto, S. Uemura, H. Shigematsu, M. Shirouzu, T. Ichimura, T.M. Watanabe, R. Nitta, Y. Okada, and N. Hirokawa. 2018. Kinesin-binding-triggered conformation switching of microtubules contributes to polarized transport. *J Cell Biol*. 217:4164-4183.
Steinmetz, M.O., and A. Akhmanova. 2008. Capturing protein tails by CAP-Gly domains. *Trends Biochem Sci*. 33:535-545.
Stenner, F., H. Liewen, S. Gottig, R. Henschler, N. Markuly, S. Kleber, M. Faust, A. Mischo, S. Bauer, M. Zweifel, A. Knuth, C. Renner, and A. Wadle. 2013. RP1 is a phosphorylation target of CK2 and is involved in cell adhesion. *PLoS One*. 8:e67595.
Stepanova, T., J. Slemmer, C.C. Hoogenraad, G. Lansbergen, B. Dortland, C.I. De Zeeuw, F. Grosveld, G. van Cappellen, A. Akhmanova, and N. Galjart. 2003. Visualization of microtubule growth in cultured neurons via the use of EB3-GFP (end-binding protein 3-green fluorescent protein). *J Neurosci*. 23:2655-2664.
Straube, A., and A. Merdes. 2007. EB3 regulates microtubule dynamics at the cell cortex and is required for myoblast elongation and fusion. *Curr Biol*. 17:1318-1325.
Su, L.K., and Y. Qi. 2001. Characterization of human MAPRE genes and their proteins. *Genomics*. 71:142-149.
Taberner, N., and M. Dogterom. 2019. Motor-mediated clustering at microtubule plus ends facilitates protein transfer to a bio-mimetic cortex. *Biorxiv*:736728.
van der Vaart, B., C. Manatschal, I. Grigoriev, V. Olieric, S.M. Gouveia, S. Bjelic, J. Demmers, I. Vorobjev, C.C. Hoogenraad, M.O. Steinmetz, and A. Akhmanova. 2011. SLAIN2 links

microtubule plus end-tracking proteins and controls microtubule growth in interphase. *J Cell Biol*. 193:1083-1099.

van Riel, W.E., A. Rai, S. Bianchi, E.A. Katrukha, Q. Liu, A.J. Heck, C.C. Hoogenraad, M.O. Steinmetz, L.C. Kapitein, and A. Akhmanova. 2017. Kinesin-4 KIF21B is a potent microtubule pausing factor. *Elife*. 6.

Vitre, B., F.M. Coquelle, C. Heichette, C. Garnier, D. Chretien, and I. Arnal. 2008. EB1 regulates microtubule dynamics and tubulin sheet closure in vitro. *Nat Cell Biol*. 10:415-421.

Wang, Z., C. Zhang, and R.Z. Qi. 2014. A newly identified myomegalin isoform functions in Golgi microtubule organization and ER-Golgi transport. *J Cell Sci*. 127:4904-4917.

Weisbrich, A., S. Honnappa, R. Jaussi, O. Okhrimenko, D. Frey, I. Jelesarov, A. Akhmanova, and M.O. Steinmetz. 2007. Structure-function relationship of CAP-Gly domains. *Nat Struct Mol Biol*. 14:959-967.

Woodruff, J.B., B. Ferreira Gomes, P.O. Widlund, J. Mahamid, A. Honigmann, and A.A. Hyman. 2017. The Centrosome Is a Selective Condensate that Nucleates Microtubules by Concentrating Tubulin. *Cell*. 169:1066-1077.

Wu, J., C. de Heus, Q. Liu, B.P. Bouchet, I. Noordstra, K. Jiang, S. Hua, M. Martin, C. Yang, I. Grigoriev, E.A. Katrukha, A.F. Altelaar, C.C. Hoogenraad, R.Z. Qi, J. Klumperman, and A. Akhmanova. 2016. Molecular Pathway of Microtubule Organization at the Golgi Apparatus. *Dev Cell*. 39:44-60.

Yue, J., M. Xie, X. Gou, P. Lee, M.D. Schneider, and X. Wu. 2014. Microtubules regulate focal adhesion dynamics through MAP4K4. *Dev Cell*. 31:572-585.

Zanic, M., J.H. Stear, A.A. Hyman, and J. Howard. 2009. EB1 recognizes the nucleotide state of tubulin in the microtubule lattice. *PLoS One*. 4:e7585.

Zanic, M., P.O. Widlund, A.A. Hyman, and J. Howard. 2013. Synergy between XMAP215 and EB1 increases microtubule growth rates to physiological levels. *Nat Cell Biol*. 15:688-693.

Zhang, R., G.M. Alushin, A. Brown, and E. Nogales. 2015. Mechanistic Origin of Microtubule Dynamic Instability and Its Modulation by EB Proteins. *Cell*. 162:849-859.

Addendum

Summary

Masters of the tips: End Binding proteins orchestrate microtubule plus- and minus-end dynamics

Microtubules are dynamic polymers built of dimers of α- and β-tubulin, which attach to each other in a head-to-tail fashion. Microtubules can rapidly switch between phases of growth and shortening, a behavior known as “dynamic instability”. Microtubules have two distinct ends, the plus ends and minus ends. Microtubule plus ends are dynamic, whereas microtubule minus ends are more stable. Microtubule dynamic instability is closely associated with the ability of β-tubulin to bind and hydrolyze GTP. Tubulin dimers with GTP-bound β-tubulin form a stabilizing cap at growing microtubule plus ends, and this cap plays a crucial role in controlling microtubule dynamics. In cells, microtubule dynamics are also tightly controlled by numerous factors including microtubule plus end tracking proteins (+TIPs).

End Binding proteins (EBs) are highly conserved +TIPs. In mammalian cells, the EB family includes three members, EB1, EB2 and EB3. EBs are composed of the microtubule-binding N-terminal Calponin Homology domain, which is connected by a flexible unstructured linker region to the C-terminal domain responsible for dimerization and partner binding. EBs recognize growing microtubule ends by sensing the nucleotide state of β-tubulin. They form the core of the +TIP network by recruiting to microtubule ends many structurally and functionally diverse +TIPs. EB partners can be divided into two groups: proteins containing an SxIP motif, including SLAIN2 and CLASPs, and proteins containing CAP-Gly domains, such as CLIP170 and $p150^{Glued}$. In addition to binding to partners, EBs can alter the properties of microtubule plus ends by promoting GTP hydrolysis by β-tubulin and possibly by modifying microtubule end structure.

In Chapter 2, we applied CRISPR/Cas9 technology to generate a series of EB1, EB2 and EB3 mutant cell lines. We found that cell division and microtubule dynamics are only mildly affected in EB1, EB2 and EB3 triple mutant cells. Surprisingly, we found that EBs strongly affect microtubule minus-end organization. In EB1 and EB3 mutant cell lines, microtubule minus ends stabilized by CAMSAP2 were detached from Golgi membranes and the Golgi apparatus became more compact. Further studies showed that co-organization of microtubules and Golgi membranes depends on the EB1/EB3-myomegalin-AKAP450 complex, which tethers microtubules to the Golgi apparatus and counteract compaction of Golgi stacks. Disruption of EB1 and EB3 also affected cell migration, intracellular trafficking and the distribution of integrin adhesions.

In Chapter 3, we investigated how EBs and their partners affect the properties of growing microtubule plus ends. Since the EB mutant cells described above might still express the microtubule-binding domain of EB1, we have generated new EB1, EB2 and EB3 triple knockout HeLa cell lines, which lacked the three EBs. We used these cells to compare the length of EB comets in vivo and in vitro. We performed microtubule severing assays and found that there is a stable, depolymerization-resistant microtubule zone in the tip-proximal region, and this zone is not affected by the presence of EBs. We also found that EBs inhibit mobility of microtubule tips and make their growth more persistent. Experiments with EB deletion mutants showed that these properties depend on the recruitment of EB binding partners.

In Chapter 4, we explored the possibility that liquid-liquid phase separation (LLPS) plays a role in microtubule tip regulation. As a candidate for an LLPS scaffold, we focused on SLAIN2, because it shares the intrinsically disordered structure with proteins that undergo LLPS in

other cellular contexts. We found that overexpression of SLAIN2 can lead to droplet formation in cells, including EB1, EB2 and EB3 knockout cells. However, we found no evidence of SLAIN2 droplet formation at endogenous expression levels. SLAIN2 can interact with other +TIPs, including EBs, chTOG, CLASP and CLIP170, and we found that EBs and chTOG were recruited to SLAIN2 droplets, whereas CLASP and CLIP170 were not. We also found that SLAIN2 and chTOG, but not EB3, could efficiently form droplets in vitro in the presence of a crowding reagent, and the droplets containing chTOG could nucleate microtubule asters. However, we were not able to show specific colocalization of SLAIN2 condensates with growing microtubule plus ends in vitro. Further studies using the tools and insights that we have obtained would be needed to address the potential role of LLPS in SLAIN2 function at microtubule tips.

In Chapter 5, we investigated how different microtubule binding domains could affect microtubule dynamics in vitro when targeted to microtubule tips by the N-terminal part of EB3. While EB3 fusions of SLAIN2 and the C-terminal microtubule-binding fragment of spectraplakin caused no obvious changes in microtubule dynamics, similar fusion of the TOG domains of CLASP2 strongly suppressed catastrophes or induced rescues. Different TOG domain of chTOG, particularly the TOG4-TOG tandem, tested in this context, strongly increased catastrophe frequency. In contrast, EB3 fusion of the GAR domain of spectraplakin and the CAP-Gly domains of CLIP170 induced rescues, whereas an EB3 fusion of the microtubule binding domain of MAP7 strongly reduced microtubule depolymerization rate. These data indicate that different parameters of microtubule dynamics can be regulated independently of each other. The same fusion proteins did not affect microtubule dynamics in EB1, EB2 and EB3 triple knockout cells as they did in vitro, possibly because of the complex regulation of microtubule dynamics in cells.

In conclusion, we have obtained new insights into how EBs control microtubule networks and generated new tools that will help in future to unravel cellular mechanisms controlling microtubule polymerization.

Samenvatting

Maestro's van de uiteinden: Eind Bindende eiwitten dirigeren de dynamiek van microtubuli plus- en min-uiteinden

Microtubuli zijn dynamische polymeren opgebouwd uit α- en β-tubuline dimeren die via een kop-staart mechanisme aan elkaar binden. Microtubuli wisselen snel af tussen fasen van groei en krimp. Dit gedrag wordt "dynamische instabiliteit" genoemd. Microtubuli hebben twee verschillende uiteinden; een plus-uiteinde en een min-uiteinde. De plus-uiteinden van microtubuli zijn dynamisch, dit in tegenstelling tot de min-uiteinden die stabieler zijn. Dynamische instabiliteit van microtubuli is nauw geassocieerd met het vermogen van β-tubuline om GTP te binden en hydrolyseren. Tubuline dimeren waar GTP gebonden is aan β-tubuline vormen een stabiele structuur op groeiende plus-uiteinden van microtubuli en deze structuur speelt een cruciale rol in het regelen van microtubuli dynamiek. In cellen wordt microtubuli dynamiek ook sterk gereguleerd door een groot aantal factoren, waaronder plus-eind bindende eiwitten (+TIPs).

Eind Bindende eiwitten (EBs) zijn sterk geconserveerde +TIPs. In zoogdieren bestaat de EB familie uit drie leden; EB1, EB2 en EB3. EBs zijn opgebouwd uit een microtubuli-bindende N-terminale Calponine Homologie domein dat via een flexibele, ongestructureerde linker is verbonden aan een C-terminaal domein wat verantwoordelijk is voor dimerisatie en interactie met bindingspartners. EBs herkennen groeiende microtubuli uiteinden door de nucleotide status van β-tubuline te detecteren. Zij vormen de kern van het +TIP netwerk door vele structureel en functioneel verschillende +TIPs naar de microtubuli uiteinden te rekruteren. EB bindingspartners kunnen worden opgedeeld in twee groepen: eiwitten die een SxIP motief bevatten, zoals SLAIN2 en CLASPs, en eiwitten die CAP-Gly domeinen hebben, zoals CLIP170 en p150^{Glued}. EBs kunnen niet alleen aan partners binden, maar daarnaast kunnen zij ook de eigenschappen van microtubuli plus-uiteinden veranderen door GTP hydrolyse van β-tubuline te stimuleren en mogelijk ook door de structuur van microtubuli uiteinden te beïnvloeden.

In **Hoofdstuk 2** hebben we de CRISPR/Cas9 techniek toegepast om een aantal cellijnen te genereren die mutant zijn voor EB1, EB2 en EB3. We hebben gevonden dat celdeling en microtubuli dynamiek in EB1, EB2 en EB3 drievoudige mutanten slechts mild waren aangetast. Verrassend genoeg vonden we dat EBs een sterk effect hebben op de organisatie van microtubuli min-uiteinden. In een cellijn die mutant is voor EB1 en EB3 lieten de door CAMSAP2-gestabiliseerde min-uiteinden los van de Golgi membranen en het Golgi-complex werd compacter. Verder onderzoek liet zien dat co-organisatie van microtubuli en Golgi membranen afhangt van het EB1/EB3-myomegalin-AKAP450 complex, wat zorgt voor het verankeren van microtubuli aan het Golgi-complex en de verdichting van Golgi membranen tegengaat. Verstoring van EB1 en EB3 heeft ook invloed op celmigratie, intracellulair transport en de verspreiding van integrine adhesies.

In **Hoofdstuk 3** hebben we onderzocht hoe EB eiwitten en hun bindingspartners de eigenschappen van groeiende microtubuli plus-uiteinden beïnvloeden. Aangezien de hierboven beschreven cellijnen met EB mutanten mogelijk nog steeds het microtubuli-bindende domain van EB1 bevatten, hebben we nieuwe EB1, EB2 en EB3 drievoudige knockout HeLa cellijnen gemaakt die alle drie de EB eiwitten missen. We hebben deze cellen gebruikt om de lengte van EB kometen in vivo en in vitro met elkaar te vergelijken. We hebben experimenten gedaan waar microtubuli werden doorgesneden en hebben hierbij gevonden dat er een stabiele, depolymerisatie-resistente microtubuli zone is in de tip-proximale regio, en dat deze zone niet

wordt beïnvloed door de aanwezigheid van EBs. We hebben ook ontdekt dat EBs de mobiliteit van microtubuli uiteinden remmen en dat dit zou kunnen zorgen voor meer aanhoudende groei. Experimenten met EB deletie mutanten hebben laten zien dat deze eigenschappen afhankelijk zijn van EB bindingspartners.

In **Hoofdstuk 4** verkennen we de mogelijkheid dat vloeistof-vloeistof fase-separatie (VVFS) een rol speelt bij microtubuli tip regulatie. We focussen ons op SLAIN2 als een kandidaat VVFS "kapstok", omdat het, net als eiwitten die VVFS ondergaan in andere cellulaire contexten, als kenmerk heeft dat het intrinsiek ongestructureerde is. We hebben ontdekt dat overexpressie van SLAIN2 kan leiden tot druppelformatie in cellen, inclusief cellen waar EB1, EB2 en EB3 afwezig zijn. Echter, we hebben geen bewijs gevonden dat SLAIN2 druppels kan vormen onder endogene expressie niveaus. SLAIN2 kan interacties aangaan met andere +TIPs, zoals EBs, chTOG, CLASP en CLIP170. We hebben gevonden dat EBs en chTOG, maar niet CLASP en CLIP170, naar SLAIN2 druppels kunnen worden gerekruteerd. Eveneens vonden wij dat SLAIN2 en chTOG, maar niet EB3, in vitro efficiënt druppels konden vormen in de aanwezigheid van een crowding reagentia, en dat druppels die chTOG bevatten konden zorgen voor de nucleatie van microtubuli asters. We konden echter geen colokalisatie detecteren van SLAIN2 condensaten met groeiende microtubuli plus-uiteinden in vitro. Met behulp van het ontwikkelde gereedschap en de behaalde inzichten, kunnen wij onderzoek doen om de mogelijke rol van VVFS bij SLAIN2 functie aan microtubuli uiteinden verder te ontrafelen.

In **Hoofdstuk 5** onderzoeken wij hoe verschillende microtubuli bindende domeinen invloed kunnen hebben op in vitro microtubuli dynamiek wanneer deze door het N-terminale deel van EB3 naar het microtubuli uiteinde worden gerekruteerd. Terwijl EB3 fusies met SLAIN2 en de C-terminus van het microtubuli-bindende fragment van spectraplakine geen duidelijke verandering van microtubuli dynamiek veroorzaakten, zorgden vergelijkbare fusies van de TOG domeinen van CLASP2 voor sterke onderdrukking van catastrofes of verminderde rescues. Verschillende TOG domeinen van chTOG, specifiek het TOG4-TOG5 tandem, die in deze context getest werden, zorgden voor sterke toename in catastrofe frequenties. In tegenstelling tot deze bevinding, resulteerde fusies van EB3 met het GAR domein van spectraplakine en de CAP-Gly domeinen van CLIP170 voor rescues, terwijl een fusie van EB3 met het microtubuli bindende domein van MAP7 leidde tot sterk gereduceerde microtubuli depolymerisatie snelheid. Deze data geven aan dat verschillende microtubuli dynamiek parameters onafhankelijk van elkaar kunnen worden gereguleerd. Dezelfde fusie-eiwitten hadden in cellen waar geen EBs aanwezig zijn niet dezelfde effecten op microtubuli dynamiek als in vitro wat mogelijk zou kunnen worden veroorzaakt door de complexe regulatie van microtubuli dynamiek in cellen.

Samengevat, hebben wij nieuwe inzichten verkregen in hoe EBs microtubuli netwerken kunnen beïnvloeden en hebben wij nieuw gereedschap ontwikkeld dat in de toekomst kan worden gebruikt bij het ontrafelen van cellulaire mechanismen die betrokken zijn bij groei van microtubuli.

Curriculum Vitae

Chao YANG was born on August 26th, 1988 in Pengzhou, China. In 2011, he received his Bachelor of Agriculture degree, majoring in Veterinary Medicine from Sichuan Agricultural University, Ya'an, China. In the same year, he enrolled in Chinese Academy of Agricultural Sciences as a Master student and continued to study Veterinary Medicine in Harbin Veterinary Research Institute. During the Master program, he used MHC-B haplotype of chicken breeds to study the association of natural killer cells with Marek's disease in the lab of Lingxia Han, and obtained the Master of Veterinary Medicine degree in 2014. In October 2014, he started his PhD training within the Graduate School of Biomembranes under the supervision of Prof. Dr. Anna Akhmanova. Here, he investigated the mechanisms of regulation of microtubule dynamics by End Binding proteins. The research described in this thesis was performed in the division of Cell Biology, Neurobiology and Biophysics in the Department of Biology, Faculty of Science, Utrecht University.

List of publications

Yang, C.*, J. Wu*, C. de Heus, I. Grigoriev, N. Liv, Y. Yao, I. Smal, E. Meijering, J. Klumperman, R.Z. Qi, and A. Akhmanova. 2017. EB1 and EB3 regulate microtubule minus end organization and Golgi morphology. *J. Cell Biol.* 216:3179–3198. doi:https://doi.org/10.1083/jcb.201701024

Atherton, J., Y. Luo, S. Xiang, **C. Yang**, K. Jiang, M. Stangier, A. Vemu, A.D. Cook, S. Wang, A. Roll-Mecak, M.O. Steinmetz, A. Akhmanova, M. Baldu, and C.A. Moores. 2019. Structural determinants of microtubule minus end preference in CAMSAP CKK domains. *Nat. Commun.* 5236. doi:10.1038/s41467-019-13247-6

Fréal, A., D. Rai, R.P. Tas, X. Pan, E.A. Katrukha, D. van de Willige, R. Stucchi, A. Aher, **C. Yang**, A.F.M. Altelaar, K. Vocking, J.A. Post, M. Harterink, L.C. Kapitein, A. Akhmanova, and C.C. Hoogenraad. 2019. Feedback-Driven Assembly of the Axon Initial Segment. *Neuron*. 305–321. doi:10.1016/j.neuron.2019.07.029.

Wu, J., C. de Heus, Q. Liu, B.P. Bouchet, I. Noordstra, K. Jiang, S. Hua, M. Martin, **C. Yang**, I. Grigoriev, E.A. Katrukha, A.F.M. Altelaar, C.C. Hoogenraad, R.Z. Qi, J. Klumperman, and A. Akhmanova. 2016. Molecular Pathway of Microtubule Organization at the Golgi Apparatus. *Dev. Cell*. 1–17. doi:10.1016/j.devcel.2016.08.009.

Co-first author

Acknowledgments
I am really glad I managed it. My PhD journey was not easy, especially the first year, when I faced a completely foreign environment while starting my projects in the lab. Just imagine, I came to the Netherlands hoping to practice my English, only to find that people were speaking Dutch! Then when I tried to speake Dutch, they would switch to English!!! With my limited cell biology knowledge, I began exploring the molecular mechanisms controlling microtubule dynamics. Thank you, my dear colleagues and friends. I cannot imagine how I could have managed it without your support, help and company. Here, I would like to express my gratitude to all the amazing people around me. Thank you for supporting me to achieve not just this thesis, but also for fantastic PhD years.

First of all, I would like to particularly thank my supervisor, Prof. dr. Anna Akhmanova. Thank you so much for trusting me and accepting me into your lab, it has opened a new world for me. Thanks for sharing valuable experience and your persistent encouragement in improving my English all these years. Thanks to your immense help, I was able to present in both America and Singapore, which were big things for me. They were wonderful trips from which I gained both experience and confidence, and I am very proud of that. I learned a lot of things from you, including a critical attitude and dedication to science, both of which will be my fortune for my whole life. I sincerely thank you for everything you have done for me, for your support in testing my various ideas; for supervising my research projects, which made my PhD productive; for sharing your personal experience, which encouraged me to overcome difficulties; for the critical discussions which not only helped give me a clear vision, but also shaped my way of looking at things, and for your great input and patience, particularly when I wrote my paper and this thesis. Under your complimentary mentorship, I gained skills, strength, experience, insight and managed to have a fantastic PhD. It was a great honor to have you as my supervisor and I wish you all the best.

Thanks to everyone in my PhD evaluation committee: Prof. Sander van den Heuvel, Prof. Marileen Dogterom, Prof. Lukas Kapitein, Prof. Judith Klumperman, Prof. Susanne Lens. Thank you for your kind words and for taking the time to evaluate my thesis.

I would like to express my thanks to my greatest friends and paranymphs. Qiongyi Chen, I am fond of your Taiwanese accent as much as my Sichuanese. I am amazed by your sweet, dynamic, joyful and strong-minded nature. Conversations with you are always comfortable. Thanks for sharing your wisdom. Fangrui Chen, your passion for science is infectious and I really appreciate your honesty and optimism. Thank you for all the things you did for my family. Thanks for all the nice conversations and delicious dishes. All the best for your family, experiments and papers.

Thanks to the colleagues and collaborators who made a great contribution to this thesis. Ilya Grigoriev, thank you for introducing me to the microscopes, which are my good friends now. Thanks for all the experiments you did and analyzed for me, as well as extensive discussions. Ankit Rai, you are such a wise person and you have encouraged me a lot. Thank you for introducing me to the in vitro reconstitution approach and for the experiments you did for my project. You will have a great lab and I would like to visit you in the future. All the best with your family. Jingchao Wu, thanks for your help and contribution to my paper. Thank you, Eugene Katrukha, for giving me the surprise balloon ride when I just arrived in the Netherlands. Thank you for taking the time to analyze the data for my project and doing so with such incredible

speed, the results are amazing too. Ruddi, thank you for the nice chats and for introducing me to the FCS world. Amol Aher, thanks for the extensive discussions and for sharing me great Indian movies. Thank you to my Mater students. Cédric Gerwoud van der Ham, you did a very good job, the EB2 knockout cell lines are very useful. Jacob Hepkema, you showed a great amount of growth during your internship. Thank you for helping me make a lot of constructs. I am really glad that you got a PhD position to study bioinformatics, and I wish you all the best. Thanks to my collaborators: Cecilia de Heus, Nalan Liv, Yao Yao, Ihor Smal, Erik Meijering, Robert Z. Qi for your help with the JCB paper.

I would like to express my gratitude to the PIs and faculties in the division. Lukas Kapitein, thanks for your great inputs in the Monday and Friday discussion as well as during casual chats. I do think biophysics is cool and I recognize your passion for both microtubule and microscopy. Casper Hoogenraad, thanks for the nice discussion and I wish you all the best with your new group in Genentech. Corette Wierenga, thanks for the inputs at meetings and nice chats. Ginny Farias Galdames, I enjoyed our conversations during the lab outing, thanks for nice discussions. Harold MacGillavry, thanks for the nice smile and chats. Sabrina Santos Oliveira, thanks for the encouragement and for making me realize that nanobodies are full of potential. Paul van Bergen en Henegouwen, thanks for introducing me to nanobodies. Esther de Graaff, thanks for the nice chats. Florian Berger, welcome to our division and good luck with your attractive research.

Thanks to the colleagues in our group. Kai Jiang, I am very grateful for your help, advice, and instructions. The sharing of your experience and wisdom meant a lot to me, and enabled me to make it through the difficult start. I am proud of you for winning the young 1000 talent program. I wish all the best with your new group, and I am looking forward to seeing your papers. Shasha Hua, I am so grateful for your friendly, welcoming and warm chats which comforted and encouraged me, especially when I was upset with the results from my experiments. They helped me to remove the dark clouds in my mind and see and feel the brightness and warmth of the sun. I can still feel it. Qingyang Liu, what a wonderful person you are, defended on time and found a job seamlessly, all followed by a happy wedding. Wonderful! I feel very inspired by you. Thanks for your help in the morning subgroup working discussion. Thanks for cheering me up when I was feeling defeated. I am very grateful not just for your help with experiments, but also for the nice chats, advice, and suggestions in general. Thanks for providing your powerful suggestions and advice whenever I needed. Wish you all the best with your family. Benjamin Bouchet. I do not remember how many times you came to ask me to refill things or close the hood. Thanks to your persistence, I formed good habits in cell culture. I am also grateful for your help and suggestions with experiments and scientific discussions in our office. Ivar Noordstra, thanks for inviting me to the wedding party, it was the first wedding party I attened in the Netherlands. Thanks for helping me whenever I came to you, even renting a car and lifting my fridge upstairs. York Ammon, I am amazed by your organization skills. Maybe sometime in the future, we can go together to Germany to watch a live football match there in person. Peter Jan Hooikaas, thanks for helping to organize the lab and for useful discussions in the morning subgroup meetings. Cyntha van den Berg, it was super nice and comfortable to have conversations with you. Dipti Rai, thanks for your time to find proteins and constructs I needed. Joyce Meiring, you are a great Dutch - Australian person, welcome to your other base. Funso Ogunmolu, I am so grateful for all the conversations, no matter the topics, science, China or Postdoc. You are so helpful and enthusiastic, good luck with all your experiments. Boris Shneyer, thanks for being a handsome guy. Babet van der Vaart, big thanks for translating

my thesis summary into Dutch, you did a truly superb job. Also thanks for your great work on SLAIN2, a beautiful protein. Hugo Damstra, thank you for the nice discussions in the morning subgroup. Kyle Quinney, thanks for taking over my EB cells and preparing cells for me. Milena Pasolli, thanks for all the great friendly chats. Thanks for Helma van Riel, Ruben Schmidt and Andrea Marques for the nice smile and chats. Maud Martin, good luck with your new job in Belgium. Carol Yu, thanks for introducing me to the lab and showing me where everything is.

I would like to express my gratitude to colleagues in my old office, O522 and new office, O502, thanks for all the knowledge about the Netherlands, conversations, and food or cookies. Wilco Nijenhuis, you have inspired me a lot. Thanks for sharing your intelligence and the knowledge about the Netherlands. I am grateful for your support, encouragement and helps. Wish you all the best with your grants and papers. Eitan Zahavi, thanks for sharing the information about the vacancy in the new office, O502, which enabled us to be office mates again, which is something I really want to continue being. Dennis Kruijssen, thanks for nice chats and information about PhD defense. Carlijn Peerboom, Marvin Ruiter and Lotte Herstel, thanks for the nice conversations and creating pleasant office environment. I am grateful to you, Marjolein Haagsman, for supporting me in fighting back against my bad landlord.

Thanks to my scientific friends in Utrecht. Yujie Cao, thanks for all the nice conversations, I am amazed by your seemingly limitless passion and knowledge. Your words were really powerful, you know, and comforted me when I was upset with my experimental results, encouraged me when I came up with new ideas, and directed me when I felt confused. Thanks for your help and support whenever I needed it. I am really grateful to have you as my dearest friend. Xingxiu Pan, you have inspired me with your ambition and knowledge, and thanks for sharing these with me. Jian Liang, thanks for your non-sense jokes, I am astonished by the breadth of your horizon, and I am looking forward to hearing your updates. Liu He, thanks for sharing information with me. Chats with you are always cheerful and comfortable. All the best with your experiments on worms.

I would like to express my gratitude to everybody in the Cell Biology, Neurobiology, and Biophysics division. Thank you all for the nice conversations and contributing to the nice atmosphere in the division. Phebe Wulf, thanks for taking care of my orders. Thanks for providing your assistance whenever I come to you. Riccardo Stucchi, good luck with your new job in Switzerland, all the best with your baby. Mithila Burute, thanks for all the nice talks. Your knowledge and suggestions were very helpful. Martin Harterink, Thanks for the wonderful conversations and I wish you all the best with your grants. Desiree Salas, I am glad we played football together, thanks for the friendly chats. Anne Janssen and Roderick Tas, thanks for all the nice experiences together. Cátia Frias, Anna Bodzeta and Sofia Doulkeridou, thanks for distracting me outside the lab and all the nice chats. Amélie Fréal, Lisa Catsburg, Jelmer Willems, Klara Jansen and Giel Korsten, thanks for your help with experiments, it was super nice to collaborate with you. René van Dorland and Bart de Haan, thanks for your support. Feline Lindhout, Robin Buijs, Jessica Hummel and Katerina Xenaki, it was super nice to have you as lab mats. Nazmiye Özkan, Marijn Siemons, Yolanda Gutierrez, Arthur de Jong, Lena Will, Daphne Jurriens, Robbelien Kooistra, Sybren Portegies, Nicky Scheefhals, Manon Westra, Malina Iwanski, thanks for joyful conversations. Thomanai Lamtha, Vida Mashayekhi, Sara Pompe and Yingxin Yu, thanks for sharing the latest understanding of nanobodies with me.

Thanks to all the members in the developmental biology division. Sander thanks for nice smiles

and encouragement. Mike, Inge, Vincent, João, Juliane, Molly, Lars and Sannne, thanks for all the nice talks during lab-out and discussions during Monday meetings.

相信，即便多年以后，我仍然能记得乌特Sunway足球队的朋友们。队长，毅哥，伴我在广州恒大路上停不下来。还有各位：柳泽光、刘磊华、常富强、桃子、瑞学、陈晨、娄博、宏凯、春晖、志雄、曦晨、李洋、吕俊、小韦、韩宇浩，张正越、蔡嘉诚，文斌、王豪、孙哲、刘超、金帝、云路、庆一、Gary、Gert、Alex，小强、杜杰、白哥、亚洵，还有球队的其他兄弟朋友。场上，感谢大家给我传球，让我有机会空门打飞机，感谢大家的鼓励让我使劲跑。为被我踢过踩过的人，真诚的道歉。场下，帮我洗训练背心，帮我开灯，借我鞋穿，开我玩笑，给我指点，带我（流）浪，让我在异国他乡感到温暖。每周最盼的就是周五，到了踢球时间，实验可以退一退，开会可以挪一挪，就盼着各位能早点来，让精彩开始。生活中还给我做饭，帮我开车，帮我找房，帮我搬家，甚至借宿，各位的大恩大德，没齿难忘。跟大家一起踢球，看球，吹牛和各种活动，生活真的是安逸的板。太巴适了。谢谢各位，给了我这么一段美好的时光，这段时光值得我珍藏到永远。

最后，感谢我的父母和家人。感谢妈妈从小到大的关心与照顾，感谢爸爸对家庭的付出。特别感谢你们的理解和支持，任何言语都无法表达我对你们无私关怀和照顾的感激之情。感谢关心，理解，支持和鼓励我的亲朋好友。愿你们身体健康，生活幸福。谢谢！

The biggest thanks to my dearest wife, Liling SHAN. First of all, thank you for accompanying me to the Netherlands, facing a totally foreign country with unpredictable difficulties. Thanks for your delicious cooking, which allows me to survive here. Thanks for all your support, patience, understanding, and encouragement over all these years. Your joyful and fun chats energized me, your wisdom and knowledge helped me find my way. Thank you for the surprise gift, our happy baby, Andong YANG. This little creature gives me more joy than I could ever have imagine possible. Thanks for taking greater responsibility for the family. Sometimes, when I think of it, I realize how happy I am with you. You are truly amazing. I wish you all the best with your defense, I am proud of you. I love you!

Chao YANG (杨超)
Jan 2020, Utrecht. The Netherlands.